Function of Meteorins in commissural axon guidance and their role as novel regulators of left-right patterning in the zebrafish embryo

Fanny Eggeler

THESE DE DOCTORAT DE SORBONNE UNIVERSITE ÉCOLE DOCTORALE 158

« ED3C CERVEAU COGNITION COMPORTEMENT »

Institut De la Vision Paris, Département Biologie du Développement Équipe Del Bene

« Développement et fonctionnement du système visuel des vertébrés »

„Function of Meteorins in commissural axon guidance and their role as novel regulators of left-right patterning in the zebrafish embryo”

Présentée et soutenue publiquement par

Fanny EGGELER

a Paris, le 10 mars 2023

Directeur de thèse:

Dr. Filippo DEL BENE

Devant le Jury composé de :

Dr. Juan R. MARTINEZ-MORALES, CABD	Rapporteur
Dr. Marion COOLEN, INSERM	Rapporteur
Dr. Pierre-Luc BARDET, Sorbonne Université	Examinateur
Dr. Alessandra PIERANI, INSERM	Examinateur/Président du Jury
Dr. Marie BREAU, INSERM	Examinateur
Dr. Filippo DEL BENE, INSERM	Directeur de thèse

Versprochen ist versprochen !

I. ACKNOWLEDGEMENTS

Who would have thought, that I would be sometime in the position to write my acknowledgements…for my PHD thesis, so often I would not have believed it myself. That's why I want to thank everyone who supported, encouraged and believed in me all these years.

First of all, of course, a big thank you to Filippo, to give me this amazing opportunity to work in your lab, not just for my PhD, but also for an internship during my Master which shaped my wish to pursue a PhD (I would have even payed to join your lab at this time ;). Thank you for always pushing me to do my best but also for leaving me some freedom to make mistakes and to learn from them. Your enthusiasm and encouragement helped me over many hurdles during my PhD journey.

I am also exceptionally thankful to the members of my TAC committee, Sonia and Pierre-Luc, for all the encouragements, suggestions and questions. I always enjoyed the TAC meetings very much, starting them so nervously but leaving them full of beans. A big thank you also to my PhD Jury (Marion Coleen, Juan R. Martinez-Morales, Alessandra Pierani, Marie Breau, Pierre-Luc Bardet) for accepting to evaluate my over-four-years PhD work.

I am very thankful to Alain for the great collaboration and all the input to the Meteorin project. One of the biggest thank you goes to Yvrick and Manuela, for being so patient with me and for all your support and help. Without you, the whole project would be somewhere totally else and surely not as progressed as it is now. Thank you Yvrick, for introducing me into the mystery of cell culture and biochemistry and for having endured some crazy PhD-student moods. Thank you, Manuela, for all your help and expertise with the Mass spec approach, I would have been lost without you.

Even if no one ever wanted to join me for a run (some of the excuses were phenomenal), a deep thank you goes to the Del Bene lab. I spend so many hours in the lab and mostly because of you, even the toughest days were bearable. Shahad, thank you for support and for being there in the lab, whenever I needed you. Your supervision during my first months in Filo's lab was the best and your encouraging smiles made so many steps back not as bad. Karine, without you, the lab would be lost. I am so grateful for your patience with me, for your help whenever I needed it and for not getting to angry when I now and again broke something! Malo, thank you for your calmness and your kindness (no matter how crazy things got in the

lab), it was great working with you. Jonathan, I cannot be grateful enough for your help with the KV-particle tracking and your contagious enthusiasm and good mood. Elena and Giulia, without you, lab days would have been so much duller and more boring, our lunch breaks so often changed my mood after a stressful morning (also thank you for putting up with me through some moody phases). Thank you also for giving me some crash courses into the Italian mentality. Julie, you are the new generation of Del Bene PhD students, stay strong, you will do great and I wish you all the best. A special thanks goes to Laura, you were the first student I was allowed to supervise. It was such a great experience for me and I believe I nearly learned as much from our work together as you during your internship. Thank you so much for this adventure. Please keep up your amazing motivation, kindness and positive mood, you will do great.
Also, a thank you to all the “old” Del Bene lab members (Celine, Christoph, Gokul, Marion, Valerie, Flavia) it was a pleasure and you all helped on some way during my PhD journey. Especially Flavia, thank you for introducing me to the Meteorins.

My biggest gratitude goes to my “Parisian” friends (Paul, Reto, Tonia) and especially to coloc “Labat” (Raly, Ani, Sam, Marie-Philipine), you are the best and I don’t know how else to say but this you are/were a bit like family far away from home and I owe you so, so much.

Amore, grazie per tutto!
It is difficult to articulate how thankful I am, for all your support, your help and patience and for just being by my side. Thank you for being my boyfriend collaborator and for being my personal chef during weekend writing sessions. Thank for all the scientific bathtubs and discussions, thank for the balcony coding sessions, office breakfasts and pizza Fridays. Thank you for always having an open ear as I try to explain my daily experiments and my struggles with lazy fish. Thank you being my running mate and for supporting me with my crazy ideas (like running a marathon…what did I get myself into?). I could go on and on like this and everything means the world to me.

Das mit größte Dankeschön geht an meine Freunde und Familie zu Hause. Ihr wart oft so weit weg aber trotzdem irgendwie da. Jessi, Lisa, Hanna danke für eure Freundschaft und die vielen Telefonate und Skype Sessions. Sie waren oft das Highlight meines Tages! Danke für euer Verständnis, eure Geduld und ich weiß, ich kann immer auf euch zählen. Oma Elfie, Oma Heidi, ihr seid die Besten. Danke für eure unerbittliche Unterstützung, die Carepakete oder ein Bett in „Hotel Oma“ wann immer ich es brauche. Alex, ich weiß, ich bin nicht immer die einfachste große Schwester und ich glaube wir haben beide nicht so wirklich Ahnung was der andere während des Tages in seinem Beruf so treibt. Aber ich wollte dir nur sagen, wie stolz

ich auf dich bin und ich weiß, wenn es hart auf hart kommt, bis du da und ich kann mich immer auf dich verlassen. Mama und Papa, ich weiß gar nicht wo ich anfangen und wie ich es sagen soll (habe mir deswegen von woher ein bisschen Inspiration geholt ;) Ihr seid einfach mein Zufluchtsort, die Mitte von meinem Schiff und mein tadelloses Himmelblau! Danke, danke, danke für Alles! Ohne euch wäre ich heute nicht hier, ich weiß nicht was ich ohne eure Hilfe, Unterstützung und Glaube an mich gemacht hätte.

I think there are so many more people who supported me during my journey (Stephan, thank you for all your patience and support with imaging, Jochen and Katha, I still happily remember my days in Heidelberg, Rob, thanks for welcoming me in your lab in Hamburg…) and I am sorry that I cannot mention you all, but I am very grateful for all your help and encouragement.

Merci beaucoup à tous!!

II. RÉSUMÉ

L'un des principaux objectifs de la Neurobiologie du développement est de comprendre comment les axones des neurones nouvellement formés peuvent atteindre leurs corrects partenaires synaptiques en suivant des chemins précis et bien définis guidés par un réseau complexe d'interactions récepteur/ligand (par exemple, Netrin/DCC; Slit/Robo) [1]. Bien qu'un grand nombre de molécules de guidage des axones ait déjà été caractérisé, le tableau est loin d'être complet et un certain nombre de facteurs de guidage restent encore à découvrir.

Les précédents travaux du laboratoire ont généré des allèles de perte de fonction pour les trois gènes du poisson zèbre de la famille des protéines sécrétées Meteorin (Metrns). De façon remarquable, nous avons pu caractériser des défauts de développement axonal spécifiques chez ces poissons mutants, y compris des défauts dans plusieurs populations de neurones commissuraux.

Soutenus par nos résultats préliminaires, nous avons émis l'hypothèse que les Metrn jouent un rôle important au cours du développement du système nerveux central (SNC) des vertébrés et du franchissement de la ligne médiane axonale et en particulier dans le guidage des axones commissuraux.

À partir de ces prémisses, l'objectif de mon projet de doctorat était d'étudier la fonction des Metrns chez le poisson zèbre, d'élucider leurs voies de signalisation biochimique et, surtout, d'identifier le ou les récepteurs des Metrns.

La Metrn a d'abord été découverte comme un facteur neurotrophique sécrété qui favorise la croissance des neurites *in vitro*. Elle est exprimée dans les progéniteurs neuronaux radiaux et dans la glie radiale [2], [3]. Chez les vertébrés, les Metrn sont hautement conservées, y compris deux membres chez les mammifères et trois chez le poisson zèbre (Metrn, Metrnl1 et Metrnl2). Chaque gène *Metrn* ou *Metrnl* code pour une protéine d'environ 300 acides aminés contenant une séquence signal N-terminale ainsi qu'un domaine de type Netrin à l'extrémité C-terminale [3].

Par conséquent, une partie de mon projet de thèse consistait à évaluer la localisation des protéines Metrns *in vivo* et à caractériser leur fonction sur le développement des axones commissuraux chez le poisson zèbre. Dans ce but, j'ai réalisé des hybridations *in situ* en double fluorescence afin de comparer les expressions de *metrn* et *metrnl1* à l'expression du facteur de guidage axonal bien établi Slit. Les résultats obtenus ont montré que metrn et *metrnl1* co-localisent avec *slit1a, slit1b* et *slit2* au niveau de la ligne médiane à 2dpf. J'ai également validé la conservation de ce modèle d'expression chez la souris. Cette colocalisation soutient le rôle des Metrns comme nouveaux acteurs dans le guidage axonal le long des Slits et d'autres facteurs impliqués dans ce processus.

De plus, il a été rapporté que l'expression de nodal, lefty ainsi que p-smad2 est régulée à la baisse dans les cellules ES dépourvues de Meteorin [4]. Par le biais de la qPCR et de l'hybridation *in situ*, j'ai découvert non seulement que le facteur Nodal était significativement altéré chez les triple mutants *metrns* mais aussi que chez le poisson zèbre de type sauvage, *metrnl1* tout particulièrement, est exprimé plus tôt qu'on ne le pensait auparavant (avant 6hpf). De plus, j'ai observé des mouvements aléatoires ou symétriques du cœur chez les triples mutants, similaires à ceux décrits chez les mutants *spaw* et lefty [5]. En outre, en utilisant les lignées knockout CRISPR/Cas9 de *meteorins*, j'ai pu montrer des défauts dans les propriétés de la vésicule de Kupffer (KV), causés par une altération de l'assemblage et de la migration de cette vésicule formant les cellules précurseures dorsales (DFCs). Enfin, nous avons pu démontrer que les Meteorins interagissent génétiquement avec ItgαV et Itgβ1b au niveau des DFCs. Ces résultats indiquent que les Météorines sont de nouveaux composants essentiels pour un patterning gauche-droite correct au cours du développement embryonnaire des vertébrés.

Malgré les récents progrès dans la compréhension des multiples fonctions des Meteorins, le ou les premiers récepteurs des Meteorins n'ont été identifiés que récemment. Il a été proposé qu'en activant un récepteur inconnu, les protéines Metrn puissent activer la voie de signalisation Jak/Stat3 [2]. Cependant, il a été récemment démontré que Metrnl favorise la réparation cardiaque en se liant à la tyrosine kinase du récepteur KIT et établit METRNL comme un ligand du récepteur KIT dans le contexte de la réparation des tissus ischémiques [6]. De plus, il a été révélé que Metrn se lie à Htr2b pour réguler les niveaux d'espèces réactives de l'oxygène dans les cellules souches/progénitrices hématopoïétiques [7]. Cependant, nous pensons que les Metrn doivent également agir par le biais d'un récepteur supplémentaire au cours des processus de structuration précoce ainsi que du guidage axonal. Par conséquent, l'une des principales ambitions de ma thèse était d'identifier d'autres récepteurs Metrn et Metrnl à l'aide d'approches indépendantes et d'analyser leurs fonctions dans le développement neurologique, le guidage axonal et la structuration gauche-droite chez le poisson zèbre.

Pour valider si les Metrn sont capables de se lier aux axones exprimant leur(s) récepteur(s) hypothétique(s) et afin de visualiser la distribution des possibles récepteurs Metrn, j'ai cloné des constructions pour produire des protéines de fusion Metrn-AP/Metrnl-AP. Ces protéines de fusion ont été utilisées comme sondes sur des sections de moelle épinière de souris et de poisson zèbre pour détecter une éventuelle liaison des Metrn. En effet, nous avons pu montrer que les protéines de fusion Metrns AP se lient près de la ligne médiane de la moelle épinière. Ceci soutient l'hypothèse que les Metrns sont de nouveaux facteurs de guidage axonal également chez la souris, facilitant le franchissement de la ligne médiane, et que les récepteurs possibles sont situés là où les axones viennent de franchir la ligne médiane.

En collaboration avec le Dr Alain Chedotal et Yvrik Zagar ainsi que Manuela Argentini de son équipe, j'ai travaillé à la mise au point de deux méthodes indépendantes de réticulation/pull-down pour identifier le(s) récepteur(s) des Metrns : l'approche Fc-tag [8] et AP-tag [9]. Nous avons récemment obtenu une liste de candidats à partir de ces cribles biochimiques combinés et nous effectuons des tests *in vivo* pour les valider en tant que récepteurs authentiques de la Meteorins.

En conclusion, les travaux de thèse suggèrent que les protéines Meteorin sont de nouveaux acteurs au cours du développement du SNC des vertébrés et du franchissement de la ligne médiane axonale, en particulier au cours du guidage des axones commissuraux et de nouveaux facteurs potentiels pour la formation correcte du KV et du schéma gauche-droite des vertébrés.

III. SUMMARY

One of the major goals of developmental neurobiology is to understand how axons of newborn neurons can reach their correct synaptic partners by following precise and well-defined paths guided by a complex network of receptor/ligand interactions (e.g. Netrin/DCC; Slit/Robo) [1]. Although a big set of axon guidance molecules has been already characterized, the whole picture is far from being complete and a number of guidance factors still remain to be discovered.

Previous work in the laboratory has generated loss-of-function alleles for all three zebrafish genes from the Meteorin (Metrn) family of secreted proteins. Remarkably, we could characterize specific axonal development defects in these mutant fish including defects in several commissural neuron populations.

Supported by our preliminary results, we hypothesized that Metrns play an important role during the development of the vertebrate central nervous system (CNS) and axonal midline crossing and especially in commissural axon guidance.

From these premises, the goal of my PhD project was to investigate the function of Metrns in zebrafish, to elucidate their biochemical signaling pathways and, most notably, to identify Meteorins receptor(s).

Metrn was first discovered as a secreted neurotrophic factor which promotes neurite outgrowth *in vitro*. It is expressed in radial neuronal progenitors and radial glia [2], [3]. In vertebrates Metrns are highly conserved including two members in mammals and three in zebrafish (Metrn, Metrnl1 and Metrnl2). Each Metrn or Metrnl gene codes for a protein of around 300 amino acids containing an N-terminal signal sequence as well as a Netrin-like domain at the C-terminus [3].

Hence, one part of my PhD project was to evaluate the Metrns protein localization *in vivo* and characterize their activity on commissural axons development in zebrafish. With this intent, I performed double fluorescence *in situ* hybridizations to compare the expressions of *metrn* and *metrnl1* to the expression of the well-established axonal guidance factor Slit. The results showed that *metrn* and *metrnl1* co-localizes with *slit1a*, *slit1b* and *slit2* at the floorplate at 2dpf. I further validated the conservation of this expression pattern in mouse. This colocalization supports the role of Metrns as novel players in axonal guidance along Slits and other factors implicated in this process.

Furthermore, it has been reported that *nodal* and *lefty* expression as well *p-smad2* levels are downregulated in Meteorin-null ES-cells [4]. Via qPCR and *in situ* hybridization I discovered not only that Nodal factors were significantly altered in triple *metrn* mutants but also that in wild-type zebrafish, especially *metrnl1* is expressed earlier than previously assumed (earlier

than 6hpf). Additionally, I observed randomized or symmetric heart jogging and looping in triple mutants, similar to the ones described in *spaw* and *lefty* mutants [5]. Furthermore, using the Meteorins CRISPR/Cas9 knockout lines I could show defects in properties of the Kupffer's vesicle, caused by impaired assembly and migration of the Kupffer's vesicle (KV) forming Dorsal forerunner cells (DFCs). Finally, we could demonstrate that Meteorins genetically interact with *itgaV* and *itgβ1b* at the level of the Dorsal forerunner cells. These results indicate that Meteorins are new essential components for proper left-right patterning during embryonic vertebrate development.

In spite of the recent advancement in understanding the multiple functions of Meteorins, first receptor(s) of Metrns were identified just recently. It has been proposed that through activating an unknown receptor Metrn proteins may activate the Jak/Stat3 signaling pathway [2]. However, it was lately shown that Metrnl is promoting heart repair via binding to KIT receptor tyrosine kinase and is establishing Metrnl as a KIT receptor ligand in the context of ischemic tissue repair [6]. Additionally, it was revealed that Metrn is binding to Htr2b to regulate reactive oxygen species levels in hematopoietic stem/progenitor cells [7]. However, we believe that Metrns must act also through an additional receptor during early patterning processes as well as axonal guidance. Therefore, a key ambition of my PhD was the identification of further Metrn and Metrnl receptor(s) using independent approaches and the analysis of their functions in neurodevelopment, axon guidance and left-right patterning in zebrafish.

To validate if Metrns are able to bind axons expressing their hypothesized receptor(s) and to visualize the distribution of possible Metrn receptor(s), I have cloned constructs to produce Metrn-AP/Metrnl-AP fusion proteins. These fusion proteins were used as probes on mouse and zebrafish spinal cord sections to detect possible Metrns binding. Indeed, we could show that Metrns AP-fusion proteins bind close to the midline of the spinal cord. This supports the hypothesis of Metrns as novel axonal guidance factors also in mouse, facilitating midline crossing, and possible receptors are located where axons just crossed the midline.

In collaboration with Dr. Alain Chedotal and Yvrik Zagar as well as Manuela Argentini from his team, I worked on developing two independent crosslinking/pull-down methods to identify the Metrns receptor(s): the Fc-tag [8] and the AP-tag [9] approach. We recently obtained a list of candidates from these combined biochemical screens and we are testing *in vivo* to validate as *bona fide* Meteorin receptors.

In conclusion, I hypothesize Meteorin proteins as novel players during the development of the vertebrate CNS and axonal midline crossing, especially in commissural axon guidance and potential novel factors for proper KV formation and vertebrate left-right patterning.

IV. TABLE OF CONTENTS

I. ACKNOWLEDGEMENTS 3

II. RÉSUMÉ 6

III. SUMMARY 9

IV. TABLE OF CONTENTS 11

V. ABBREVIATIONS 16

1 INTRODUCTION 18

1.1 Meteorins – an extremely interesting and diverse protein family 18

1.1.1 The discovery of the Meteorin protein family 19

1.1.2 The structures and homologies of Meteorins 20

1.1.3 The expression patterns of *Metrn* and *Metrnl* during development 21

1.1.4 The roles of Meteorins during development and regeneration 23

1.1.5 Meteorins in CNS pathologies (neuropathic pain, gliosis, neurogenesis after stroke) 26

1.1.6 The new faces of Metrnl as an adipokine, fat thermogenesis regulator, cytokine, myokine and its role in diabetes pathologies 28

1.1.6.1 Metrnl as an adipokine, myokine and cytokine 28

1.1.6.2 The role of Metrnl in adipogenesis and its involvement in diabetes pathogenesis 31

1.1.6.3 Further diverse functions of Metrnl 36

1.2 The novel role of the Meteorin gene family in the establishment of the left-right axis during early embryonic development 38

1.2.1 General mechanisms of early embryonic patterning and symmetry breaking 38

1.2.2 Main components of the Nodal signaling pathway 38

1.2.3 Roles of Nodal signaling during embryonic development 40

1.2.3.1 Endoderm and mesoderm specification during germ layer formation 40

1.2.3.2 The role of Nodal signaling and antagonism during neural patterning 41

1.2.3.3 Nodal signaling in patterning the dorsal-ventral and the anterior-posterior axis as well as in the maintenance of undifferentiated ES cells 42

1.2.3.4 Nodal signaling and the establishment of the embryonic left-right axis 43

1.2.4 The role of DFCs and the KV for left-right patterning processes 44

1.2.5 The function of αV/β integrins during early embryonic patterning 47

1.2.6 Recent findings in zebrafish left right patterning research 48

1.2.7 Meteorins in early embryonic development and open questions in the field 49

1.3 The function of Meteorins in axon guidance and hunting for Meteorins receptor(s) 51

1.3.1 General mechanisms of axonal guidance 51

1.3.1.1 Crossing the midline – the remarkable role of the midline in axonal guidance 53

1.3.2 Axon guidance factors 55

1.3.2.1 Slit family and Robo receptors 56

1.3.2.2 Netrins and their receptors 57

1.3.2.3 Ephrins and Ephrin receptors 58

1.3.2.4 Semaphorin family and known receptors 59

1.3.2.5 Non-canonical axonal guidance molecules 59

1.3.3 Axon guidance mechanisms in Zebrafish 61

1.3.4 Open questions in the field 64

1.3.5 The hunt for the Meteorins receptor(s) 65

1.4 AIMS OF THE STUDY 67

2 MATERIALS AND METHODS 68

2.1 Zebrafish husbandry 68

2.2 CRISPR-Cas9-mediated mutagenesis of metrn, metrnl1 and metrnl2 and whole embryo genomic DNA extraction 68

2.3 Mutants genotyping and generation of triple mutants 69

2.4 Whole embryo RNA extraction and cDNA synthesis 69

2.5 Quantitative Real-Time PCR (q-RT-PCR) 70

2.6 *In situ* hybridization in zebrafish and chicken 70

2.7 Hybridization chain reaction (HCR) 72

2.8 Analysis of DFC phenotype and migration 72

2.9 mRNA synthesis and injection 73

2.10 Design and injection of antisense morpholino oligonucleotides 73

2.11 Whole-mount immunohistochemistry and quantification 74

2.12 Fluorescent microspheres injection and analysis 74

2.13 Molecular cloning 75

2.14 Western Blots 77

2.15 Immunohistochemistry on COS7 cells 77

2.16 AVEXIS 78

2.17 Production of Metrn/Metrnl1-AP fusion probes 78

2.18 Cryosection and AP-assays on sections and cells 79

2.19 Co-IP binding assay 80

2.20 Ecto-Fc ligand-receptor interaction screen 80

2.20.1 Production and purification of extracellular domain Fc-fusion bait proteins 80

2.20.2 Prey extraction from fresh tissue 81

2.20.3 Preparation for mass spectrometry 81

2.20.4 Mass spectrometry analysis 81

2.21 Figures 82

3 RESULTS 83

3.1 The role of Meteorins during the establishment of the left-right axis throughout early embryonic development 83

3.1.1 Summary article 1 83

3.1.2 Article 1: “Meteorins as novel regulators of left-right patterning in the zebrafish embryo” 83

3.1.3 Annex to “Meteorins as novel regulators of left-right patterning in the zebrafish embryo” 120

3.1.3.1 DFC phenotype cannot be rescued via co-injection of metrn and/or metrnl1 mRNA and metrns overexpression leads to DFC phenotype 120

3.1.3.2 Heart looping phenotype can be rescued by injection of metrn and/or metrnl1 mRNA and metrns overexpression seems to have no severe effect 121

3.2 Function of Meteorins in commissural axon guidance 122

3.2.1 Summary article 2 122

3.2.2 Article 2: “A novel role of Meteorin proteins during the development of the vertebrate CNS and axonal midline crossing” 122

3.3 Hunting for Meteorin receptors 143

3.3.1 Candidate approach with AVEXIS 144

3.3.2 Candidate approach with AP-binding assays 146

3.3.3 Establishing a receptor candidate library with Ecto-Fc ligand-receptor interaction screen 148

4 DISCUSSION AND PERSPECTIVES 154

4.1 Meteorins during the establishment of the left-right axis throughout early embryonic development 154

4.2 Meteorin proteins during the development of the vertebrate CNS and axonal midline crossing 159

4.2.1 Possible models for modulation of axonal pathfinding induced by Meteorin proteins: direct interaction and/or FP induction 161

4.3 The (long) Meteorins receptor hunt….to be continued 164

4.4 CONCLUSION 168

5 REFERENCES 169

VI. LIST OF FIGURES 202

VII. ANNEX 206

V. ABBREVIATIONS

AC	anterior commissure
AVEXIS	Avidity-based extracellular interaction screen
BAT	brown adipose tissue
BMP	Bones morphogenetic protein
CAD	coronary artery disease
circRNA	Circular RNA
CNS	central nervous system
Co-IP	Co-immunoprecipitation
COPD	chronic obstructive pulmonary disease
CRC	colorectal cancer
DCC	Deleted in Colorectal Cancer
DFCs	dorsal forerunner cells
dpf	days post fertilization
DRC	dorsal rostral cluster
DRG	dorsal root ganglia
DSCAM	Down syndrome cell adhesion molecule
ECM	extracellular matrix
EGF	epidermal growth factor
ES-cell	embryonic stem cells
FP	floor plate
GDF	growth differentiation factor
gli	Gli Family Zinc Finger 2
HEK293	Human embryonic kidney 293 cell
hpf	hours post fertilization
HSPGs	Heparan sulfate proteoglycans
Htr2b	5-hydroxytryptamine receptor
Ig	immunoglobulin
IM	intermediate mesoderm
ko	knockout
KV	Kupffer’s vesicle
LOF	loss of function
LPM	lateral plate mesoderm
LRR	leucine-rich repeat
Metrn	Meteorin
Metrnl	Meteorin-like

Metrns	Meteorins
mRNA	messenger RNA
miRNA	microRNA
MLF	medial longitudinal fascicle
MS	mass spectrometry
Neo	Neogenin
NSC	neural stem cell
NT	non-transfected
Ntn	Netrin
o.n.	overnight
PCOS	polycystic ovary syndrome
PM	paraxial mesoderm
PMP	plasma membrane protein
PNS	peripheral nervous system
POC	post-optic commissure
RGC	retinal ganglion cell
ROBO	Roundabout
shh	sonic hedgehog
SOT	supra-optic tract
SVZ	subventricular zone
TGF	Transforming growth factor
TM	transmembrane
TPOC	tract of the post-optic commissure
triplMut	triple Meteorins mutant (*metrn*$^{-/-}$, *metrnl1*$^{-/-}$, *metrnl2*$^{-/-}$)
VRC	ventro-rostral cluster
WAT	white adipose tissue
WB	Western Blot
YSL	yolk synthetic layer

1 INTRODUCTION

1.1 Meteorins – an extremely interesting and diverse protein family

Around 14% of the total human proteome is expected to be secreted via classical or non-classical secretory cascades [10], [11]. Secreted proteins are used as biomarkers and in disease therapies since they are known to play major roles in physiological as well as pathological processes [12]–[15]. Hence, one of the major questions in present biology is how a cell is able to tightly control its multifaceted outputs, ensuring that correctly folded and properly functioning proteins reach their correct destinations.

Meteorins were discovered as a novel family of secreted proteins. In the last few years Meteorin's function has been studied broadly and revealed that they are implicated in a wide range of biological processes. However, a wide spectrum of possible Metrns functions and mechanisms of their actions remain to be investigated. Within this first part of the introduction, I will outline the discovery, structure and homological characteristics, expression patterns and to date characterized Metrns functions as well as pathways of these new family of secreted proteins (*Figure 1*).

This will set the premises for the main part of the thesis in which I will focus on the suggested roles of Metrns during the development of the vertebrate CNS and axonal midline crossing, especially in commissural axon guidance and as potential novel factors for proper KV formation and vertebrate left-right patterning.

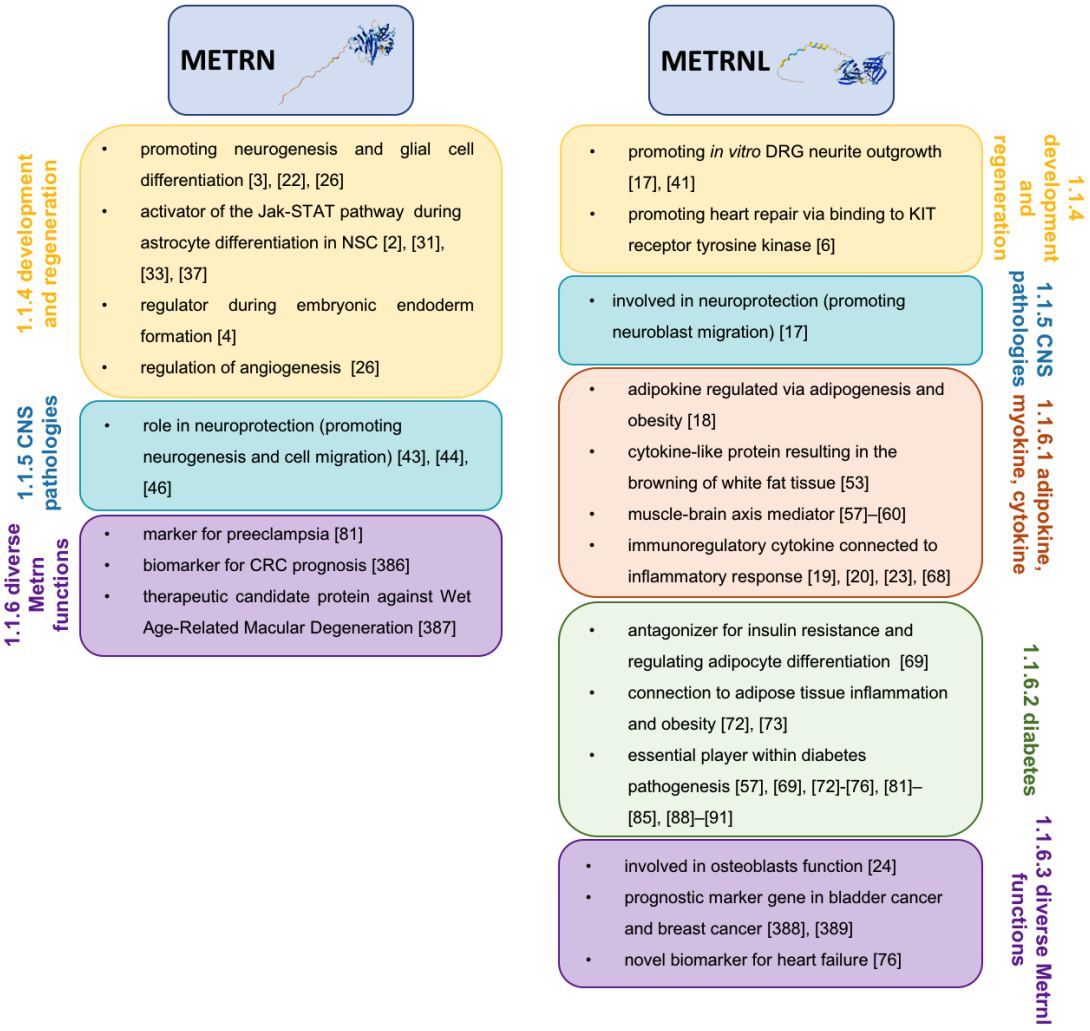

Figure 1: **Meteorins are an extremely interesting and diverse protein family:** Overview about the different up-to-date known functions of Metrn and Metrnl.

1.1.1 The discovery of the Meteorin protein family

Meteorin (Metrn) was first discovered as a secreted neurotrophic factor during a screen for genes with induced expression during neurogenesis. It was described having the ability to induce glial cells differentiation and to promote axonal extension in dorsal root ganglion (DRG) explants *in vitro* [3]. Meteorin-like (Metrnl), named like this for the close homology to Metrn, has been first mentioned as a downstream target of Pax2/5/8 signaling during otic vesicle development [16] and later found to have neurotrophic properties comparable to the ones of Metrn [17]. Independently, Metrnl was also early described as highly expressed adipokine in subcutaneous adipose tissue of caloric restricted adult rats [18]. Metrnl is additionally named Cometin [17], Subfatin [18], IL-41 [19] or Metrnß [20] depending on organism and described function. However, for the sake of clarity, we will continue naming Metrnl.

1.1.2 The structures and homologies of Meteorins

Metrn and Metrnl are highly conserved in vertebrates with two members in mammals (Metrn, Metrnl), one in *Xenopus tropicales* (Metrnl) and three in zebrafish (Metrn, Metrnl1, Metrnl2). However, no detectable orthologues were found in invertebrate models such as *Drosophila melanogaster* or nematodes like *Caenorhabditis elegans* [3], [17], [21], [22]. A comparative analysis performed by our lab between the sequences of human, mouse and zebrafish Meteorins revealed that homologue and paralogue proteins display an overall high degree of sequence conservation with about 50% of identity and even higher levels of similarity suggesting a common biological function for Meteorin proteins.

Metrn cDNA encodes for a small protein with a size of around 300 amino acids, 10 conserved cysteine residues and it is located on chromosome 17 (A3.3) in mouse and chromosome 16 (p13.3) in human. The mouse and human Metrn protein share a similarity of 82% with a total of 238 identical amino acids. Its sequence shows no common conservation with already identified proteins except of a putative signal peptide on the NH_2-term (*Figure 2*) [3]. The actual secretion of Meteorin was first proven by Nishino et al. (2004) [3]. Metrn shows approximately 40% amino acid identity with Metrnl [17], [21]. The *Metrnl* gene, mostly annotated as *Cometin* in mouse and human, encodes for a 311 amino acid protein including a NH_2-terminal signal peptide resulting in a secreted 30kDa protein of 266 amino acids. *METRNL* is located on the human chromosome 17 (q25.3) whereas mouse *Metrnl* is found on chromosome 11 (qE2) [17], [18]. When compared, mouse Metrnl shares 78% similarity with human METRNL, 79% with cow, 77% with rabbit and 72% with chicken. Similarly, the identity between mature mouse and Xenopus Metrnl is 62%, and 55% between mouse and zebrafish Metrnl1 [17].

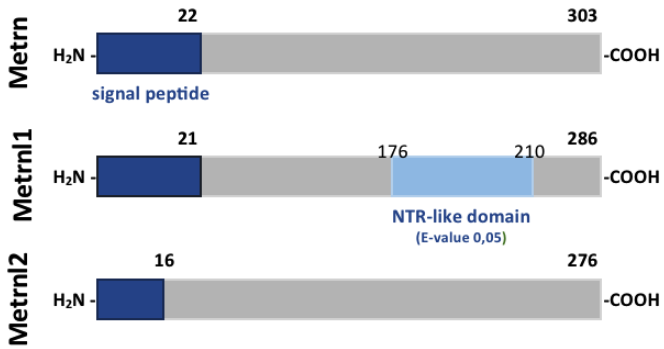

Figure 2: **Meteorins are small, secreted proteins:** Schematic for the three members of the Meteorin family in zebrafish, visualizing the signal peptide at the N-terminal of each protein and an NTR-like domain in Metrnl1.

Like Metrn, Metrnl displays no structural relations with already identified proteins, classifying Meteorins as a novel family of proteins. However, it was shown that mouse and rat Metrnl displays one potential N-glycosylation site and is indeed glycosylated with N-linked oligosaccharides. Such N-glycosylation site could not be found in mouse Metrn and in any

other species Metrnl sequence, indicating a non-conserved feature and potentially without high functional significance [17], [18].

1.1.3 The expression patterns of *Metrn* and *Metrnl* during development

The expression of *Metrn* in mouse was discovered to start early in development. During the blastocyst stage first *Metrn* expression is restricted to the inner cell mass. From E6.5 *Metrn* is expressed ubiquitously throughout cells of the epiblast and extraembryonic ectoderm. Starting from stage E7.0–E7.5 *Metrn* expression was found to be sustained in the epiblast as well as in the extra-embryonic ectoderm and the epiblast [4]. During later stages of development *Metrn* expression is mostly restricted to the central and peripheral nervous system (PNS). In the spinal cord at E9.5 *Metrn* is expressed in all layers, but its expression appears limited to the ventricular zone one day later. In the PNS *Metrn* expression can be detected in migrating neural crest during early embryonic development [3]. During continuing neural tissue development *Metrn* expression becomes limited to glial cells and in the dorsal root ganglion, to the site of Schwann cell progenitors and to the nerve roots. From E12.5 *Metrn* started to be expressed in ganglia, in newly emerged satellite glial cells and expression continued in Schwann cells. Furthermore, *Metrn* expression is apparent in radial glia and in the cerebellum where *Metrn* expression starts in the ventricular zone from E14.5 [2], [3]. *Metrn* transcripts could be detected also in Bergmann glia at P8 indicating that in general *Metrn* was present in neural progenitors and cells of the glial cell linage [3]. Specifically, in the mouse retina *Metrn* expression appears in all cell layers at E10.5 and becomes restricted to only the external layer containing retinal progenitor cells from E14.5. In the postnatal retina, Müller glia cells express *Metrn* [3]. During postnatal development *Metrn* expression is restricted to the corpus callosum as well as to the lateral ventricle subventricular zone, places which home glial progenitors and astrocyte precursors [3].

In adult mouse *Metrn* is mainly expressed in the spinal cord. Within the brain, *Metrn* transcripts can be detected predominantly in the cerebellum, brainstem and medulla. Within the cerebellum *Metrn* expression can be found in the Bergmann glia, where the expression is mainly restricted to the cytoplasm along radial processes. Additionally, throughout the cerebellar parenchyma *Metrn* transcripts are present in cells with glial morphology, mostly in clusters around blood vessels [22]. *Metrn* transcripts can also be found in several neuronal populations and in different regions of the brain, including the superficial layers of the superior colliculus. Furthermore, *Metrn* is expressed in raphe and pontine nuclei, in the ocular motor nucleus as well as in various thalamic nuclei [22]. In contrast to embryonic development where *Metrn* is expressed in the migrating neural crest, the transcript levels of *Metrn* in the PNS of adult mice are low [22]. During neurogenesis *Metrn* transcripts appear in CNS regions containing neural progenitors, cells able to generate oligodendrocytes, neurons as well as

astrocytes [3]. *Metrn* expression can also be detected in some specific organs such as heart, ovary, kidney and skeletal muscle, even though in smaller amounts [22].

Metrnl transcripts can be found in numerous tissues. In mouse, *Metrnl* expression is dominant in the developing CNS as well as the adult brain. The earliest described onset time of *Metrnl* expression is at stage E9.5, during which transcripts were detected in floor plate cells throughout the neural tube. Starting from E13.5 *Metrnl* transcripts can be detected within the inner ear and in DRG, where the expression level of *Metrnl* is slightly stronger in spinal cord DRGs compared to DRGs at the hindbrain level [17]. From E14.5 *Metrnl* is expressed in the cartilage primordia, in the epithelial layer lining the bronchioles and in the olfactory epithelium [17]. *Metrnl* is expressed in adult mouse brain, however when compared to *Metrn* expression in adult hind-, mid- as well as forebrain, *Metrnl* expression is found to be weaker in all three parts [18], [23]. In adult mouse, *Metrnl* is expressed in several tissues including heart, muscle and liver. With the exception of lipid droplets, *Metrnl* transcripts can be detected in subcutaneous adipose tissue and omental adipose tissue. It exhibits a dispersed distribution through these adipose tissues, being concentrated in stromal cells and adipocytes [18]. Additionally, it was shown that *Metrnl* displays a high expression in activated monocytes as well as in the skin, fibroblasts, respiratory and digestive mucosal tissue [23]. Furthermore, *Metrnl* transcripts were detected in hypertrophic chondrocytes and in active osteoblasts along the trabecular bone of rats [24]. *METRNL* was also shown to be expressed in the gastrointestinal tract of human and mouse, mainly in intestine epithelial cells (Figure 3) [25].

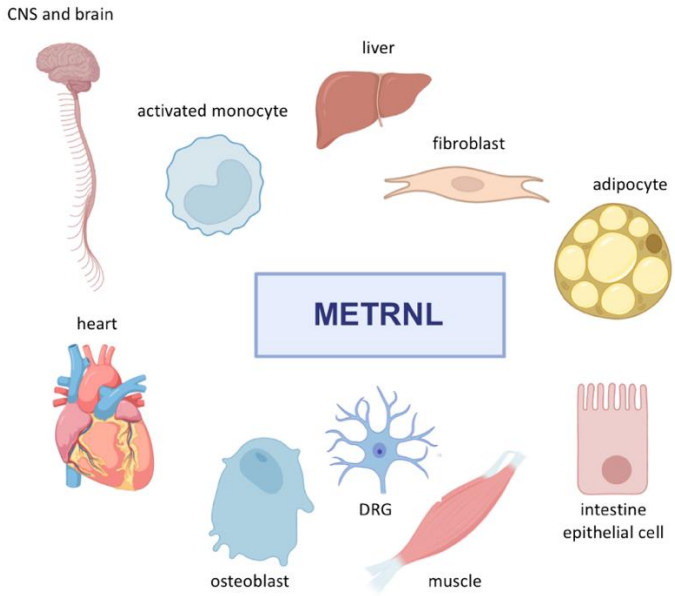

Figure 3: ***Metrnl* is expressed in numerous tissues:** Schematic representation of examples for tissues with *Metrnl* expression.

In our favorite model organism, the zebrafish (*Danio rerio*), previous unpublished work of our laboratory has shown that *metrn* as well as *metrnl1* are maternally expressed. At 6 hours post fertilization (hpf), *metrnl1* expression can be detected over the whole animal cap whereas starting *metrn* expression can be observed at the yolk syncytial layer (YSL) at this developmental stage. From 9 hpf *metrn* expression is restricted to the developing lateral plate mesoderm (LPM) and the leading edge of the shield. In contrast, *metrnl1* is expressed throughout the whole enveloping layer and the developing midline. At 12 hpf, the expressions of both paralogs are restricted to the area around the KV (*metrn*) and the midline (*metrnl1*). At 14hpf both *metrn* genes are expressed in the KV. Additionally, *metrn* and *metrnl1* transcripts can be found around the PM (paraxial mesoderm), the IM (intermediate mesoderm) and the LMP. At 14hpf *metrnl1* is still expressed along the midline while the first *metrn* expression in the developing brain can be detected at this stage. By 24 and 48 hpf, both genes are strongly expressed in the CNS. At 24hpf *metrnl1* expression can also be detected at the midbrain/hindbrain boundary, in regions close to hindbrain rhombomeres as well as in the area of the presumptive otic vesicles. At 48hpf *metrn* and *metrnl1* expression can be visualized especially along the midline as well as in CNS periventricular regions. *Metrnl2* expression can be detected from 24hpf and displays a broad expression in the embryonic brain. From 48hpf *metrnl2* transcripts mostly localized in the otic vesicles and at the somite boundaries. At stages later than 2 days post fertilization (dpf) the expression of *meteorins* within the CNS decreases significantly. Therefore, we suggest that Meteorin function is required just during early developmental stages, especially in the context of CNS development. Excitingly, the expression patterns of Meteorins in zebrafish and mouse display strong similarities, especially within the CNS like strong expression at the floor plate and along the midline.

In conclusion, both Metrn and Metrnl are specifically present during vertebrate neurodevelopment and their genes display diverse expression patterns during later developmental stages.

1.1.4 The roles of Meteorins during development and regeneration

The first discovery of Metrn as a secreted neurotrophic factor was during a screen for novel neurogenesis genes in mouse [3]. Nishino et. al (2004) [3] named the novel discovered protein after “meteor”, because Metrn protein could transform glial cells into cells with elongated trails. Since then, many investigations have focused on the role of Metrn during diverse developmental and regenerating processes within the nervous system. Metrn was described to induce neurite outgrowth from *in vitro* DRG cell culture, to promote astrocyte formation in cerebrocortical cell culture and to have the ability to induced cerebellar astrocytes to become radial glia [3], [22], [26]. Astrocytes, belonging to the family of macroglial cells, are one of the most common cell type within the CNS [27], [28]. Their roles within the network are diverse,

reaching from supporting neuron in their correct functioning, being key factors in 'gliotransmission' [28], maintaining the blood-brain barrier [26], [29] to the regulation of the blood flow [30]. Reactive gliosis describes the astrocytic response to diverse CNS pathologies causing molecular as well as morphological changes in resting glia like hypertrophy, upregulation of *Gfap* and *S100β* expression [31], [32]. The induction of DRG neurite outgrowth and the ability to promote astrocyte formation were the first indicators for an important role of Metrn in axonal network formation during neurogenesis and glial cell differentiation. Furthermore, *Metrn* was mentioned as a gene related to nervous system development in a screen for genes influenced by cadmium exposure during neurulation in C57 mice [33]. Under treatment with cadmium, a teratogen which can provoke lethality and numerous defects during development, *Metrn* expression was downregulated indicating a possible role of Metrn during the development of the nervous system [33].

Yoon-Young Kim et al. [4] investigated the physiological role of Metrn in several developmental processes using a *Metrn* knockout (ko) mouse model. The authors demonstrated embryonic lethality in these *Metrn*$^{-/-}$ mice and assumed a probable death between E7.0 and E8.5, the time of mesendoderm cell specification [34]. Although still viable, *Metrn*$^{-/-}$ embryos at E7.5 were significantly smaller, especially in the embryonic region, via expression analysis of several mesoderm markers and genes of the nodal signaling pathway in an *in vitro* ES cells culture, the authors could demonstrate that these essential signaling pathways were disrupted in *Metrn* ko models. The authors described *Metrn* as a novel gene important for embryonic development and as a new *Nodal* transcription regulator important for maintaining sufficient Nodal levels for proper embryonic endoderm formation [4].

The first publication investigating Metrn downstream pathways, which mediate its functions, explains the activation of the Jak-STAT3 pathway through Metrn [2]. The Jak-STAT3 pathway is a key regulator for astrocyte differentiation in NSC (neural stem cells) [35] and important for catalyzing the onset of gliogenesis [36] which is consistent with known Metrn properties. Since *Gfap* expression in *Metrn* expressing P19 cells was increased after neuroglial induction it was suggested that Metrn promotes the linage commitment of cells characterized as glial within the NSC. Intriguingly, cell treatment with Metrn reliably induced tyrosine phosphorylation of STAT3, an increase of nuclear concentration of STAT3 as well as phosphorylation of Erk1/2, demonstrating that Metrn indeed might be an activator of the Jak-STAT pathway [2], [37]. Since the promoter of GFAP contains a STAT3 binding element, Jak-STAT signaling stimulates astrocyte generation and that *Gfap* expression was increased in *Metrn* expressing cell culture suggests that the Jak-STAT3 pathway could have been activated by Metrn. Moreover, this activation could have increased the GFAP promoter activity which was in turn essential for glial differentiation [2]. Additionally, it was shown that GP130 is recruited by Metrn as it activated Jak- STAT3 signaling and that Metrn may have complementary function to the IL-6 cytokine

intracellular signaling machinery [2], [37]. This hypothesis was supported by the observation that Metrn-induced glial differentiation is impaired when the Jak-STAT pathway was inhibited. Interestingly, inhibiting the Mek-Erk1/2 pathway, a pathway reported to control neuronal differentiation of NSCs [38], did not result in disturbed glial differentiation [2]. In conclusion, Metrn promoted the differentiation of glial cell in NSC as an upstream signaling unit of the Jak-STAT3 pathway activation [2], [31].

Another hypothesized property of Metrn is the regulation of angiogenesis, first described by Park et al. (2008) [26]. Within the CNS, blood vessels are enclosed by a basement membrane made of a tight astrocyte cytoplasmic process network, establishing an endothelial barrier named gliovascular interface [29], [39]. Forming these highly selective endothelial barrier the permeability plays an essential role in the homeostatic regulation and maintenance of the brain environment [29]. Since Metrn was described to affect astrocyte and neuronal development [3], [22] it seemed plausible also to play a role in astrocytes - gliovascular interface endothelial cells interplay. Indeed, the authors could demonstrate colocalized *Metrn* and *Gfap* (an astrocyte marker) expression in cells with direct contact to blood vessels in mice and as well as *Metrn* expression around blood vessels of the ganglion cell layer of the human retina. These results indicated that Metrn might reflect the vessel function at the gliovascular interface and is involved in diverse blood vessel maturation [26]. Moreover, Metrn was shown to positively regulate thrombospondin-1/-2 levels (potent inhibitors of angiogenesis), which demonstrates its putative antiangiogenic activity via astrocyte-derived TSP-1/-2 level regulation in an indirect manner. Interestingly, exposure of astrocytes to Metrn induced Erk1/2 phosphorylation. Since ERK1/2 is a known contributor to the expression pathway of TSP-1/-2[40] Metrn was suggested to regulate TSP-1/-2 via the Erk1/2 signaling cascade [26].

Alike its protein family member Metrn, Metrnl is described as a vertebrate specific, conserved secreted neurotrophic protein including tissue defined expression during development and adulthood [17], [18], [21]. *Metrnl* is expressed in DRG and is able to promote *in vitro* DRG neurite outgrowth through the Jak-STAT3 pathway including further involvement of the MEK-ERK signaling cascade [17], [41]. Remarkably, the addition of Metrn and Metrnl simultaneously to cell culture medium revealed an additive effect resulting in a notably higher number of neurites than in DRG cells stimulated with Metrn or Metrnl alone [17]. Interestingly, in contrast to Metrn, which effects are so far described only upstream of the Jak-STAT3 pathway with additional participation to the MEK-ERK signaling cascade, Metrnl1 got also linked with latent process genes and adenylate cyclase-activating peptide (PACAP)-forskolin signaling [41]. Latent process genes are essential for the decondition of extracellular stimuli into cellular functions, involved in numerous cellular function preparations like for instance neurite

extension [41], which supports the important role of Metrnl alongside Metrn during neurodevelopment.

In spite of the recent advancement in understanding the multiple functions of Meteorins, receptor(s) of Metrns were yet unknown. It was only recently shown that METRNL is promoting heart repair via binding to KIT receptor tyrosine kinase and is establishing METRNL as a KIT receptor ligand in the context of ischemic tissue repair (Figure 4A) [6]. Short after the publication of the METRNL receptor, also the first receptor for Metrn was published. Metrn was shown to be a functional 5-hydroxytryptamine receptor 2b (Htr2b) ligand. In this context Metrn was described to regulate oxygen species levels in Hematopoietic stem/progenitor cells via phospholipase C signaling direction (Figure 4B) [7]. Nevertheless, the detailed pathway(s) and other possible receptor(s) for Metrns and their binding property(s) still have to be investigated.

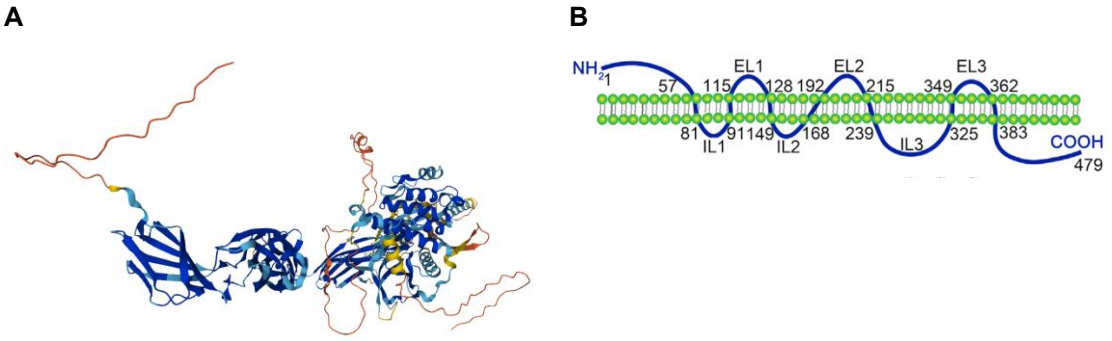

Figure 4: **There are two published receptors for Meteorins so far, one each per member of the Meteorin family:** Schematic representation of the published receptors, **A** the KIT receptor (from www.uniprot.org/uniprotkb/A0A0U2N547/entry) and **B** Htr2b (adapted from [7]).

1.1.5 Meteorins in CNS pathologies (neuropathic pain, gliosis, neurogenesis after stroke)

Neurotrophic factors are essential for proper development and maintenance of the nervous system. In addition, they also gained interest in clinical research as they connected to several neurological disorders like for instance neuropathic pain [42]. Based on Metrn and Metrnl known functions and expression in the nervous system in normal development and physiology, it was investigated if Metrn as a neurotrophic factor has therapeutic potential concerning peripheral neuropathy and associated pain [22], [43]. Jorgensen et al. [44] published first results describing neuroprotective properties of Metrn *in vivo*. Responding to excitotoxic injury, *Metrn* displayed an upregulated expression in glial cells. As Metrn was delivered via a lentivirus directly to the stratium of rats before excitotoxin (quinolinic acid) injections, the number of striatal neurons lost as well as the lesion size was significantly reduced compared to rats getting quinolinic acid injections only [44]. It could be demonstrated that Metrn might promote neurogenesis and cell migration. Via *in vitro* and *in vivo* experiments, it was shown that Metrn

stimulated subventricular zone neuroblast migration in neonatal rat SVZ (subventricular zone) culture explants as well as in stroke-subjected adult rat models through chemokinetical mechanisms. Metrn treatment of SVZ cells exposed to excitotoxin NMDA reduced significantly the number of apoptotic cells and displayed neuroprotective properties of Metrn, like described from Jorgensen et al. (2011) [44]. Additionally, direct Metrn infusion into stroke-damaged rat ischemic striatum stimulated cell proliferation within the SVZ [45]. A further supporting role of Metrn during CNS pathology was described by Wright et al. (2016) [46]. Several previous studies described that after striatal injury neuroblasts, generated in the SVZ, are able to migrate into the injured striatal parenchyma where they differentiate into neurons. However, the survival rate of these new mature neurons is very poor [47]–[49]. It was discovered that the overexpression of *Metrn* within damaged striatum is able to drive gliogenesis after striatal injury and might take the novel role of a newborn neuron survival factor after striatal injury [46]. It was demonstrated that Metrn injections could successfully mediate a long-lasting reversal of pain-associated behavior in rat models depending in the dose. Hence, Metrn is suggested to have disease modifying properties and might be able to support restoration of neuronal function [43]. Additionally, in a quinolinic acid rat model implant-delivered Meteorin successfully protected brain cells against quinolinic acid-induced toxicity [50]. Strikingly, also Metrnl, as a secreted neurotrophic factor, was associated with a role of promoting neuroblast migration in rat SVZ [17]. These results possibly suggest an important role of both Meteorins (Metrn, Metrnl) in neuroprotection and neurogenesis.

Since *Metrn* is highly expressed by astrocytes of the adult brain [22] and that Metrn is moreover able to stimulate glial cell differentiation as well as the *Gfap* expression in NSCs [2], it was hypothesized that Metrn might play a role in reactive gliosis as well [31]. Furthermore, it was demonstrated that *Metrn* expression within reactive astrocytes was increased after brain injury *in vivo*. These results were similar to *in vitro* observations, where primary mouse cortex astrocytes culture cells were treated with TGF-β1(known reactive gliosis-promoting factor) and increased *Metrn* expression was detected [31]. Compared to Metrn properties in neural progenitor cell differentiation, where it induces phosphorylation of STAT3 and activation of Erk1/2 [2], in astrocytes Metrn doesn’t seem to phosphorylate STAT3, still signaling through Erk1/2 activation [31]. Further, Metrn was described as negative feedback loop factor in reactive gliosis, with possible support resolving glial activation and cell reversion into their resting state [31]. This finding is in line with already mentioned Metrn properties having neuroprotective effects in several neuropathological models [43]–[45], [50].

Additionally, Metrn was mentioned during a study investigating the effect of miR-615 expression on Müller cells in the context of retinal neurodegeneration [51]. Transfection with miR-615 reduced the expression of *Metrn* significantly. Silencing of cZNF609, a sponge for miR-615, displayed the same effect. However, overexpression of *Metrn* in cZNF609 silenced

conditions was able to rescue glial cell proliferation, normally inhibited in these conditions. These findings demonstrate a possible regulation pathway in retinal neurodegeneration for Metrn in connection with the circular RNA-ZNF609 [51].

1.1.6 The new faces of Metrnl as an adipokine, fat thermogenesis regulator, cytokine, myokine and its role in diabetes pathologies

In contrast to Metrn, whose properties are mostly restricted to the nervous system, investigated and revealed Metrnl functions became more diverse over the last years with assigned roles in various tissues and systems.

1.1.6.1 Metrnl as an adipokine, myokine and cytokine

One of the first studies revealing new Metrnl characteristics was published by Li et al. (2014) [18] defining Metrnl as an adipokine regulated via adipogenesis and obesity. Adipokines, proteins secreted by adipose tissue, play a role in numerous physiological functions like insulin sensitivity, metabolic homeostasis, inflammation and immunity [18], [52]. In an adipose rat model *Metrnl* expression was predominant in subcutaneous white adipose tissue (WAT) but *Metrnl* transcripts could also be found in mesenteric adipose tissue and perivascular brown adipose tissue (BAT). In general *Metrnl* displayed a diffuse expression distribution through adipose tissue and was significantly increased during adipogenesis and obesity [18]. Since *Metrnl* expression was higher in the WAT compared to expression in BAT and considering the fact that energy is deposed in white tissue and surplus energy is burned in brown fat tissue, Metrnl as a new adipokine was described to be involved in energy storage [18].

In line with the abundant expression in adipose tissue, Metrnl has been recognized to regulate thermogenesis and anti-inflammatory processes acting as a novel cytokine-like protein resulting in the browning of white fat tissue [53]. Interestingly, it was revealed that expression of *PGC-1α4*, a known transcriptional cell fat regulator and muscle energy-sensing network marker, promotes WAT browning, specifically in muscles, and that *Metrnl* might be an important PGC-1α4 target gene within skeletal muscles. Furthermore, it was presented that *Metrnl* expression could be induced after concurrent exercise in skeletal muscle and that an increasing amount of circulating Metrnl could be detected one day after eccentric exercise. In addition to showing that Metrnl seemed to be regulated by exercise, it was also demonstrated that exposure to acute cold could elevate *Metrnl* expression in BAT, WAT and epididymal fat depots. Since acute cold exposure didn't induce the expression of *Metrnl* in skeletal muscle and eccentric exercise could induce its expression in skeletal muscle but couldn't in adipose tissue the authors defined Metrnl as cytokine-like protein which could be induced in different tissues in a selective manner. Excitingly, an increase of circulating Metrnl increased the expression of beige fat thermogenesis associated genes and anti-inflammatory cytokines

within WAT [53]. Increasing the amount of circulating Metrnl elevated also the expression of alternative macrophage activation genes like *Clec10a* or *Retnla* and IL-4, IL-13. These findings indicate that *in vivo* Metrnl could stimulate a phenotypic switch within adipose tissue macrophages via cytokines IL-4/IL-13 induction. In summary, Metrnl was characterized as an upon physiological stimuli (cold, exercise) inducible protein with the ability of recruiting and engaging recruited immune cell types to stimulate thermogenesis (Figure 5) [53]. These findings portray new physiological roles of Metrnl. Interestingly, a cleaved fragment of the axon guidance molecule Slit2 has been linked to exert the same function in adipose tissue [54].

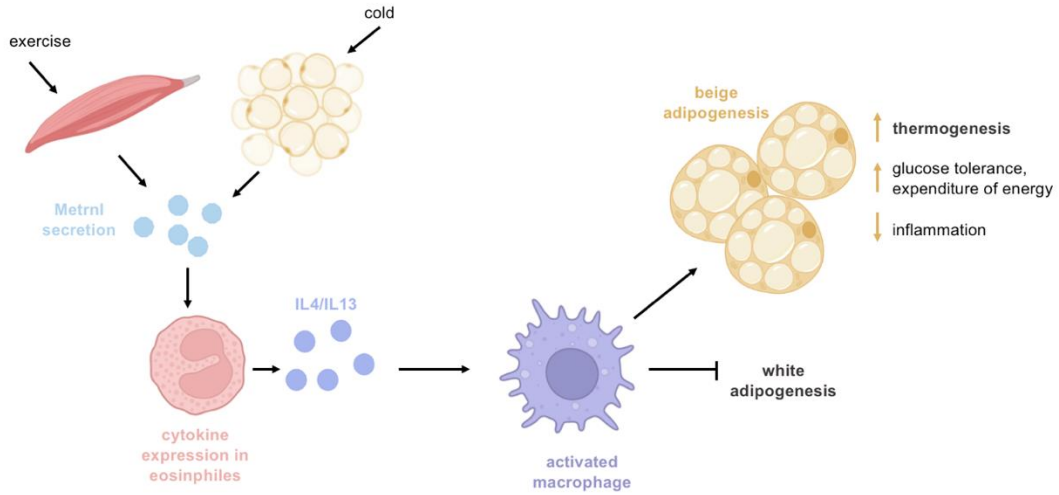

Figure 5: **Metrnl is a regulator of beige fat thermogenesis:** Schematic representation of the role of Metrnl in beige fat thermogenesis visualizing the secretion of Metrnl induced by exercise or cold exposure, promoting adipocyte browning due to IL4/IL13 expression and secretion as well as macrophage activation. Adapted from [53].

To analyze the direct effect of training on Metrnl, the levels of MP-activated protein kinase, PGC-1α (proteins of muscle energy-sensing network) and circulating Metrnl in mice under normal diet, high-fat diet and different training routines were investigated [55], [56]. It was confirmed that regular exercise upregulated Metrnl protein levels as well as the muscle energy-sensing network, resulting in the reduction of fat mass and general body weight [55]. Furthermore, Metrnl was proposed as a therapeutic target for obesity since it was suggested that exercise induced Metrnl within the muscle could decrease the accumulation of fat via the upregulation of Metrnl in adipose tissue. Additionally, Jung Ok Lee et al. (2020) [57] demonstrated that Metrnl levels increased under electrical-pulse-stimulation *in vitro* as well as *in vivo* in mice. These results support the role of Metrnl as a newly defined myokine induced by exercise. In line with the results in mouse models, *METRNL* expression was also described to be connected to resistance exercise training in a rat model [58] and short high intense training as well to acute high interval exercises in human [59].

Interestingly, METRNL was hypothesized as a muscle-brain axis mediator since it could be shown that METRNL is able to cross over the blood-brain-barrier and that METRNL concentration in the cerebrospinal fluid is elevated with blood-brain-barrier dysfunctions [60]. With exercise or muscle contraction the expression as well as secretion of METRNL increases and might lead to higher METRNL quantities crossing the blood-brain-barrier, modulating directly brain plasticity and/or brain function [57]–[60].

Aligned to previous publications describing Metrnl as a secreted protein important for stimulation of inflammatory cytokines expression [53] Metrnl was proposed to be a novel cytokine by itself [23]. Cytokines are signaling molecules, generally produced by activated leukocytes, and upon receptor-specific binding are responsible for triggering signal transduction cascades. They act as molecular messengers between immune system cells and are crucial for a correct development and control of immune responses. The fine tuning and control of cytokine expression is crucial, since deregulated cytokine expression is linked to severe inflammatory abnormalities and alleviation of diseases like psoriasis or rheumatoid arthritis [61], [62]. It was analyzed that *Metrnl* is dominantly expressed and secreted from IL-4 induced M2 macrophages, which are connected with “anti-inflammatory” properties [23], [63]. Since *METRNL* expression was upregulated in human diseases like rheumatoid arthritis, psoriatic arthritis, osteoarthritis [19], [62], [64], prurigo nodularis and actinic keratosis [23], in Familial Primary Localized Cutaneous Amyloidosis (FPLCA) [65] and in chronic obstructive pulmonary disease (COPD) [66], an anti-inflammatory role of METRNL protein within the pathology of these human diseases was hypothesized.

Metrnl was further described as a new immunoregulatory cytokine connected to inflammatory responses using a *Metrnl*$^{-/-}$ mouse model. Via mouse bone marrow-derived macrophages cell culture and the addition of various cytokines it could be demonstrated that Metrnl production within the mouse bone marrow is regulated by numerous cytokines like TGFβ, IFNγ, IL17a, IL12, IL4, IL-1β and TNFα as the strongest *Metrnl* expression inducer. Interestingly, Metrnl was also acting as an inducer for IL-10, CXCL1 and CCL2 in bone marrow-derived macrophages cell culture indicating that the production of Metrnl is regulated by numerous cytokines but it self also regulates the expression of different cyto- and chemokines [20]. Additionally, lipopolysaccharide (LPS) in macrophages strongly induced *Metrnl* expression and the amount of circulating Metrnl was significantly increased by an induction of an inflammatory response in a mouse model. These results indicated that *Metrnl* is expressed *in vivo* dominantly during inflammatory responses and mostly in response to inflammatory stimuli [20]. *Metrnl*$^{-/-}$ mice displayed normal weight gain, a normal development, fertility and an overall good health. However, they displayed decreased levels of IgG in serum, an upregulated immunoglobulin M level and especially a significantly decreased ability to produce CCL3 and CCL4 chemokines. Besides, *Metrnl*$^{-/-}$ mice were shown to be very affected and vulnerable to endotoxin shock and

older *Metrnl*$^{-/-}$ mice were more common to developed inflammatory lesions [20]. The authors conclude that Metrnl has several functional roles within diverse immune responses. Metrnl upregulation was also described in hypo-responsive Th2 cells of mice, indicating another possible role of Metrnl within the immune system [67].

Finally, the effect of METRNL and exercise on the activation of the NLRP3 inflammasome was investigated. Javaid et al. [68] described that the induction of METRNL in muscles and the anti-inflammatory effects within macrophages is partly associated with adipose tissue NLRP3 inflammasome suppression during/after exercise.

Summarizing, METRNL is annotated as a novel key player within the inflammatory response regulation with possible roles in human inflammatory diseases pathogenesis.

1.1.6.2 The role of Metrnl in adipogenesis and its involvement in diabetes pathogenesis

In connection to Metrnl characteristics as a adipokine and its expression in WAT [53], Metrnl was described as an antagonizer for insulin resistance via the PPARy signaling pathway [69]. Insulin resistance is a known condition strongly connected with morbid obesity and a key pathogenic factor in diabetes mellitus type 1 or type 2 [70]. Interestingly, Rao et al. [53] suggested that Metrnl might not directly interact with adipocytes to stimulate a thermogenic gene program. Instead, it was demonstrated that secreted Metrnl regulated adipocyte differentiation by upregulating adipocyte mature-specific markers and the expression of the PPARy receptor [69], whose activation causes insulin sensitization [71]. The role of Metrnl was further analyzed using a Metrnl adipocytes specific conditional knock-out as well as an overexpressing mouse model. Whereas normal diet *Metrnl* ko mice presented no changes in food intake, body weight or serum insulin levels, a high-fat diet in *Metrnl* ko mice severely stimulated insulin resistance and decreased the size of white adipocytes. In contrast, in the *Metrnl* overexpression mouse model insulin resistance induced trough high-fat diet was significantly reduced and white adipocyte size was increased. These findings demonstrated a pro-differentiation effect of Metrnl in white adipocytes and its influence in insulin resistance. Furthermore, the phosphorylation of AKT within WAT normally stimulated by insulin was markedly decreased in *Metrnl* ko mice and increased in *Metrnl* overexpressing mice. *PPARy* expression was also upregulated in *Metrnl* overexpressing mice. Remarkably, the inhibition of PPARy entirely abolished the Metrnl insulin sensitizing effect in *Metrnl* overexpressing mice [69]. Rao et al. [53] demonstrated that Metrnl stimulated white adipose browning by IL4 expression increase and M2 macrophages activation. However, no white adipose browning could be detected in the *Metrnl* transgenic overexpression and adipocyte-specific knockout mice [69]. It was concluded that Metrnl as an adipokine improved general insulin resistance by an autocrine/paracrine manner in local adipose tissue. However, no correlation could be found between METRNL serum concentration and BMI in adult human subjects [69]. Loeffler at al.

(2017) [72] described METRNL as adipokine and its expression in WAT in a study with human samples from the Leipzig Adipose Tissue Childhood cohort, bringing its properties into clinical application. In contrast to the upregulated expression of *Metrnl* during adipocyte differentiation in mouse [18], *METRNL* expression decreased during human preadipocytes differentiation [72]. However, *METRNL* expression within adipocytes was higher in obese than in lean children. Besides, expression of *METRNL* was shown to be correlated with insulin in an independent manner. These findings indicated that the expression of *METRNL* seems to be connected with adipose tissue inflammation and obesity [72], [73]. The fact that the accumulation of adipose tissue in children is related to adipose tissue inflammation and insulin resistance [74], a connection between *METRNL* expression within adipocytes and adipose tissue proliferation parameters as well as differentiation factors could be possible. Indeed, a positive correlation between *METRNL* expression with preadipocyte proliferation, fasting insulinemia and adipocyte hypertrophy was demonstrated [72]. Additionally, METRNL was shown to ameliorate inflammatory responses via PPARδ and AMPK-dependent pathways and might be a potential suppressor against endothelial inflammation [73]. It was also shown that browning of white human adipocytes does not induce *METRNL* expression. Possible functional involvements of METRNL in adipose tissue alterations linked with obesity were evaluated in human adipocytes via a *METRNL* overexpression and knockdown study. The overexpression of *METRNL* inhibited the differentiation of human adipocytes and decreased *PPARγ* expression. Conversely, the knock down of *METRNL* resulted in a slight increase of adipogenic capacity and *PPARγ* expression. Thus, *METRNL* expression downregulation seemed to stimulate adipogenesis and *METRNL* overexpression might inhibited the differentiation of human adipocytes, however adipocyte proliferation was increased under *METRNL* overexpression [72]. The contradiction of several results in the mouse model described by Zhi-Yong Li et al. (2015) [69] and Li et al. (2014) [18], like the downregulation of *METRNL* during human adipocyte differentiation or the inhibitory effect of *METRNL* overexpression on *PPARγ* expression, might hint at possible species-specific differences regarding the role of Metrnl on adipogenesis.

Besides, it was suggested that METRNL as a novel myokine is able to alleviate insulin resistance and inflammation [75]. Additionally, it was described that *Metrnl*-PPARδ signaling is an important factor for the induction of the fatty acid oxidation within skeletal muscle. Cell culture treatment with Metrnl displayed a negative correlation with inflammatory markers like the translocation of the nuclear factor κB (NFκB), the expression of *Interleukin-6* (IL-6) as well as with pro-inflammatory cytokines *TNFα* and *MCP-1*. In skeletal muscle of high-fat diet mice the treatment with Metrnl reduced the altered insulin response, rescued the general glucose intolerance and increased the expression of *PPARδ* and phosphorylation of AMPK. Since the treatment also improved the expression of fatty acid oxidation-associated and AMP-activated

kinase (AMPK), and PPARδ suppression reversed these expression of fatty acid oxidation-associated genes, the authors concluded a positive correlation between Metrnl treatment and insulin resistance, inflammation and fatty acid oxidation via a PPARδ or AMPK associated pathway [75], [76]. Additionally, it was shown that Metrnl has an ameliorating effect on β cell function by the inhibition of their apoptosis and promotion of β cell proliferation through activating the WNT/β-catenin pathway [77]. Since progressive pancreatic β cell dysfunction is a known hallmark for T2D [78] METRNL was suggested as an essential player within diabetes pathogenesis (Figure 6).

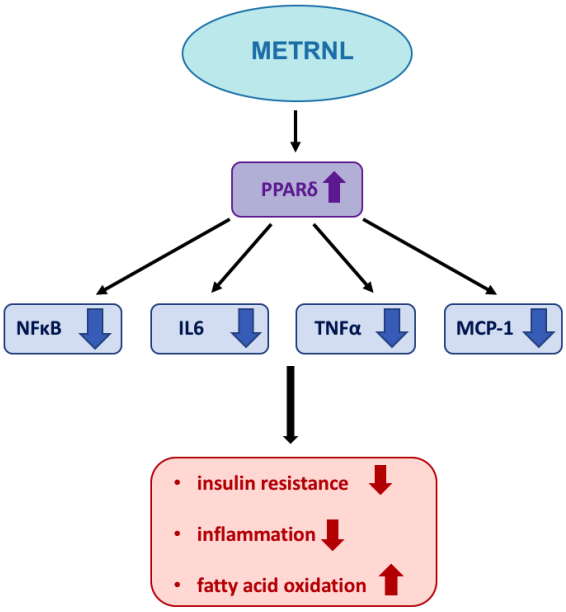

Figure 6: **Metrnl as an important player within diabetes pathogenesis:** Schematic representation of the described influence of secreted Metrnl on the expression of PPARδ and resulting effects on the expression of pro-inflammatory cytokines leading to decreased insulin resistance, inflammation as well as fatty acid oxidation as described in [69], [72]–[76].

Besides, the role of Metrnl as an exercise induced myokine, also the properties of Metrnl as a protein improving glucose tolerance via the already hypothesized AMPK pathway were investigated [57]. AMPK is a known major metabolic homeostasis regulator and especially activated as the energy levels of the cell are low. Skeletal muscle glucose uptake and the induction of fatty acid oxidation in fat tissue are stimulated under AMPK activation [79]. In C2C12 mouse skeletal muscle cells, the treatment with Metrnl increased the phosphorylation of AMPKα and acetyl-CoA carboxylase, an AMPKα downstream factor. Furthermore, the authors showed that this phosphorylation of AMPKα via Metrnl is facilitated by increasing the concentrations of intracellular calcium. These findings indicated that glucose uptake of skeletal muscle cells via AMPK signaling was stimulated by Metrnl. Since p38 MAPK phosphorylation was increased by Metrnl treatment, it was proposed that Metrnl-mediated uptake of glucose is probably due to the participation of p38 MAPK acting downstream of AMPK. Metrnl treatment upregulated HDAC5 phosphorylation, *Glut4* expression and the amount of GLUT4 protein

which is crucial for tissue glucose uptake. Since the addition of Metrnl decreased the binding of HDAC5 to the propter region of GLUT4 the authors concluded that *Glut4* expression is normally upregulated by Metrnl via HDAC5 release from the GLUT4 promoter region [57]. Using a high fat-induced obesity mouse model it was suggested that Metrnl has also the same glucose tolerance improving ability via AMPK *in vivo*. Therefore, Metrnl was confirmed as a candidate for therapy in type 2 diabetes and other glucose-related diseases (Figure 7) [57]. Beside, Metrnl was further connected to the AMPK-PAK2 signaling pathway [80]. In a myocardial ischemia/reperfusion (MI/R) cell model it was shown that via AMPK-PAK2 Metrnl attenuates cardiomyocytes apoptosis induced by MI/R injury. Since the overexpression of Metrnl showed an inhibitory effect to inflammation, endoplasmic reticulum stress and apoptosis *in vitro,* the authors claim Metrnl as a possible target for future myocardial ischemia treatment [80].

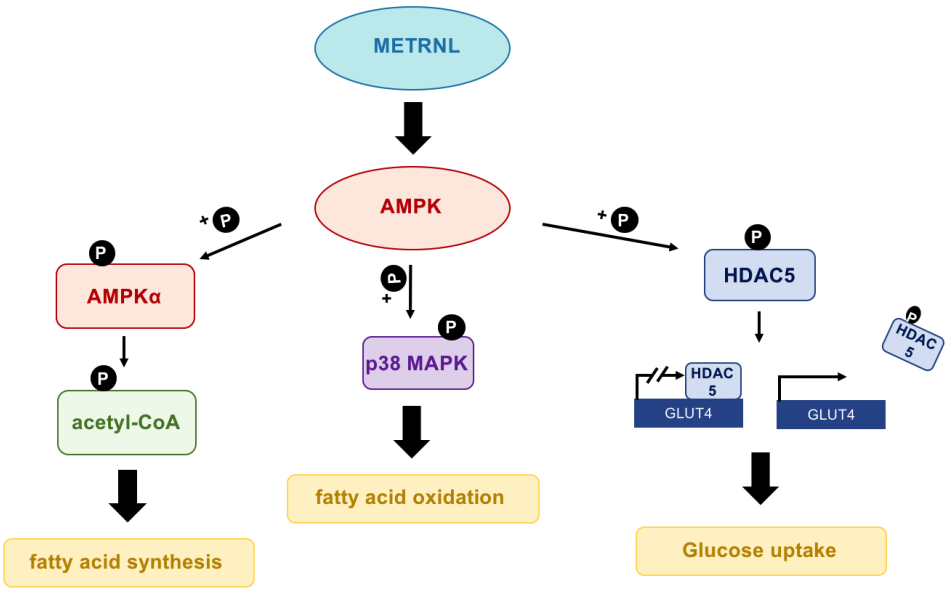

Figure 7: **Metrnl is improving glucose tolerance:** Schematic representation of the described influence of Metrnl treatment on fatty acid synthesis, fatty acid oxidation and glucose uptake as published from [57].

In the following years the role of METRNL in connection with diabetes was extensively studied. Especially the level of secreted and circulating METRNL in correlation with type 2 diabetes mellitus in human was investigated [81]–[85].

Several secreted proteins have already been established for the treatment against insulin resistance as well as diabetes in form of therapies and biomarkers [12]–[15]. For instance, it was shown that proinflammatory cytokines like IL-6 and TNF-a are upregulated in patients

suffering from type 2 diabetes [86]. It was demonstrated that METRNL serum levels were dominantly decreased in diabetic subjects compared to non-diabetic patients, and that METRNL levels displayed a negative correlation with insulin resistance and the level of glucose serum. No correlation could be detected regarding the BMI [82]. Hence, in line with the results published by Zhi-Yong Li et al. (2015) [69], it was assumed that there could be a correlation between glucose homeostasis and METRNL serum levels, however METRNL levels and the human BMI might be independent from each other. Besides, the connection between levels of METRNL and visceral fat obesity in type 2 diabetes was investigated [87]. Subjects suffering from visceral fat obesity displayed a lower METRNL serum level compared to controls indicating an inverse correlation between METRNL serum levels and visceral fat obesity in type 2 diabetes [87]. Additionally, METRNL concentrations in the serum were shown to be inversely correlated with diabetic nephropathy as well as renal function [85].

In connection with the adipokine properties of Metrnl [18], the correlation between METRNL concentration in diabetic patients with insulin resistance was investigated, including inflammatory cytokine levels and patients suffering from obesity induced coronary artery disease (CAD) [88], [89]. Again, a decreased level of METRNL in patients with diabetes as well as CAD could be found. A decrease in METRNL serum levels was associated with higher risk of diabetes and CAD incidences [66], [88], [89]. In patients suffering from type 2 diabetes and CAD the levels of IL-6 and TNF-α were significantly increased. In line with these results, METRNL was shown to have a negative correlation with IL-6 and TNF-α [88].

Another focus in diabetes research is the correlation between the amount of secreted METRNL, impaired endothelial function, atherosclerosis and declining glucose tolerance in adult human [90]. In patients suffering from type 2 diabetes, METRNL levels were dominantly decreased compared to patients with normal oral glucose tolerance. This finding goes in line with other publications describing the negative Metrnl serum level- type 2 diabetes correlation [69], [82], [89], [91]. Also, a negative correlation between METRNL levels and fasting blood glucose, fasting insulin, IL-6, TNF-a, insulin tolerance (HOMA-IR), vascular cell adhesion molecule-1 and intercellular adhesion molecule-1 among others was described. Thus, a negative link between METRNL levels, impaired endothelial function (vascular cell adhesion molecule-1, intercellular adhesion molecule-1), glucose tolerance, HOMA-IR and massive weight loss were concluded [90]–[92].

Strikingly, Garcés et al. (2015) [81] demonstrated a negative correlation between METRN serum level and glucose level and no correlation with BMI, insulin or HOMA-IR in healthy pregnant women. However, so far, no further investigations of METRN and its possible connections to diabetes pathogenesis were published.

Overall these results indicate for a new possible role for Meteorins especially METRNL in type 2 diabetes pathogenesis include atherosclerosis and endothelial dysfunction pathogenesis.

In contrast to these results, some studies describe a positive correlation between diabetic subjects and the concentration of circulating METRNL [84], [93]–[96]. In these publications METRNL levels were also associated to blood pressure, the lipid profile and fasting plasma glucose of human subjects[84], the onset of type 1 diabetes in a mouse model [96] as well as to Irisin levels [94]. Irisin, described as a secreted hormone and myokine by itself, was demonstrated to be present in adipocytes and muscle tissue and being upregulated by PGC-1α to induce white adipose tissue thermogenesis [97], [98]. METRNL and Irisin displayed a positive correlation. In patients with type 2 diabetes and obese background plasma METRNL and Irisin levels were higher than in non-diabetic, normal weight control subjects [94].
Interestingly, studies discovered that bariatric surgery, a form of therapy for diabetes 2, is sufficient to regulate the level of METRNL in obese patients and that METRNL could act as a biomarker for weight loss after bariatric surgery [99]–[101].
In conclusion METRNL seems to play a crucial role in the pathogenesis of type 2 diabetes and concomitant diseases and it could be a putative candidate for diabetes 2 treatment strategies.

1.1.6.3 Further diverse functions of Metrnl

Indicating the enormous diversity of of Meteorins' possible biological functions, *METRNL* was also identified via a screen for genes involved in osteoblasts function [24]. As osteoblast differentiation is extremely coordinated, complex and composed of many factors, several signaling pathways and functions of specific osteoblast-expressed genes are so far not understood [24], [102]. The activation of the activator protein-1 (AP-1) was used as read out in this study since it is known to have an essential role in the proliferation and differentiation of bone cells [103]. METRNL was shown to be able to interfere with AP-1 activity as its overexpression notably reduced AP-1 basal activity. Also, it was demonstrated that *METRNL* overexpression inhibits osteosarcoma-derived MG63 cell differentiation. Thus, it could be demonstrated that METRNL might be associated with the activity of the AP-1 transcription factor complex and osteoblasts function as well as differentiation [24].
Based on Metrn-Jak/Stat3 signaling for heat rate regulation [104], connecting to the abundant expression of *Metrnl* in the cardiac muscle [18] and METRNL`s possible role in myocardial ischemia treatment [80], Hu et al. [105] described a connection between Metrnl and doxorubicin-induced cardiotoxicity by SIRT1 activation via the cAMP/PKA cascade. Since cardiac-specific *Metrnl1* overexpression improved apoptosis, oxidative stress and the overall survival of the mouse model, Metrnl was hypothesized as a new therapeutic key player to prevent doxorubicin-induced cardiotoxicity. Additionally, it was shown that METRNL inhibits the development of cardiac hypertrophy with a direct effect on cardiac cells, and that the concentration of METRNL could be a novel biomarker for heart failure independent from prognostic value [76].

These results show that the heart is one of the sources of *Metrnl* expression as well as one of the targets for Metrnl, going in line with a recent study describing heart repair promoted by METRNL through the endothelial KIT receptor tyrosine kinase [6].
Overall, Metrns carry a great potential as novel biomarkers or therapeutic target for numerous pathologies and are therefore a promising protein family for further investigations and discoveries.

1.2 The novel role of the Meteorin gene family in the establishment of the left-right axis during early embryonic development

It has been reported that genes essential for early embryonic patterning are downregulated in *Meteorin*-null embryonic stem cells (ES-cells). Per se, *Metrn* was hypothesized to be a new gene essential for embryonic development as well as a Nodal transcription regulator [4]. Since in mouse the ko of *Metrn* resulted in early embryonic lethality we used a zebrafish model to further investigate the role of Metrns in early embryonic development *in vivo*. Now, in the second part of the thesis introduction I will highlight the general mechanisms and main components of early embryonic patterning mechanisms, with a specific emphasis on the role of Nodal signaling and the establishment of the left-right axis.

1.2.1 General mechanisms of early embryonic patterning and symmetry breaking

During early vertebrate development the embryo has to establish three main body axes, the anterior-posterior, the dorsal-ventral and the left-right axis.

The distribution of signaling molecules at the right time and the right place within the developing embryo is essential for proper cell fate specification and pattern coordination. Specific cell types develop from stereotypical locations within the embryo and that different cell fates can be induced by the exposure to essential signaling molecules. These signaling molecules are often expressed and secreted in the embryonic location giving rise to these cell fates. Furthermore, these signaling molecules acting together with their extracellular antagonists are able to induce certain cell fates also in surrounding tissues. Since the dose and location of these signaling molecules is essential for correct cell fate specification and excess signaling or removal of these signaling molecules leads to disturbed embryonic patterning, the correct distribution is fundamental for the correct development of the embryo [106]–[111]. Among these signaling molecules are BMP and Nodal the two key players for coordinated embryonic patterning [112], [113]. Nodal signaling was first described in mouse with its identification as a new members of the TGFβ family [112].

1.2.2 Main components of the Nodal signaling pathway

Ligands of the nodal signaling pathway belong to the transforming growth factor β (TGFβ) protein family and are known to bind to type I and type II serine-threonine kinase receptors. They are signaling via Smad2/Smad3 phosphorylation, which leads to their interaction with Smad4. This interaction results in transcriptional complex formation within the nucleus, acting as transcriptional activators with regulatory factors like for example Forkhead box protein H1 (FoxH1) (Figure 8). Essential for Nodal signaling and exclusive to the nodal pathway are co-receptors belonging to the EGF-CFC family [114]–[117]. Additionally, it was shown that Leftys,

soluble inhibitors belonging to a subclass of TGF factors, can antagonize nodal signaling (Figure 8) [118], [119]. Nodal ligands are conserved in vertebrates with one ligand in mouse, chick and human (Nodal), three in zebrafish (Cyclops, Squint, Southpaw) and multiple in frogs (encoded by six xNr genes) [111].

Remarkably, via *in vivo* experiments it was shown that also additional TGF ligands, beside Nodal ligands, utilize the core components of the nodal pathway and induce Nodal-like responses. [120], [121] Three of such ligands are the mammalian growth differentiation factor 1 (Gdf1) and Gdf3 or zebrafish Vg1 (Vtg1) [120]–[122].

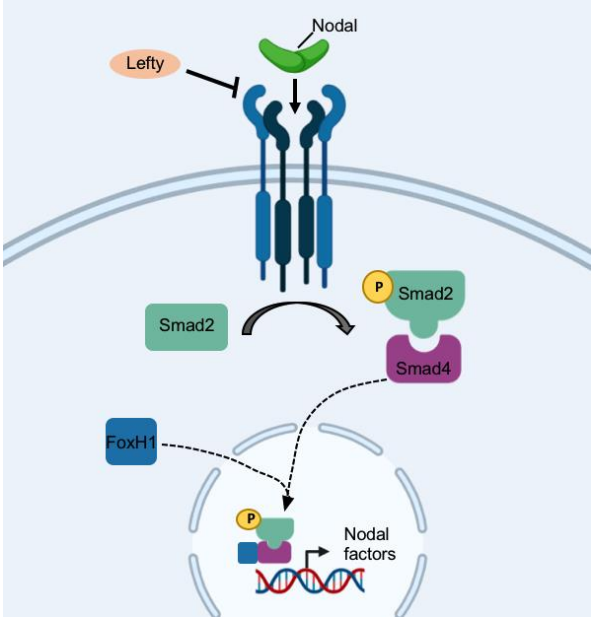

Figure 8: **Nodal ligands are conserved in vertebrates:** Schematic for Nodal signaling with Nodal binding to type I and type II serine-threonine kinase receptors (possible inhibition via Leftys), inducing Smad2 phosphorylation, which leads to interaction with Smad4 resulting in transcriptional complex formation within the nucleus acting as transcriptional activators with FoxH1. Modified from [123].

A common characteristic of all Nodal ligands is that they are able to induce receptor-mediated responses [114]. They are signaling via the type I serine-threonine kinase receptor ALK4 (ActRIB/Acvr1b) together with ActRIIB (Acvr2b) or the type II receptors ActRII (ActRIIA; Acvr2a) [124]–[126] but lacking signaling ability without EGF-CFC co-receptors [119], [125], [126] which are essential for type I receptor ALK4 specificity by protein interactions [124], [125]. Genes encoding for EGF-CFC belong to a small family, with only two members in mammals (*Cripto, Cryptic*), one in zebrafish (*one-eyed pinhead*) and three in frogs (*FRL1/XCR1*, *XCR2*, *XCR3)* [115], [127]. The activities of nodal ligands can be modulated by various extracellular inhibitors. One major group are the Lefty proteins. Also belonging to the TGF superfamily, they are known to antagonize nodal signaling through blocking of receptor complex formation by interacting with EGF-CFC proteins and other ligands of the nodal signaling pathway [119], [128]. However, it was shown that Leftys don't act as direct competitive inhibitors for ALK4 or ActRIIB [119], [128], but that they are targets downstream of nodal signaling, functioning in an essential negative feedback loop [129], [130]. Proteins belonging to the Cerberus family are

another group of well characterized nodal antagonizers that are blocking Nodal signaling via direct ligand interactions. This cysteine-rich extracellular protein family is primarily a Nodal inhibitor in mouse, in *Xenopus* however Cerberus was shown to antagonize Wnt and BMP signaling as well [131]–[133]. The activity of Nodal downstream of the ActRII and ALK4 receptors is transduced via Smad2, Smad3 and Smad4 together with the FoxH1 transcription factor and the Mixer subclass of homeodomain proteins [134]. FoxH1 and Mixer contain interaction motifs for Smads, enabling active transcription complex formation on enhancers of target genes belonging to the Nodal pathway [135], [136]. The response to Nodal signals is mostly the transcriptional activation of Nodal pathway targets, like Nodal, Pitx2 and Lefty1, and just in a few cases the transcription of target genes is repressed. The expression of *Nodal* is positively autoregulated by an asymmetric enhancer situated in the first *Nodal* Intron and a left-side specific enhancer, located upstream [137]–[142].

The properties of Nodal ligands are associated with the ones of classical morphogens, signaling over a distance to induce responses in a dose dependent manner in a field of developing and responsive cells [143]. For instance, it was discovered that in *Lefty2* mouse mutants the Nodal pathway is activated ectopically in the right lateral plate mesoderm (LPM), indicating that an excess of the normally left sided Lefty2 long-range diffused to the other side [144]. In zebrafish, Lefty1 and Squint are known to function as long-range signals for mesoderm induction [118] and in chick embryos it was discovered that Lefty2 or Nodal proteins are able to travel over long distances [145].

The Nodal signaling pathway is strictly regulated by various mechanisms like positive- and negative-feedback loops, soluble antagonist expressions and the use of co-receptors. Nevertheless, all distinct molecular mechanisms of the Nodal signaling pathway, the different levels, activities and transcriptional responses remain to be revealed.

1.2.3 Roles of Nodal signaling during embryonic development

Nodal signaling displays many biological activities during early embryonic development. Especially well conserved are the roles of Nodal signaling for mesoderm and endoderm specification, neural patterning as well as the establishment of the left-right axis.

1.2.3.1 Endoderm and mesoderm specification during germ layer formation

During gastrulation, the specification of distinct lineages into mesoderm, endoderm and ectoderm (the three germ layers) is achieved by an intricate interplay between signaling molecules along the embryo`s anterior-posterior (A-P) and proximo-distal (P-D) axes. The signaling molecule Nodal is essential for endoderm and mesoderm specification and the patterning of the germ layers. [112], [116].

In the mouse embryo an interlinked slow and fast positive regulatory loop is used for the formation of the primitive streak. The unprocessed Nodal ligand was shown to induce *Furin, Pace4* and *Bmp4* expression via signaling from the epiblast to the connected extraembryonic ectoderm. Successively, *Wnt3* expression is activated via Bmp4 back signaling to the epiblast resulting in upregulation of *Cripto* and *Nodal* expression in the epiblast [146], [147].
In zebrafish, the two nodal-related genes, crucial for mesoderm and endoderm specification are *squint (sqt)* and *cyclops (cyc)* with redundant and overlapping functions (Figure 9A) [148]. *Sqt* was shown to be expressed in the yolk syncytial layer (YSL), a known source of signaling molecules important for organizer development and the formation of the mesendoderm (Figure 9B) [149]. The mis- expression of *sqt* resulted in mutant mesoderm phenotypes in zebrafish, and *sqt,cyc* double mutants displayed a lack of mesendodermal derivatives as well, indicating an important role of these nodal related genes within the mesendoderm formation and organizer development [148]. However, it was shown that for mesoderm patterning in zebrafish only long-range graded Nodal signaling along the animal-vegetal axis, not the D-V axis, is needed [150].

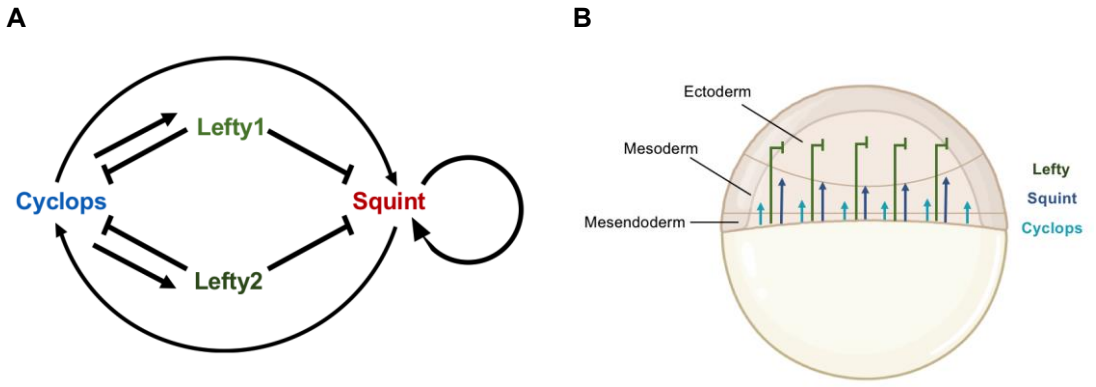

Figure 9: **Nodal signaling is regulated by positive- and negative-feedback loops: A** Schematic model for the cross-regulation between zebrafish Squint, Cyclops, Lefty1 and Lefty2 during the germ layer specification. Adapted from [130]. **B** Schemata for endoderm and mesoderm induction in the zebrafish embryo, with *cyclops, squint and leftys* being expressed close to the YSL and acting with long-range activity (squint, leftys) and short-range activity (cyclops). Adapted from [110].

1.2.3.2 The role of Nodal signaling and antagonism during neural patterning

Beside endoderm and mesoderm specification, Nodal signaling has two essential roles during neural development. First, Nodal inhibition is important for the generation of anterior neural tissue. Second, Nodal signaling is required for the subsequent patterning and maintenance of the neural tissue since this depends on the via Nodal signaling generated axial mesendoderm [114]. The activation of Cerberus-like (Cerl) and Lefty1 (Lft1), within the anterior visceral

endoderm by Nodal signaling is essential for anterior neural patterning. For instance, in *Xenopus* the expression of *Cerberus* within the anterior endoderm is antagonizing Wnt and Nodal ligands and is allowing the formation of the head [131]. Since Cerl as well as Lft1 belong to group of Nodal antagonists, their activation in the distal visceral endoderm is restricting the expression of Nodal target genes to the proximal region [129], [151]–[153]. Additionally, high Nodal activity is also crucial for the ventral patterning of the neural tube as well as the maintenance of anterior forebrain territory. Strong Nodal activity within the posterior epiblast is vital for anterior endoderm and prechordal mesoderm generation and necessary for neural tube patterning and forebrain maintenance [114], [154].

1.2.3.3 Nodal signaling in patterning the dorsal-ventral and the anterior-posterior axis as well as in the maintenance of undifferentiated ES cells

Interestingly, novel and unexpected roles of Nodal signaling have emerged over the last couple of years. Three of them are the role of Nodal in dorsal-ventral as well as anterior-posterior axis establishment and the maintenance of human and mouse undifferentiated ES cells.

Alike Nodal, also BMP belongs also to the TGFβ protein family. It is important for ventral fates specification and a key player for the patterning of the dorsal/ventral axis [155], [156]. It was recently shown that in zebrafish also maternal transcripts for *sqt* act as dorsal determinants, since maternal *sqt* transcrips were shown to localize in dorsal blastomeres (4 cell stage and 8 cell stage), and that maternal *sqt* morpholino knock-down resulted in ventralized phenotypes [157]. However, also zygotic *sqt* mutants resembled the described maternal-zygotic *sqt* mutants, indicating that for dorsal specification maternal *sqt* transcripts might not be essential [114], [158].

For A-P patterning in mouse Nodal signaling was shown to be required for at least two aspects: for the formation and for the directional movement of the anterior visceral endoderm [114]. The anterior visceral endoderm does not form properly and an A-P axis is not evident with a reduced amount or the absence of Nodal [142], [159]. Furthermore, in hypomorphic *Nodal* or *Cripto* mutants the anterior visceral endoderm seems to form correctly but is not able to translocate [142], [160], [161]. Additionally, *Lefty1* and *Cer1* expression in distal visceral endoderm was shown to have a light asymmetric bias toward the prospective anterior side [162], [163] and was described to mediate directional anterior visceral endoderm movements. Finally, it was suggested recently that the NODAL pathway is also involved in the maintenance of undifferentiated human and mouse embryonic stem (ES) cells, since crucial components of the NODAL signaling pathway were shown to be highly expressed in these cells [164]. Also, *NODAL* overexpression in human ES cells was inhibiting mesoderm differentiation in embryoid bodies and maintained ES cells in their undifferentiated state [165].

1.2.3.4 Nodal signaling and the establishment of the embryonic left-right axis

From outside, the body plan of a vertebrate appears bilaterally symmetric. Nonetheless the positioning and morphology of internal organs often display a strict L-R asymmetry. For instance, in vertebrates the heart generally lies on the left side, the liver as well as the pancreas are found on the right and the gut undertakes asymmetric rotations. Regulated Nodal signaling was shown to be involved in several important early embryonic patterning events, essential for the establishment of this left-right (L-R) axis during vertebrate embryonic development [166]–[170]. In general, the vertebrate L-R axis is the one determined last, and abnormal left-right pattering often results in less severe defects than disturbed P-D or A-P patterning [171]. For proper establishment of the L-R asymmetry four consecutive steps have to be completed. First, during late neural-fold stage the initial L-R symmetry has to be broken in or near the node [172]. The node, also named “organ of asymmetry”, is placed at the anterior of the primitive streak and is essential for the establishment of the L-R axis (further descriptions see 1.2.4).
Within the node cila undergo rapid, clockwise rotation, creating leftward flow of the extra-embryonic fluid and acting as a left-side determinant. [173]–[176]. For the second step, the L-R biased signals have to be transferred from the node to the LPM, and for the third step, signaling molecules like *Nodal* or *Lefty1/2* have to be asymmetrically expressed. During the late neural-fold stage *Nodal* is symmetrically expressed around both sides of the node (where it forms heterodimers with GDF1 and activates Nodal signaling) but is later detected asymmetrically in the left LPM in mouse as well as chicken and zebrafish [112], [177]–[179]. The upregulation of Nodal activity on the node’s left side is hypothesized to be generated via Notch pathway activity and asymmetric Ca2+ signaling, and since it occurs in all investigated vertebrate species it is considered the conserved key moment which leads to laterality decisions in a tissue specific manner [114].
The Lefty proteins (Lft1, Lft2) are Nodal antagonists. They are both expressed asymmetrically and transiently. Alike *Noda*l, *Lefty2* is expressed in only the left LPM, where the expression begins, slightly after *Nodal*, adjacent to the node in just a small region and is later expanded along the A/P axis in a bidirectionally manner until 6-7 somite stage [171], [177]–[181]. *Lefty1* displays expression on the left side of the prospective floor plate, beginning near the node with anterior expansion till the 5-6 somite stage [171]. The expression of *Nodal* in the mouse node is crucial for the subsequent asymmetric expression within the LPM [182], [183]. In contrast, zebrafish *spaw* expression around the KV seems not essential for subsequent *spaw* expression in the LPM, hinting for another factor being involved in the transmission of the left-sided information [178]. The expression of *Noda*l is then spreading rapidly through the left LPM, inducing the expression of *Pitx2* and is subsequently downregulated via a negative-feedback loop involving *Lefty2* [114]. The asymmetric expression of *Nodal* within the LPM of mouse is induced and maintained through two different kinds of inhibitions. On the right side

of the node *Nodal* is inhibited by Cerl2/Dand5, which belongs to the group of secreted TGFβ antagonists [132], and at the midline Lefty1 is restricting the activity of Nodal to the left [184]. Lefty1 was shown to also act via a lateral-inhibition and self-enhancement feedback system [185]. Via mathematical modeling it was shown that the *Nodal-Pitx2-Leftys* expression cassette is generating a reaction- diffusion mechanism, which is important for the propagation of Nodal in an uniform manner through the left LPM, and keeps it from spreading to the right [185]. The final necessary step for proper establishment of the L-R asymmetry is the morphogenesis of the visceral organs in an asymmetrical manner induced by these asymmetrically expressed signaling molecules [171].

In summary, Nodal signaling is the key player for the L-R axis specification since its activity controls the propagation of positional information for the developing left side of the embryo (Figure 10).

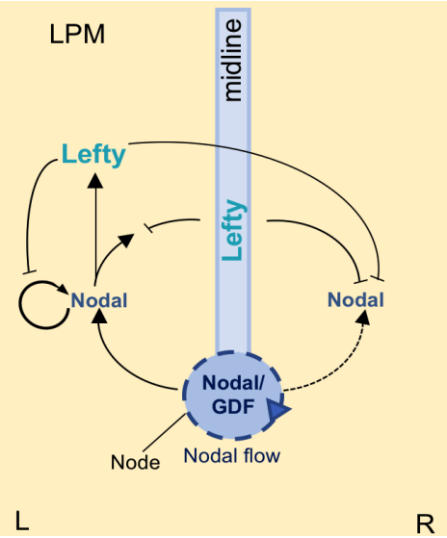

Figure 10: **Nodal signaling is the key player for the L-R axis specification:** Simplified model for the establishment of the left-right axis by Nodal and Lefty visualizing Nodal/GDF1 heterodimers formed at the node, activating Nodal signaling in the LPM. Caused by the leftward Nodal flow, Nodal activation is biased toward the left, succeeding the autoregulation of Nodal, *Lefty* expression induction as well as Lefty's long-range inhibition towards the right. Adapted from [110].

1.2.4 The role of DFCs and the KV for left-right patterning processes

Left-right patterning mechanisms have been well studied in mice. Symmetry-breaking in this animal model was shown to be initiated in the Node, formed by a morphologically distinct cluster of cells located on the tip of the early embryo [186]–[188]. The general structure of the node is made of a surface layer of endoderm, covering crown cells, which are surrounding small columnar pit cells in the node`s center [189]. At E7.5 stage the node has a concave, teardrop-shape and is located distally on the ventral surface of the mouse embryo. It is made of around 250 cells and is approximately 50 µm deep, 50–60 µm wide and 70–90 µm long [174], [176], [189].

Importantly, the node pit cells have a monocilium which is projecting into the extra-embryonic space. The formations of these cilia depend on a core machinery including intraflagellar transport particles, a specific kinesin-2 motor as well as a retrograde cytoplasmic dynein motor

[190]. In mouse, the monocilia within the node are reaching up to 3–5 microns at E8 [176]. Node monocila were shown to undergo rapid, clockwise rotation with a frequency of around 600 rpm, creating leftward flow of the extra-embryonic fluid, called “Nodal flow”, acting as a left-side determinant [173]–[176].

The Nodal flow is described to be conserved in numerous vertebrates [173], [175], [191], [192] and is proposed to be one of the key point for L-R symmetry breaking [173]–[175]. The proper functioning of the node is fundamental since the leftward-directed Nodal flow within the node results in asymmetric expression of Nodal genes, like Nodal/spaw, Lefty1 and Lefty2, crucial for proper left right pattering [188], [193]. However, the detailed mechanisms by which the nodal flow is translated into these asymmetric expressions are still to be fully understood.

The Hensen’s node in chicken, in Xenopus the gastrocoel roof plate and in zebrafish the Kupffer’s vesicle (KV) are equivalent structures [186], [194]–[196]. The KV, the zebrafish organ of laterality, was first described in 1868 by C. Kupffer and its structure is conserved among teleost fish [194], [197]. Compared to the relatively flat shaped mouse node, the zebrafish KV is a fluid-filled sphere (Figure 11).

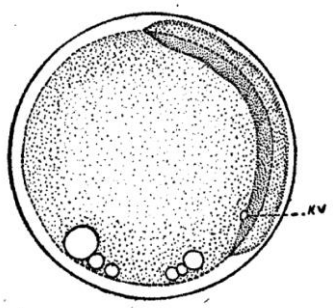

FIG. 24.—Egg 24 hours after fertilization; KV, Kupffer's vesicle.

Figure 11: **In zebrafish the KV is the organ of laterality:** Drawing from a teleostean fish egg at 24hpf highlighting the Kupffer’s vesicle [198].

The KV, is formed by Dorsal forerunner cells (DFCs) (Figure 12A) [194]. These cells first emerge as cells of the epithelium of the dorsal surface in direct contact with the yolk syncytial layer at around 4hpf and are advancing further towards the vegetal pole during embryonic epiboly movements [194], [199], [200]. With advancing epiboly, the cluster of DFCs becomes more and more separated from the dorsal marginal deep cells, however remaining in direct contact with the enveloping layer margin which is advancing dorsally [200]. At around 80%, epiboly DFCs form a compact and oval-shaped cluster by converging dorsally and intercalating between each other. Interestingly, it was shown that during this dorsal convergence a subset of DFCs forms progressively into a bottle-shaped structure and remains linked to the dorsal enveloping layer by tight-junction components and Protein kinase C zeta enriched attachment points. Besides, the remaining DFC subset stays unpolarized and forms random dynamic cell protrusions. Overall, the DFC movement is coupled to the enveloping layer movement by

physical tissue linkage [194], [199]–[201]. At the final phase of epiboly and after reaching the vegetal pole, the DFC cluster is separating from the dorsal marginal enveloping layer cells and is becoming more compact with a flattened sphere rosette-like shape. Short after, the interior KV lumen is formed by incorporating the unpolarized DFCs into a rosette structure of merged widely spaced apical focal points and migrating into the zebrafish embryo [194], [199], [200], [202]. Between 1-somite and 4-somite stage the lumen volume then increases around 12-fold [200]. Intriguingly, it was discovered that the formation of the lumen was directly coupled to ciliogenesis since Tubulin-rich cilia were detected at the lumen-facing membrane side of polarized DFCs at the time of lumen initiation. This indicated that the DFC polarization, which is happening during epiboly, is essential for the formation of the distinct rosette-like structure and later KV formation and ciliogenesis. The distinct architecture of the zebrafish KV enables a circular counterclockwise flow of fluid within the lumen. Cells located at the KV`s anterior tip have a more columnar shape, causing a higher cilia density and therefore developing a faster fluid flow in the anterior left segment of the KV resulting in L-R asymmetric Nodal flow strength [203], [204]. In summary, the asymmetric Nodal flow within the ciliated Node/KV results in asymmetric Nodal genes expression and is therefore the major modulator of vertebrate L-R symmetry breaking (Figure 12B). The correct development and formation of the “organ of asymmetry” is essential for a proper further embryonic development.

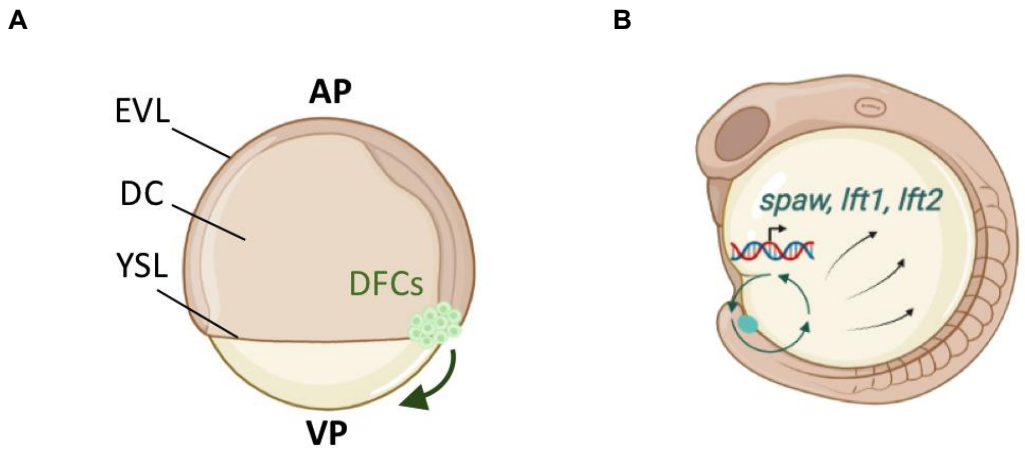

Figure 12: **The KV is formed by DFCs and is important for asymmetric Nodal gene expression: A** Schematic representation of an 8hpf zebrafish embryo visualizing animal pole (AP) to vegetal pole (VP) dorsal forerunner cell (DFC) migration. EVL, enveloping layer; DC, deep cells; YSL, yolk syncytial layer **B** Schematic for the asymmetric Nodal flow within the ciliated KV which results in asymmetric Nodal gene expression.

1.2.5 The function of αV/β integrins during early embryonic patterning

Integrins are a family of cell adhesion receptors which are able to recognize primarily cell-surface ligands and extracellular matrix ligands. In mammals there are eighteen α and eight β integrin subunits which can form 24 different αβ heterodimers (Figure 13A).

Integrin αV was shown to be crucial during early developmental processes since αV mutant mice displayed disturbed embryonic cerebral blood vessel formation and defects in the axon and glia interactions in the CNS [205]–[207]. The αV integrin subunit can bind to any of the five β integrin subunits β1, β3, β5, β6 or β8 [208]. During vertebrate embryonic development, αV integrins are expressed with wide overlapping distributions in mammalian, zebrafish and avian embryos [209]–[212]. Integrin αVβ1 has not yet been studied extensively in mammals *in vivo*, due to their extreme broad expression overlapping with other integrins and the nonexistence of antibodies and inhibitors specific for αVβ1. Nevertheless, several *in vitro* studies connected αVβ1 to developmental processes. For instance αVβ1 was shown to be implicated in embryonic astrocytes and oligodendrocyte precursors migration in rodents [213], neural cell adhesion molecule L1 cell binding [214] and in the spreading and adhesion of mouse embryonic cells on fibronectin [215]. Interestingly, it was described that Integrin αVβ1b (Figure 13B) in zebrafish is a regulator for the establishment of the vertebrate left-right axis since it was defined as a mediator of cellular interactions which are important for the clustering and movement of DFCs. In zebrafish, αV as well as β1b morphants show mislocalization of DFCs, KV malformation and left-right body asymmetry defects [209].

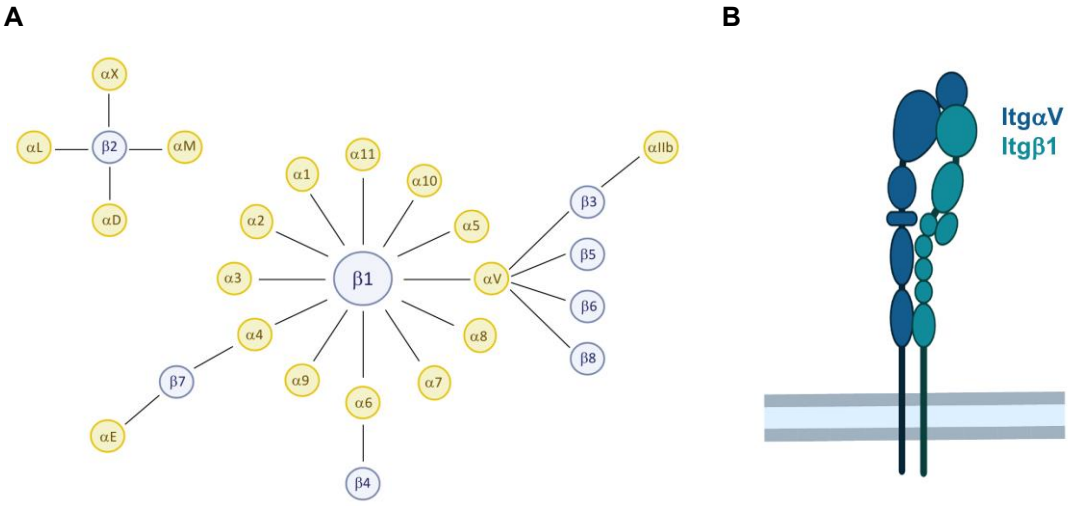

Figure 13: **The Integrins α and β can form heterodimers: A** Schematic overview for known Integrin α and β interactions. Adapted from [216]. **B** Schematic representation of an Integrin αβ heterodimer.

1.2.6 Recent findings in zebrafish left right patterning research

In zebrafish, *southpaw* (*spaw*) is the Nodal related gene important for the establishment of the left-right axis. *Spaw* was shown to be expressed the left LPM and bilaterally in paraxial mesoderm precursors, overlapping with other left-sided expressed genes like *lefty2* during later somite stages [178]. It was recently shown that Nodal-mediated left-right patterning function is also conserved in zebrafish using mutants for the *Nodal* orthologue *spaw* as well as the Nodal inhibitors *dand5* and *lefty1* (Figure 14) [5]. Like *Nodal* mouse mutants, zebrafish mutants for *spaw* failed to initiate *spaw* expression in the LPM and displayed heart looping and jogging defects [5], [182]. Zebrafish *dand5* and *lft1* mutants displayed bilateral *spaw* expression as well as heart looping and jogging defects [5], [217]. Besides, *lefty1* loss of function fish displayed accelerated *spaw* progression, indicating that *lefty1* as well as *dand5* inhibition control the localization, timing and speed of *spaw* expression [5]. In *lefty1* mutants the application of a Nodal inhibitor drug was sufficient to rescue the heart looping and jogging phenotypes and the bilateral *spaw* expression. These results indicate that the location of Lefty1 activity is not essential, but that Lefty1 activity dampens Nodal activity, preventing it from extending to the embryo`s right side [5].

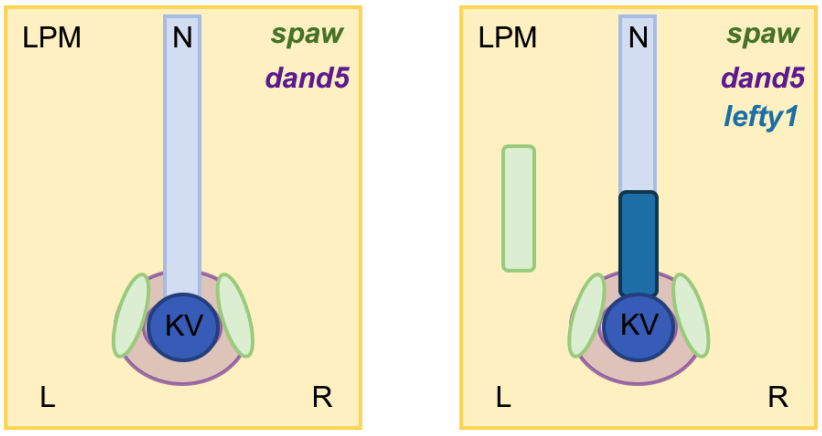

Figure 14: **Nodal related genes are important for the establishment of the left-right axis:** Schematic for the expression patterns in zebrafish at 6 somite stage (left) and 12 somite stage (right) for *spaw, dand5* as well as *lefty1*. LPM, lateral plate mesoderm; KV, Kupffer's vesicle; N, notochord

Additionally it was shown that Vg1 and Spaw are forming heterodimers, similar to mouse, where Nodal-Gdf1 heterodimers are important for left-right axis patterning [5], [218]. These results demonstrated the conservation of left-right patterning processes between mouse and zebrafish. Surprisingly, it was shown that zebrafish Lefty1 and Lefty2 can be replaced with a Nodal inhibitor drug also during mesendoderm patterning, shining a light specifically on the Lefty inhibitory feedback loop during Nodal patterning (Figure 10). *Lefty* mutant phenotypes

could be rescued by ectopic *lefty* expression distant from the normal expression domain as well as by temporally and spatially uniform Nodal inhibitor drug exposure. These results signify that in zebrafish the patterning of the mesendoderm without the Lefty inhibitory feedback is possible but less robust. Lately it was revealed that also *jnk* genes, downstream components of the Nodal cilia patterning planar cell polarity signaling pathway, might play a role in establishing the left-right asymmetry [219]–[221]. In zebrafish mutants for *jnk1a*, *jnk1b* and *jnk2,* the length of the KV cilia was significantly reduced as well as the counter-clockwise nodal flow within the KV and *spaw* expression disrupted [221]. However, the exact way in which *jnk* genes co-ordinate the length of cilia remains so far unresolved.

In summary, even if many questions are still unanswered, zebrafish and its now well-established Nodal factor mutants display a huge potential for further understanding of the left-right axis establishment in vertebrates.

1.2.7 Meteorins in early embryonic development and open questions in the field

It has been reported that *Nodal, Lefty* as well *p-Smad2* expression is downregulated in *Meteorin*-null ES-cells [4]. Per se, *Metrn* was hypothesized to be a novel gene crucial for embryonic development and regulator of *Nodal* transcription, important for maintaining sufficient Nodal levels for proper embryonic endoderm formation. In mice however, the disruption of the *Metrn* gene resulted in early embryonic lethality and made it not possible to investigate the role of Metrn proteins in early embryonic development *in vivo* [4]. Consequently, we are aiming to continue the investigation of the role of Metrns in early embryonic development *in vivo*, using zebrafish as model organism.

Especially, the receptor(s) through which Metrns are acting in the context of early embryonic patterning is/are still unknown. It was recently shown that METRNL is binding to KIT receptor ligand in the background of ischemic tissue repair [6] and that Metrn is interacting with Htr2b for in the context of hematopoietic stem/progenitor cell mobilization control [7]. But, since zebrafish *kita/b* as well as *htr2b* seem to be not expressed earlier than 9hpf and not in proximity to DFCs and the forming KV we assume that Metrns act through another, so far unknown receptor during early patterning processes.

Another open question in the field of left-right patterning is how the Nodal flow is finally converted in asymmetric nodal gene expression, and what is the downstream signaling of the Nodal pathway to drive asymmetric changes. Furthermore, it is still unknown how precise timing and localization of nodal pathway components is achieved during left-right patterning. It was recently shown that *jnk1a, jnk1b, jnk2* triple zebrafish mutants display disturbed Nodal flow, however they do not show the loss of the stereotypical asymmetric organ placement as described in *spaw* or our *metrns* mutants [5], [221]. This indicates that there might be other mechanisms beside the Nodal flow which are important for the establishment of the

asymmetric organ positioning during early embryonic development. Also, how entire tissue movement is coordinated by different forces (intrinsic and extrinsic in different layers) and the ways how an organ shape is influenced by physical properties of the extracellular matrix and surrounding cells still have to be investigated specifically in the context of KV formation.

Overall, in spite of recent progress in understanding the breaking of embryonic L-R symmetry in vertebrates, the totality of all aspects of proper establishment of the left-right axis and execution of asymmetric organogenesis is far from being fully understood.

1.3 The function of Meteorins in axon guidance and hunting for Meteorins receptor(s)

Despite over million years of evolution, the principal features of the brain wiring diagram in bilaterians are highly conserved, including the presence of a subset of axons interconnecting neurons on both sides of the central nervous system (CNS) called commissures [222]. It was shown that the formation of the ratio of correct commissural and non-commissural axons is strictly balanced and is essential for sensory stimuli integration and the CNS physiology [223]. A number of of neurological disorders can have their origin in the failure of proper axon midline crossing during development [224], [225] indicating that the understanding of controlled midline crossing mechanisms will help understand the etiology of these complex severe neurological diseases. Despite extensive studies in the past years, the molecular repertoire for midline guidance is more diverse than initially imagined and far from being fully understood.

Meteorin was discovered as a secreted neurotrophic factor, promoting neurite outgrowth *in vitro*, with expression in radial neuronal progenitors and radial glia [2]. In vertebrates Metrn and Metrnl are highly conserved including two members in mammals and three in zebrafish (Metrn, Metrnl1 and Metrnl2). Recently it was investigated that *Metrn* and *Metrnl* mRNAs are highly expressed by floor plate cells and in other midline structures in the CNS of zebrafish and mouse indicating them as suitable animal models for further research to work out the function of the Meteorins, as new family of secreted proteins, during the development of the CNS [2].

Therefore, in the final part of this thesis introduction I will give an overview about general axon guidance mechanisms, established axonal guidance factors, the particular role of the midline during axonal navigation and about the hunt for Meteorins receptors to fully understand the way of function of our favorite family of proteins.

1.3.1 General mechanisms of axonal guidance

During embryogenesis, developing axons have to navigate significant distances to be able to reach their final targets. Amazingly, this axon growing occurs in a highly stereotyped and extreme ordered manner. The mechanisms to solve the hard challenge of guiding thousands/millions of axons along their way are largely conserved in invertebrates and vertebrates. During the past decades, one of the major goals of developmental neurobiology has been to understand how the axons of newly generated neurons can reach their correct synaptic partners by following precise and well-defined paths. With the help of invertebrate model organisms such as the nematode *Caenorhabditis elegans* or the fruitfly *Drosophila melanogaster*, our understanding and knowledge of axon guidance mechanisms has progressed at lot. However, we are still far away from understanding the full picture. The primary connections of neurons are achieved through processes of guidance events. A

complex network of receptor/ligand interactions (e.g. Netrin/DCC; Slit/Robo) in the close environment, orchestrates these processes, ensuring the proper establishment of neuronal connections [1], [226]. The response of an axon to environmental guidance signals is mainly controlled by the highly motile growth cone, a structure on the axon's distal tip. The growth cone was first described by Ramon y Cajal, over a century ago (1890). The axonal growth cone is characterized by an exceptionally dynamic cytoskeleton as well as its division into two domains. The first domain is the central domain, enriched with microtubules. The second peripheral domain houses actin-rich lamellipodia and filopodia (Figure 15A). Generally, a distinct set of axonal guidance receptors is localized at the growth cone. This helps the growing neurites to "read" their extracellular environment and to understand their correct directions for their navigation. In case of changes in the environment, the assembly or disassembly of cytoskeletal component of the growth cones leads to changes in the morphology, influencing in turn axonal navigation and elongation [227]–[231]. The pioneer axon is the first axon initiating the formation of an axonal tract. This single axon establishes the future trajectory for subsequently following axons from the same neuronal population. Neurons which are developing later can then grow along the track pathways which have been pathed by the pioneers axons to reach their appropriate targets [227], [232]. The parameters which are allowing the growth cone's correct neuronal paths are specified by tightly regulated sets of instructive guidance cues along the track of the navigating axon. These guidance cues can be mediated by ECM or cell membrane bound molecules but also by diffusible factors [227], [233]. Four different types of guidance cues can be generated by the different guidance factor's coordinate actions. Guidance cues can act repellent or attractant and as long-range or short-range cue. These roles are not necessarily mutually exclusive. Rather they act in a concert-like manner together to warrant reproducible as well as correct elongation of the navigating axons. This means that for instance particular neurites can be repelled by a long-range repellent guidance cue, but attracted from the opposite side by a long-range attractant cue, resulting in tightly bundled neurites navigating along their designated tract [234], [235]. The whole navigation of growing axons is an extremely dynamic process, as one guidance molecule might be able to act in a bifunctional manner, as an attractant or repellant. This dynamic enables different axonal responses to the same cue. Furthermore, especially in the case of long distances navigation, it might be necessary for one same axon to be able to change its reaction to one particular axonal guidance factor during its journey (Figure 15B) [222], [227], [234], [235].

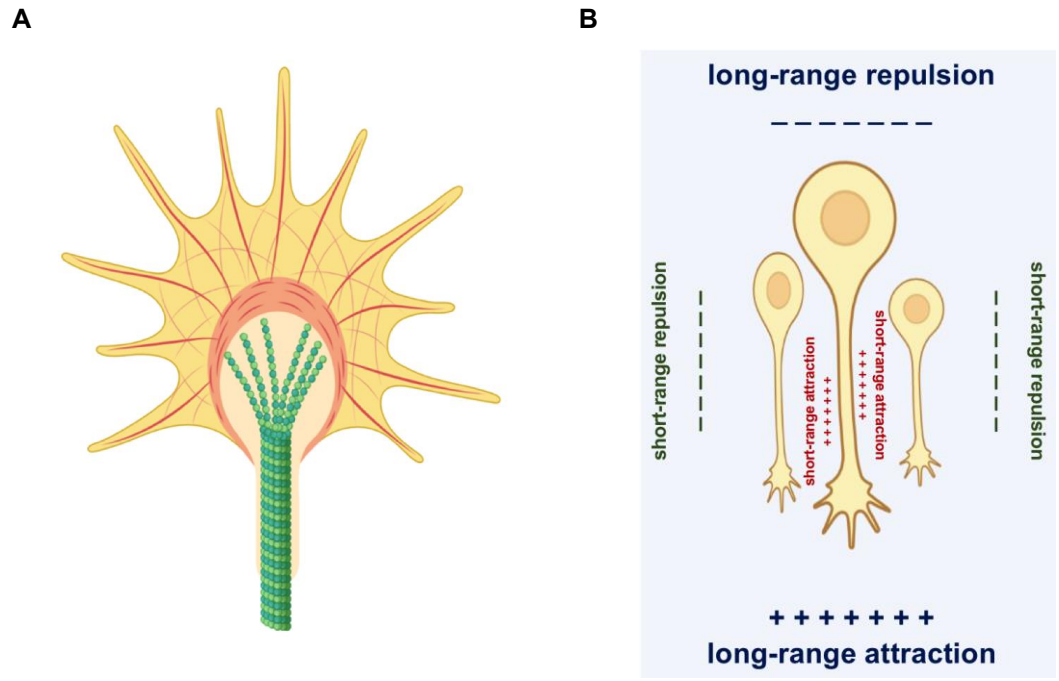

Figure 15: **General mechanisms of axonal guidance: A** Schematic representation of a growth cone highlighting its central domain, enriched with microtubules (green) and the organization of its peripheral domain housing actin filaments cytoskeletal components. **B** Schematic representation of the different possible guidance cues acting on the growth cone and the developing axon including long-range attractant and long-range repellent enabling axonal navigation and short-range repulsion as well as attractive cues keeping the growing axon in a tight bundle.

1.3.1.1 Crossing the midline – the remarkable role of the midline in axonal guidance

From this complex and tightly regulated process of axonal guidance longitudinal projections are established. They are forming ipsilateral circuits and are situated in parallel to the midline along the AP body axis. Additionally, commissural connections are established as well. Commissures are interconnection neurons on both sides of the CNS, and therefore are crossing the midline. The balance between commissural and non-commissural axons within the CNS is tightly regulated and crucial for sensory stimuli integration as well as the general CNS physiology [222], [223]. For the achievement of these structures, axons have to cross the midline. In bilaterians the CNS is developing along a bilateral symmetry axis which is located at the midline [236]. At the ventral midline, or also named floor plate (FP), a population of specialized glia cells is located. These cells are a main source of diffusible axonal guidance molecules secretion and therefore the midline is one of the main organizers for neurodevelopment, also acting as “choice point” or “intermediate target” for navigating axons [233], [236], [237]. For instance, for commissure navigation, the developing axons have to be first attracted to the midline and after actually crossing the midline, the attracting forces have to be switched off and responsiveness to midline repellents has to be switched on. These

mechanisms are then facilitating the growth of commissural axons away from the midline and enabling them to move on to the other side of the CNS (Figure 16A) [237].

During the last decades two key questions were the leading force for numerous neurodevelopmental studies, especially in context of midline crossing. The first concerns the mechanisms by which commissural axons are attracted to the midline and how their growth cones are able to receive and integrate the huge diversity of midline cells released signals. The second key question is how are commissural axons instructed to leave the midline after successful midline crossing, and what are the signaling as well as molecular changes to switch to longitudinal growth mode. In general, midline axonal guidance factors are expressed in independent locations and different time points, which is enabling the control of this diverse biological process of axonal midline crossing [1]. The extreme significance of the midline and especially its ventral part, the FP was illustrated in numerous studies using different model organisms, all above *D. melanogaster* [238]–[242]. In *D. melanogaster* single-minded (*sim*) mutants the specification of midline cells is abolished. This disturbed midline formation was shown to result in axonal guidance defects such as abrogated commissural tracts formation as well as a collapse of the longitudinal bundles [242]. On the other hand, in *D. melanogaster* mutants for *slit*, the cells of the midline seem to differentiate correctly but they appear displaced ventrally. This leads to initial commissural tracts formation, but also to the fusion and collapsing of the longitudinal tracts onto the midline, due to the mis-positioned midline [239]. In mouse, Danforth's short-tail (*Sd*) mutants, which are missing the notochord as well as the FP, display failures of proper commissural axons development. Due to the missing midline-secreted axonal guidance factors in these mutants, commissures in the spinal cord are not able to elongate towards the FP dorso-ventrally, cross the midline and then turning rostrally. Rather, commissural axons in *Sd* mutants are reaching the FP but are not able to properly cross the midline due to the lack of guidance factors [240]. Likewise, it was published that in chick embryos, the ablation of the notochord inhibits FP formation, and consequently causes errors in commissural axons turning [238]. Similar mutant phenotypes were also described in mouse Gli Family Zinc Finger 2 (*Gli2*) mutants. *Gli2* mutants are missing the FP as well, due to the mutation of the Gli2 transcription factor, which is involved in Shh signaling regulation [241]. Additionally, *Gli2* mutants suffer also from severely defasciculated axons in the hindbrain, due to longitudinal axonal trajectories defects (Figure 16B) [243]. Remarkably, also the primary cilium, located on commissural neuron's cell bodies, got assigned a significant role within axonal guidance along the midline. It was described to be crucial for transcriptional changes of guidance receptors, resulting in a repulsive response of commissural axons after crossing the midline [244].

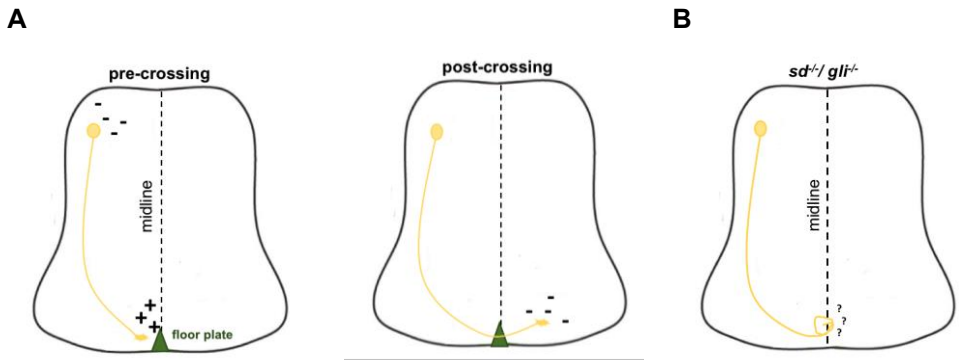

Figure 16: **Axonal guidance at the midline: A** Schematic representation of a mouse embryonic spinal cord section and an axon crossing the midline, guided by repulsive and attracting guidance cues. **B** Schematic representation of a *sd* or *gli* mouse mutant missing the floorplate, which results in commissural axons stuck at the midline.

It was recently suggested that the FP is not the sole mediator of midline axon guidance, since also other cells in close proximity to the midline, for instance neuronal progenitor cells, might be involved in instructive guidance molecules secretion and therefore in the process of midline axon guidance [245], [246]. Moreover, beside axonal guidance, the midline got also associated with multiple pathways regulating left-right asymmetry. Even though the midline tissue itself doesn't appear morphologically asymmetric it is suggested to function as a border for different pathways essential to establish left-right asymmetry as well as for organ positioning. Disturbed midline development was demonstrated to influence correct left-right asymmetry development, especially in the heart and gut [247], [248].

1.3.2 Axon guidance factors

Two molecular couples of ligand and respective receptor have been associated with an important role in midline guidance processes: Netrin1/DCC (Deleted in Colorectal Cancer) is known to act as a mediator of commissural axon growth towards the CNS midline and Slit/Robo (Roundabout) which is essential for hindrances of axons to post-cross away from the midline and to prevent ipsilaterally projecting neurons from crossing the midline. A fine-tuning between repulsion and attraction is provided by various molecular interactions between the Netrin1/DCC and the Slit/Robo pathway. It was shown that numerous additional molecules in other protein families (Cell-adhesion molecules, Semaphorins, Ephrins, etc.) have an influence in crossing the CNS midline within complex regulatory mechanisms [249], [250]. In general, to the family of "canonical axon guidance molecules" four major protein families belong: Slits, Netrins, Ephrins and Semaphorins. These protein families have been studied extensively and their role and effects on axonal behavior have been investigated [234].

1.3.2.1 Slit family and Robo receptors

For the last few years, the Slit protein family has been intensively studied as crucial axon guidance regulators and cell migration mediators in Drosophila and vertebrates. Slit proteins are highly conserved across species. They are mostly secreted, however frequently associate with the extracellular matrix (ECM) and the cell membrane [251], [252]. In most vertebrates, the Slit protein family contains three members (Slit1-3). They have a size of ~200kDa each and include four stretches of leucine-rich repeat (LRR) domains (D1-D4), seven to nine repeats of the epidermal growth factor (EGF), one Agrin-Perlecan-Laminin-Slit (ALPS)/Laminin-G-like domain, as well as a cysteine knot on the C-terminal [251].

Slit proteins were simultaneously identified twice, as negative regulators but also positive regulators during axonal guidance [253]. The first discovery was led by search for factors that are able to stimulate axonal branching and the surprising purification of a cleaved mammalian Slit2 protein fragment in rat brain extracts indicated Slit2 as a branching and elongation stimulator [254]. The second Slits discovery was with a genetic screen in *D. melanogaster* for genes affecting the navigation of axons and as the repulsive Robo ligand [255]–[257].

The Robo receptors are the main receptors for Slits. Four Robo orthologs exist in mammals and zebrafish, one in *C. elegans* (SAX-3) and three in Xenopus and chick [256]. The first descriptions of a *robo* gene and also the name giving discoveries were in Drosophila: *robo* Drosophila mutants displayed midline stalled commissural axon resulting in a creation of an axonal 'ROundaBOut' [255], [257]–[259]. Robo proteins are single-pass transmembrane receptors without any enzymatic or autocatalytic activity, hence, to mediate their function, Robo receptors might depend on scaffolding molecules as well as downstream signaling. Most of the Robo extracellular domains have five immunoglobulin-like domains (Ig1-5) and three fibronectin repeats (FNIII 1-3). The Cytoplasmic tail of Robo receptors mostly contains "cytoplasmic conserved" domains, which can vary between species [260]. Robo-Slit interaction occurs through the binding of the Slits LRR2 domain to the Robos first Ig domain (Figure 17) [261].

The role of Slit/Robo signaling, especially within the organization and navigation of commissural axons in the spinal cord and hindbrain, has been studied extensively. In a *Slit1/2/3* mutant mouse model an increased number of misrouting axons was observed, with axons navigating several times across the floorplate or axons stalling at the midline [262]. In mice mutants for *Robo,* it was discovered that the function of Slit is just partially mediated by proteins of the Robo family. *Robo1*$^{-/-}$,*Robo2*$^{-/-}$, *Robo3*$^{-/-}$ mice displayed just a partial copy of the described *Slit1*$^{-/-}$, *Slit2*$^{-/-}$, *Slit3*$^{-/-}$ mutant mice phenotype [263].

Furthermore, it was recently described that Robo3 has exceptional properties in mammals and that it is no longer able to bind to Slits due to several amino acid changes within its Ig1 domain [264]. *Robo3* is normally extensively expressed on commissural axons during midline crossing.

Interestingly, in *Robo3*$^{-/-}$ mice commissural neurons are not able to cross the midline, indicating that Robo3 function within axonal guidance differ from the one of Robo1 and Robo2 [265], [266]. It was shown that Robo3 acquired new signaling properties and that it interacts with the Netrin1/Dcc signaling pathway, indicating that Robo3 instead of counteracting repulsion, rather promotes the attraction to the midline [251], [264].
In summary, Slit proteins and their receptors are key regulators in axonal guidance as mediators of cell and axon migration and as a linkage between axonal repulsion and axonal branching.

1.3.2.2 Netrins and their receptors

The first Netrin (Ntn) and in general the first described molecule influencing axonal navigation was Unc-6 (the orthologue of the vertebrate Netrin1) in *C.elegans* 25 years ago [267]–[269]. Since the initial discovery, the phylogenetically conserved Netrin protein family, with proteins of a size of about 70–80 kDa, has been studied intensively and implemented as crucial axonal guidance factor family, besides other important functions in many biological processes. In mammals the Netrin family is composed of secreted proteins (Netrin-1, -2, -3, -4, and -5) as well as membrane-bound proteins (Netrin-G1 and -G2) via glycosylphosphatidylinositol linkages [270]. Structurally, proteins of the Netrin family contain an N-terminal domain (VI), which is followed by epidermal growth factor-like domains (V-1, V-2, V-3, etc.) and then a C-terminal domain with positive charge [270], [271]. Netrin1 was discovered in 1994 and is so far the most investigated and studied within the Netrin protein family [272], [273]. Since its first description as guidance molecule of commissural axons in the vertebrate CNS development, Netrin1 became also associated with angiogenesis, organ morphogenesis as well as got attributed a crucial role in cell migration [272], [274]. Netrin1 is secreted from neural progenitor cells and floor plate cells and can act both as a chemorepellent or as a chemoattractant [246], [272], [275]. *Netrin1* expression was described in regions of the developing but also adult nervous system, including the forebrain, the spinal cord, the cerebellum and the optic disc. Additionally, *Netrin1* expression was detected also in the developing heart, the intestine, the lung, the pancreas and mammary gland [267]. Though their wide expression in numerous tissues, Netrins have largely been studied as axonal guidance factors during neural development. It was shown that *Netrin1* is expressed by floor plate cells and it was initially proposed that a Netrin1 protein gradient is established in the embryonic spinal cord when commissural axons are extending towards the ventral midline [272], [275], [276]. Furthermore, it was demonstrated that a Netrin1 source is able to attract extending commissural axons and to deflect these axons from their dorsoventral path within the embryonic neural tube [275]. Additionally, it was shown that ventricular zone progenitors produce high levels of Netrin1, which seem to carry the main responsibility for navigating commissural axons. However, the

role of floor plate cells secreted Netrin1 is so far not clear since its selective genetic ablation within FP cells does not interfere with commissural axon guidance [245], [246]. On the other hand, it was recently demonstrated that FP derived Netrin1 is indeed essential for navigating corticospinal axons across the midline [277].

The activities of Netrin are mediated by distinct receptors; which include in vertebrates DCC (deleted in colorectal cancer) and four Unc5 proteins (Unc5A-D) [270]. Compared to DCC, which is required for attractive responses to Netrin1, Unc5 proteins are mediating repulsive responses to Netrin1, acting alone or together with DCC [267], [270]. The majority of studies describing and investigating Netrin signaling focuses on the DCC receptor. DCC was first discovered as a candidate tumor suppressor in humans, with an allelic deletion of the 18q21chromosome in colon cancer [278]. Structurally, DCC receptors are composed of four Ig domains and six fibronectin type III domains in the extracellular space. Intracellularly, proteins of the DCC family contain three sequences termed the P1-3 motif which are highly conserved [279]–[281]. Besides DCC and Unc5 proteins, Netrins were shown to also bind to Down syndrome cell adhesion molecule (DSCAM) and Neogenin, a DCC paralogue (Figure 17) [270], [282].

1.3.2.3 Ephrins and Ephrin receptors

Another protein family within canonical guidance cues are Ephrins. They are cell-surface signaling molecules and were shown to play essential roles in numerous developmental processes, including axon guidance [283]. The Ephrin protein family can be divided into two subfamilies. There are five class A Ephrins which are linked to the cell surface by GPI linkages and three class B Ephrins which are characterized as transmembrane molecules [234]. Ephrins were allotted an essential role in organizing the connections of topographic projections. For instance, Ephrins were shown to be crucial for the connection of retinal ganglion cells to the proper layer of the optic tectum or the lateral geniculate nucleus [283], [284]. Ephrins can act as positive regulators as well as negative regulators for axonal branching and they can function as repellents for some axons but also as attractants for other axons. This versatility is the base of the mapping functions of the Ephrin protein family [283], [285]. Additionally to their role in topographic mapping, Ephrins were shown to be implicated in the pruning of axonal trajectories as well as short-range repellents and attractants in central and peripheral axon guidance [283], [285], [286].

The Ephrin receptors are named EphA (EphA1–8) and EphB (EphB1–4, EphB6) depending on the binding subgroup of Ephrin ligands, whereby EphA can bind most of A-type Ephrins and EphB most of the B-type Ephrins. Only EphA4 was shown to bind A-type and most B-type Ephrins. Additionally, a unique feature for Ephrins and their receptors is that an Ephrin receptor can also act as a ligand and an Ephrin can on the other hand also act as a receptor (Figure

17) [283], [285]. In general, the functions of the Ephrin receptors are often redundant, since their Ephrins binding affinities are quite promiscuous and their expression patterns are frequently overlapping. These features make the genetic analysis of the Ephrins and their receptors challenging, but also illustrate their highly variable putative function in a wide range of neuronal and non-neuronal cellular environments [283].

1.3.2.4 Semaphorin family and known receptors

Another protein family of secreted or membrane molecules that plays diverse roles in axon guidance is the Semaphorin family. In higher vertebrates there are around 20 different Semaphorins which all contain a Semaphorin-specific domain of approximately 500 amino acids. Semaphorins are known to function in short-range but also long-range guidance [234], [287]. The transmembrane protein Semaphorin 1a, or Fasciclin IV was the first identified and was described as an axon guidance factor of the pioneer sensory axons during the grasshopper limb development [288]. In vertebrate the first identified protein of the Semaphorin family was the secreted Sema3A, or Collapsin-1. It was identified *in vitro* during a biochemical brain extracts purification for factors with axonal repelling functions [289].

The signature 500 amino acids Semaphorin domain is essential for protein homo-dimerization as well as for the interactions between Semaphorin and their receptors [287]. The Plexin protein family is the best characterized class of Semaphorin receptors. Plexins are a single-pass transmembrane protein family with nine members in vertebrates (Plexins A1-A4, B1-B3, C1, D1). In invertebrates two orthologues have been identified (PlexA and PlexB). [290] Most Semaphorins can directly bind to Plexins, but their ligand/receptor binding can also be modulated by other molecules, like for instance by transmembrane proteins named Neuropilins [291]. Since the disruption of *Sema3A* in a mouse model resulted in defasciculating of several peripheral tracts, it was hypothesized that Semaphorin3A secretion into a motor and sensory axon surrounding environment is defining a permissive corridor in where the developing projections are able to grow in a bundled manner (Figure 17). Indeed, it was shown that proteins of the Semaphorin family are exerting a repellent action on axonal projections which is resulting in local repulsions, essential for correct fasciculation of numerous peripheral nerves [287], [292]. Additionally, via *in ovo* RNAi experiments in chicken it was recently demonstrated, that the receptor complex formation of PlexinA2 and the Nogo-66 receptor 1 is essential for proper midline crossing and the following turning of post-crossing axons [293].

Interestingly, beside axonal guidance, Semaphorins were shown to be involved in processes during tumorigenesis, angiogenesis and vascular development [294], [295].

1.3.2.5 Non-canonical axonal guidance molecules

Besides the canonical axonal guidance factors, also other molecules were assigned a role in navigating axons. Several of them are ECM components, including Collagen, Fibronectin,

Laminin, HSPGs and Tenascin. ECM components were shown to form stable complexes with numerous secreted axon guidance factors and to modulate their signaling, hence to influence the axonal outgrowth. Additionally, ECM components can regulate axon elongation and cell motility via neuronal Integrins interactions and therefore were shown to influence axonal navigation as well [296], [297].

Another class of molecules involved in axonal guidance are growth factors. They act mainly as attractive cues and mostly just on a subset of responsive neurons, indicating their specialized functions within axonal guidance. It was demonstrated that sensory axons show sensitivity to Neurotrophins and that Neuregulins induce responses in thalamocortical axon [298], [299]. Furthermore, Hepatocyte growth factor (HGF), Glial cell-derived neurotrophic factor (GDNF) as well as Fibroblast growth factors (FGFs) were shown to have the ability to instruct subsets of motor axons [300]–[302].

A third class of non-canonical axonal guidance molecules are secreted morphogenic factors. Normally morphogenes are crucial during early embryonic development to coordinate cell proliferation as well as fate-specification. Members of the Transforming growth factorB/Bones morphogenetic protein (TGFB/ Bmp), Wnt and Shh family were described to have a previously unknown axonal guidance role during later developmental stages, behaving as repulsive but also attractive cues. For instance, in mammals, proteins of the Wnt family have been described to establish an attractive guidance cue for post-crossing motor axons in the anterior direction. In D. melanogaster Wnt proteins are able to push axons away from the posterior commissure [303], [304] .Besides, spinal cord axons along the dorso-ventral axis were shown to be pushed away by a repellent cue formed by BMPs [305]. Plus, Shh proteins secreted by FP cells, are able to attract commissural axons in the spinal cord in collaboration with Netrin1 and act as repellent guidance cues on RGCs [306], [307].

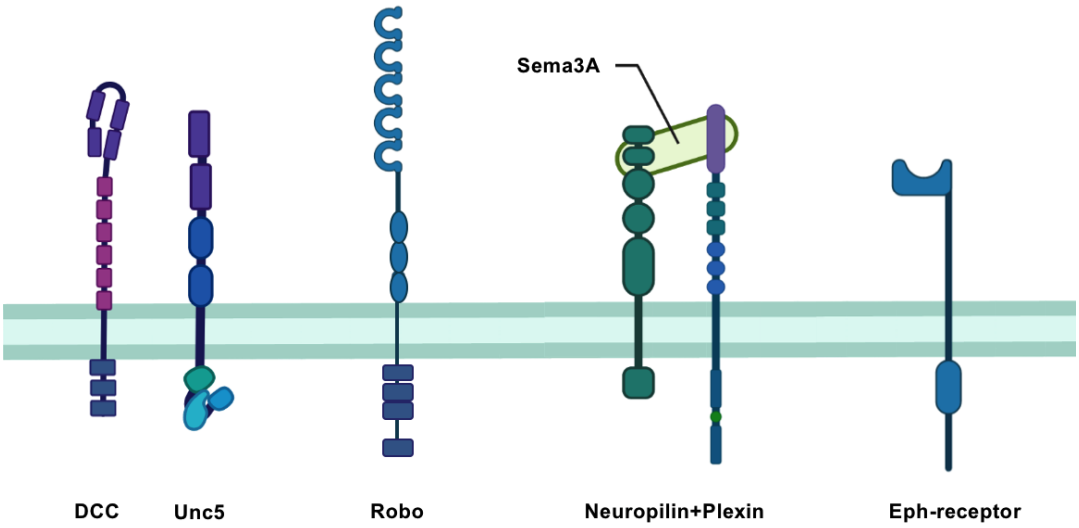

Figure 17: **Receptors of canonical axonal guidance factors:** Schematic representation of the DCC, Unc5, Robo, Neuropilin, Plexin and Eph-receptor.

1.3.3 Axon guidance mechanisms in Zebrafish

Our favorite model organism, the zebrafish, has been extensively studied to investigate regulating mechanisms for the establishment and function of neural circuits. The zebrafish nervous system is relatively simple and highly stereotypically organized. Many mechanisms and structures are highly conserved and were shown to be coordinated by the same molecules sets of mammals, especially in the context of axonal pathfinding. Hence, several embryonic axonal tracts in zebrafish have been used as models for the understanding of the conserved mechanisms which are driving the elongation of axons [308].

One of these models studied in zebrafish is the development of first commissural tracts, the anterior commissure (AC) and post-optic commissure (POC). In zebrafish, a bilaterally symmetrical axonal scaffold is developed by around 1 dpf. This scaffold structure is made of longitudinal and commissural tracts, and acts as a template for the further developing zebrafish embryonic nervous system. The ventro-rostral cluster (VRC) and the dorsal rostral cluster (DRC) are two neuronal nuclei from where two big commissures are originating, situated in the most rostral region in the developing forebrain. At 1 dpf the left and right VRCs are connected by an axon bundle and the POC is forming. Beside the commissural axons, a caudally growing longitudinal tract is also projected from the VRC, named tract of the post optic commissure (TPOC). The second commissure, the AC, is formed shortly after the POC between the dorsal rostral clusters. The supra-optic tract (SOT) is formed by a group of axons, originating from the DRC and navigating towards the VRC in the dorso-ventral direction. As soon as the developing neurites of the SOT reach the VRC, they can grow rostrally to join the axons of the VRC in the POC or be integrated in the TPOC by turning caudally (Figure 18) [309]. It has been described that this development of first commissural tracts and the axonal navigation along the POC and AC is guided by a multifaceted cluster of guidance factors. It was demonstrated that the formation of the POC and AC is severely disrupted if expressions of single or multiple axonal guidance factors are altered or absent, indicating the tight regulation of these factors during commissure development [310]–[314]. In the zebrafish mutant for the *pax2* transcription factor, named *noi* mutant, POC axons, even though they are able to cross the midline, are not able to interconnect properly and show a less fasciculated phenotype than in wt control fish. Additionally, *noi* mutants display disturbed expression of *netrin1* and *shh*, indicating a sensitivity of POC neurons for these guidance cues [310]. Another example for a zebrafish study and axonal guidance factors for commissural axon development is from Barresi et al. [315], proposing that Slit signaling is essential for proper AC and POC establishment. They describe, that *silt2* and *slit3* are expressed in the region between the AC and POC and that

Silt2 and Slit3 apply a repulsive force which keeps the high fasciculation of the axon bundles and is protecting against abnormal branching. In addition, Slit1a is described as a guidance cue forming a permissive corridor for correct axon elongation. Additionally, it was recently demonstrated that also the Collapsin response mediator protein 2 (CRMP2) and CRMP4 are playing a role in AC and POC development, signaling through the Semaphorin3/Nrp1a signaling pathway [316].

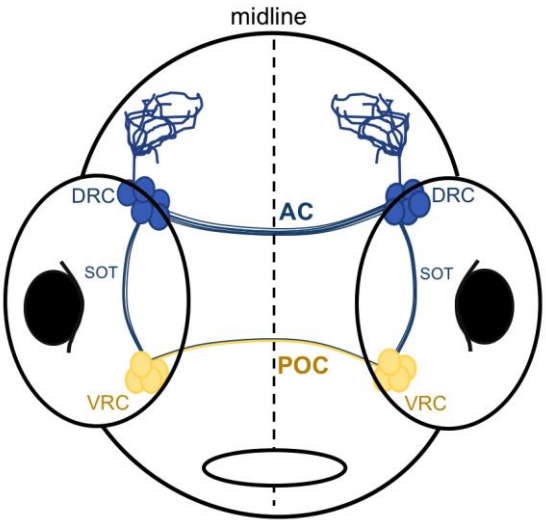

Figure 18: **Development of the first commissural tracts in zebrafish:** Frontal representation of the zebrafish anterior commissure (AC) and post-optic commissure (POC) at around 24hpf showing DRC neurons extending to and forming the SOT and AC. Beside VRC neurons are establishing the POC.

Another model for axonal guidance studies in zebrafish are the longitudinal and commissural tracts in the hindbrain. In general, the hindbrain of vertebrates is characterized by a composition of sensory-motor networks which are essential for directing crucial vital functions like respiration, locomotion and vision [317]. In the zebrafish, the distinctive morphological organization of eight segments named rhombomeres is characteristic for the embryonic hindbrain [318]. Mauthner cells, two large reticulospinal neurons, are the first emerging neurons in the zebrafish embryonic hindbrain. Their cell bodies are found symmetrically in the 4th rhombomere's center. From around 21-23 hpf, the Mauthner cells start to extend their axons and after midline crossing, they turn caudally and pioneer the hindbrain medial longitudinal fascicle (MLF), parallel to the FP. Later the MLF will grow and thicken since it will be joined ipsilaterally or contralaterally from other reticulospinal neuron axons with somas located in hindbrain rhombomeres. An additional pair of tracts, the lateral longitudinal fascicles, will grow caudally, beginning from the trigeminal sensory neurons [309]. Axonal guidance processes in the zebrafish hindbrain gained a lot of interest, since it was suggested that the FP plays a crucial role in the patterning of these axonal projections. Disturbed FP specification as well as maturation was shown to result in severe guidance mistakes of axons of the longitudinal and commissural tracts in the hindbrain.

Several studies discovered that canonical guidance molecules are playing a role in axonal guidance in the embryonic hindbrain. For instance, it was described that the Slit and Robo pathway is important for commissural axon guidance in the hindbrain, including also the Mauthner cells. In zebrafish with a loss of function for *robo3*, the commissures of the hindbrain display a high disorganization and defasciculation. Mauthner axons are not able to properly cross the midline and instead of growing across the FP and then turning caudally, they are projecting ipsilaterally to the spinal cord [319]. Same Mauthner axons disorganization and defasciculation could be observed in a study overexpressing the robo ligand *slit2* [320]. Furthermore, also Semaphorins were connected to guiding trajectories of hindbrain projections. The knock-down of *nrp-1A* or *sema3D* results in a high disorganization of the MLF [311]. Using a *dcc* mutant zebrafish model, which introduces a single amino acid substitution within the *dcc* gene resulting in the disruption of the netrin binding site also, the requirement of the netrin pathway for correct axonal guidance of commissural hindbrain neurons was demonstrated. These mutant fish displayed numerous commissural hindbrain neurons misprojections and ectopic ipsilateral neurites development [321].

Even though, zebrafish has exclusively crossed retino-tectal projections and is quite different from mammalian vertebrates, its retino-tectal system is a widely used model structure to investigate the regulating mechanisms for axonal pathfinding. The system can be divided into two main areas, the retina and the optic tectum. From the retina which is sensitive to light stimuli the visual information are transmitted through the retinal ganglion cells (RGCs) to their key midbrain target region, the optic tectum. The optic tectum is then responsible for the visual input integration, as the mammalian homologous, the superior colliculus [322], [323]. The optic nerve, made of densely bundled RGC axons exiting each eye, is navigating in the ventral diencephalon toward the midline. There, the axons of the optic nerves intercross and form the optic chiasm. As the retinal axons leave the midline they form the optic tract and grow dorso-caudally, hence reaching the optic tectum's contralateral lobe. Once reached the contralateral lobe of the tectum each single neurite is terminating its journey in an exceptionally organized manner, and the positions of their cell bodies within retina is reflected in a stereotyped retinotopic map [322]–[325]. Furthermore, it was described that RGC projections are also organizing in a regulated laminar structure, where single synaptic laminae within the tectal neuropil is innervated by one single axon [323], [326].

During the last years numerous factors influencing retino-tectal projections patterning and correct RGC guidance have been discovered. These guidance factors are affecting proper RGS growth at many different points during the axonal path, for instance exiting the eye, crossing the midline, forming the retinotopic maps or during the organization of their distinct synaptic lamination. The loss or downregulation of these factors were reported to results in disturbed RGC growth [322], [327], [328]. Strikingly, various canonical guidance molecules,

ECM components as well as midline differentiation affecting genes were associated with proper retinal axons navigation, illustrating the requirement of multiple and diverse signals for appropriate retino-tectal trajectories development and navigation [314], [328]–[331]. For instance in the well-studied *astray/robo2* zebrafish mutant the axons of the RGS show numerous misrouted axon projections to ectopic extra-tectal targets or to the ipsilateral tectum [329], [332]. It was proposed that, RGCs which are expressing *robo2*, are sensitive to the repellent guidance cues of Slit2 and Slit3, which are in turn expressed along the RGCs axonal navigation path. With the loss of function for *robo2*, RGC axons are not able anymore to react to the repulsing Slit signaling, hence instead of growing towards the contra-lateral tectum they are navigating with aberrant trajectories. Additionally, Slit/Robo signaling might be playing a role on various RGCs elongation aspects, since *robo2* loss of function also results in disturbed RGC laminar segregation in the tectal neuropil [329], [332], [333]. Additionally, it was recently further investigated how Slits (Slit2, Slit3) are acting together to facilitate proper retinal axon midline crossing. Single mutants for *slit2* or *slit3* did not show the whole severity of axonal guidance defects of robo2$^{-/-}$ mutants, however *slit2*$^{-/-}$, *slit3*$^{-/-}$ double mutants were characterized by much more severe defects than the singles mutants, and comparable with single robo2$^{-/-}$ mutants. *In vivo* time-lapse tracking experiments lead to the suggestion that Slit2 and Slit3 are both working via Robo2, however given their diverse spatial expression patterns, most likely through slightly different mechanisms [334].

In summary, these observations in the zebrafish model organisms on mechanisms for the establishment and function of neural circuits prove that during early embryonic development complex axonal guidance patterns are necessary for proper and correct axonal navigation, essential for correct CNS physiology.

1.3.4 Open questions in the field

Despite this vast set of identified players andcting often in apparently molecular redundant mechanisms, the mystery of the axonal guidance puzzle is nowhere near being solved in its totality. In fact, due to the high redundancy of biological systems, there might be the possibility that the family of axon guidance factors contains even more specific members. It is not clear if there are other major families of guidance molecules which have to be identified and/or if already established guidance factors have additional functions, especially when it comes to navigating a specific subset of responsive axons, for instance during embryogenesis with a constantly changing extracellular environment.

So far also the complete mechanisms of how axonal growth cones are capable of regulating cue specific responses are not fully understood, and how the switch from repulsive to attractive behavior at a specific time and specific place of the navigation path is modulated remains a partially unanswered question. There are different theories how this response could be

regulated, for instance by fine-tuned expression control via transcriptional, translational, and post-translational mechanisms with the right combination of expressed receptors on each growth cone. However, there are still many open questions concerning the regulation of guidance receptor expression and the respective transcription factors and how environmental guidance cues are integrated into changes in neuronal gene expressions. Also, the mechanisms which are ensuring that the numerous different signals present in the extracellular environment are properly integrated and the way different axonal guidance pathways interact to facilitate proper axonal navigation are still poorly characterized [335]–[338].

During the last years, the knowledge of axon guidance control mechanisms within the CNS midline has increased enormously right up to the identification of specific molecular axonal guidance control mechanisms [249], [250]. These mechanisms appear to be highly conserved across evolution. Exception to this rule where also recently demonstrated. For instance, it was established that a key receptor for spinal cord and hindbrain commissural axons named Robo3 has exceptional properties in mammals [264]. Interestingly, the gene DCC was shown to be lost twice during evolution in two bird lineages via a phylogeny analyses across vertebrates [339]. Together, these findings suggest that the midline guidance molecular repertoire and molecular mechanisms involved are more diverse and complex than initially assumed.

1.3.5 The hunt for the Meteorins receptor(s)

For a long time, nothing was known about the molecular nature of the Metrns receptor(s). The first publication describing Metrn downstream pathways connects its function with the activation of the Jak-STAT3 pathway[2]. The Jak-STAT3 pathway as key regulator for astrocyte differentiation in NSC [35] is crucial for catalyzing the onset of gliogenesis [36]. In a cell culture model, Metrn was shown to reliably induced tyrosine phosphorylation of STAT3, an increase of nuclear concentration of STAT3 as well as the phosphorylation of Erk1/2. These results are indicating that Metrn might be an activator of the Jak-STAT pathway [2], [37].

With rising number of possible Meteorins functions and the growing interest in the Meteorin Protein family also the hunt for the receptor(s) continues. Remarkably, it was recently shown that METRNL as a KIT receptor tyrosine kinase ligand is promoting heart repair in the context of ischemic tissue repair [6]. METRNL binding to KIT was the first description of a Metrns receptor. Interestingly, it was demonstrated that *Kit* is also expressed in commissures and that commissure in mice mutants for *Kit* display a significant delay in exiting the midline [237].

However, so far only METRNL was shown to bind to KIT and so far only in the context of ischemic tissue repair [6]. Short after the identification of the first Metrnl receptor, it was published that Metrn is binding to Htr2b to regulate reactive oxygen species levels in hematopoietic stem/progenitor cells [7]. However, we hypothesize that there might be more than one Metrnl or Metrn receptor, considering the wide range of described Metrns functions especially during early embryonic patterning processes.

Therefore, a main aim of this work is/was to hunt for further Meteorins receptor(s) since the identification of the receptor(s) will help to fully understand the downstream signaling pathways critical for Meteorin's biological function.

1.4 AIMS OF THE STUDY

Meteorin proteins were discovered as a novel independent family of secreted proteins. In the last few years *Meteorins* expressions and functions have been studied broadly and revealed a great diversity and numerous possible roles for these proteins. However, a wide spectrum of possible Meteorins functions and mechanisms of their actions remain to be investigated. Therefore, the major aims of my PhD project were:

1. the further investigation of the function of Meteorins in zebrafish during early embryonic patterning and axonal guidance
2. and most notably the identification of Meteorin receptor(s).

The first emphasis in this thesis is to unravel if Meteorins are potential novel factors for proper KV formation and vertebrate left-right patterning. Via the CRISPR/Cas9 mediated generation of *metrns* LOF alleles I analyzed *metrns* LOF phenotypes during the establishment of the embryonic left-right axis. Besides, I took advantage of the generated *meteorins* mutants to establish Meteorin proteins as novel axonal guidance factors, playing an essential role during the development of the vertebrate CNS and axonal midline crossing, especially in commissural axon guidance. To this end, I analyzed the effect of *meteorin* LOF on the axonal navigation path establishment as well as its connections to already well-established axonal guidance factors.

The identification of Metrn receptor(s) is essential to dissect Metrn pathways. Hence, for the second goal I aim to fill the crucial gap using state-of-the art biochemical screening approaches to identify in near-physiological conditions putative receptor(s) for Metrns, and to critically advance our understanding of their biological functions.

2 MATERIALS AND METHODS

2.1 Zebrafish husbandry

Zebrafish (*Danio rerio*) were kept at 28°C with a 14h light/10h dark cycle and maintained in the animal facility of Institute de la Vision. The facility was built consistent with the respective local animal welfare standards. The Committee on ethics of animal experimentation animal-approved all experimental procedures and handlings. All animal experiments were conducted in conformity with French and European Union animal welfare guidelines.

2.2 CRISPR-Cas9-mediated mutagenesis of metrn, metrnl1 and metrnl2 and whole embryo genomic DNA extraction

Guide sequences for sgRNAs were cloned into the DR274 (Addgene 42250) plasmid vector, digested before with the BsaI restriction enzyme (NEB). SgRNAs were synthetized via *in vitro* transcription (Megascript T7 transcription kit, Ambion AM1334). Following transcription, sgRNAs were purified using the Qiagen RNAeasy Mini Kit. The purified sgRNAs quality was checked via 2 % agarose gel electrophoresis. The sgRNA target sequences are the following:

	Sequence (5'->3')
metrn	CCACCACACCCGGCCCAGCC
metrnl1	GGTGTATCTCCGCTGCGCCC
metrnl2	CCAGAAACAGCGCCCCCTCC

Cas9 mRNA was made as described in Hwang, Fu et al. 2013 [340]. To achieve targeted mutagenesis at the loci of *metrn*, *metrnl*1 and *metrnl2*, 150ng/ml of *Cas9* mRNA together with 200ng/ml of sgRNA were injected into one-cell stage zebrafish embryos. Injected embryos were grown to adulthood and genotyped for mutation in their offspring.
For genomic DNA extraction, 25 5-dpf embryos were pooled and digested for 1h at 55°C with proteinase K (0.17 mg/mL, Roche Diagnostics) in 0.5mL lysis buffer (10 mM Tris, pH 8.0, 10 mM NaCl, 10 mM EDTA, and 2% SDS). Proteinase K inactivation was achieved by a following 95°C incubation for 10min. To analyze the frequency of indel mutations, target genomic loci were amplified by PCR using the Phusion High-Fidelity DNA polymerase (Thermo Scientific). Following, PCR amplicons were cloned into the pCR-bluntII-TOPO vector (Invitrogen). Plasmid DNA was extracted from single colonies and sent for Sanger sequencing (Eurofins, GATC). Mutant alleles were identified by aligning with the respective wt sequence.

2.3 Mutants genotyping and generation of triple mutants

Following genomic DNA extraction, 1 µl per extracted DNA was added to the respective PCR amplification reaction containing 1x PCR reaction buffer, 1,5mM MgCl2, 70 ng of gDNA, Taq DNA Polymerase (5U/µl) and 0.5 µM of each primer in a final volume of 20 µl.

	Sequence (5'->3')
metrn-fw	CTGTGTTGACTGCTGGCTG
metrn-rev	GTGGTTTAGTGGTGTTCTTACAATGA
metrnl1-fw	TCCCATGCCTGGACCTCATA
metrnl1-rev	AGACGGAGAGAAGAGACGCT
metrnl2-fw	TGTTGATCAGCAGTGTGTGCGTAGC
metrnl2-rev	GTCCTCCGCTGATCTACGTG

The genotyping PCRs were performed at the annealing temperature of 60°C with 35 cycles. *Metrn* and *metrnl2* PCR products were loaded on 2 % agarose electrophoresis gels to distinguish between wild type and mutant alleles (*metrn*, the size of wild type allele: 598bp, size of mutant allele: 482bp; *metrnl2*, the size of wild type allele: 242bp, size of mutant allele: 156bp). For *metrnl1*, the PCR product was digested with the PasI enzyme at 55°C overnight (o.n.) and the digestion product was analyzed on a 2% agarose electrophoresis gel (*metrnl1*, the size of wild type allele: two fragments of 107bp and 94bp, size of mutant allele: 201bp).
Triple mutants were obtained by respective incrosses of homozygous *metrn* and *metrnl1* mutants resulting in double heterozygous mutants. Double heterozygous mutants were crossed with homozygous *metrnl2* subsequently and genotyped for identification of triple heterozygous mutants. Triple heterozygous mutants were intercrossed and triple homozygous mutants were identified by genotyping.
In the described experiments, heterozygous triple mutants were obtained by outcrossing female triple mutants with male wildtype, if not stated differently.

2.4 Whole embryo RNA extraction and cDNA synthesis

Whole embryo RNA was extracted from zebrafish embryos in the respective developmental stage with TRIzol reagent (ThermoFisher Scientific) and the TURBO DNA-free kit (ThermoFisher Scientific). For cDNA synthesis 1µg RNA was retrotranscribed using the SuperScript III First-Strand Synthesis system (ThermoFisher Scientific) and random primers. The quality and concentration of extracted RNA and synthesized cDNA was determined with a NanoDrop spectrophotometer.

2.5 Quantitative Real-Time PCR (q-RT-PCR)

The SYBR Green PCR Master Mix was used for q-RT-PCR and assays were conducted according to the manufacturers protocol. *Ef1a* was used as reference gene as described from Tang, Dodd et al. 2007 [341]. All q-RT-PCR experiments were performed in at least biological triplicates with technical triplicates each. The mean values of triplicate assays were calculated with the delta CT quantification method as described from Valcu and Valcu 2011 [342]. For the p-value calculation a student T-test was applied. Primer used are the following:

	Sequence (5'->3')
metrn-fw	GCGTCAAGCCTGATCCAG
metrn-rev	CGTACATGGGCTGGGC
metrnl1-fw	GCCAAACACGCTGTCACC
metrnl1-rev	CCTGGATGTTGAAGCAGTGC
metrnl2-fw	GCACAGTATTCCAGTGATC
metrnl2-rev	CGTAGATCAGCGGAGG
spaw-fw	CGAGTGACAACATCCAGCTC
spaw-rev	CGTCTACTGATTTAACGCTGC
lft1-fw	GCAACTACGGCTACGGAGAG
lft1-rev	GTGCGTCATGTAGATAGCTGG
lft2-fw	GGCAATGCAGATATTACCGGAG
lft2-rev	GACTCTGGCGTGGTTTATCG
dand5-fw	GTCAAACTAAACCCTCATTTTCTGC
dand5-rev	CATCTCGAGCCCTTGTTTCC

2.6 *In situ* hybridization in zebrafish and chicken

Respective cDNA fragments were amplified by PCR from zebrafish cDNA using the following primers:

	Sequence (5'->3')
metrn-fw	GAAGTGGACTTTCTCAGGC
metrn-rev	CAAGGATTGTTTGGCCTGTTCG
metrnl1-fw	GTATTTGCTGTCGGTTGTGC
metrnl1-rev	CAGGGGTTGGTCCCTTGCTGCCG
metrnl2-fw	CTGAAGGCTCTCTGCAGTGG
metrnl2-rev	ATCACAGCGCTGCAGAATCT
spaw-fw	GGTACCCGCTGTACATGATGC
spaw-rev	CCGCTCAGGTTGGTAGAGC

lft1-fw	CACGAAGACATGAAAGACGC
lft1-rev	GATACATCATCGGTAGTGGC
lft2-fw	GCAATGCAGATATTACCG
lft2-rev	CACCTCTCATCTGAGAGC
dand5-fw	CGTTCAGAAATTCACCAAGTCG
dand5-rev	GTAGAGATGCAGAGAGGGGC
myl7-fw	GCAGACAGTGAACATGGC
myl7-rev	CAGTCTGTAGGGGGCAGC
gata6-fw	GGTTATAACGACACGC
gata6-rev	CCGTGTAACTTGGTG
cas-fw	GCAGTGCCACTATTTGC
cas-rev	GGTACTGGTCAAATTCACTG
ntl-fw	GCTTGAAGACGCGGAGTTG
ntl-rev	CCAGCTGTCATGAGACGC
sox17-fw	GCTCAGTCCGCTCTCAGAC
sox17-rev	GGTGTCTAAAGTTGATGGGCAG
kita-fw	CGGCTAACAGTACCACTG
kita-rev	GCAGAGACAGACTTTCACCAG
kitb-fw	GGTTACATGCCCATGAGGTC
kitb-rev	GCCTCTGCAAGCCTGG
htr2b-fw	CATCCAGCACAGCCAG
htr2b-rev	GTCACTGATGAACGAAAGG

Respective cDNA fragments were amplified by PCR from chicken cDNA using the following primers:

	Sequence (5'->3')
metrn-fw	GGATCAGTGCAGCTGGAGG
metrn-rev	CGCCAGAAATTCCCCCTCTT
metrnl1-fw	GCAGTACTCCAGCGACC
metrnl1-rev	CCAATTTCACATGGATTTAGCC
fgf8-fw	GCTCCTCGCTCTTCAGC
fgf8-rev	CTGGCGCTGGAGTTTCG

In vitro transcription of Digoxigenin/Fluorescent-labeled *in situ* probes was executed using the RNA Labeling Kit (Roche Diagnostics Corporation) according to company's instructions. Zebrafish embryos were manually dechorionated at the appropriate developmental stage(s) and fixed in 4% paraformaldehyde (in PBS, pH 7.4) for 2 hours at room temperature or 4°C o.n. Whole-mount *in situ* hybridizations were performed as described in Thisse and Thisse

2008 [343]. Chicken embryos were dissected at the appropriate developmental stage(s) and fixed in 4% paraformaldehyde (in PBS, pH 7.4) for 4 hours at room temperature or 4°C o.n. Whole-mount *in situ* hybridizations were performed as described in Streit and Stern 2001 [344]. *In situ* samples were imaged on a Leica MZ10F stereomicroscope. Images were processed and analyzed using ImageJ software. Color balance, brightness and contrast were applied uniformly.

2.7 Hybridization chain reaction (HCR)

All HCR probes and solutions were purchased from Molecular Instruments®. Dechorionated embryos at the appropriate developmental stage(s) were fixed in 4% paraformaldehyde in PBS (pH 7.4) for 2 hours at room temperature, followed by several washes with PBS to stop the fixation. With a series of MeOH washes the embryos were dehydrated and permeabilized. The HCR was performed as described from the manufacturer. HCR samples were imaged on an inverted confocal microscope Olympus FV-1000, employing a 20x oil immersion objective (NA 0.85). Z-volumes were acquired with a 5µm resolution and images were processed and analyzed using ImageJ.

2.8 Analysis of DFC phenotype and migration

In the DCF malformation analysis Bayesian inference was used to recover the maximum-likelihood value for the malformation probability. The outcome of an experiment was considered to be a binary random variable (malformed or normal phenotype) whose probability depends solely on the experimental condition. The total number of malformed phenotypes per experiment is therefore binomially distributed. The posterior distribution is obtained by inverting this binomial distribution using Bayes theorem, under a uniform prior. Under these hypotheses the maximum-likelihood estimate for the malformation probability is simply given by the empirical malformation frequency. The standard deviation of the posterior distribution was sued to provide a confidence interval for our estimate (black error bars). P-values were evaluated using Fisher exact test on the number of malformed and normal phenotypes. AP to VP DFC migration was calculated as the percentage of the total embryo length using ImageJ.

2.9 mRNA synthesis and injection

Zebrafish *spaw*, *metrn* and *metrnl1* cDNA fragments were amplified by PCR from zebrafish cDNA using the following primers:

	Sequence (5'->3')
metrn-fw	ATGGCCAGTTACTCAGAAGATCAG
metrn-rev	TCAGTCATTGACCAGAGTGCAG
metrn-Xba1-fw	GCCTCTCGAGATGGCCAG
metrn-Xho1-rev	ATAGTTCTAGAGTCAGTCATTGACC
metrnl1-fw	ATGCTCTCGCCGTTCTT
metrnl1-rev	TCAGTCTGTTTCCAAATGAC
metrnl1-Xba1-fw	GCCTCTCGAGATGCTCTC
metrnl1-Xho1-rev	ATAGTTCTAGAGTCAGTCTGTTTC
spaw-fw	ATGCAGCCGGTCATAGC
spaw-rev	GTCAATGACAGCCGCACTCC
spaw-Xba1-fw	CCTCTCGAGATGCAGCCG
spaw-Xho1-rev	GTTCTAGAGTCAATGACAGCCGC

The fragments were inserted into a pCS2+ plasmid linearized with Xho1 and Xba1 (NEB) using a Quick Ligation Kit (New England Biolabs). The ligation products were linearized subsequently using Not1 restriction enzyme. mRNAs were synthetized by *in vitro* transcription using the mMESSAGE mMACHINE Sp6 kit (Invitrogen) and 150 ng/µl were injected into 1- to 4-cell-stage zebrafish embryos.

2.10 Design and injection of antisense morpholino oligonucleotides

Used antisense morpholino oligonucleotides were previously published from Barresi et al., 2005 [315] and Ablooglu et al., 2010 [209]. The sequences are the following:

	Sequence (5'->3')
slit1a	GACAACATCCTCCTCTCGCAGGCAT
slit2	CATCACCGCTGTTTCCTCAA GTTCT
slit3	TATATCCTCTGAGGCTGATAGCAGC
itgαV1	AGTGTTTGCCCATGTTTTGAGTCTC
itgβ1b1	GGAGCAGCCTTACGTCCATCTTAAC
standard control	CCTCTTACCTCAGTTACAATTTATA

All MOs were obtained from Gene Tools (Philomath, OR, USA). MOs were injected in 1- to 4-cell-stage zebrafish embryos.

2.11 Whole-mount immunohistochemistry and quantification

Embryos were fixed at their respective stage in 4% paraformaldehyde (in PBS-Tween) for 2h at RT or o.n. at 4°C and subsequently washed three times in PBS-Tween. To promote permeabilization the samples were incubated for 30min in 1% TritonX100 (in PBS-Tween) and subsequently, for 1h at RT in blocking solution (10% Normal Goat Serum, in PBS-Tween). This followed an o.n. incubation, at 4°C, with a mouse anti acetylated tubulin monoclonal antibody (1/200 dilution in blocking solution, Sigma # T7451).

After five washes in PBS-Tween the samples were incubated with an Alexa Fluor 488 anti-mouse IgG secondary antibody (final concentration 1/200 in blocking solution, Life Technologies) o.n. at 4°C. The next day, embryos were washed five times in PBS-Tween before mounted with 1% low melting point agarose in glass-bottom cell tissue culture dishes (Fluorodish, World Precision Instruments, USA).

For imaging of the KV cilia, an inverted confocal microscope Olympus FV-1000 was used, employing a 40x oil immersion objective (NA 1.30). Z-volumes were acquired with a 0.5µm resolution and images were processed and analyzed using ImageJ. Cilia numbers were quantified using the CellCounter plugin. Cilia length and KV size were acquired using the measuring tool, whereby KV size was measured as diameter from the two most distant cilia tips. For anterior and post-optic commissure imaging an inverted confocal microscope Olympus FV-1000 was used, employing a 20x oil immersion objective (NA 0.85). Z-volumes were acquired with a 2µm resolution and images were processed and analyzed using IMARIS software.

2.12 Fluorescent microspheres injection and analysis

Embryos were manually dechorionated and mounted in 1% agarose and fish water. FluoSpheresH fluorescent microspheres (0.5 mm, Polysciences) were injected into KV at the 6ss-10ss as described in Borovina et al. 2010 [345]. Imaging was conducted with a 40x water dipping objective using an upright Yokogawa CSU-X1 spinning disk scan head, mounted on a DM6000 upright Leica microscope and a CCD CoolSnap HQ2 camera at 4 Hz using the green channel at 0.25um resolution on a single z-plane. Beads trajectories extraction was performed using an already developed toolbox [346]. The size detection parameter was set to 0.75-1.25um objects with a brightness superior to the 0.01 percentile of the whole image. Objects that travelled less than 2.5um between two consecutive frames were linked into the same

trajectory. Analyses between different genotypes were performed using a custom-made Matlab code. For legibility, trajectories plots only show 20 tracked beads. MSD analysis was conducted according to Tarantino et al. (2014) [347] using already published code (https://tinevez.github.io/msdanalyzer/). Average MSD plots only show particle tracked between 1 and 8 s. Very short tracking durations do not permit to correctly estimate displacement properties and less then 1% of the particles were tracked during more than 8 s.

2.13 Molecular cloning

The pCMV6-XL4 FLAG -Fc constructs were generated via digestion of a pCMV6-XL4 FLAG-BMP2-Fc plasmid with Not1 and Xba1 and copy and paste of our genes of interest using a Quick Ligation Kit (New England Biolabs). Respective cDNA fragments were amplified by PCR from zebrafish (Z) and mouse (m) cDNA using the following primers:

	Sequence (5'->3')
Zmetrn-fw	ATAAGAATGCGGCCGCCACCATGGAGATTTGGGGCTTCC
Zmetrn-rev	ATAAGAATTCTAGACCATCGTTCACCAGTGTACAGGG
Zmetrnl1-fw	ATAAGAATGCGGCCGCCACCATGGTGTCTCCCTTCCTGG
Zmetrnl1-rev	ATAAGAATTCTAGACCATCTGTCTCCAGGTGACAAGG
Zntn1a-fw	ATAAGAATGCGGCCGCCACCATGGGATATGGAATGAGCATGTTCG
Zntn1a-rev	ATAAGAATTCTAGACCTTGTTTTTGTTTTTCTTTCCTTTTTTCCCAGC
mMetrnl-fw	ATAAGAATGCGGCCGCCACCATGGGCTACTCGGAAGACCG
mMetrnl-rev	ATAAGAATTCTAGACCGTCCAGTGCCATCTCACATG
mMetrnl-fw	ATAAGAATGCGGCCGCCACCATGCAGTACTCCAGCGACCTGTGC
mMetrnl-rev	ATAAGAATTCTAGACCCTCCATATTGATTTCACAGGG

The pCMV6-XL4 FLAG-BMP2-Fc was a gift from Davide Comoletti (Addgene plasmid # 115771; http://n2t.net/addgene:115771 ; RRID:Addgene_115771).

The AP-tag backbone plasmid for the production of Metrn-AP/Metrnl1-AP fusion proteins were purchased from ©GenHunter Corporation. Metrns cDNA fragments were amplified from respective cDNA. Following Primers were used:

	Sequence (5'->3')
Zmetrn-fw	ATCTCGAGGAAGCGCTCTCTTCCTACTCTGAGGACCAG
Zmetrn-rev	GAGTTTTTGTTCGGGCCCTTATCGTTCACCAGTGTACAG
Zmetrnl1-fw	ATCTCGAGGAAGCGCTCTCTCAGTATAGCTCCGACCAG
Zmetrnl1-rev	GAGTTTTTGTTCGGGCCCTTATCTGTCTCCAGGTGACAAG

mMetrn-fw	AGCTGCTAGCGCCACCATGCTGGTAGCCACGCTTC
mMetrn-rev	CATGTGAGATGGCACTGGACTCCGGAAGCT
mMetrnl-fw	AGCTGCTAGCGCCACCATGCGGGGTGCGGTGTG
mMetrnl-rev	CTGTGAAATCAATATGGAGTCCGGAAGCT

The pCX-V5 and -HA constructs were generated via digestion of an empty pCX vector with EcoRV and the insertion of a gBlocks® Gene Fragment including a Kozak sequence around Met1, a linker and the V5/HA tag after the last residue of the gene of interest. The 5'->3' sequences were the following:

	Sequence (5'->3')
V5-tag	TTTTGGCAAACAATTGTGATGCCACCATGGACTGAGTCTTCGCTATGT
	GCAGAAGACGTCGAGTTCGAAGGTAAGCCTATCCCTAACCCTCTCCTC
	GGTCTCGATTCTACGTAGATCTTTAATTAAACCCCGGG
HA-tag	TTTTGGCAAACAATTGTGATGCCACCATGGACTGAGTCTTCGCTATGT
	GCAGAAGACGTCGAGTTCGAATACCCATACGACGTCCCAGACTACGC
	TTAGATCTTTAATTAAACCCCGGGATCTTT

Subsequently the generated pCX-V5 and -HA constructs were digested with BbsI-HF enzyme (NEB) and the genes of interest were inserted using a Gibson assembly kit (NEB). Respective cDNA fragments were amplified by PCR from zebrafish cDNA using the following primers:

	Sequence (5'->3')
iltgαV1-HA-fw	ACAATTGTGATGCCACCATGGCTGCTCCCGGGCGCCTG
itgαV1-HA-rev	ACGTCGTATGGGTATTCGAAGGTTTCAGAGTTTCCTTCGCCATTCTCATG
itgβ1b1-V5-fw	ACAATTGTGATGCCACCATGAATTTGCAACTGGTTTCCTG
itgβ1b1-V5-rev	ACGTCGTATGGGTATTCGAATTTTCCCTCATACTTCGGATTG
kita-HA-fw	ACAATTGTGATGCCACCATGGAATATCACTGCGTTCTGTTTAC
kita-HA-rev	ACGTCGTATGGGTATTCGAAGACTACAGGGTGACTTGG
kitb-HA-fw	ACAATTGTGATGCCACCATGGGACACTCGTGGTTTCTAC
kitb-HA-rev	ACGTCGTATGGGTATTCGAATATGCTCTGATGTTCCAGAAAAAC
gp130-V5-fw	ACAATTGTGATGCCACCATGGACACTTCACATCATTGGCTGTTG
gp130-V5-rev	GGGATAGGCTTACCTTCGAACTGCGGTCGATACCCGCTC

The AVEXIS plasmids were kindly generated and donated from the lab of Rob Meijers, EMBL Hamburg. In principal for the insertion of a gene of interest into the AVEXIS prey or bait vector, the plasmids were digested with Not1 and Asc1 and the genes of interest, amplified from

respective cDNA with fused Not1 and Asc1 restriction sides, were integrated using a Quick Ligation Kit.

2.14 Western Blots

For Western blotting, samples were diluted in Laemmli 2X buffer (4% SDS, 10% 2-mercaptoethanol, 20% glycerol, 0.004% bromophenol blue, 0.125 M Tris-HCl, pH adjusted to 6.8) and incubated at 95°C for 5min. Subsequently, samples were separated on 4-15% Mini-Protean TGX Tris-Glycine-buffer SDS-PAGE and transferred onto a 0.2µm Trans-Blot Turbo nitrocellulose membranes (both from Biorad). Membranes were blocked for 1h at RT in 1xTBS (10mM Tris pH 8.0, 150 mM NaCl,) supplemented with 5%(w/v) dried skim milk powder. Primary antibody incubation was carried out overnight at 4°C, with the following antibodies: rabbit anti-AP (1:2000, GenHunter), mouse anti-V5 (1:2000, Invitrogen), goat anti- Human IgG, Fc gamma fragment specific (1:500, Jackson Immunoresearch), rabbit anti-HA (1:2000, Sigma #H6908). For detection, goat anti-rabbit-HRP, goat anti-mouse-HRP, donkey anti-goat-HRP coupled secondary antibodies were used (1:10000, Jackson ImmunoResearch, West Grove, PA). In between and after antibody incubations, membranes were extensively washed in TBS-T (TBS containing 2.5% Tween-20). Western blots (WB) were visualized using the enhanced chemiluminescence method (ECL prime Western Blotting detection reagent, Amersham).

2.15 Immunohistochemistry on COS7 cells

For the immunohistochemistry on COS7 cells 24-well plates were used. For plate preparation, round glass slides (stored in EtOH) were placed in each well and incubated with 300µl polylysine (2mg/ml) for 3h at RT. After 3 PBS washes, COS7 cells (150µl) and respective Medium (350µl) were plated in each well. The next day, the cells were transfected (10µl Optimem + 0,3µg/0,6µg ADNA, 10µl Optimem + 0,4µl lipofectamine) with the respective pCX-HA plasmids and incubated in 500µl Medium. After 48h, the immunohistochemistry staining was performed. Therefore, the cells were washed 3x for 10min with PBS-Tween and subsequently fixed with 4% paraformaldehyde (in PBS-Tween) for 30min at RT. After 3x washes for 10min with PBS-Tween, the cells were incubated in blocking solution (PBS-Tween, 0,5% gelantine) for 90min at RT. The primary antibody (rabbit anti-HA, Sigma) was applied and incubated for 3h at RT (1:500, in blocking solution). Following, the cells were washed 3x for 10min with PBS-Tween and subsequently incubated with the secondary antibody incl. DAPI (α-rabbit-Cy3, 1:500, in blocking buffer) for 2h at RT. Next, the cells were washed 3x for 10min with PBS and mounted with mowiol. For imaging, a 5X objective on an upright Microscope

system (Leica DM6000B) including a CCD CoolSnap HQ2 camera was used. Images were processed and analyzed using ImageJ.

2.16 AVEXIS

The avidity-based extracellular interaction screen (AVEXIS) was performed as described in Bushell et al. 2008 [348] and more in detail in Kerr and Wright 2012 [349]. AVEXIS constructs were transfected into Human embryonic kidney 293 (HEK293) cells in 50ml Freestyle293 media. As transfections reagent Polyethyleneimine solution (PEI) was used (Sigma-Aldrich #03880). For bait normalization a Dotplot was used to determine the relative levels at which the bait proteins are expressed. Therefore, dilution series (1, 1:2, 1:4, 1:8, …) of respective dialyzed bait proteins were brought onto a 0.45µm nitrocellular membrane and detected with αrat CD4 antibody (BioRad # MCA1022R), then αmIgG-HRP (Thermo Fisher #32230) and ECL enhance substrate. For prey normalization, the β-lactamase enzyme activity was utilized. Therefore, a prey protein dilution series was incubated with Nitrocefine (Calbiochem®) and every minute for 20 min the absorbance at 485 nm was measured. For the AVEXIS screening, streptavidine coated plates (Thermo Scientific #10143632) were first incubated with normalized biotinylated monomeric bait proteins and after with normalized pentamerized prey proteins. Interactions between bait and prey were visualized by nitrocefine incubation and quantified by analyzing the absorbance at 485 nm. A positive interaction resulted in a color change of the nitrocefin solution from yellow to red (visible even by eye).

2.17 Production of Metrn/Metrnl1-AP fusion probes

AP-tag plasmids for the production of Metrn-AP/Metrnl1-AP fusion proteins were transfected into HEK293 cells (8µg per contruct) using Lipofectamine 2000 reagent (Invitrogen). After 24h, the cell medium was exchanged with OptiMEM medium and subsequently after 48h the media were collected, spin down and the supernatant transferred into a fresh flask. The presence of the fusion protein in the supernatant at the expected molecular weight was validated via Western blot (WB) using an α-AP antibody (1:6000, GenHunter).

The supernatants were used directly without additional purification for the binding assay or stored at -20°C. Before each binding assay the Alcaline Phosphatase activity was measured. Therefore, 30µl per sample were incubated at 72°C for 20min to inactivate the endogenous phosphatases. Then, 2X AP solution (1 M diethanolamine (pH 9.8) 0.5 mM $MgCl_2$, 10 mM L-homoarginine, 0.5 mg/ml BSA, 12 mM p-nitrophenyl phosphate) was diluted with water and 200 µl were added to each sample. Positive AP activity could be detected with a color change into bright yellow.

2.18 Cryosection and AP-assays on sections and cells

For zebrafish sections, 5dpf embryos were fixed in 4% paraformaldehyde in PBS (pH 7.4) for 2h at RT. After the fixation, the samples were cryoprotected overnight in a solution of 30% sucrose/0.02% sodium azide/PBS. Subsequently, the sucrose was removed and the embryos were embedded in OCT and stored at -80°C or placed on dry ice for immediate following sectioning. The sections were cut with a 20µm thickness and mounted on Fisherbrand Superfrost plus slides. For mouse samples, E14 fresh-frozen spinal cord samples were cut with 20µm thickness and mounted on Fisherbrand Superfrost plus slides as well. The sections were equilibrated at -20°C in the cryostat. For fixation the cryosection samples cooled in 100% Methanol for 8 minutes (30min for mouse). After 3x wash in PBS1 X, $MgCl_2$ 4mM the sections were incubated in blocking solution (in PBS 1X, $MgCl_2$ 4mM, 10% FBS) for 1 hour at RT. For the binding, AP-fusion proteins were diluted (1/5 to 1/20 if high AP activity) in PBS 1X. Then, the slices were incubated with the fusion probes for 2 hours at room temperature. Subsequently, the samples were washed 5x in PBS 1X, MgCl2 4mM. For bound ligand fixation, to sections were incubated for 2 minutes in 60% acetone, 4% Paraformaldehyde, 20mM Hepes pH7 and the washed 3x in PBS1X. To inactivate the endogenous phosphatases, the sections were treated at 65°C for 2 hours in PBS 1X and then washed again 2X with PBS 1X. Ligand bound to sections was revealed in Tris pH 9.5, 5 mM MgCl2, 100 mM NaCl, 0.3 g liter–1 4-nitro blue tetrazolium chloride, 0.25 g liter–1 5-bromo-4-chloro-3-indolyl-phosphate (Roche). After sufficient staining the reaction was stopped with PBS1X and slices were mounted in Mowiol.

For the AP-binding assay on COS7 cells 24-well plates were used. For plate preparation, round glass slides (stored in EtOH) were placed in each well and incubated with 300µl polylysine (2mg/ml) for 3h at RT. After 3 PBS washes, COS7 cells (150µl) and respective Medium (350µl) were plated in each well. The next day the cells were transfected (10µl Optimem + 0.3µg ADNA, 10µl Optimem + 0.4µl lipofectamine) with the respective pCX-V5 and/or -HA plasmids and incubated in 500µl Medium. After 48h, the AP-binding assay was performed. Therefore, the respective AP-proteins (Metrn-AP, Metrnl1-AP ect.) were defrozen and tested for AP activity (see 2.17). The transfected COS7 cells were washed per well with 400µl freshly prepared HBHA solution (50mg BSA, 20mM Hepes, 10ml HBSS, H_2O up to 100ml) 2X for 15min. Cells were probed with diluted AP-proteins (diluted in HBHA, AP alone 1:100, Netrin-AP1:20, others 1:50) for 90min at RT. Subsequently, the cells were washed 7x with HBHA for 10min each under light shaking. 1/3 of wash buffer 1 (150mM NaCl, 20mM Hepes) was stored at 65/70°C. For fixation, cells were fixed well by well for 30sec each with fixation buffer (60% Acetone, 3% PFA, 20mM HEPES) and then immediately washed with wash buffer 1. Next, fixed cells were washed again with wash buffer1 for 5min. For inactivation of the endogenous

AP, cells were incubated for 20min at 70°C with preheated wash buffer 1. After the inactivation, the cells were washed with wash buffer 2 (100mM Tris HCL pH 9,5, 100mM NaCl, 5mM MgCl) for 10min. For revelation, cells were incubated in 400µl staining buffer (10mM L-homogenine, 0.17mg/ml BCIP, 0.33mg/ml NBT in wash buffer 2) at RT, in the dark, for up to 72H. After sufficient staining the reaction was stopped with 10% EDTA (in PBS) solution and slices were mounted in Mowiol.

2.19 Co-IP binding assay

For the Co-immunoprecipitation (Co-IP) approach, COS7 cells were transfected with respective pCX expression vectors using Lipofectamine 2000 according to the manufacturer's protocol (Invitrogen). After 48h, COS7 cells were lysed with in radioimmunoprecipitation assay (RIPA) buffer (50 mM Tris-HCl, pH 7.4, 150 mM NaCl, 20 mM EGTA, 1% NP-40, 0.5% sodium deoxycholate, 0.1% SDS) supplemented with protease inhibitor cocktail and phosphatase inhibitor cocktail. The lysate was incubated at 4°C for 20 min. After centrifugation at 14,000g for 10 min, the supernatants were incubated for 2h at 4°C with the following antibodies: rabbit anti-HA (Sigma), mouse anti-V5 (Invitrogen). Complexes were incubated with Protein-G Sepharose Fast-Flow beads (Sigma) for 1h at 4°C. Subsequently, complexes were washed with cold lysis buffer and boiled in Laemmli SDS protein sample buffer. Then, the samples were processed for migration, transfer and visualized as already described above (see 2.14) using goat anti-mouse, donkey anti-goat or goat anti-rabbit HRP (Jackson ImmunoResearch, West Grove, PA) as secondary antibodies and ECL Western Blotting detection reagent (Amersham).

2.20 Ecto-Fc ligand-receptor interaction screen

The majority of the Ecto-Fc ligand-receptor interaction screen was conducted as described the Nature Protocol of Savas et al. 2014 [8]. For the molecular cloning see 2.13.

2.20.1 Production and purification of extracellular domain Fc-fusion bait proteins

Ecto-Fc bait proteins were produced as described in Savas et al. 2014 [8]. Per Ecto-Fc bait protein (mMetrn-Fc, zMetrnl1-Fc, zMetrn-Fc, zNtn1-Fc), HEK293 cells on 25 10cm plates were transfected using Lipofectamine 2000 reagent (Invitrogen). For the purification, ecto-Fc bait proteins were purified from 250ml of surpernatant using a HiTrap® MabSelect™ PrismA 1ml (Cytiva, 17549854) on a fast protein liquid chromatography (Äkta go) according to the manufacturer's instructions. Fraction 4 to 8 were collected, pooled and transfered to a Slide-A-Lyzer (10 K MWCO; Thermo Scientific, 66383) and dialyzed at 4°C o.n. with two buffer

changes. After dialysis the purified proteins were concentrated using an Amicon Ultra-4 (10K UFC801024, Millipore). The concentration was measured with Bradford reagent.

2.20.2 Prey extraction from fresh tissue

For prey protein extraction, CNS structures (whole brain and spinal cord) were dissected from E13 mouse embryos. For one experiment (one interaction) 16 embryos were dissected to achieve a final protein concentration of ~4mg. The tissue homogenization and the plasma membrane enrichment were conducted according to the AB65400kit (abcam) protocol and resulted in ~400µg plasma membrane enriched protein extract. Subsequently, the extract was incubated with 25µl of Netrin or Meteorin coated beads (5µg of Fc-fused proteins) o.n.

2.20.3 Preparation for mass spectrometry

The bait-prey beads solution was washed 3x with 500 µl of lysis buffer (50 mM Tris-HCl, pH 7.4, 150 mM NaCl, 20 mM EGTA, 1% NP-40, 0.5% sodium deoxycholate, 0.1% SDS) and subsequently boiled in Laemmli SDS protein sample buffer supplemented with DTT 5mM. After, the samples were processed for short migration in an SDS-PAGE gel. Finally, the gel was stained with Coomassie blue and the Coomassie stained protein gel regions were cut (Figure 19), digested with trypsin and send for mass spectrometry analysis.

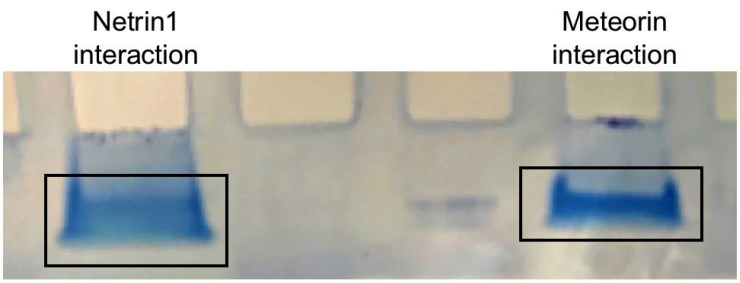

Figure 19: **Example for a short migration in an SDS-PAGE gel of an Meteorin- and Netrin-interaction sample.** (cut regions marked with squares)

2.20.4 Mass spectrometry analysis

The mass spectrometry analysis was performed from the platform at Institute Jacques Monod. The peptides were filtered with an FDR (False Discovery Rate) of 1% and a Homo sapiens database including the sequences of our FC-tagged bait proteins was used.

The result of the mass spectrometry analysis was a list of detected proteins and their abundance in the sample. This list contained several hundreds to few thousands of proteins for each sample. The abundance was annotated as "area", "number of unique detections" or "number of spectra". To restrict this to a shortlist of some tens of putative candidates all non-transmembrane proteins were filtered out, and preferentially proteins that were enriched in the Meteorin sample compared to the Netrin sample were considered.

For the first step, UniProt was queried using a program written in python, that given the accession number of the detected protein would obtain the corresponding UniProt page. It would then parse the page to assess whether the protein contains a transmembrane domain, and whether it was annotated with one of the following keywords: "Mitochondrion", "Endoplasmic reticulum", "Golgi apparatus" or "Nucleus".
For the second step the detected proteins were subdivided in three different classes, depending on whether they were found in only the Meteorin sample, only the Netrin sample, or in both. For the latter the realtive enrichment as the logarithm of the Meteorin area divided by the Netrin area was evaluated. For proteins present in only one sample the number of spectra to quantify abundance was used instead.

2.21 Figures

Schematic Figures were created/partially created with BioRender.com. (Figure 3, Figure 5, Figure 8, Figure 9B, Figure 12, Figure 13, Figure 15, Figure 17, Figure 27B) or PowerPoint/Illustrator.

3 RESULTS

3.1 The role of Meteorins during the establishment of the left-right axis throughout early embryonic development

3.1.1 Summary article 1

From the exterior the vertebrate body plan appears bilaterally symmetric, though often the morphology and positioning of internal organs display left-right asymmetries. Nodal, a ligand belonging to the TGFβ protein family is one major regulator for the establishment of the vertebrate left-right axis. Symmetry-breaking in mouse was shown to be initiated in the Node or by equivalent structures such as the KV in zebrafish. The zebrafish KV is formed by DFCs. Achieved by an oriented rotation of cilia in the node (or KV), a leftward flow of extraembryonic fluid named Nodal flow is established, which is considered the key point for L-R symmetry breaking and results in asymmetric expression of several nodal factors and asymmetric Nodal signaling. In the paper "Meteorins as novel regulators of left-right patterning in the zebrafish embryo" we demonstrate that Meteorin proteins are important for the left-right patterning since they are required for the correct formation of the Kupffer's vesicle as well as for correct properties of the KV like the cilia length, cilia number, KV size and expression of Nodal flow genes. Furthermore, we show that Metrns act together with Itgα V1 and Itgβ1b, and that they are necessary for proper DFC clustering and migration by mediating necessary cellular interactions. We present Metrn proteins as novel potential factors within the establishment of the L-R asymmetry during embryonic development.

3.1.2 Article 1: "Meteorins as novel regulators of left-right patterning in the zebrafish embryo"

"Meteorins as novel regulators of left-right patterning in the zebrafish embryo" (in preparation)

Fanny Eggeler[1], Jonathan Boulanger[1], Laura Belleri[1], Karine Duroure[1], Flavia De Santis[2,3], Thomas O. Auer[2,4], Shahad Albadri[1], Filippo Del Bene[1]

[1] Sorbonne Université, INSERM, CNRS, Institut de la Vision, Paris, France

[2] Institut Curie, PSL Research University, Inserm U934, CNRS UMR3215, Paris, France

[3] ZeClinics SL, Badalona, Spain

[4] Center for Integrative Genomics, Faculty of Biology and Medicine, University of Lausanne, CH-1015 Lausanne, Switzerland

Meteorins as novel regulators of left-right patterning in the zebrafish embryo

Fanny Eggeler[1], Jonathan Boulanger[1], Laura Belleri[1], Karine Duroure[1], Flavia De Santis[2,3], Thomas O. Auer[2,4], Shahad Albadri[1], Filippo Del Bene[1]

[1] Sorbonne Université, INSERM, CNRS, Institut de la Vision, Paris, France

[2] Institut Curie, PSL Research University, Inserm U934, CNRS UMR3215, Paris, France

[3] ZeClinics SL, Badalona, Spain

[4] Center for Integrative Genomics, Faculty of Biology and Medicine, University of Lausanne, CH-1015 Lausanne, Switzerland

ABSTRACT

During vertebrate embryonic development left-right symmetry-breaking is innated by a ciliated organ called the Node or left-right organizer. Within the node, a leftward flow of extraembryonic fluid named the Nodal flow mediates the asymmetric expressions of Nodal factors. Although downstream Nodal pathway components leading to the establishment of the embryonic left-right axis are well known, less is known about the development and formation of the embryonic Node itself.

Here we reveal a novel role for the Meteorin protein family in the establishment of the left-right axis and in the formation of the Kupffer's vesicle, the node equivalent structure in zebrafish. We show that the CRISPR-Cas9 mediated knockout for each or all three members of the zebrafish Meteorin family (*metrn*, *metrn-like 1* and *metrn-like 2*) leads to defects in properties of the Kupffer's vesicle, caused by impaired assembly and migration of the Kupffer's vesicle forming dorsal forerunner cells. In addition, we demonstrate that Meteorins genetically interact with integrins ItgaV and Itgβ1b at the level of the dorsal forerunner cell clustering and that *meteorins* loss-of-function results in disturbed Nodal factor expression and consequently in randomized or symmetric heart looping and jogging.

These results identify a new role for the Meteorin protein family in the left-right asymmetry patterning during embryonic vertebrate development.

INTRODUCTION

From the outside the vertebrate body plan appears bilaterally symmetric. However internal organs positioning and morphology often displays left-right asymmetries. For instance, in vertebrates the heart generally lies on the left side, the liver and the pancreas are positioned on the right and the gut presents asymmetric rotations.

In vertebrates, one major regulator for the establishment of the left-right (L-R) axis is Nodal, a ligand belonging to the TGFβ protein family [1]–[6]. Its signaling is activated in the left lateral plate mesoderm (LPM), whereas Nodal remains inactive in the right LPM, creating an embryo-scale left-right asymmetry [3]. In mice, this asymmetry is achieved by an oriented rotation of the cilia of a structure called the node generating a leftward flow of extraembryonic fluid named the Nodal flow. This results in an asymmetric expression of several Nodal factors and Nodal signaling. Participating in this patterning, Leftys, soluble inhibitors belonging to a subclass of TGF factors, antagonize Nodal signaling [7], [8].
The node and the Nodal flow were shown to be conserved in numerous vertebrates. In chicken it is known as the Hensen's node, in Xenopus the gastrocoel roof plate and in zebrafish the Kupffer's vesicle (KV) [9]–[15] and all are key points of the L-R symmetry breaking during the embryonic development [12], [14], [16].

Compared to the relatively flat shaped mouse node, the zebrafish KV is a fluid-filled sphere with a ciliated epithelium and it is formed by dorsal forerunner cells (DFCs) [9]. DFCs first emerge as cells of the epithelium of the dorsal surface in direct contact with the yolk syncytial layer [17]. During gastrulation DFCs form a cluster of non-involuting cells remaining at the leading edge of the shield. During the epibolic movements they migrate toward the vegetal pole organizing into an ovoid, rosette like pattern. At the final phase of epiboly and after reaching the vegetal pole, the DFC cluster is separating from the dorsal marginal enveloping layer cells. Short after, the interior KV lumen is formed by incorporating the unpolarized DFCs into a rosette structure and migrating into the zebrafish embryo [9], [17], [18]. It was shown that the proper functioning of the KV is fundamental since the leftward directed flow within the KV results in asymmetric expression of zebrafish Nodal genes, like *spaw*, *lefty1* and *lefty2* that are crucial for proper L-R pattering [19], [20]. However, the molecular mechanisms involved in correct DFC migration and clustering that will form the KV remain largely elusive.
In this context, it has been reported that *nodal, lefty* as well as *p-smad2* expression are downregulated in *Meteorin*-null ES-cells. As such, Meteorin (Metrn) was hypothesized to be a novel important regulator of Nodal transcription [21].

Meteorin (Metrn), a secreted neurotrophic factor, is expressed during early mouse development and is already detected at the blastocyst stage in the inner cell mass and then expands through the extraembryonic ectoderm to the central (CNS) and peripheral nervous system (PNS) during later developmental stages [21]. It was first described to induce glial cells differentiation and to promote axonal extension in dorsal root ganglion (DRG) explants *in vitro* [22]. Its paralog, Meteorin-like (Metrnl) has been first reported as a downstream target of the Pax2/5/8 signaling during otic vesicle development [23] and was shown later to have neurotrophic properties comparable to the ones of Metrn [24]. The disruption of *Metrn* resulted in early embryonic lethality [21] and made it not possible to investigate the role of Metrn proteins in early embryonic development *in vivo* and in particular as supposed for the L-R patterning.

Highly conserved in vertebrates, Metrn proteins account for three in zebrafish (Metrn, Metrnl1, Metrnl2). Here using the zebrafish larva as model system and using CRISPR/Cas9 to generate knockout lines for all three zebrafish *metrn* genes, all viable, we reveal organ patterning defects with randomized or symmetric heart looping and jogging in *metrns* mutant embryos. We could observe that, like in mouse, *metrn* genes are expressed during early development already from the 2-cells stage. We detected transcripts in DFCs as well as in the KV structure and demonstrate that *metrns* loss of function led to DFC disorganization and Nodal flow formation defects within the KV. Together our study reveals a critical role for Metrn proteins in the DFC clustering and KV formation and in the establishment of the L-R axis.

RESULTS

Metrns are required for proper heart looping and visceral organs correct positioning

To study the functions of Meteorin proteins, we stablished we performed CRISPR/Cas9 - mediated knockout in the second exon that encodes for the signal peptide sequence in all three genes and generating zebrafish mutant lines carrying out-of-frame deletions in the coding sequence of *metrn*, *metrnl1* and *metrnl2* (supp Figure 1A). In contrast to published embryonic lethal *Metrn* mouse mutants [21], constitutive homozygote mutants for all three genes individually (*metrn*$^{-/-}$; *metrnl1*$^{-/-}$; *metrnl2*$^{-/-}$), in double (*metrn*$^{-/-}$, *metrnl1*$^{-/-}$; *metrn*$^{-/-}$, *metrnl2*$^{-/-}$; *metrnl1*$^{-/-}$, *metrnl2*$^{-/-}$) and triple (*metrn*$^{-/-}$, *metrnl1*$^{-/-}$, *metrnl2*$^{-/-}$ or triplMut) mutant zebrafish lines were all adult viable and did not show any obvious morphological defect (Figure 1A). To validate our that mutagenic approach resulted in the generation of null alleles, we performed *in situ* hybridization as well as qPCR experiments. From 2-cells stage to 2 days post-fertilization (dpf), no expression could be detected for *metrn* and *metrnl1* in the triplMut embryos as well as in the single mutant embryos via *in situ* hybridization (supp Figure 1B-C). Additionally, significant reduction of the *metrn* genes expression at 14 hpf (and at 48 hpf for *metrnl2*) could be detected via qPCR, suggesting that the mRNA produced by the targeted locus is degraded by non-sense-mediated decay (supp Figure 1D).

Remarkably, using *myl7* antisense riboprobe *in situ* hybridization in single mutant embryos, we analyzed disturbed heart morphogenesis. In wild type control embryos, most had D-looped shaped hearts (Figure 1B-C). In *metrn*$^{-/-}$ and *metrnl1*$^{-/-}$ single mutant embryos and in particular in the triplMut, a higher proportion of embryos displayed randomized (no/mild loop, S-loop) heart phenotypes (Table 1, Figure 1B-C). The injection of *metrn* and/or *metrnl1* mRNA into one-cell stage triplMut zebrafish embryos could partially rescue the observed phenotype (Table 1, supp Figure 1E). These results indicate that while Metrns are not implicated in the specification of the heart (*myl7* expression being detected in all analyzed genetic backgrounds), their loss of function can impact on the L-R asymmetry positioning of this organ.

In addition to the heart, morphological L–R asymmetry of the visceral organs was also perturbed in TriplMut embryos. To determine if L–R asymmetry of the visceral organs is affected in these embryos, we used *gata6* as a maker. A larger portion of triplMut embryos failed to show normal L–R asymmetry of the pancreatic bud and gut, with 10.49% embryos exhibiting symmetrical placement of the gut and pancreas with respect to the midline and 9.88% showing heterotaxic phenotypes compared to the wild type embryos (wt: 93.84% normal L–R asymmetry, 1.37% heterotaxia, 4.79% L–R symmetry) (Figure 1D-E).

The left-jogged heart or the right-positioned liver are just two of many examples for determined L-R asymmetry in zebrafish and are well-studied readout for altered L-R pattering processes

Taken together, these results show that Metrns play a critical role in the establishment of L–R asymmetry at an early step.

Metrns are required for proper Nodal factor genes expression

Nodal signaling is one of the major regulatory pathways for the establishment of the left-right axis during vertebrate development. In zebrafish, null mutants for several Nodal factors like *spaw* (a zebrafish nodal orthologue), *dand5* or *lefty1* all display symmetric or randomized heart looping and jogging [25], [26], similar to *Nodal* mutant mice [27], [28]. We asked whether Metrns loss of function affects also the expression of these Nodal factors and therefore assessed *metrns* loss-of-function effect on *dand5* expression and subsequently as well as on *spaw*, *lft* and *left2* expression. Via qPCR we first measured a significant reduction of *dand5* expression at 14 hpf in triplMut embryos compared to wild type controls (Figure 2A). We next characterized *dand5* specific R > L bias expression pattern in triplMut embryos. Via *in situ* hybridization, we did not detect *dand5* expression in more than 61% triplMut embryos and in 23% an abnormal R > L bias (Figure 2 B-C). In single *metrn* and *metrnl1* mutants *dand5* expression pattern was also altered (supp Figure 2A). These results are in line with previous findings reporting that *dand5* expression in the KV is only altered if upstream symmetry breaking mechanisms are disrupted [29]–[31].

Additionally, we assessed the expression of *spaw*, *lefty1* as well as *lefty2* in the absence of Metrns proteins. *These* Nodal factors were all downregulated in triplMut embryos compared to the wild type embryos as revealed by qRT-PCR (Figure 2D). We then analyzed their gene expression patterns by *in situ* hybridization (supp Figure 2B). At 16 hpf *spaw* is normally expressed adjacent to the KV and in the left LPM. In *metrn*$^{-/-}$ and *metrnl1*$^{-/-}$ single mutants as well as triplMut embryos, we could not detect any *spaw* expression in the left LPM and only faintly around the KV (supp Figure 2B). The Spaw inhibitor *lefty1* is expressed along the midline at this stage. In all analyzed *metrn* mutants (single *metrn* and *metrnl1* and triplMut), *lft1* expression was severely disrupted at the midline (supp Figure 2B, middle panel). The same was observed for *lft2* which expression in the left heart field was either absent or randomized in *metrn* mutants, single or triplMut embryos, compared to the wild type embryos (supp Figure 2B, lower panel). These results indicate that Metrns are required for the proper expression of Nodal factor genes.

***Metrns* are expressed during early zebrafish development**

Since the establishment of the vertebrate left-right axis takes place and Nodal factors are expressed from the first stages of embryonic development we sought to analyze the expression of all three zebrafish *metrn* genes during this time. We investigated the expression pattern of *metrn* and *metrnl1* in zebrafish by *in situ* hybridization and hybridization chain

reaction (HCR) experiments. At the 2-cells stage, we detected both *metrn* and *metrnl1* were maternally expressed (Figure 3A, supp. Figure 3A). At 6 hpf (also called to shield stage), *metrnl1* expression could be detected over the whole animal cap whereas *metrn* expression onset was observed only around the yolk syncytial layer (YSL) at this developmental stage (Figure 3A). *Metrn* expression was then restricted to the developing LPM and to the leading edge of the shield from 9 hpf. In comparison, *metrnl1* was found expressed throughout the whole enveloping layer and developing midline (Figure 3A, supp Figure 3B). At 12 hpf, the expression of *metrn* was restricted to the the KV area while *metrnl1* transcript were found instead in the midline (*metrnl1*) (Figure 3A-B). At 14 hpf, we found both genes expressed in the KV (Figure 3B). At this stage, *metrnl1* transcripts were additionally found in the region of the paraxial mesoderm (PM) and intermediate mesoderm (IM) and we could still detect them along the midline. Instead *metrn* first expression in the developing brain could be detected at this stage (Figure 3C). By 24 and 48 hpf, both genes were found strongly expressed in the central nervous system (CNS) (supp Figure 3C). Finally, *metrnl2* expression onset started from 24 hpf broadly in the embryonic brain. At 48 hpf, *metrnl2* transcripts were mostly found in the otic vesicles and at the somite boundaries (supp Figure 3C).

By double fluorescence *in situ* hybridization, we next analyzed the relative expression of *metrns* genes to landmarks of the KV structure like *casanova* (*cas*), a well-studied DFC marker [32], [33]. We observed a complete colocalization of *metrn*/*cas* and *metrnl1*/*cas* signals at 10 hpf, validating the expression of *metrns* genes in DFCs that are meant to form the KV (Figure 3D). To assess whether *metrn* and *metrnl1* expression in the KV structure is conserved among vertebrates, we performed *in situ* hybridization for *metrn* and *metrnl1* in the chick embryo at early stages. Around stage HH6, we could visualize *metrn* as well as *metrnl1* expression around the Hensen's node and the primitive streak (the latter matching the expression of the primitive streak landmark *fgf8*) (supp Figure 3D). Remarkably, the chick *metrn* and *metrnl1* expression patterns were reminiscent of the ones of the zebrafish *metrn* genes, with *metrn* being expressed more restricted to the node and *metrnl1* displaying a more diffused expression around the node area.

Metrns loss-of-function leads to DFC disorganization and migration defects

Due to the specific expression of *metrn* and *metrnl1* in DFCs and in the KV area, we asked whether Metrns could play a role for DFCs and for KV formation and function. Because *metrnl2* expression does not appeare before 24 hpf, we hypothesize that Metrnl2 does not play a role in this process. However, due to possible genetic compensation effects, we used the triple mutant line triplMut that we generated throughout all our analysis if not stated otherwise [34]. To assess how the loss of Metrn proteins function affected their migratory and clustering

properties, we labeled DFCs in 9 hpf (80-90% epiboly) gastrulating mutant embryos using *cas* [32], [33], *ntl* [35] or *sox17* [32] as markers. Compared to wild type embryos displaying usual ovoid DFC clustering, about 65% of the triplMut embryos displayed disorganized DFC assembly forming disorganized segregated clusters or arranged in an abnormal linear distribution as shown using *cas* as DFC marker (Figure 4A-B, supp Figure 4A). Similarly, *metrn*$^{-/-}$ as well as *metrnl1*$^{-/-}$ single mutant embryos presented *cas*-expressing DFC clustering defects compared to wild type embryos (Figure 4B, supp Figure 4A-B). In single or triplMut$^{+/-}$ heterozygous embryos, DFC clustering was not significantly or very mildly affected as revealed by the *cas* labeling of these cells (supp Figure 4A). These observations led us to the conclusion that Metrns are required for the proper clustering of DFCs that will then form the KV. The observed defects were also present when using *ntl* and *sox17* DFC markers which expression could be detected at 8 and 10 hpf indicating that although disorganized, the DFCs identity was not altered by the absence of *metrns* expression (supp Figure 4C).

It was reported that proper adherent cell assembly is crucial for directional collective cell migration, as for DFCs during their animal to vegetal pole (AP to VP) journey [36] (Figure 4C). We thereby evaluated the migration capacity of DFCs during the early hours of development in the absence of Metrn proteins. To do so, first labeled *cas*-expressing DFCs by *in situ* hybridization in wild type and triplMut embryos and measure the distance from AP to the VP over the total embryo length at 6 hpf, 8 hpf and 10 hpf. Compared to wild type embryos, DFC cells in triplMut embryos showed migratory delays of about 8% to 13% of the total embryo length at all analyzed developmental stages (Figure 4D and supp Figure 4D). Together our results indicate that DFCs migrate significantly slower in triplMut embryos compared to wild type DFCs, suggesting that Metrn proteins are important for both the proper clustering and the migration of DFCs.

Metrns loss-of-function impairs the KV formation and function

At the end of gastrulation, DFCs that migrated in clusters to deeper layers of the developing zebrafish embryo form a lumen to shape the KV, a ciliated organ transiently present that is crucial for initiating left-right asymmetric patterning [9], [18]. Dand5, belonging to the Cerberus/Dan family of secreted factors, was reported to be expressed adjacent to the KV with a right – left (R > L) bias between 11 and 14 hpf in zebrafish [37]. It was also shown that *dand5* expression is directly influenced by the direction and the strength of the Nodal flow in the KV [38]. Dand5 is also known to contribute to the left-biased expression of *spaw* in the LPM and to antagonize Spaw activity [37]. Furthermore, it was shown that the leftward-directed flow within the KV results in the asymmetric expression of Nodal genes, like *spaw*, *lefty1* (*lft1*) and *lefty2* (*lft2*) [19], [20].

The specific expression of *metrn* and *metrnl1* in the KV area, the disturbed expression of several Nodal factors like *dand5, spaw* or *leftys* as well as the disturbed DFC clustering and migration in the absence of Metrns led us to hypothesize that Metrn proteins might be important for the proper formation and function of the KV. To assess this question, we measured diameter and cilia number in the KV both in wild type and triplMut embryos (Figure 5A). Compared to wild type control embryos, the KV diameter and the number of KV cilia were significantly reduced in the triplMut embryos (Figure 5B-C). As it was shown that these two parameters present high variability from one embryo to the other, we measured the overall KV cilia length that was reported to show less variation from one embryo to the next [39]. With respect to the wild type controls, triplMut embryos also displayed a significant reduction in the KV cilia length (Figure 5D). These results indicate that the loss of Metrns function impacts on the proper KV formation.

We next evaluated whether the KV function was impaired by the absence of Metrn proteins and compared the Nodal flow in the KV of triplMut and triplMut$^{+/-}$ embryos to the one of wild type embryos. The movement generated by the KV cilia was monitored by injecting fluorescent microspheres into the KV at 12-14 hpf. To quantify flow, movement of individual microbeads was tracked in wt control embryos (n = 363 beads) and in triplMut (n = 318 beads) and used to calculate an average bead velocity (Figure 5E). Beads movement analysis within the KV showed a counter-clockwise rotation of the flow in wild type control (Figure 5E, supp Movie 1). In contrast, this movement was severely impaired in triplMut embryos (Figure 5E, supp Movie 2). Furthermore, measurement of average bead velocity showed an overall reduction in the speed displacement of the beads in the triplMut$^{-/-}$ mutant embryos compared to the wild types (supp Figure 5). These results demonstrate that the observed defects in the KV formation in the absence of Metrns also severely impacts the Nodal flow.

Genetic interaction of ItgaV/Itgb1b and Metrns on the level of the DFCs

In order to uncover one of the mechanisms through which Metrn proteins act in the establishment of the early L-R patterning, we finally assessed the possible relationship between Metrns and both ItgαV1 and Itgβ1b at the level of DFCs, in particular for their proper clustering and migration. Indeed *itgαV* as well as *itgβ1b* were also shown to be expressed in DFCs and *itgαV* and *itgβ1b* morpholino -injected embryos display similar DFC phenotypic defects reminiscent to those observed in *metrn* mutants [40]. In order to examine the possible genetic interactions between ItgaV1 and Itgβ1b and Metrns, we injected morpholinos for *itgβ1b* (0.5 ng) or *itgαV1* (0.41ng) into 1 to 4 -cell stage in triplMut$^{+/-}$ embryos to generate insufficient doses of both proteins in a heterozygous *metrns* mutant background. The injection of the morpholinos at these doses and at sufficient doses (*itgβ1b:* 0.7ng, *itgαV1:* 1.25ng) reproduced

the previously reported defects on DFCs (Figure 6A, Table 2) [40]. The injection of low doses of either *itgβ1b* or *itgαV1* morpholino into wild type embryo controls did not affect DFC clustering, similarly to non-injected triplMut$^{+/-}$ embryos (Figure 6A, Table 2). A significantly higher percentage of embryos with DFC clustering defects could be observed upon the injection of either morpholino at low dose into triplMut$^{+/-}$ (Figure 6A, Table 2). These results are consistent with the hypothesis that both Integrins might genetically interact with Metrn proteins for the proper clustering of DFCs.

DISCUSSION

Our results demonstrate a novel role for Meteorin proteins during vertebrate embryonic development. We showed that Metrns are required for the establishment of the L-R patterning. We demonstrated that Metrns ensures this function by acting together with ItgαV1 and Itgβ1b for the proper clustering and migration of DFCs to form the KV. We could show that Metrns are essential for several aspects of the KV formation and function like the cilia length, cilia number, KV size and expression of Nodal flow genes and that the regulation of all these parameters by Metrn proteins is critical for the proper positioning of vital organs like the heart (Figure 6B).

From 9 hpf the expression of *metrn* was visible around the developing LPM close to the midline and the leading edge of the shield. *Metrnl1* expression was found expressed throughout the whole enveloping layer and the developing midline. It was shown that the embryonic midline plays an important role in vertebrate L-R development. Zebrafish midline mutants display altered *lft1* and *lft2* expression patterns as well as discordance among heart, gut and brain gene expression patterns [41]. However, we hypothesize that the described body asymmetry defects in our Metrn mutants probably do not originate from impaired midline structures but rather impaired DFC clustering and migration. TriplMut$^{-/-}$ embryos indeed had intact *ntl*-positive notochords (supp Figure 4C) as well as randomized visceral organs positioning (Figure 1D-E), phenotypes that are not characteristic for defects of the anterior midline [41].

DFCs are precursors of the zebrafish KV, organ of laterality, essential for the L-R axis establishment. DFCs develop at the beginning of gastrulation and form the KV by the end of gastrulation [9], [18]. Given the early onset of *metrn* and *metrnl1* expression and their specific expression within the DFCs we investigated their role for the clustering and migration capacity of DFCs during these early embryonic developmental steps. In the course of their migration, DFC progenitors intercalates mediolaterally and results in an oval-rosette shape cluster of DFCs by mid-gastrulation that will form the KV [17]. *Metrn*$^{-/-}$, *metrnl1*$^{-/-}$ and triplMut zebrafish embryos displayed DFC assembly defects and delayed migration of these cells during gastrulation. Since DFCs in triplMut still express DFC specific markers (*sox17, cas, ntl*), we concluded that Metrns are not required for the specification of DFCs per se but rather that Metrns are solely important for their proper clustering and migration.

It is important to note that the DFC clustering and migration defects observed in Metrn mutants does not only appears to be affected on the mediolateral axis but also apical ventrally since the connection between DFCs and the YSL/EVL seems also to be disrupted in these mutants (Figure 4A). It is therefore possible that the defects observed are due to impaired embedding of the DFCs into the cells of the EVL, the deep cell layer and the EVL. Another possibility is

that some DFCs connected to the EVL during epiboly movements might not be able to migrate properly, leading to the misclustering defects that we observe in Metrn mutants. Since the proper connection between DFC and EVL enables a subset of DFCs to have apical contacts with the EVL and to be pre-polarized, one can speculate that Metrns play a role in the polarization of DFCs [17], [18], [42], [43].

Additionally it was shown that the formation of the developing KV lumen was directly connected to ciliogenesis as polarized DFCs initiated developing cilia at their membrane domain facing the forming lumen [17]. This indicates that proper DFC polarization is essential for the KV formation and for ciliogenesis. The decreased number of cilia and reduced cilia length in *metrn* mutants suggest an impairment of the DFC polarization that consequently leads to a disturbance of the tissue interaction between the EVL and DFCs and consequently to KV formation defects.

In line with the impaired KV formation and function in *metrns* mutants, it was shown that knockdown of integrin αV as well as β1b in zebrafish also results in L-R asymmetry defects [40]. This was explained by DFC organization and migration defects and disturbed KV formation. Integrin αVβ1 has not yet been studied extensively in mammals, mostly due to their broad expression and connection with other integrins as well as the lack of antibodies and inhibitors specific for αVβ1. However, several *in vitro* studies already connected αVβ1 to developmental processes. For instance αVβ1 was shown to be implicated in embryonic astrocytes and oligodendrocyte precursors migration in rodents [44] and neural cell adhesion molecule L1 cell binding [45]. Our results suggest that integrin αV/β1b genetically interacts with Metrn proteins as one mechanism to properly cluster DFCs.

In spite of the recent advancement in understanding the multiple functions of Meteorins, Metrns receptor(s) are still unknown. It was recently shown that METRNL is promoting heart repair through its binding to KIT tyrosine kinase receptor, establishing METRNL as a KIT receptor ligand in the context of ischemic tissue repair [46]. At 9 hpf *kita* is solely expressed in prechordal plate and from 11 hpf in the lateral borders of the anterior neural plate (supp Figure 6A). *Kitb* expression could be detected from 11 hpf in the anterior ventral mesoderm (supp Figure 6B) as previously reported [47]. Recently it was shown that Metrn is a ligand for the 5-hydroxytryptamine receptor 2b (Htr2b). Additionally Metrn was associated to regulating reactive oxygen species levels in hematopoietic stem/progenitor cells via directing phospholipase C signaling [48]. However, analyzing the expression pattern of *htr2b* during zebrafish development (supp Figure 6B), we could detect *htr2b* expression only from around 2 dpf in the developing heart (supp Figure 6B).

Thus, the absence of *kita/b* as well as *htr2b* expression at early embryonic stages in proximity of the DFCs and in the forming KV suggests that Metrns act through another receptor during to ensure its L-R patterning function. Future studies focusing at identifying this receptor will be important to further investigate the pathway through which this family of proteins act during early embryogenesis.

MATERIAL AND METHODS

Zebrafish husbandry

Zebrafish (Danio rerio) were maintained at 28°C o.n. a 14h light/10h dark cycle. Fish were housed in the animal facility of our laboratory which was built according to the respective local animal welfare standards. All animal procedures were performed in accordance with French and European Union animal welfare guidelines with protocols approved by the committee on ethics of animal experimentation of Sorbonne Université (APAFIS#21323-2019062416186982).

CRISPR-Cas9-mediated mutagenesis of *metrn*, *metrnl1* and *metrnl2* and whole embryo DNA extraction

SgRNA guide sequences were cloned into a BsaI digested DR274 plasmid vector. The sgRNAs were synthetized by in vitro transcription. After transcription, sgRNAs were purified using a RNAeasy Mini Kit. The target sequences were the following:

	Sequence (5'->3')
metrn	CCACCACACCCGGCCCAGCC
metrnl1	GGTGTATCTCCGCTGCGCCC
metrnl2	CCAGAAACAGCGCCCCCTCCTGC

Cas9 mRNA was generated as described in Hwang, Fu et al. 2013 [49]. To induce targeted mutagenesis at the *metrn, metrnl1* and *metrnl2* loci, 200 ng/ml of sgRNA were injected into one-cell stage zebrafish embryos together with 150 ng/ml of *Cas9* mRNA. Injected embryos were grown to adulthood and screened for mutation in their offspring.

For genomic DNA extraction, 5dpf embryos were digested for 1 h at 55 °C in 0.5 mL lysis buffer (10 mM Tris, pH 8.0, 10 mM NaCl, 10 mM EDTA, and 2% SDS) with proteinase K (0.17 mg/mL, Roche Diagnostics) and inactivated 10 min at 95 °C. To check for frequency of indel mutations, target genomic loci were PCR amplified using a Phusion High-Fidelity DNA polymerase (Invitrogen). PCR amplicons were subsequently cloned into a pCR-bluntII-TOPO vector (Thermo Fisher). Plasmid DNA was isolated from single colonies and Sanger sequencings was performed by Eurofins. Mutant alleles were identified by comparison with the wild-type sequence using Geneious software.

Mutants genotyping and generation of triple mutants

Genotyping of *metrns* mutants was performed as follows: after genomic DNA extraction PCR amplification reactions were conducted in final volumes of 20 µl containing 1x PCR reaction buffer, 1,5mM MgCl2, 70 ng of gDNA, Taq DNA Polymerase (5U/µl) and 0.5 µM of each primer.

	Sequence (5'->3')
metrn-fw	CTGTGTTGACTGCTGGCTG
metrn-rev	GTGGTTTAGTGGTGTTCTTACAATGA
metrnl1-fw	TCCCATGCCTGGACCTCATA
metrnl1-rev	AGACGGAGAGAAGAGACGCT
metrnl2-fw	TGTTGATCAGCAGTGTGTGCGTAGC
metrnl2-rev	GTCCTCCGCTGATCTACGTG

The DNA amplification was performed with 35 cycles at the annealing temperature of 60°C. Metrn and metrnl2 amplicons were loaded on 2 % agarose gel to discriminate between wild type and mutant alleles (for *metrn*, the size of wild type allele is 598bp while the mutant is 482bp long; for *metrnl2*, the size of wild type allele is 242bp while the mutant is 156bp long). Metrnl1 PCR product was digested at 55°C o.n. with the PasI enzyme and the resulting digestion was subsequently analyzed on a 2% agarose gel. The wildtype allele results in two fragments of 107bp and 94bp length, respectively. The mutant alleles show one band at 201bp. Triple mutants were obtained by incrossing homozygous *metrn* and *metrnl1* mutants to generate double heterozygous mutants. Double heterozygous mutants were crossed with homozygous *metrnl2* and genotyped to identify triple heterozygous mutants. Triple heterozygous mutants were intercrossed and genotyped to identify triple homozygous mutants. In the described experiments, heterozygous triple mutants were obtained by outcrossing female triple mutants with male wildtype, if not stated differently.

Hybridization chain reaction (HCR)

All HCR probes and solutions were purchased from Molecular Instruments®. Decorionated embryos at the appropriate developmental stage(s) were fixed in 4% paraformaldehyde in PBS (pH 7.4) for 2 hours at room temperature, followed by several washes with PBS to stop the fixation. With a series of methanol MeOH washes the embryos were dehydrated and permeabilized. The HCR was performed described as described from the manufacturer. HCR samples were imaged on an inverted confocal microscope Olympus FV-1000, employing a 20x oil immersion objective (NA 0.85). Z-volumes were acquired with a 5µm resolution and images were processed and analyzed using ImageJ.

In situ hybridization in zebrafish and chicken

The respective cDNA fragments were amplified by PCR from zebrafish or chicken cDNA.
In vitro transcription of Digoxigenin/Fluorescent-labeled probes was performed using an RNA Labeling Kit according to manufacturer's instructions. Zebrafish whole-mount *in situ* hybridizations was performed described in Thisse and Thisse 2008 [50]. Whole-mount in situ hybridizations in chicken were performed as described in Streit and Stern 2001 [51]. *In situ hybridizations* were imaged on a Leica MZ10F stereomicroscope. Images were processed and analyzed using ImageJ software. Color balance, brightness and contrast and were applied uniformly. Fluorescent-labeled samples were imaged using an inverted confocal microscope Olympus FV-1000, employing a 40x oil immersion objective (NA 1.30). Z-volumes were acquired with a 0,5µm resolution and images were processed and analyzed using ImageJ.

Analysis of DFC phenotype and migration

For the DCF clustering analysis Bayesian inference was used to recover the maximum-likelihood value for the malformation probability. The outcome of an experiment was considered to be a binary random variable (malformed or normal phenotype) whose probability depends solely on the experimental condition. The total number of malformed phenotypes per experiment is therefore binomially distributed. The posterior distribution is obtained by inverting this binomial distribution using Bayes theorem, under a uniform prior. Under these hypotheses the maximum-likelihood estimate for the malformation probability is simply given by the empirical malformation frequency. The standard deviation of the posterior distribution was used to provide a confidence interval for the estimate (black error bars). P-values were evaluated using Fisher exact test on the number of malformed and normal phenotypes. AP to VP DFC migration was calculated as the % of the total embryo length.

qPCR and analysis

For gene expression analysis total RNA was prepared from zebrafish embryos with TRIzol reagent and TURBO DNA-free reagents. Total RNA was cleaned up using RNeasy Mini Kit (Qiagen) following the manufacturer's instructions and treated twice with DNase I (1 unit/µg RNA, Qiagen). The RNA concentration was quantified using nanodrop2000 (Thermo Fisher). RNA (1 µg) was retrotranscribed using random primers and a SuperScript III First-Strand Synthesis system. For q-RT-PCR, the SYBR Green PCR Master Mix was used according to the manufacturers protocol. *Ef1a* was used as reference genes as reported from Tang, Dodd et al. 2007 [52]. All assays were performed in triplicates. The mean values of triplicate experiments were calculated according to the delta CT quantification method (Valcu and Valcu 2011 [53]) and a student T-test was applied for the p-value calculation.

mRNA synthesis and injection

Zebrafish *metrn* and *metrnl1* cDNA fragments were amplified by PCR from zebrafish cDNA. The fragments were inserted into a pCS2+ plasmid linearized with Xho1 and Xba1 using a Quick Ligation Kit (NEB). Each plasmid was linearized with NotI restriction enzyme. mRNAs were synthesized by in vitro transcription with 1 µL of GTP from the kit added to the mix and lithium chloride precipitation (using the mMESSAGE mMACHINE sp6 Ultra kit #AM1340, Ambion) and 150ng/µl were injected into 1- to 4-cell-stage zebrafish embryos.

Design and injection of antisense morpholino oligonucleotides

MOs used were previously published from Ablooglu et al., 2010 [40]. All MOs were obtained from Gene Tools (Philomath, OR, USA). MOs were injected in respective concentrations in 1- to 4-cell-stage zebrafish embryos.

Whole-mount immunohistochemistry and quantification

Embryos were fixed in 4% paraformaldehyde in PBS-Tween for 2h at RT and subsequently washed three times in PBS-1% Triton X 100 to promote their permeabilization. Consequently, they were incubated for 1 hour at room temperature in blocking solution (10% Normal Goat Serum, in PBS-Tween) followed by overnight incubation, at 4 °C, with a 1/200 dilution of a mouse anti acetylated tubulin monoclonal antibody (Sigma T6793) in blocking solution. After five washes in PBS-Tween, the embryos were incubated overnight with an Alexa Fluor 488 anti-mouse IgG secondary antibody (Life Technologies) diluted at a final concentration of 1/200 respectively in blocking solution. The following day embryos were washed five times in PBS-Tween and mounted in 1% low melting point agarose in glass-bottom cell tissue culture dish. An inverted confocal microscope Olympus FV-1000 was used for imaging, employing a 40x oil immersion objective (NA 1.30). Z-volumes were acquired with a 0,5µm resolution and images were processed and analyzed using ImageJ.

Fluorescent microspheres injection and analysis

Embryos were dechorionated and mounted in 1% agarose and fish water. FluoSpheresH fluorescent microspheres injection was conducted as described in Borovina et al. 2010 [54]. Imaging was performed with a 40x water dipping objective using an upright Yokogawa CSU-X1 spinning disk scan head, mounted on a DM6000 upright Leica microscope and a CCD CoolSnap HQ2 camera at 4 Hz using the green channel at 0.25um resolution on a single z-plane. Beads trajectories extraction was performed using an already developed toolbox [55]. The size detection parameter was set to 0.75-1.25um objects with a brightness superior to the 0.01 percentile of the whole image. Objects that travelled less than 2.5um between two consecutive frames were linked into the same trajectory. Analyses between different

genotypes were performed using a custom-made Matlab code. For legibility, trajectories plots only show 20 tracked beads. MSD analysis was conducted according to Tarantino et al., 2014 [56] using already published code (https://tinevez.github.io/msdanalyzer/). Average MSD plots only show particle tracked between 1 and 8 s. Very short tracking durations do not permit to correctly estimate displacement properties and less then 1% of the particles were tracked during more than 8 s.

FIGURES

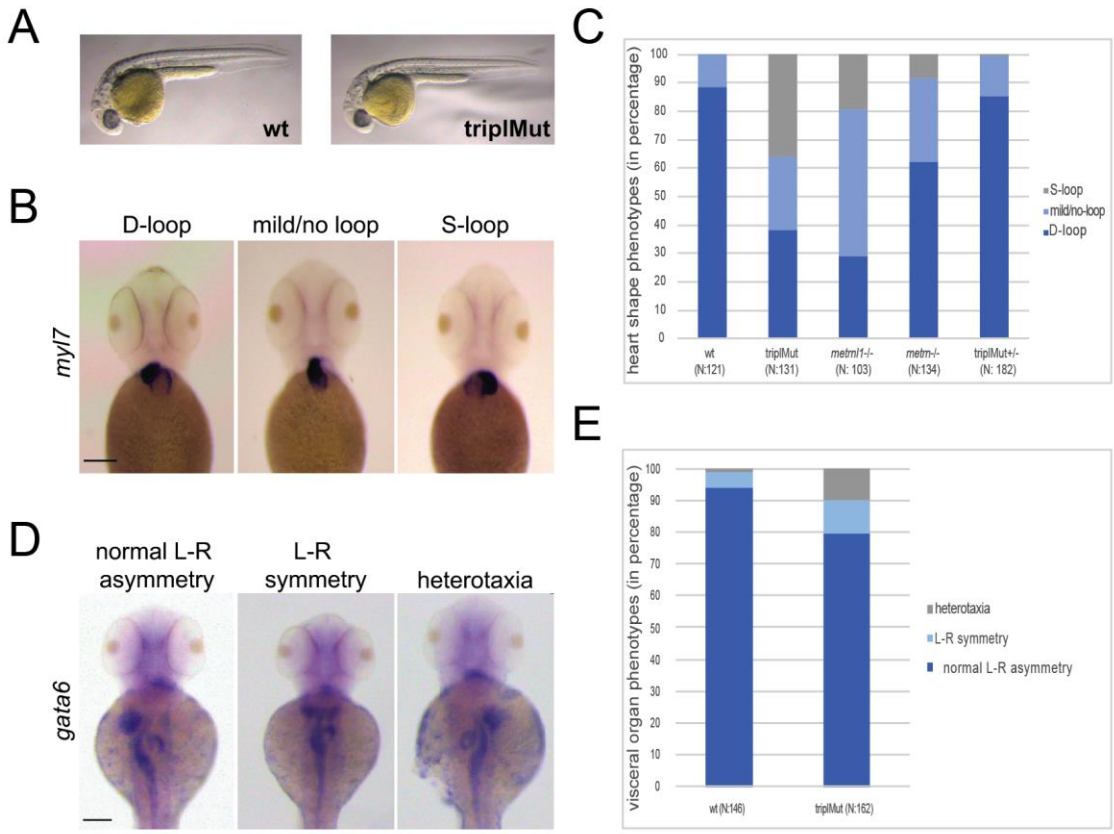

Figure 1: **Metrns LOF cause defects in heart looping and visceral organs positions, A** 48hpf zebrafish display no significant malformation in the *metrn*$^{-/-}$, *metrnl1*$^{-/-}$, *metrnl2*$^{-/-}$ (triplMut) background compared to WT embryos. **B** 2 dpf *myl7* antisense RNA probe *in situ* hybridization showing different phenotypes of heart looping. **C** Quantification of heart looping phenotypes at 2 dpf in wild-type and mutant embryos (triplMut, *metrn*$^{-/-}$, *metrnl1*$^{-/-}$, triplMut$^{+/-}$) showing the percentage of embryos (scale: 0.25mm). **D** 56 hpf *gata6* antisense RNA probe *in situ* hybridization showing different phenotypes of visceral organ positioning (scale: 0.25mm). **E** Quantification of visceral organ positioning phenotypes at 56 hpf in wild-type and triplMut embryos showing the percentage of embryos.

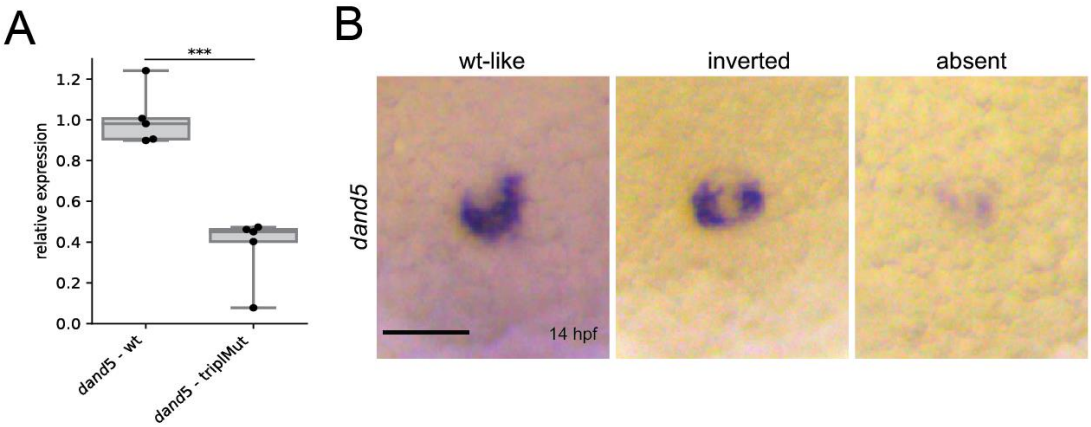

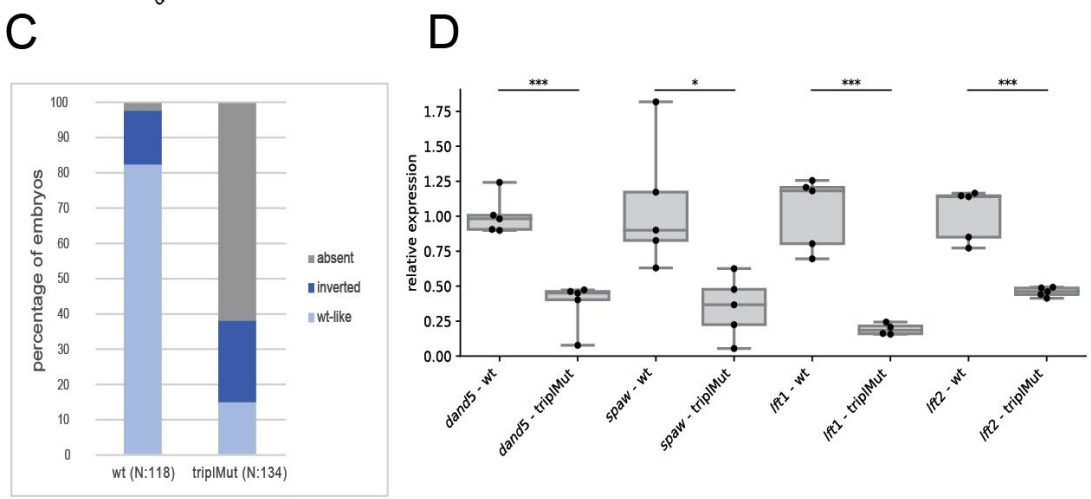

	wt-like	inverted	absent
wt (N=118)	82.20%	15.25%	2.54%
triplMut (N=134)	14.92%	23.13%	61.94%

Figure 2: **Metrns are required for proper Nodal factor genes expression, A** Quantification via qRT-PCR of *dand5* expression in 14hpf triple mutants compared to 14hpf wild type fish (student t-tests pvalue: 0.00019). **B** 14hpf *dand5* antisense RNA probe *in situ* hybridization showing different phenotypes of *dand5* expression (scale: 0.1mm). **C** Quantification of *dand5* expression phenotype at 14hpf in wild-type and mutant embryos showing the percentage of embryos. **D** Quantification via qRT-PCR of *spaw, lft1* and *left2* expression in 14hpf triple mutants compared to 14hpf wild type fish (student t-tests pvalues: *spaw* 0.014; *lft1* 0.0004; *lft2* 0.00019).

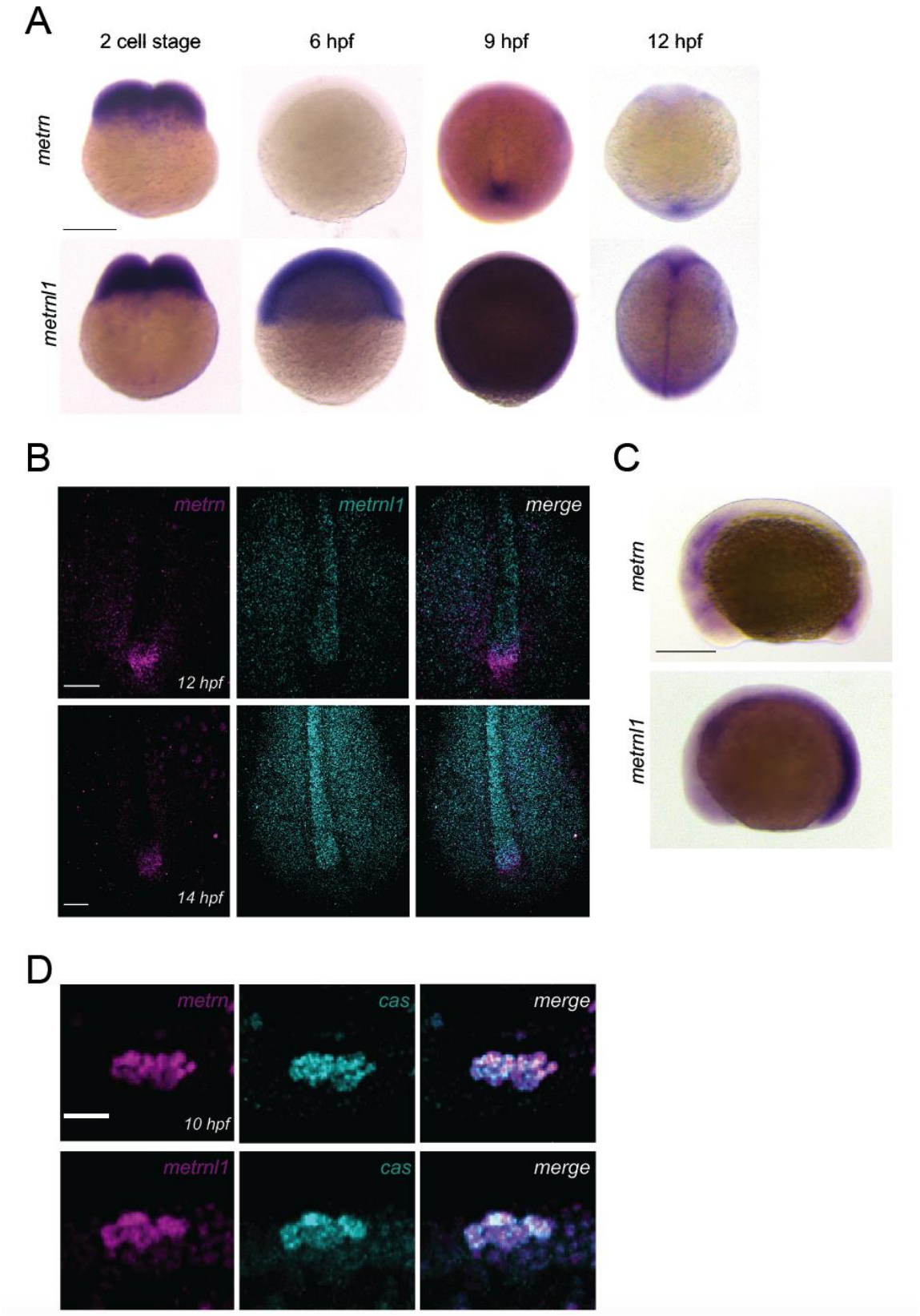

Figure 3: ***Metrns* are expressed during early zebrafish development, A** Expression pattern of *metrn* and *metrnl1* during early embryonic development visualized via *metrn/metrnl1* antisense RNA probe *in situ* hybridization (scale: 0.25mm). **B** Expression pattern of *metrn* and *metrnl1* at 12 hpf and 14 hpf visualized via HCR for *metrn* and *metrnl1* showing specific expression in the area of the KV

(scale: 0.25mm). **C** Expression pattern of *metrn* and *metrnl1* at 14 hpf visualized via *metrn/metrnl1* antisense RNA probe *in situ* hybridization, showing *metrn/metrnl1* expression along the midline and first *metrn* expression in the developing brain (scale: 0.25mm). **D** Double fluorescence *in situ* hybridization with *cas* and *metrn/metrnl1* antisense RNA probes on 10 hpf wt samples visualizing the expression of *metrn* an *metrnl1* within DFCs (scale: 50µm).

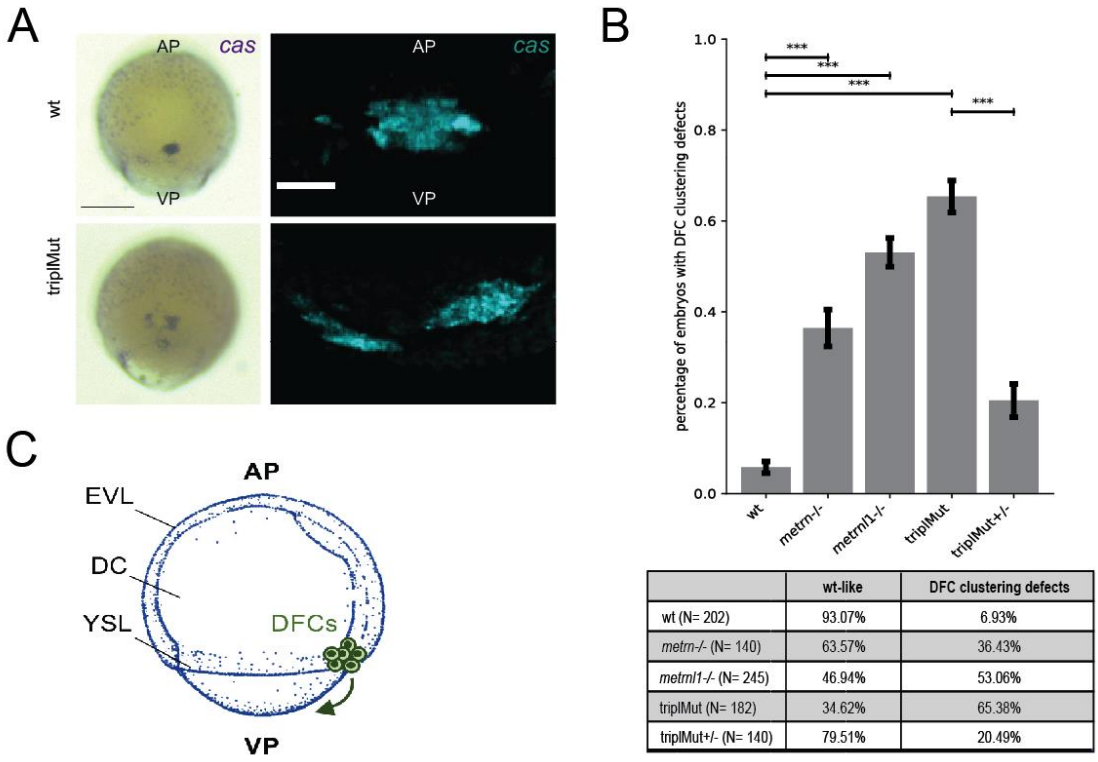

	wt-like	DFC clustering defects
wt (N= 202)	93.07%	6.93%
metrn-/- (N= 140)	63.57%	36.43%
metrnl1-/- (N= 245)	46.94%	53.06%
triplMut (N= 182)	34.62%	65.38%
triplMut+/- (N= 140)	79.51%	20.49%

	6 hpf	8 hpf	10 hpf
wt	59.32% (+/- 7.65%, N=27)	78.18% (+/- 7.94%, N=19)	93.67% (+/- 2.48%, N=16)
triplMut	46.26% (+/- 9.83%, N=24)	69.94% (+/- 6.22%, N=24)	80.67% (+/- 6.56%, N=20)

Figure 4: ***Metrns* loss-of-function leads to DFC disorganization and migration defects, A** *cas* antisense RNA probe *in situ* hybridization (scale: 0.25mm) and fluorescent situ hybridization (scale: 50µm) visualize DFC malformation at 9hpf (AP animal pole, VP vegetal pole). **B** Quantification of DFC malformation phenotype at 9hpf in wild-type and mutant embryos (p-values evaluated with Fisher exact test indicating statistical significance, ****p*-value < 0.0001 with wt, *metrn*$^{-/-}$ 1.6e-07; wt,

metrnl1$^{-/-}$ 3.5e-40; wt, triplMut 1.5e-49; triplMut, triplMut$^{+/-}$ 7.9e-15). **C** Schematic representation of an 8hpf zebrafish embryo visualizing animal pole (AP) to vegetal pole (VP) dorsal forerunner cell (DFC) migration, adapted from [57]. EVL, enveloping layer; DC, deep cells; YSL, yolk syncytial layer **D** The analysis of the die DFC migration between 6hpf and 10hpf shows a slower DFC migration in triplMut compared to wt embryos. Per condition and group 16 to 27 embryos were analyzed and the migration was calculated as the % of the total embryo length (p-values evaluated with Fisher exact test, ****p*-value < 0.0001 with 6hpf 2.5e-06; 8hpf 0.00038; 10hpf 1.1e-08).

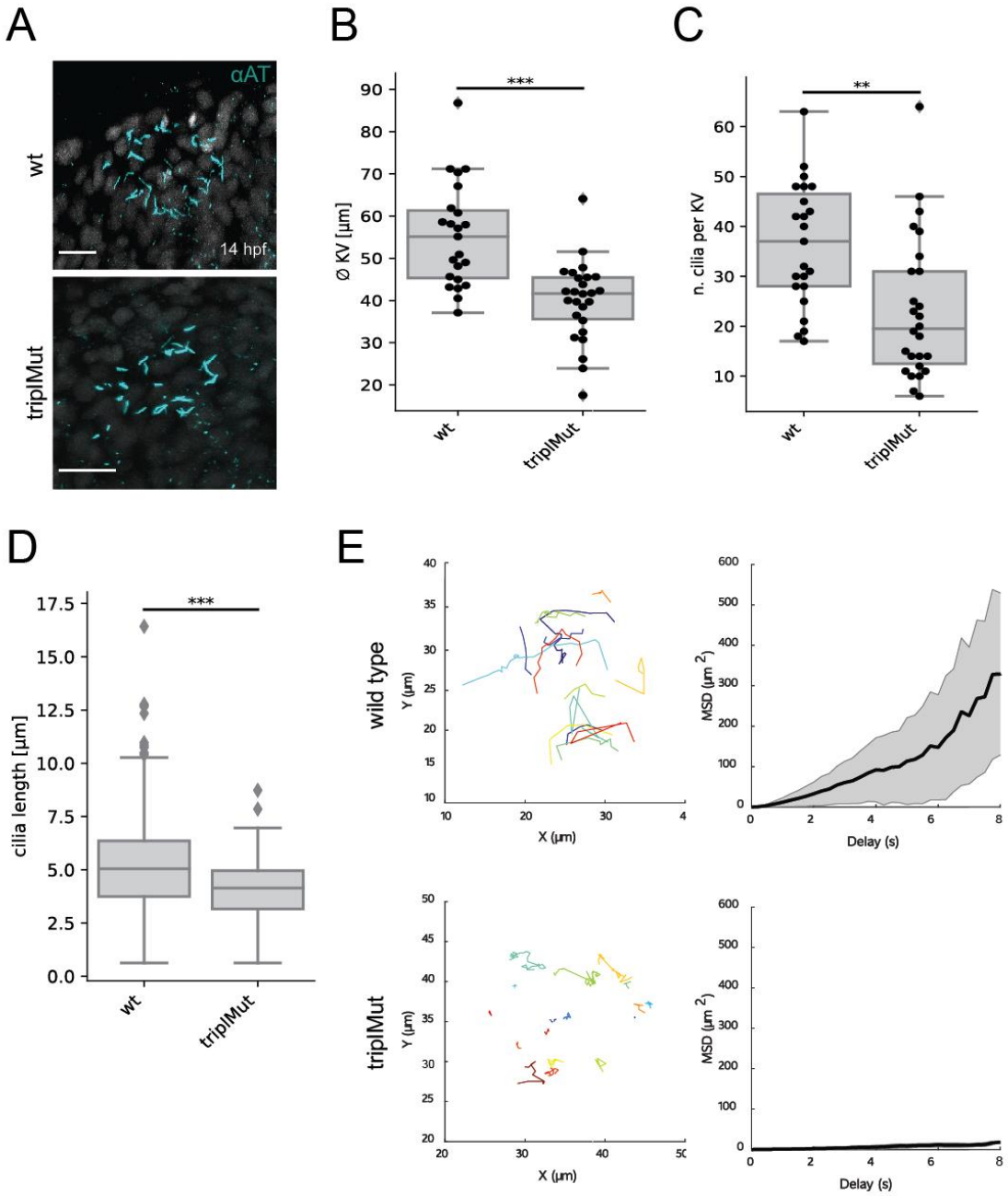

Figure 5: ***Metrns* loss-of-function impairs the KV formation and function, A** 14hpf wt and triplMut acetylated tubulin immunostaining visualizing the cilia in the KV (scale: 20µm). **B-D** Properties of the KV are changed in *Metrns* LOF embryos. **B** The KV size **C** the number of cilia per KV as well as **D**

the length of each individual cilia are decreased in triplMut, with student t-tests indicating statistical significance, **p*-value < 0.01, ***p*-value < 0.001 and ****p*-value < 0.0001 and n.s. = not significant, KV size pvalue: 9.7e-06, cilia number pvalue: 0.0012 and cilia length pvalue: 1.2e-20. **E** Examples for the tracking of single microbeads in the KV of 6ss-10ss embryos and the mean square displacement (MSD), visualizing a directed trajectory in wt samples in contrast to triplMut, displaying short and undirected trajectories**.**

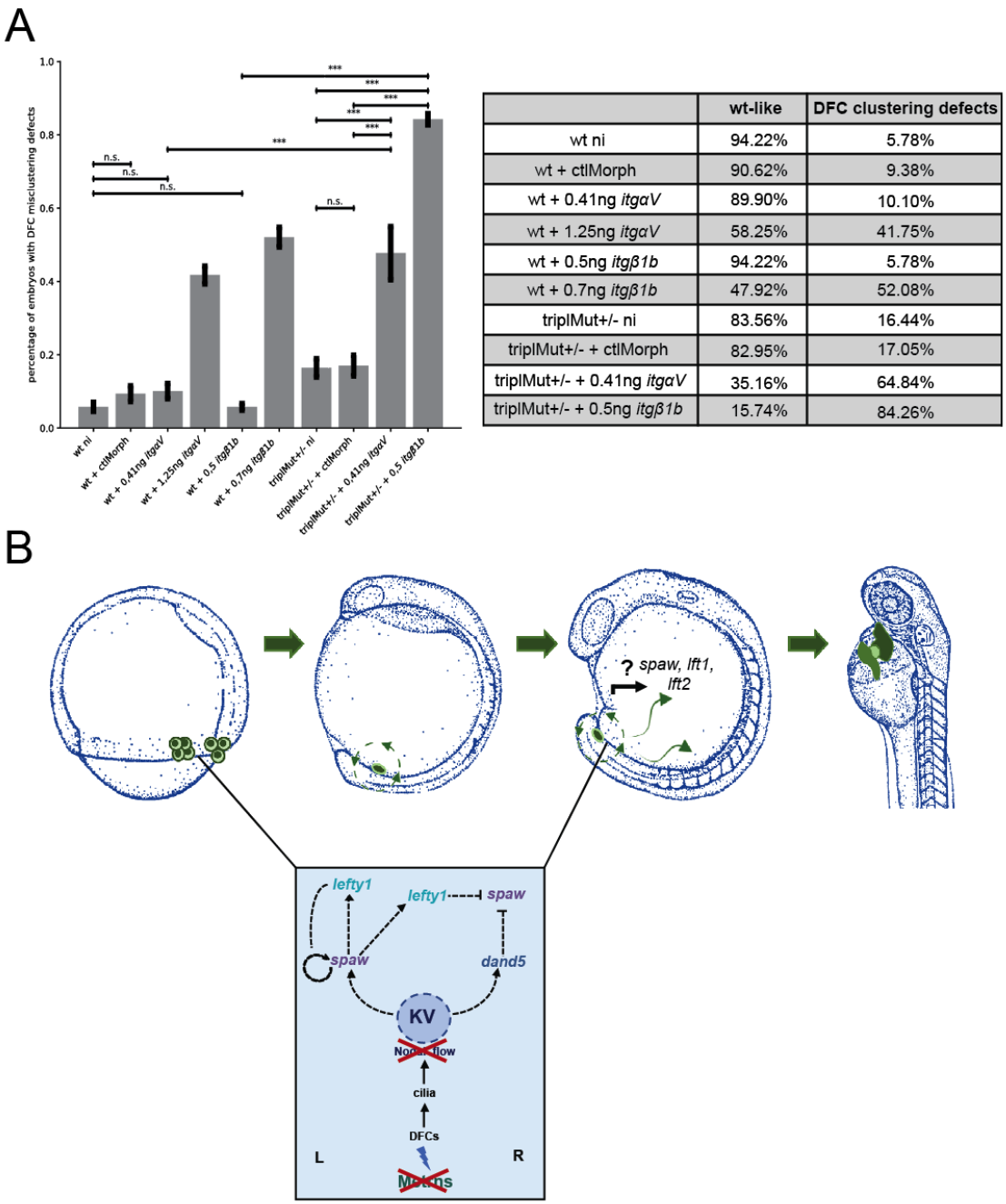

	wt-like	DFC clustering defects
wt ni	94.22%	5.78%
wt + ctlMorph	90.62%	9.38%
wt + 0.41ng *itgαV*	89.90%	10.10%
wt + 1.25ng *itgαV*	58.25%	41.75%
wt + 0.5ng *itgβ1b*	94.22%	5.78%
wt + 0.7ng *itgβ1b*	47.92%	52.08%
triplMut+/- ni	83.56%	16.44%
triplMut+/- + ctlMorph	82.95%	17.05%
triplMut+/- + 0.41ng *itgαV*	35.16%	64.84%
triplMut+/- + 0.5ng *itgβ1b*	15.74%	84.26%

Figure 6: Genetic interaction of ItgαV/Itgβ1b and Metrns on the level of the DFCs, A Quantification of DFC malformation phenotype at 9hpf for wt non injected (wt ni), wt + 2.5ng control morpholino (wt + ctlMorph), wt + insufficient doses *itgαV/itgβ1b* morpholinos (wt + 0.41ng *itgαV*; wt +

0.5 *itgβ1b*), wt + sufficient *itgαV/itgβ1b* dosages (wt + 1.25ng *itgαV*; wt + 0.7ng *itgβ1b*), heterozygous triple mutants non injected (triplMut$^{+/-}$ ni), heterozygous triple mutant + 2.5ng control morpholino (triplMut$^{+/-}$ + ctlMorph) and heterozygous triple mutants with insufficient doses of *itgαV/itgβ1b* morpholinos (triplMut$^{+/-}$ + 0.41ng *itgαV*; triplMut$^{+/-}$ + 0.5 *itgβ1b*) showing the percentage of malformation (P-values evaluated with Fisher exact test indicating statistical significance, **p*-value < 0.01, ***p*-value < 0.001 and ****p*-value < 0.0001 and n.s. = not significant). **B** Schematic for the hypothesized role of Metrns in DFC assembly and migration and their influence on proper KV formation and nodal factor expression, crucial for correct left-right axis establishment, adapted from [57].

REFERENCES

[1] M. Blum, K. Feistel, T. Thumberger, and A. Schweickert, “The evolution and conservation of left-right patterning mechanisms,” *Development*, vol. 141, no. 8, pp. 1603–1613, Apr. 2014, doi: 10.1242/dev.100560.

[2] M. Blum and T. Ott, “Animal left–right asymmetry,” *Current Biology*, vol. 28, no. 7, pp. R301–R304, Apr. 2018, doi: 10.1016/j.cub.2018.02.073.

[3] D. T. Grimes and R. D. Burdine, “Left–Right Patterning: Breaking Symmetry to Asymmetric Morphogenesis,” *Trends in Genetics*, vol. 33, no. 9, pp. 616–628, Sep. 2017, doi: 10.1016/j.tig.2017.06.004.

[4] A. Kawasumi *et al.*, “Left–right asymmetry in the level of active Nodal protein produced in the node is translated into left–right asymmetry in the lateral plate of mouse embryos,” *Developmental Biology*, vol. 353, no. 2, pp. 321–330, May 2011, doi: 10.1016/j.ydbio.2011.03.009.

[5] W. W. Branford and H. J. Yost, “Nodal Signaling: CrypticLefty Mechanism of Antagonism Decoded,” *Current Biology*, vol. 14, no. 9, pp. R341–R343, May 2004, doi: 10.1016/j.cub.2004.04.020.

[6] X. Zhou, L. Lowe, H. Sasaki, B. L. M. Hogan, and M. R. Kuehn, “Nodal is a novel TGF-β-like gene expressed in the mouse node during gastrulation,” *Nature*, vol. 361, no. 6412, pp. 543–547, Feb. 1993, doi: 10.1038/361543a0.

[7] Y. Chen and A. F. Schier, “Lefty Proteins Are Long-Range Inhibitors of Squint-Mediated Nodal Signaling,” *Current Biology*, vol. 12, no. 24, pp. 2124–2128, Dec. 2002, doi: 10.1016/S0960-9822(02)01362-3.

[8] C. Chen and M. M. Shen, “Two Modes by which Lefty Proteins Inhibit Nodal Signaling,” *Current Biology*, vol. 14, no. 7, pp. 618–624, Apr. 2004, doi: 10.1016/j.cub.2004.02.042.

[9] J. J. Essner, J. D. Amack, M. K. Nyholm, E. B. Harris, and H. J. Yost, “Kupffer’s vesicle is a ciliated organ of asymmetry in the zebrafish embryo that initiates left-right development of the brain, heart and gut,” *Development*, vol. 132, no. 6, pp. 1247–1260, Mar. 2005, doi: 10.1242/dev.01663.

[10] J. Gros, K. Feistel, C. Viebahn, M. Blum, and C. J. Tabin, “Cell Movements at Hensen’s Node Establish Left/Right Asymmetric Gene Expression in the Chick,” *Science*, vol. 324, no. 5929, pp. 941–944, May 2009, doi: 10.1126/science.1172478.

[11] P. Vick *et al.*, “Flow on the right side of the gastrocoel roof plate is dispensable for symmetry breakage in the frog Xenopus laevis,” *Developmental Biology*, vol. 331, no. 2, pp. 281–291, Jul. 2009, doi: 10.1016/j.ydbio.2009.05.547.

[12] S. Nonaka, H. Shiratori, Y. Saijoh, and H. Hamada, “Determination of left–right patterning of the mouse embryo by artificial nodal flow,” *Nature*, vol. 418, no. 6893, pp. 96–99, Jul. 2002, doi: 10.1038/nature00849.

[13] A. Schweickert *et al.*, “Cilia-Driven Leftward Flow Determines Laterality in Xenopus,” *Current Biology*, vol. 17, no. 1, pp. 60–66, Jan. 2007, doi: 10.1016/j.cub.2006.10.067.

[14] Y. Okada, S. Takeda, Y. Tanaka, J.-C. I. Belmonte, and N. Hirokawa, “Mechanism of Nodal Flow: A Conserved Symmetry Breaking Event in Left-Right Axis Determination,” *Cell*, vol. 121, no. 4, pp. 633–644, May 2005, doi: 10.1016/j.cell.2005.04.008.

[15] Y. Tanaka, Y. Okada, and N. Hirokawa, “FGF-induced vesicular release of Sonic hedgehog and retinoic acid in leftward nodal flow is critical for left–right determination,” *Nature*, vol. 435, no. 7039, pp. 172–177, May 2005, doi: 10.1038/nature03494.

[16] S. Nonaka *et al.*, “Randomization of Left–Right Asymmetry due to Loss of Nodal Cilia Generating Leftward Flow of Extraembryonic Fluid in Mice Lacking KIF3B Motor Protein,” *Cell*, vol. 95, no. 6, pp. 829–837, Dec. 1998, doi: 10.1016/S0092-8674(00)81705-5.

[17] P. Oteíza, M. Köppen, M. L. Concha, and C.-P. Heisenberg, “Origin and shaping of the laterality organ in zebrafish,” *Development*, vol. 135, no. 16, pp. 2807–2813, Aug. 2008, doi: 10.1242/dev.022228.

[18] M. S. Cooper and L. A. D’amico, “A Cluster of Noninvoluting Endocytic Cells at the Margin of the Zebrafish Blastoderm Marks the Site of Embryonic Shield Formation,” *Developmental Biology*, vol. 180, no. 1, pp. 184–198, Nov. 1996, doi: 10.1006/dbio.1996.0294.

[19] N. Hirokawa, Y. Tanaka, Y. Okada, and S. Takeda, “Nodal Flow and the Generation of Left-Right Asymmetry,” *Cell*, vol. 125, no. 1, pp. 33–45, Apr. 2006, doi: 10.1016/j.cell.2006.03.002.

[20] R. P. Harvey, “Links in the Left/Right Axial Pathway,” *Cell*, vol. 94, no. 3, pp. 273–276, Aug. 1998, doi: 10.1016/S0092-8674(00)81468-3.

[21] Y.-Y. Kim *et al.*, “Meteorin Regulates Mesendoderm Development by Enhancing Nodal Expression,” *PLoS ONE*, vol. 9, no. 2, p. e88811, Feb. 2014, doi: 10.1371/journal.pone.0088811.

[22] J. Nishino, K. Yamashita, H. Hashiguchi, H. Fujii, T. Shimazaki, and H. Hamada, “Meteorin: a secreted protein that regulates glial cell differentiation and promotes axonal extension,” *EMBO J*, vol. 23, no. 9, pp. 1998–2008, May 2004, doi: 10.1038/sj.emboj.7600202.

[23] M. Ramialison *et al.*, “Rapid identification of PAX2/5/8 direct downstream targets in the otic vesicle by combinatorial use of bioinformatics tools,” *Genome Biol*, vol. 9, no. 10, p. R145, 2008, doi: 10.1186/gb-2008-9-10-r145.

[24] J. R. Jørgensen *et al.*, “Cometin is a novel neurotrophic factor that promotes neurite outgrowth and neuroblast migration in vitro and supports survival of spiral ganglion neurons in vivo,” *Experimental Neurology*, vol. 233, no. 1, pp. 172–181, Jan. 2012, doi: 10.1016/j.expneurol.2011.09.027.

[25] T. G. Montague, J. A. Gagnon, and A. F. Schier, “Conserved regulation of Nodal-mediated left-right patterning in zebrafish and mouse,” *Development*, vol. 145, no. 24, p. dev171090, Dec. 2018, doi: 10.1242/dev.171090.

[26] S. Long, N. Ahmad, and M. Rebagliati, “The zebrafish *nodal* -related gene *southpaw* is required for visceral and diencephalic left-right asymmetry,” *Development*, vol. 130, no. 11, pp. 2303–2316, Jun. 2003, doi: 10.1242/dev.00436.

[27] J. Brennan, D. P. Norris, and E. J. Robertson, “Nodal activity in the node governs left-right asymmetry,” *Genes Dev.*, vol. 16, no. 18, pp. 2339–2344, Sep. 2002, doi: 10.1101/gad.1016202.

[28] Y. Saijoh, S. Oki, S. Ohishi, and H. Hamada, “Left–right patterning of the mouse lateral plate requires Nodal produced in the node,” *Developmental Biology*, p. 13, 2003, doi: 10.1016/s0012-1606(02)00121-5.

[29] J. L. Pelliccia, G. A. Jindal, and R. D. Burdine, “Gdf3 is required for robust Nodal signaling during germ layer formation and left-right patterning,” *eLife*, vol. 6, p. e28635, Nov. 2017, doi: 10.7554/eLife.28635.

[30] M. Hojo *et al.*, “Right-elevated expression of charon is regulated by fluid flow in medaka Kupffer’s vesicle: Left-right asymmetric expression of charon,” *Development, Growth & Differentiation*, vol. 49, no. 5, pp. 395–405, Jun. 2007, doi: 10.1111/j.1440-169X.2007.00937.x.

[31] F. Gourronc, N. Ahmad, N. Nedza, T. Eggleston, and M. Rebagliati, “Nodal activity around Kupffer’s vesicle depends on the T-box transcription factors notail and spadetail and on notch signaling,” *Dev. Dyn.*, vol. 236, no. 8, pp. 2131–2146, Aug. 2007, doi: 10.1002/dvdy.21249.

[32] J. Alexander, M. Rothenberg, G. L. Henry, and D. Y. R. Stainier, “casanova Plays an Early and Essential Role in Endoderm Formation in Zebrafish,” *Developmental Biology*, vol. 215, no. 2, pp. 343–357, Nov. 1999, doi: 10.1006/dbio.1999.9441.

[33] Y. Kikuchi *et al.*, “*casanova* encodes a novel Sox-related protein necessary and sufficient for early endoderm formation in zebrafish,” *Genes Dev.*, vol. 15, no. 12, pp. 1493–1505, Jun. 2001, doi: 10.1101/gad.892301.

[34] M. A. El-Brolosy *et al.*, “Genetic compensation triggered by mutant mRNA degradation,” *Nature*, vol. 568, no. 7751, pp. 193–197, Apr. 2019, doi: 10.1038/s41586-019-1064-z.

[35] J. D. Amack and H. J. Yost, “The T Box Transcription Factor No Tail in Ciliated Cells Controls Zebrafish Left-Right Asymmetry,” *Current Biology*, vol. 14, no. 8, pp. 685–690, Apr. 2004, doi: 10.1016/j.cub.2004.04.002.

[36] T. Matsui, I. Hiroshi, and B. Yasumasa, “Cell collectivity regulation within migrating cell cluster during Kupffer’s vesicle formation in zebrafish,” *Frontiers in Cell and Developmental Biology*, vol. 3, p. 8, 2015, doi: 10.3389/fcell.2015.00027.

[37] H. Hashimoto *et al.*, “The Cerberus/Dan-family protein Charon is a negative regulator of Nodal signaling during left-right patterning in zebrafish,” *Development*, vol. 131, no. 8, pp. 1741–1753, Apr. 2004, doi: 10.1242/dev.01070.

[38] P. Sampaio *et al.*, “Left-Right Organizer Flow Dynamics: How Much Cilia Activity Reliably Yields Laterality?,” *Developmental Cell*, vol. 29, no. 6, pp. 716–728, Jun. 2014, doi: 10.1016/j.devcel.2014.04.030.

[39] J. J. Gokey, Y. Ji, H. G. Tay, B. Litts, and J. D. Amack, “Kupffer’s vesicle size threshold for robust left-right patterning of the zebrafish embryo: Size Threshold For KV Function,” *Dev. Dyn.*, vol. 245, no. 1, pp. 22–33, Jan. 2016, doi: 10.1002/dvdy.24355.

[40] A. J. Ablooglu, E. Tkachenko, J. Kang, and S. J. Shattil, “Integrin αV is necessary for gastrulation movements that regulate vertebrate body asymmetry,” *Development*, vol. 137, no. 20, pp. 3449–3458, Oct. 2010, doi: 10.1242/dev.045310.

[41] B. W. Bisgrove, J. J. Essner, and H. J. Yost, “Multiple pathways in the midline regulate concordant brain, heart and gut left-right asymmetry,” *Development*, vol. 127, no. 16, pp. 3567–3579, Aug. 2000, doi: 10.1242/dev.127.16.3567.

[42] L. Solnica-Krezel *et al.*, “Mutations affecting cell fates and cellular rearrangements during gastrulation in zebrafish,” *Development*, vol. 123, no. 1, pp. 67–80, Dec. 1996, doi: 10.1242/dev.123.1.67.

[43] E. Pulgar *et al.*, “Apical contacts stemming from incomplete delamination guide progenitor cell allocation through a dragging mechanism,” *eLife*, vol. 10, p. e66483, Aug. 2021, doi: 10.7554/eLife.66483.

[44] R. Milner, G. Edwards, C. Streuli, and C. ffrench-Constant, “A Role in Migration for the αvβ1 Integrin Expressed on Oligodendrocyte Precursors,” *J Neurosci*, vol. 16, no. 22, pp. 7240–7252, Nov. 1996, doi: 10.1523/JNEUROSCI.16-22-07240.1996.

[45] B. Felding-Habermann *et al.*, “A Single Immunoglobulin-like Domain of the Human Neural Cell Adhesion Molecule L1 Supports Adhesion by Multiple Vascular and Platelet Integrins,” *Journal of Cell Biology*, vol. 139, no. 6, pp. 1567–1581, Dec. 1997, doi: 10.1083/jcb.139.6.1567.

[46] M. R. Reboll *et al.*, “Meteorin-like promotes heart repair through endothelial KIT receptor tyrosine kinase,” *Science*, vol. 376, no. 6599, pp. 1343–1347, Jun. 2022, doi: 10.1126/science.abn3027.

[47] E. M. Mellgren and S. L. Johnson, “kitb, a second zebrafish ortholog of mouse Kit,” *Dev Genes Evol*, vol. 215, no. 9, pp. 470–477, Sep. 2005, doi: 10.1007/s00427-005-0001-3.

[48] Y.-W. Dai *et al.*, “Meteorin links the bone marrow hypoxic state to hematopoietic stem/progenitor cell mobilization,” *Cell Reports*, vol. 40, no. 12, p. 111361, Sep. 2022, doi: 10.1016/j.celrep.2022.111361.

[49] W. Y. Hwang *et al.*, “Efficient genome editing in zebrafish using a CRISPR-Cas system,” *Nat Biotechnol*, vol. 31, no. 3, pp. 227–229, Mar. 2013, doi: 10.1038/nbt.2501.

[50] C. Thisse and B. Thisse, “High-resolution in situ hybridization to whole-mount zebrafish embryos,” *Nat Protoc*, vol. 3, no. 1, pp. 59–69, Jan. 2008, doi: 10.1038/nprot.2007.514.

[51] A. Streit and C. D. Stern, “Combined Whole-Mount in Situ Hybridization and Immunohistochemistry in Avian Embryos,” *Methods*, vol. 23, no. 4, pp. 339–344, Apr. 2001, doi: 10.1006/meth.2000.1146.

[52] R. Tang, A. Dodd, D. Lai, W. C. McNabb, and D. R. Love, “Validation of Zebrafish (Danio rerio) Reference Genes for Quantitative Real-time RT-PCR Normalization,” *ABBS*, vol. 39, no. 5, pp. 384–390, May 2007, doi: 10.1111/j.1745-7270.2007.00283.x.

[53] M. Valcu and C.-M. Valcu, “Data transformation practices in biomedical sciences,” *Nat Methods*, vol. 8, no. 2, pp. 104–105, Feb. 2011, doi: 10.1038/nmeth0211-104.

[54] A. Borovina, S. Superina, D. Voskas, and B. Ciruna, “Vangl2 directs the posterior tilting and asymmetric localization of motile primary cilia,” *Nat Cell Biol*, vol. 12, no. 4, Art. no. 4, Apr. 2010, doi: 10.1038/ncb2042.

[55] I. F. Sbalzarini and P. Koumoutsakos, “Feature point tracking and trajectory analysis for video imaging in cell biology,” *Journal of Structural Biology*, vol. 151, no. 2, pp. 182–195, 2005, doi: 10.1016/j.jsb.2005.06.002.

[56] N. Tarantino *et al.*, “TNF and IL-1 exhibit distinct ubiquitin requirements for inducing NEMO–IKK supramolecular structures,” *Journal of Cell Biology*, vol. 204, no. 2, pp. 231–245, Jan. 2014, doi: 10.1083/jcb.201307172.

[57] C. B. Kimmel, W. W. Ballard, S. R. Kimmel, B. Ullmann, and T. F. Schilling, “Stages of embryonic development of the zebrafish,” *Developmental Dynamics*, vol. 203, no. 3, pp. 253–310, 1995, doi: 10.1002/aja.1002030302.

Supplement Figures

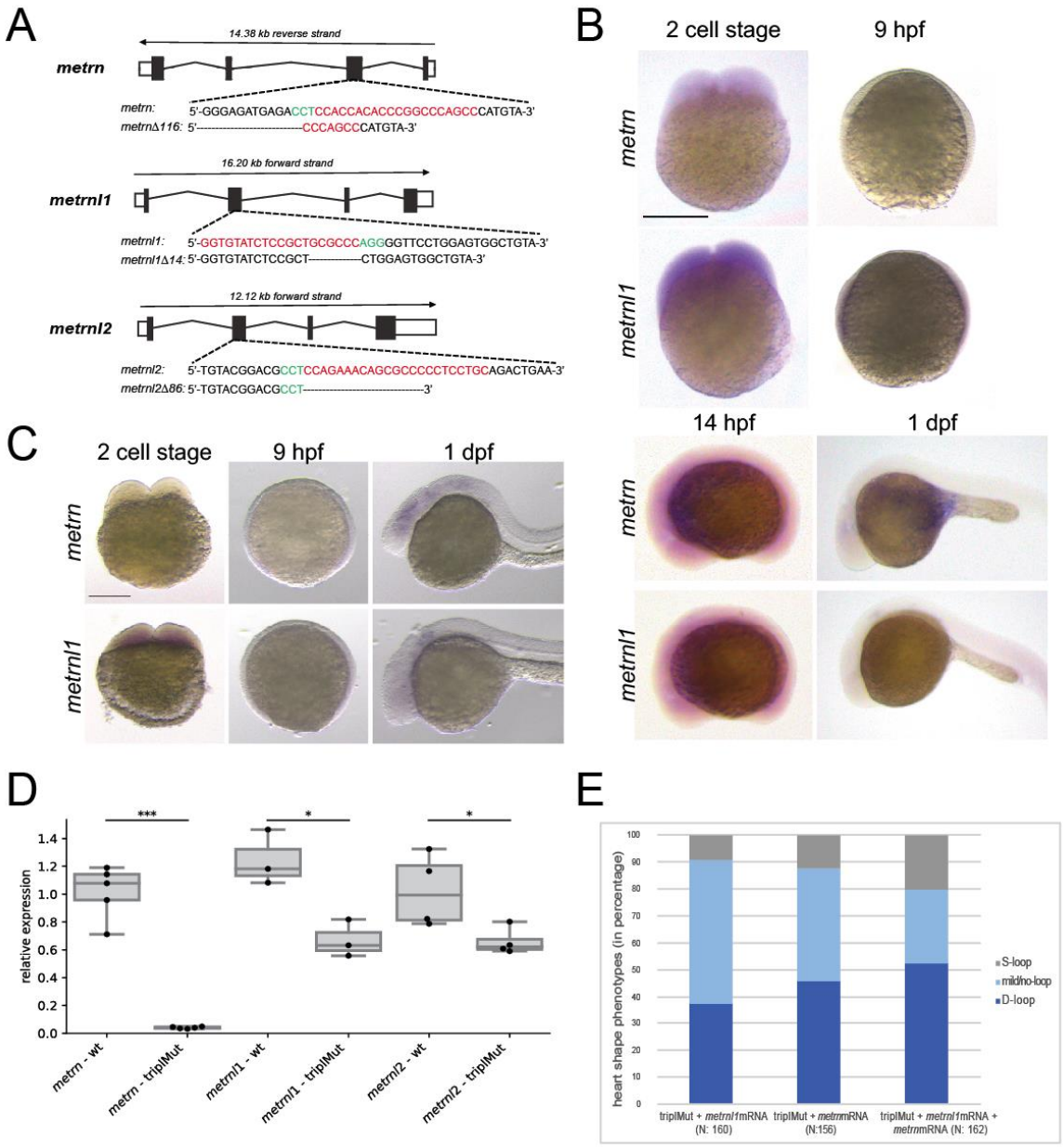

Supplement Figure 1: Metrns LOF cause defects in heart looping and visceral organs positions, A Schematic representation of the three targeted *metrn* loci in the zebrafish genome for the LOF generation. Targeted nucleotides in exon 2 of each gene are indicated in red; the PAM sequences are highlighted in green. **B** *Metrn* and *metrnl1 in situ* hybridization on triplMut showing a reduction of the amount of *metrn* transcripts in triple mutants over several developmental stages (scale: 0.25mm). **C** *Metrn* and *metrnl1 in situ* hybridization showing a reduction of the amount of *metrns* transcripts in metrn$^{-/-}$ or metrnl1$^{-/-}$ embryos over several developmental stages (scale: 0.25mm). **D** Quantification via qRT-PCR of the reduction of *metrns* expression in triple mutants compared to wild type fish (*metrn/metrnl1*: 14hpf, *metrnl2*: 48hpf, student t-tests pvalues: *metrn* 3.1e-

06; *metrnl1* 0.014; *metrnl2* 0.04). **E** Quantification of the mRNA injection rescue heart looping phenotypes at 2dpf in injected triplMut showing the percentage of embryos.

A

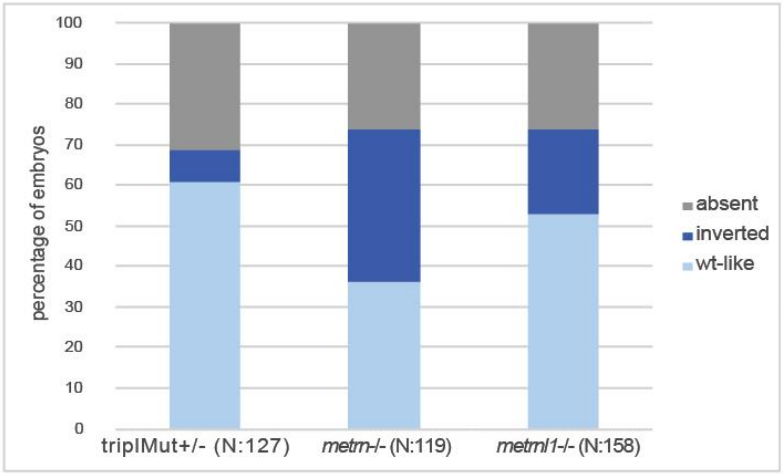

	wt-like	inverted	absent
triplMut+/- (N=127)	60.63%	7.87%	31.50%
metrn-/- (N=119)	39.50%	40.33%	28.57%
metrnl1-/- (N=158)	53.16%	20.89%	25.95%

B

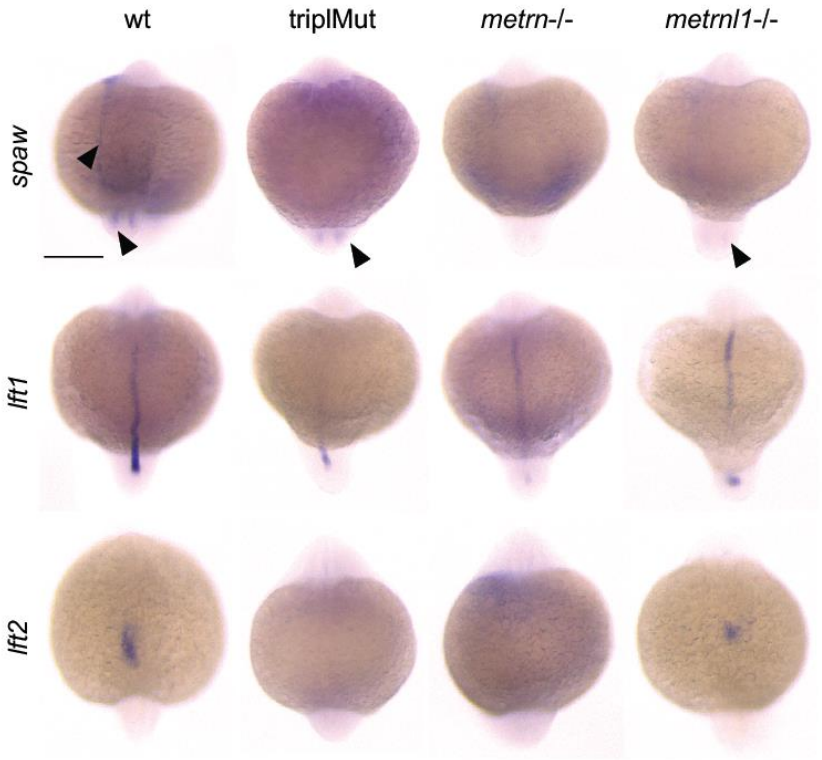

Supplement Figure 2: Metrns are required for proper Nodal factor genes expression, A Further quantification of *dand5* expression phenotype at 14hpf in triplMut$^{+/-}$ and single mutant embryos showing the percentage of embryos. **B** 16hpf *in situ* hybridization for *spaw*, *lft1* and *lft2* show altered expression patterns in triplMut, *metrn* and *metrnl1* mutants (scale: 0.25mm).

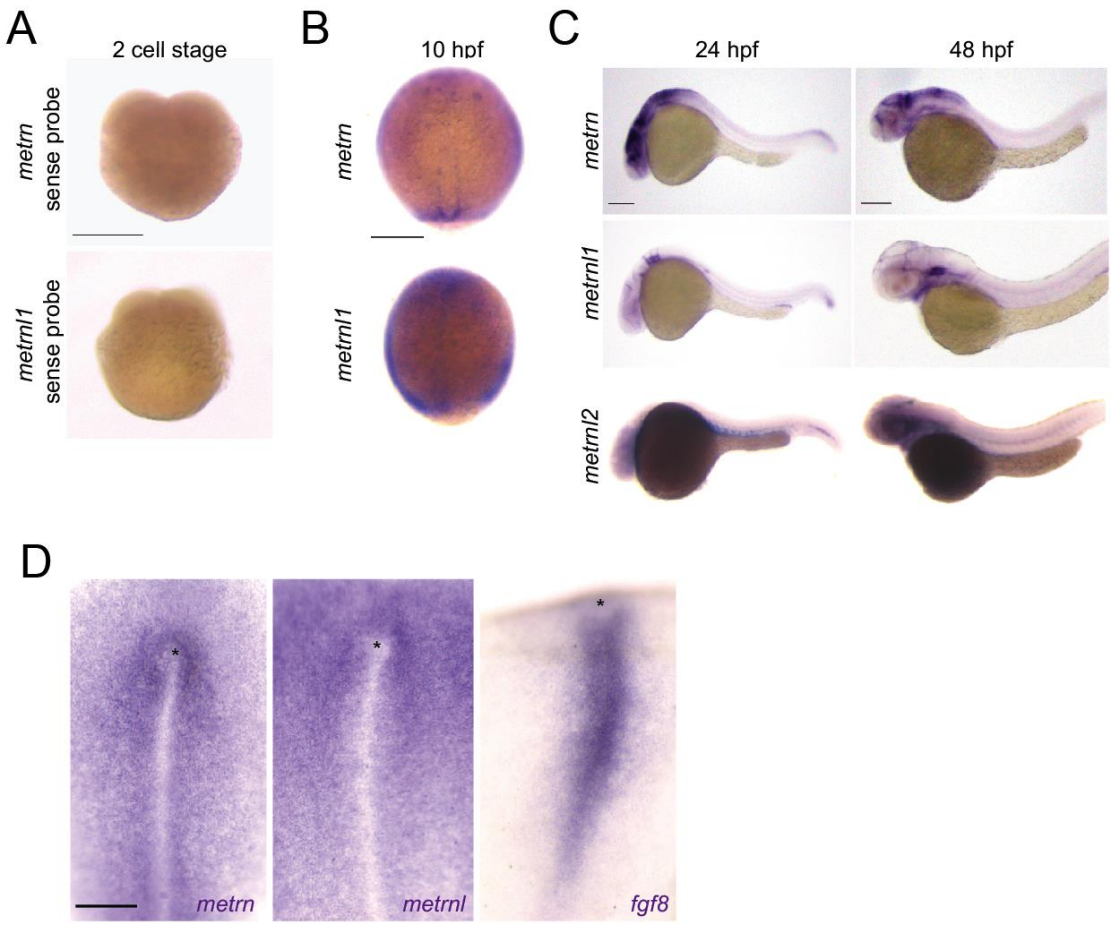

Supplement Figure 3: *Metrns* are expressed during early zebrafish development, A 2 cell stage *metrn/metrnl1* sense RNA probe *in situ* hybridization (scale: 0.25mm). **B** Expression patterns of *metrn* and *metrnl1* at 10 hpf, visualized via *metrn/metrnl1* antisense RNA probe *in situ* hybridization (scale: 0.25mm). **C** Expression patterns of *metrn, metrnl1* and *metrnl2* at 24 hpf and 48hpf, visualized via *metrn/metrnl1/metrnl2* antisense RNA probe *in situ* hybridization (scale: 0.25mm). **D** RNA probe *in situ* hybridization in HH6 chick embryos for *metrn*, *metrnl* as well as *fgf8,* visualizing expression around the Hensen's node (*) and the primitive streak (scale: 0.25mm).

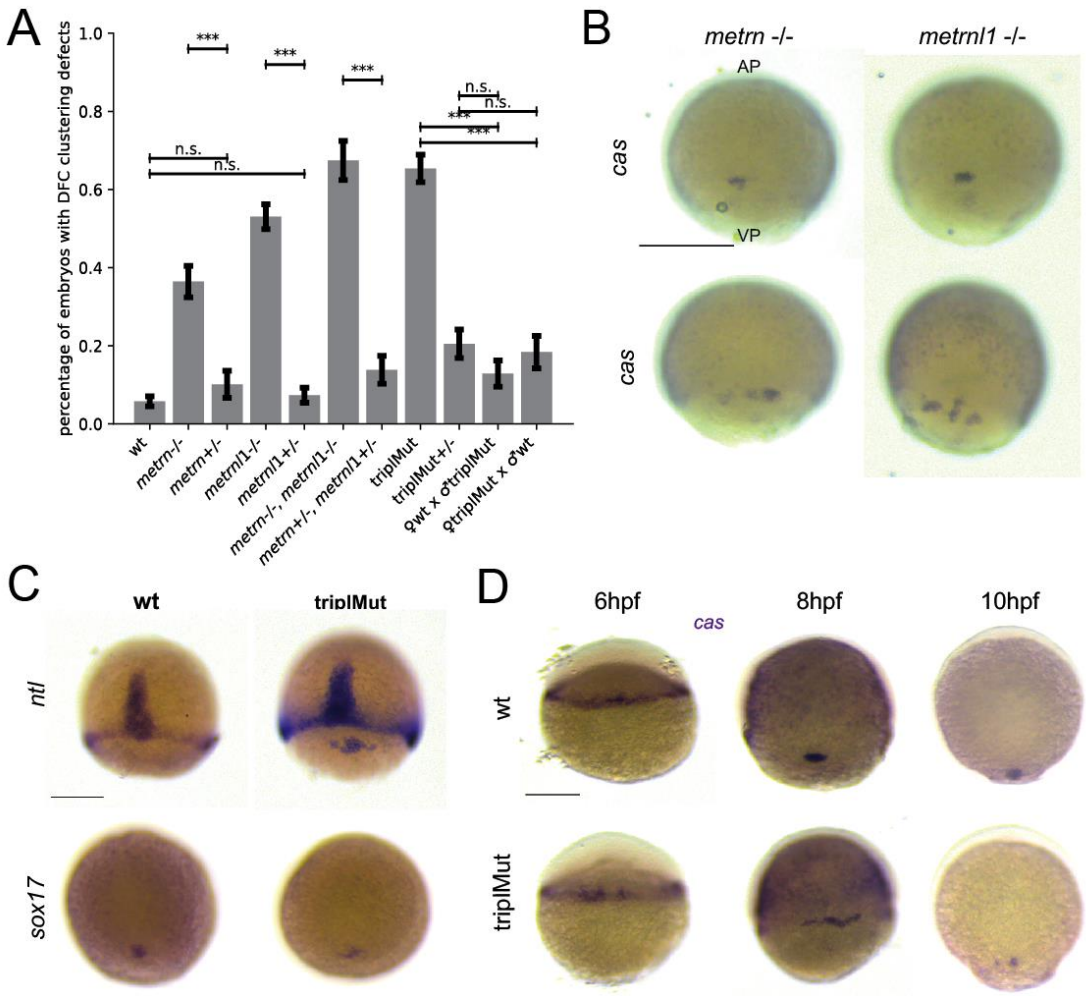

Supplement Figure 4: *Metrns* loss-of-function leads to DFC disorganization and migration defects, A Further quantification of DFC malformation phenotype at 9hpf. **B** *cas* antisense RNA probe *in situ* hybridization on 9hpf *metrn*$^{-/-}$ or *metrnl1*$^{-/-}$ embryos showing wt-like DFC phenotypes and disturbed DFC cluster phenotypes (scale: 0.50mm). **C** *ntl* and *sox17 in situ* hybridization on wt and triplMut (*ntl*: 8hpf, *sox17*: 10hpf) showing specific expression in DFCs independent from genotype (scale: 0.25mm). D *cas* antisense RNA probe *in situ* hybridization show DFC migration between 6hpf and 10hpf (scale: 0.25mm).

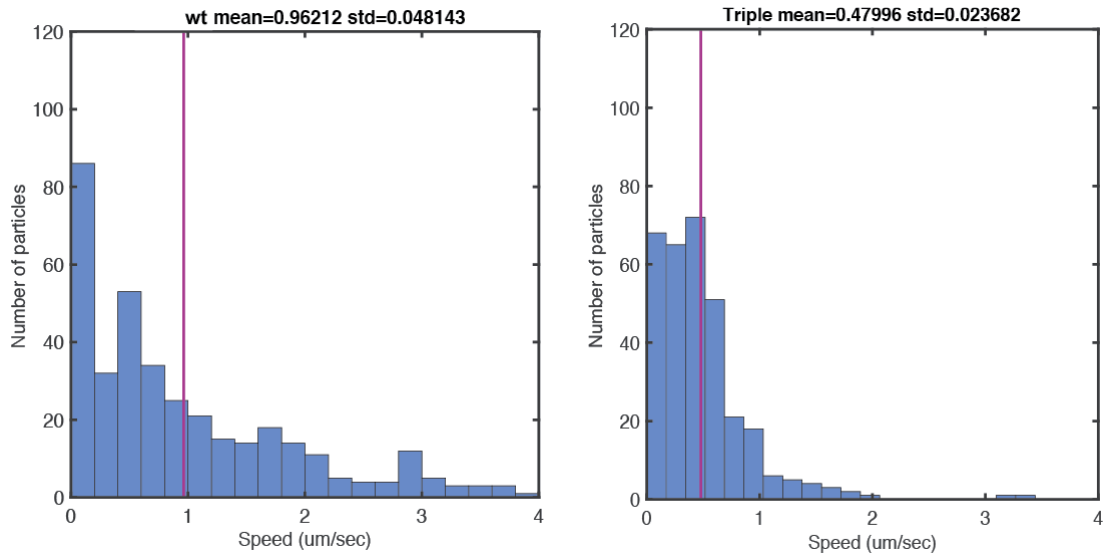

Supplement Figure 5: *Metrns* loss-of-function impairs the KV formation and function, Analysis for the overall speed of tracked microbeads per condition, marking the mean and the standard deviation (std).

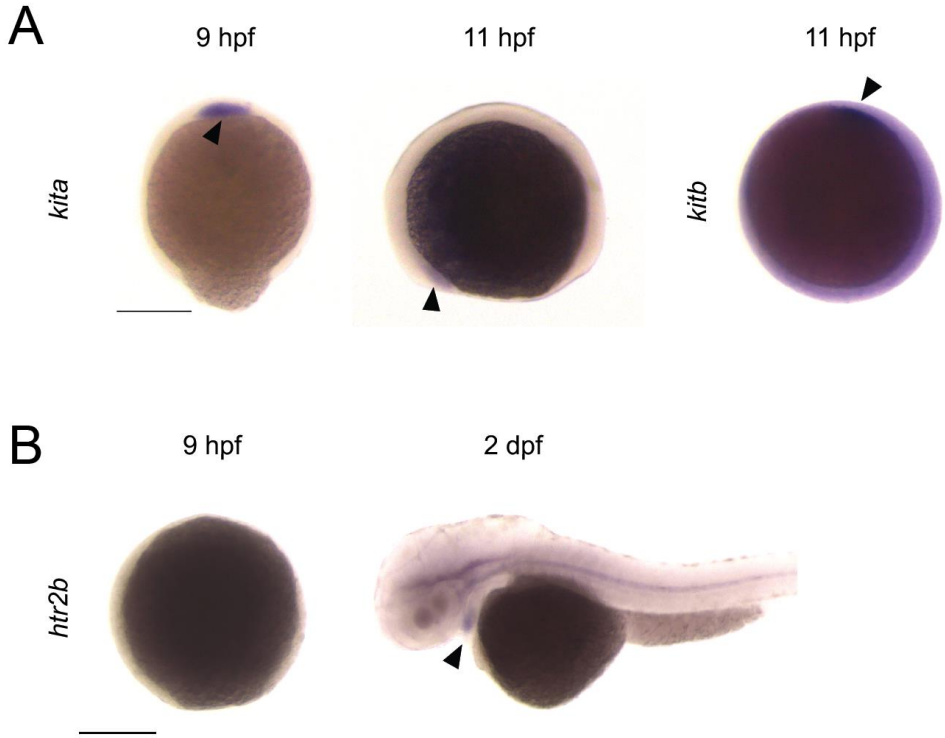

Supplement Figure 6: Antisense RNA probe *in situ* hybridization for the expressions of *kita, kitb* and *htr2b*, A At 9hpf *kita* is expressed in the prechordal plate (black arrow) and from 11hpf in the lateral borders of the anterior neural plate (black arrow), *kitb* expression could be detected from 11hpf in the anterior ventral mesoderm (black arrow), (scale: 0.25mm). **B** At *9hpf* no *htr2b* expression could be detected, solely from 2dpf *htr2b* transcripts could be visualized in the developing heart (black arrow).

Supplement Movies

Movie 1: Microbeads tracking the KV of 6ss-10ss wt embryos showing a distinctive anti-clockwise rotation.

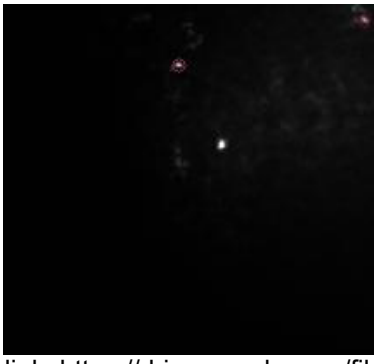

link: https://drive.google.com/file/d/1n-wMx4h9n5teO2SlbRK_KJOwXYuZE7ux/view?usp=share_link

Movie2: Microbeads tracking the KV of 6ss-10ss triplMut embryos showing the loss of the distinctive anti-clockwise rotation.

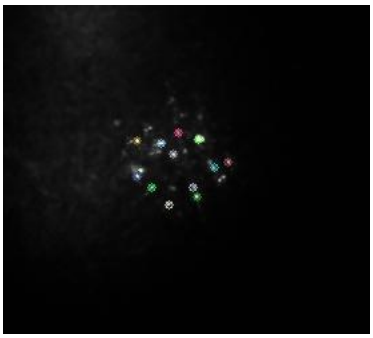

link: https://drive.google.com/file/d/19ZIugQExelhy6yhh2gTmMZi5Pm3BYtWc/view?usp=share_link

Tables

	D-loop	mild/no-loop	S-loop
wt (N = 121)	88.43%	11.57%	0%
***metrn*$^{-/-}$** (N = 131)	61.19%	29.10%	8.21%
***metrnl1*$^{-/-}$** (N = 104)	28.85%	51.92%	19.23%
triplMut (N = 134)	38.17%	25.95%	35.88%
triplMut$^{+/-}$ (N = 182)	85.16%	14.29%	0.55%
triplMut + *metrnl1* mRNA (N = 160)	37.5%	53.13	9.37%
triplMut + *metrn* mRNA (N = 156)	45.51%	42.31%	12.18%
triplMut + *metrnl1* + *metrn* mRNA (N = 162)	52.47%	27.16%	20.37%

Table1: Quantification of heart looping phenotypes at 2 dpf using *myl7* riboprobe *in situ* hybridization on wild-type, *metrn*s single and triple mutants and *metrn* and/or *metrnl1* mRNAs -injected embryos. 'Mild/no loop' designates hearts with no particular L-R orientation. D-loop, dextral loop; mild/no-loop and S-loop.

Experiment	Number of embryos
WT non injected	346
WT + ctrl MO	192
WT + 0.41 ng *itgαV* MO	208
WT + 0.5 ng *itgβ1b* MO	623
WT + 1.25 ng *itgαV* MO	412
WT + 0.7 ng *itgβ1b* MO	336
triplMut$^{+/-}$ non injected	219
triplMut$^{+/-}$ + ctrl MO	176
triplMut$^{+/-}$ + 0.41ng *itgαV* MO	182
triplMut$^{+/-}$ + 0.5 ng *itgβ1b* MO	559

Table2: Number of embryos with DFC clustering defects at 9 hpf upon *itgβ1b*, *itgαV* or control (ctrl) morpholino (MO) injection in wild type (WT) or triplMut$^{+/-}$ embryos.

3.1.3 Annex to "Meteorins as novel regulators of left-right patterning in the zebrafish embryo"

3.1.3.1 DFC phenotype cannot be rescued via co-injection of metrn and/or metrnl1 mRNA and metrns overexpression leads to DFC phenotype

We wondered if the mutant DFC phenotype could be rescued by co-injection of *metrn* and/or *metrnl1* mRNA. However, embryos independent from their injected mRNA (*metrn, metrnl1, metrn+metrnl1*) didn't show a significant increase of wt-like DFC phenotypes compared to Triple mutants (triplMut N=182, 34.62% normal, 65.38% malformation; triplMut+*metrn* N=181, 47.51% normal, 52.49% malformation; triplMut+*metrnl1* N=185, 41.62% normal, 58.38% malformation, triplMut+*metrn+metrnl1* N=146, 39.73% normal, 60.27% malformation). Therefore, we assume that the disturbed mutant DFC formation cannot be rescued by an ectopic source of Metrns (Figure 20A). Besides, we investigated the influence of *metrns* overexpression on the assembly and cluster formation of DFCs. Via *metrn* and/or *metrnl1* mRNA injection we could observe that an ectopic source of Meteorins is disturbing proper DFC clustering (wt N=202, 93.07% normal, 6.93% malformation; triplMut N=182, 34.62% normal, 65.38% malformation; wt+*metrn* N=160, 38.75% normal, 61.25% malformation; wt+*metrnl1* N=137, 30.66% normal, 69.34% malformation, wt+*metrn+metrnl1* N= 142, 41.55% normal, 58.45% malformation), with nearly the same severity as in triplMut (Figure 20B).Therefore, we hypothesize that the right dosage and the right expression location of Meteorins are necessary for correct DFC assembly.

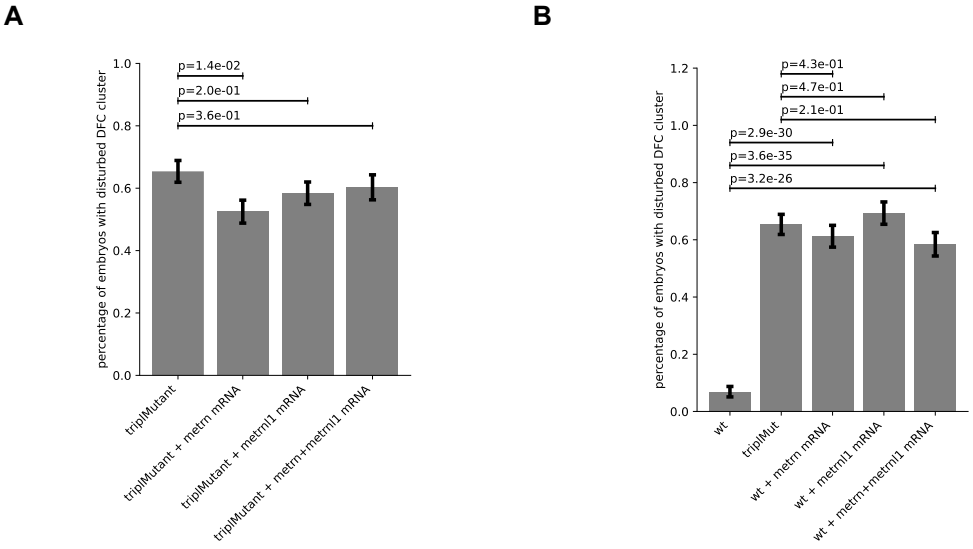

Figure 20: **Metrns LOF fish show DFC phenotype, which cannot be rescued by an ectopic source of metrns and is mimicked by *metrns* overexpression: A** Quantification of DFC malformation phenotypes in triplMut at 9hpf with *metrns* mRNA injection. **B** Quantification of DFC malformation phenotypes in wt samples at 9hpf with *metrns* mRNA injection.

3.1.3.2 *Heart looping phenotype can be rescued by injection of metrn and/or metrnl1 mRNA and metrns overexpression seems to have no severe effect*

As the DFC phenotype could not be rescued via *metrns* mRNA injection and the overexpression of *metrns* also lead to a defect in DFC clustering, we were wondering if the final formation and looping of the heart would be disturbed as well. Surprisingly, embryos independent from their injected mRNA (*metrn, metrnl1, metrn+metrnl1*) showed an increase of wt-like heart looping phenotypes. Also, *metrns* overexpression did not seem to have a significant effect on the heart looping (Figure 21).

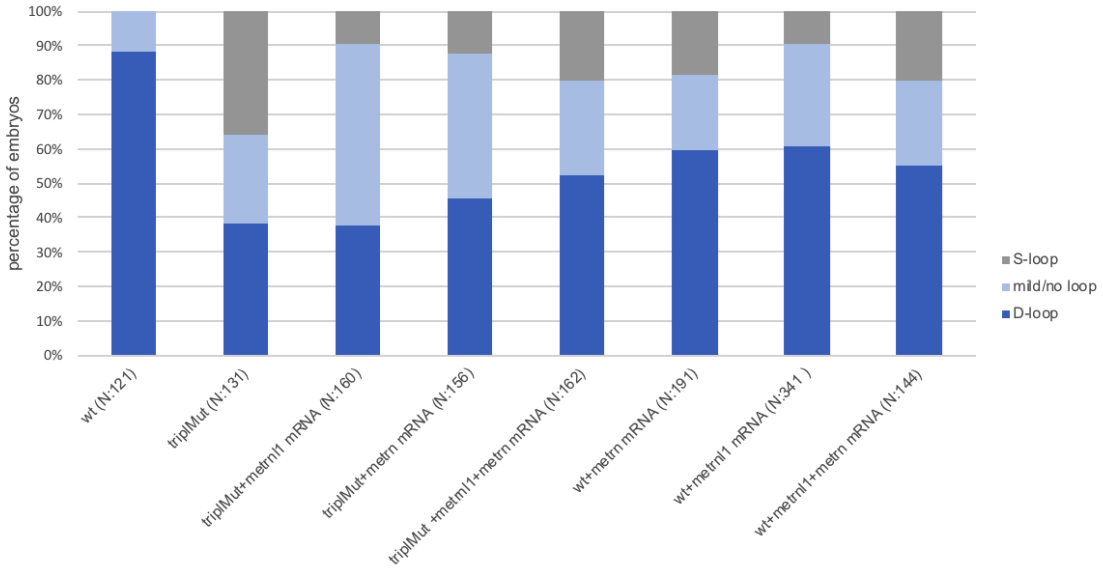

Figure 21: **Metrns LOF fish show heart looping phenotype, which can partially be rescued by an ectopic source of metrns and is not strongly influenced by *metrns* overexpression:** Analysis of heart looping phenotypes in triplMut at 2dpf with *metrns* mRNA injections and in wt samples at 2dpf with *metrns* mRNA injections.

These results indicate, that the heart looping phenotype might be more robust (as described also from Grimes et al.,2020 [350]) and just only a total LOF of *metrns* is sufficient for a significant increase of mutant phenotypes.

3.2 Function of Meteorins in commissural axon guidance

3.2.1 Summary article 2

One of the driving goals of developmental neurobiology research is to unravel the mechanisms of how axons of newborn neurons are able to reach their correct synaptic partners by following well-defined paths guided and by being navigated by a complex network of receptor/ligand interactions. Although a big set of axon guidance molecules has already been characterized, the whole picture is far from being completely understood and a number of axon guidance factors still remain to be revealed. We have generated loss-of-function alleles for all three zebrafish genes from the Meteorin (Metrn) family of secreted proteins. Remarkably, we could characterize specific axonal development defects in these mutant fish including defects in several commissural neuron populations. For instance, *meteorins* triple mutants showed significant defects in the correct development of axonal projections of commissures in the optic tectum, in which bundles of axons have been shown to cross the midline multiple times. In addition, we could show that *Metrn* mRNAs are highly expressed by floor plate cells and in other midline structures of the CNS of zebrafish and mouse. Supported by our results, we hypothesized that Metrns play an important role during the development of the vertebrate CNS and axonal midline crossing, especially in commissural axon guidance.

The following article is based on an earlier manuscript in preparation published in the PhD Thesis of Flavia de Santis (2017). Since the start of my PhD I contributed substentionally to this work and will be a Co-first author. In particular I demonstrated the genetic interaction beween Meteorins and Slits as well as between Meteorins and Integrins ItgαV/Itgβ1b. Furthermore, I performed single and double fluorescent *in situ* hybridizations.

3.2.2 Article 2: "A novel role of Meteorin proteins during the development of the vertebrate CNS and axonal midline crossing"

"A novel role of Meteorin proteins during the development of the vertebrate CNS and axonal midline crossing" (in preparation)

Fanny Eggeler[1*], Flavia De Santis[2,3*], Yvrick Zagar[1], Laura Belleri[1], Natalia Belen Beiza-Canelo[2], Vincenzo Di Donato[2,3], Karine Duroure[1], Thomas O. Auer[2,4], Alain Chédotal[1], Filippo Del Bene[1]

[1] Sorbonne Université, INSERM, CNRS, Institut de la Vision, Paris, France

[2] Institut Curie, PSL Research University, Inserm U934, CNRS UMR3215, Paris, France

[3] ZeClinics SL, Badalona, Spain

[4] Center for Integrative Genomics, Faculty of Biology and Medicine, University of Lausanne, CH-1015 Lausanne, Switzerland

"A novel role of Meteorin proteins during the development of the vertebrate CNS and axonal midline crossing"

Fanny Eggeler[1*], Flavia De Santis[2,3*], Yvrick Zagar[1], Natalia Belen Beiza-Canelo[2], Laura Belleri[1], Vincenzo Di Donato[2,3], Karine Duroure[1], Thomas O. Auer[2,4], Alain Chédotal[1], Filippo Del Bene[1]

[1] Sorbonne Université, INSERM, CNRS, Institut de la Vision, Paris, France
[2] Institut Curie, PSL Research University, Inserm U934, CNRS UMR3215, Paris, France
[3] ZeClinics SL, Badalona, Spain
[4] Center for Integrative Genomics, Faculty of Biology and Medicine, University of Lausanne, CH-1015 Lausanne, Switzerland

ABSTRACT

In the embryonic nervous system axons are guided toward their specific targets by attractive and repulsive cues in the extracellular environment. Here, we present a family of secreted proteins (the Meteorin family) whose members represents novel uncharacterized molecules involved in the process of axon guidance. By investigated the role of Meteorin proteins in directing the navigation of axonal projections in the developing nervous system of zebrafish embryos, we identified a number of axonal tracts responsive to the Meteorin signal. We demonstrated that, if Meteorin function is disrupted, axons from the anterior commissure, the retinal ganglion cells and the trigeminal neurons display several navigation errors. Supported by our results, we suggest that Meteorins play an essential role in the vertebrate CNS development as novel axonal guidance factors for axonal midline crossing.

INTRODUCTION

A functional nervous system is composed by a stereotyped pattern of neuronal circuits in which different populations of neurons are linked to each other by specific synaptic contacts. The central nervous system (CNS) of bilateral organisms is composed by a combination of commissural circuits, connecting the left and right side of the brain, and ipsilateral connections, established by neurons located on the same side of the longitudinal body axis. It was shown that the appearance of commissural and non-commissural axons underlies a strict balance which is essential for sensory stimuli integration and the CNS physiology. Multitude of neurological disorders can have their origin in the failure of proper axon midline crossing during development indicating that the understanding of controlled midline crossing mechanisms will help understand the etiology of these complex severe neurological diseases [1]–[4].
The assembly of the brain wiring pattern starts during the early stages of embryonic development, when differentiated neurons begin to extend their axons and to elongate them toward their correct synaptic partner. While navigating along their path, axons are exposed to environmental attractive and repulsive guidance cues, most of which are produced by specialized cells located at the midline. During the last years, the knowledge of axon guidance control mechanisms within the CNS midline has increased enormously right up to the identification of specific molecular control mechanisms [5], [6]. These mechanisms appear to be highly conserved across evolution. Two molecular couples of ligand and respective receptor have an important role in midline guidance processes: Netrin1/DCC (Deleted in Colorectal Cancer) is known to act as a mediator of commissural axon growth towards the CNS midline and Slit/Robo (Roundabout) which is essential for hindrances of axons to post-cross away from the midline and to prevent ipsilaterally projecting neurons from crossing the midline. Hence, a fine-tuning between repulsion and attraction is provided by various molecular interactions between the Netrin1/DCC and the Slit/Robo pathway. Nevertheless, it was shown that numerous additional molecules in other protein families (Cell-adhesion molecules, semaphoring, ephrins, etc.) have an influence in crossing the CNS midline within complex regulatory mechanisms [5], [6]. Despite this apparent molecular redundancy and complexity, the mystery of the midline crossing puzzle is nowhere near from being solved in its totality.

Metrn was first discovered as a secreted neurotrophic factor which promotes neurite outgrowth *in vitro*. It is expressed at the blastocyst stage during early mouse embryonic development [7] and later in neural and glial progenitors of the central and peripheral nervous systems [8]–[10]. In vertebrates Meteorins (Metrns) are highly conserved including two members in mammals and three in zebrafish (Metrn, Metrnl1 and Metrnl2) [9]–[12]. Each *Metrn* or *Metrnl* gene codes for a protein of around 300 amino acids containing an N-terminal signal sequence as well as

a Netrin-like domain at the C-terminus [9]. In the last few years *Meteorins* expressions and functions have been studied broadly and revealed a great diversity and numerous possible roles for these proteins, which reaches from neurodevelopment, angiogenesis, adipogenesis to novel the ability to alleviate insulin resistance and inflammation [9], [13]–[15].

Recently, we determined that Metrns act together with ItgαV1 and Itgβ1b in controlling the migration and clustering of dorsal forerunner cells (DFC). Additionally, we could demonstrate that Metrns they are required for the proper formation of the Kupffer's vesicle (KV) , a ciliated organ equivalent to the mouse node and essential for initiating left-right asymmetric patterning during embryonic development [16], [17].
Intrigued by the fact that, the midline plays a significant role for the vertebrate's left-right asymmetry but also is one of the main organizers for neurodevelopment, acting as "choice point" or "intermediate target" for navigating axons [18]–[20] we hypothesized a novel role for Meteorin proteins also in axonal guidance. At the ventral midline, or likewise named floor plate (FP), a population of specialized glia cells is located. These cells are a main source of diffusible axonal guidance molecules secretion. Consequently, with the aim to identify new axonal guidance factors which are regulating axonal development as well as navigation, we decided to deeper our understanding in the functions of Meteorins within these processes.

Here we show in Meteorin triple mutants that axonal development defects including defects in several commissural neuron populations are present. Additionally, we could determine that Metrns act together with proteins of the Slit family as well as Integrins ItgαV1/Itgβ1b on the level of the anterior commissure (AC) formation and colocalize at the spinal cord and the ventral midline. Supported by our results, we hypothesized that Metrns play an important role during the development of the vertebrate CNS and axonal midline crossing, especially in commissural axon guidance.

RESULTS

Meteorin genes are expressed by floor plate cells and in other midline structures in the CNS of zebrafish and mouse

To investigate if Meteorin proteins could indeed be implemented also in axonal guidance processes we performed in *situ hybridization* to analyze if *metrns* are expressed in regions of the developing CNS. As already published (Eggeler et al. in preparation) we found out that *metrns* are expressed maternally and from very early stages of zebrafish development (from around 6hpf), however since the development of the CNS doesn't take place in the first hours we focused now on stages between from 24hpf to 3dpf.

In general, from 24 to 48hpf all three zebrafish *meteorin* genes show expression in the CNS. At 24hpf *metrnl1* expression could be detected at the midbrain/hindbrain boundary, in regions close to hindbrain rhombomeres as well as in the area of the presumptive otic vesicles. *Metrn* expression could be broadly localized in the developing embryonic brain and also *metrnl2* transcripts could be detected in the embryonic brain at this stage. (Figure 1A, C) At 48hpf *metrn* and *metrnl1* expression could be visualized especially along the midline as well as in CNS periventricular regions. From this stage, *metrnl2* transcripts mostly localized in the otic vesicles and at the somite boundaries (Figure 1A, C). At stages later than 2dpf, the expression of *metrns* within the CNS displayed a significant decrease. (data not shown) Hence, we assume that Meteorin function in aspect of axonal development and guidance is just required during early developmental stages.

Additionally, we analyzed the expression pattern of *Metrn* and *Metrnl* in mouse. On mouse spinal cord sections, we could remarkably discover that both genes show a high expression specifically in floor plate cells and in other midline structures in the CNS. (Figure 1B).

Excitingly, the expression patterns of *Meteorins* in zebrafish and mouse display strong similarities, especially within the CNS like strong expression at the floor plate and along the midline. Therefore, we hypothesize that Meteorin proteins might play indeed an important role during these early neurodevelopmental processes.

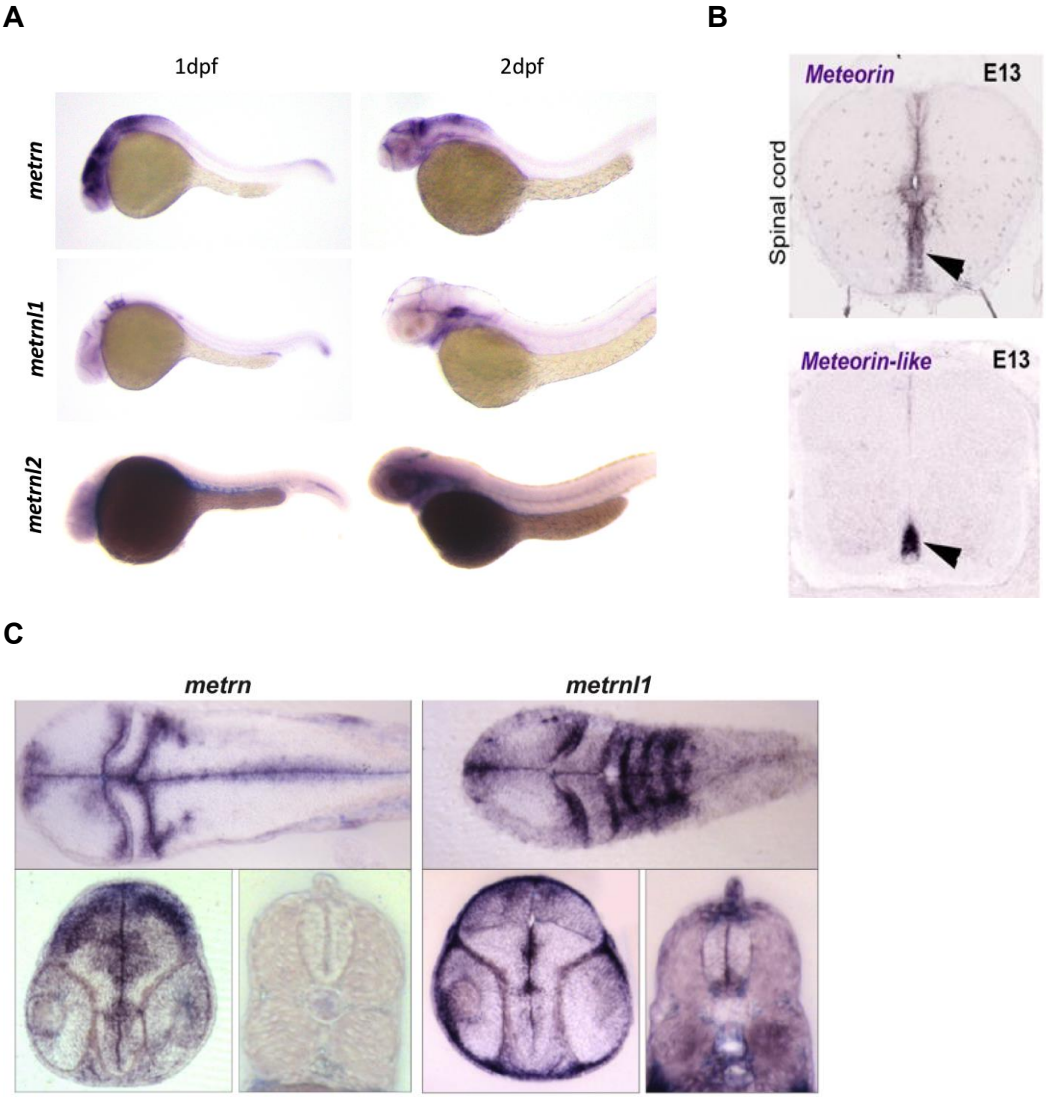

Figure 1: **Metrns are expressed in CNS structures during early zebrafish neurodevelopment: A)** Expression patterns of *metrn, metrnl1, metrnl2* at 1dpf and 2dpf in CNS structures are visualized via *metrn/metrnl1/metrnl2* antisense RNA probe *in situ* hybridization in whole mount samples. **B)** *In situ hybridization* on E13 spinal cord sections displaying *Meteorin* and *Meteorin-like* expression at the floor plate (black arrows). **C)** *In situ hybridization* on longitudinal (upper panels) and transversal (lower panels) vibratome sections of 2dpf embryos visualizing the expression patterns of *metrn* and *metrnl1* at the midline in the dorso-ventral and antero-posterior axis and metrnl1 expression at the floor plate in the spinal cord.

Meteorins mutants show specific axonal development defects including defects in the development of the AC

Since their significant expression patterns in the developing brain we assume that Meteorin proteins might play a role during the elongation of the primary axonal tracts extending within embryonic zebrafish brain. Using our already established CRISPR/Cas9 knockout lines for all three members of the zebrafish Meteorin family, we investigated if Meteorins influence the

development of the dorsal anterior commissure (AC) and the ventral post-optic commissure (POC). Both commissural tracts, as examples for the first developing stereotyped axonal scaffolds, should fully developed during the stages of high *metrns* expression within the brain and connect the right and left side of the brain [21]. Therefore, we stained the axonal projections by acetylated tubulin staining of 28hpf wild type (wt) and mutant embryos. As expected, 28hpf wt samples displayed a complete and fully organized and developed POC and AC (Figure 2A left). Remarkably, in *Metrns* triple mutant (triplMut) samples at the same stage, the formation of the formation of the AC seemed to be reduced and delayed, with a thinner with compared to wt samples, repeatedly defasciculated or even absent (Figure 2A right). While, the formation of the POC did not seem effected in triplMut samples (Figure 2A). We next wondered if the observed AC phenotype in triplMut samples is caused by the loss of function of one single *meteorin* gene or by the synergistic activity of the three Meteorin proteins. Therefore, we analyzed the thickness of the AC axonal bundles, in triplMut, single mutants as well wt controls. Interestingly, we could observe a significant reduction of the AC thickness in triplMut and *metrn*$^{-/-}$ samples. On the other hand, in *metrnl1*$^{-/-}$ and *metrnl2*$^{-/-}$ embryos we could not detect an effect on the thickness and formation of the AC. Additionally, we could not detect a significant difference between triplMut and *metrn*$^{-/-}$ samples (Figure 2B). Hence, we assume the loss of other paralogues does not influence the disrupting effect on the AC development and that Meteorin is the solely involved, among the other Meteorins family members, in the correct development of the AC.

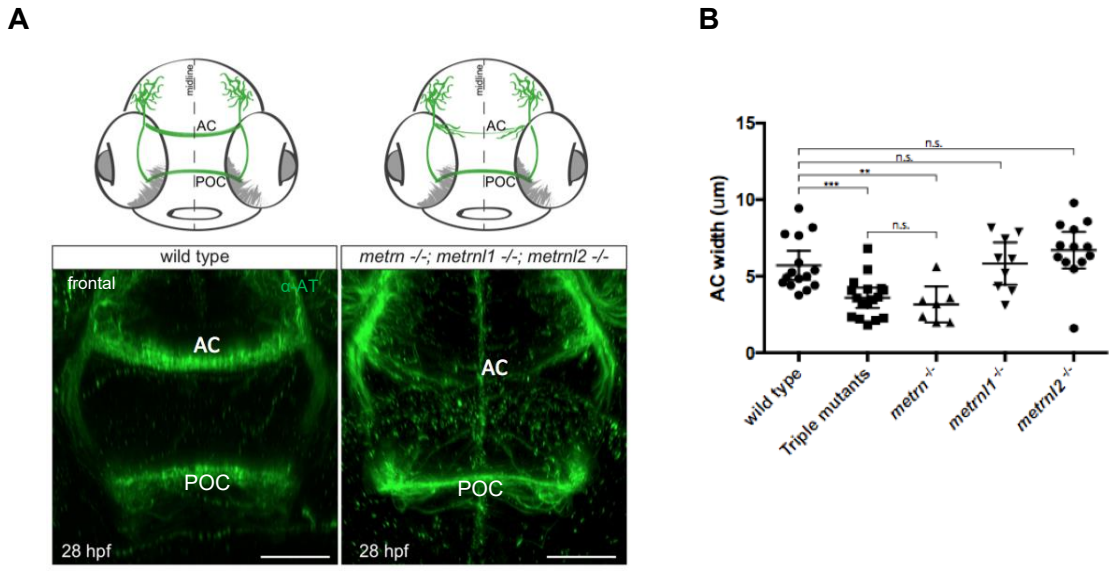

Figure 2: **Metrns are required for the formation of the AC: A)** Schematic representation of the wt (upper left) and mutant (upper right) anterior (AC) and post-optic commissures (POC) in the rostral forebrain of a 28hpf zebrafish embryo and the frontal views of the AC and POC in a wt (lower left) and triple mutant (lower right) embryo, visualizing a fully developed AC and POC in wt fish while triplMut fish show incomplete development of the AC. AT, acetylated tubulin (scale bar: 30 µm) **B)** Analysis of the commissure phenotype measured by AC width in triplMut, single mutants and wt control (wt= 5.7+/-0.44mm, N=15; triplMut=3.6+/-0.31mm, N=17; *metrn*$^{-/-}$ = 3.16+/-0.48mm, N=7; *metrnl1*$^{-/-}$= 5.82+/-0.60 mm, N=9; *metrnl2*$^{-/-}$= 6.70+/-0.55mm, N=13. Wt vs triplMut: p=0.0004; wt vs *metrn*$^{-/-}$: p=0.0023; wt vs *metrnl1*$^{-/-}$: p=0.872; wt vs *metrnl2*$^{-/-}$: p=0.165; triplMut vs *metrn*$^{-/-}$: p=0.456; unpaired t-test).

Since it is reported that disturbed patterning and formation of the AC or POC is frequently connected to later pathfinding errors of retinal ganglion cells (RGCs) [22], [23], we were wondering if the *metrns* loss of function would also influence the navigation of RGCs projections. Consequently, by injecting a *isl2b*:Gal4:GFP-Caax plasmid into one cell stage wt, triple mutant and single mutant embryos we were able to genetically labeled single RGCs in these samples. After 5 days, we imaged the RGC terminals in the tectal neuropil. Remarkably, we could observe that Meteorin proteins are indeed influencing the laminar organization of RGC axons since in about half of the triplMut fish (n=4/9) we could observe misrouted axons meandering between multiple laminae of the tectum. In wt samples as well as single mutant fish we could not observe any lamination defects (Figure 3A). Therefore, we suggest that this biological context Meteorins might act in a redundant manner on RGC axons.

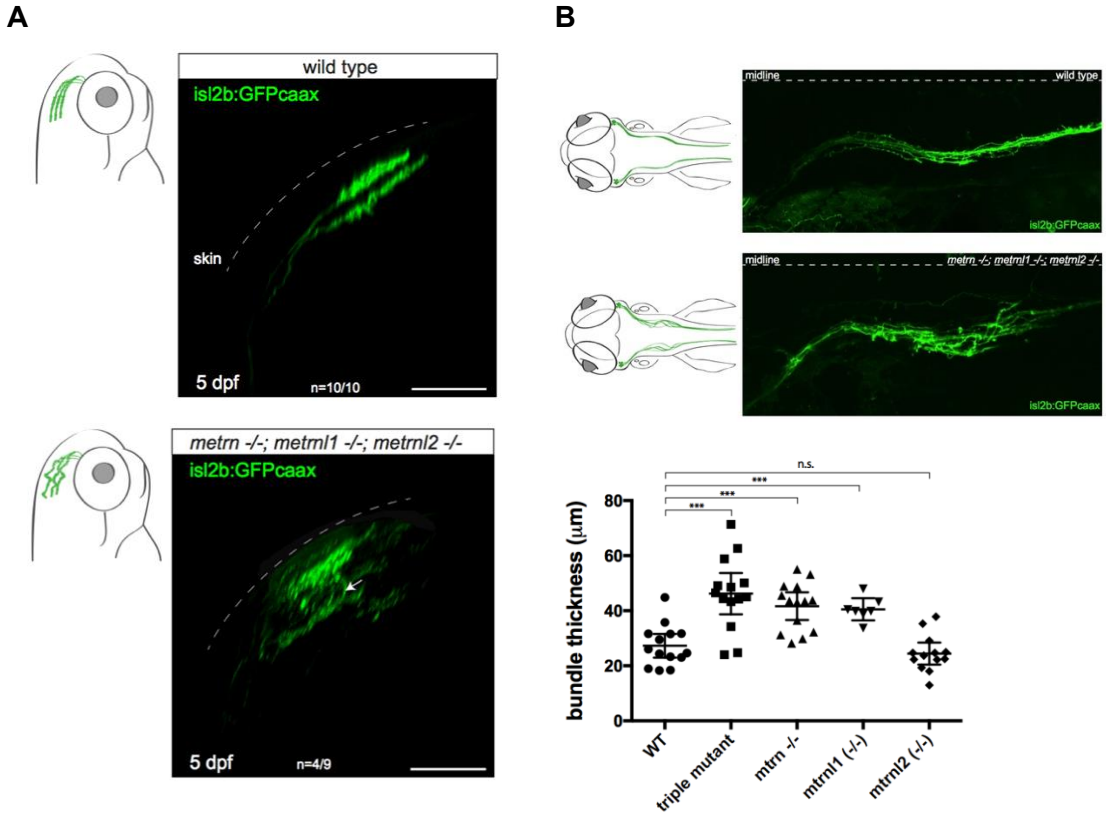

Figure 3: **Metrns are influencing the laminar organization of RGC axons: A)** Schematic representation of the retinotopic targeting of RGC within the tectum in wt (upper left) and triplMut fish (lower left) and confocal images of 5dpf *isl2b*:Gal4:GFP-Caax injected fish visualizing the disrupted laminar organization of RGC in triplMut samples. **B)** Schematic representation and dorsal view (transiently expressing islt2b:GFPcaax) of the wild type and triplMut trigeminal nerve fasciculation (scale bar: 30mm) and analysis of the width of the trigeminal tract in wt, single mutants and triplMut displaying a significant increase in bundle thickness in triplMut and single metrn and metrnl1 mutants compared to wt controls (wt=27.29mm +/- 1.99, n=14; triplMut=46.22mm +/- 3.48, n=14; metrn-/-=41.66mm +/- 2.33, n=14; metrnl1-/-=40.53 mm +/- 1.65 n=6; metrnl2-/-= 24.43mm +/-1.85, n=13. Wt vs triplMut: p<0,0001; wt vs metrn-/-: p<0,0001; wt vs metrnl1-/-: p=0,0004; wt vs metrnl2-/-: p=0,303; unpaired t-test; Error bars = SEM).

Additionally, due to their significant expression at the hindbrain midline, we assume that Meteorins might also affect the elongation profile and navigation of longitudinal tracts growing in the hindbrain. Axons of trigeminal sensory neurons are normally forming a tight axonal bundle which is growing laterally to the midline in the spinal cord and hindbrain. Hence, we think that the trigeminal nerve might be sensitive to the biological activity of Meteorins. And indeed, in 3dpf *isl2b*:gal4:GFP-Caax injected triplMut fish the trigeminal nerve seems strongly defasciculated, showing axons approaching the midline as they navigate to the posterior direction. Additionally, we could observe significant defasciculated trigeminal nerves also in

metrn$^{-/-}$ and *metrnl1*$^{-/-}$ fish, while metrnl2 didn't seem to play a role in navigating trigeminal projections (Figure 3B). These results let us assume that that trigeminal axons are sensitive to signaling of Meteorin proteins and that Meteorins are crucial to maintain the axonal navigation parallel to the midline.

In general, these results show that Meteorins could play an important role during commissural axon guidance, RGC lamination and the fasciculation of trigeminal neurons and are therefore possible new axonal guidance factors for these neuron populations.

Meteorins and *slits* co-localize at the spinal cord and the ventral midline and genetically interact in regulating commissure development

Interestingly, a cleaved fragment of the axon guidance molecule Slit2 has been recently associated to the same function as Metrnl in adipose tissue [24], [25]. To establish Meteorins as novel axon guidance factors we were wondering if they are connected to the already established and known axon guidance factors of the Slit family also in the context of axonal guidance.

Indeed, especially the expression of *metrnl1* at the level of the floorplate seems highly reminiscent of the guidance factors belonging to the Slit family. To investigate if *metrnl1* and *slits* are expressed by the same cells or at least partially from the same population, we performed double fluorescent *in situ* hybridization experiments. Interestingly, we could observe that *metrnl1* is co-localizing with tree out of the four slit paralogues (*slit1a, slit1b* and *slit2*) at the level of the hindbrain floorplate as well as spinal cord (Figure 4A). To further investigate a possible connection between Meteorins and Slits we analyzed if there might be genetic interactions between members of these two protein families on the level of the AC formation.

In order to examine possible slits and Metrns genetic interaction, we injected morpholinos for *slit1a* (0.1ng), *slit2* (0.3ng) or *slit3* (0.3ng) into 1 to 4 -cell-stage triplMut$^{+/-}$ embryos to generate insufficient doses of both proteins in heterozygous *metrns* background. The single injection of low dose *slit1a*, *slit2* or *slit3* morpholino into wt embryo controls did not affect the formation of the AV, similarly to non-injected triplMut$^{+/-}$ embryos.

Interestingly, the injection of *slit2* or *slit3* morpholino at low dose into triplMut$^{+/-}$ embryos lead to a significant increase in the percentage with embryos showing misrouted AC axons. The injection of *slit1a* morpholino at low dose into triplMut$^{+/-}$ embryos didn't seem to influence the proper formation of the AC (Figure 4B).

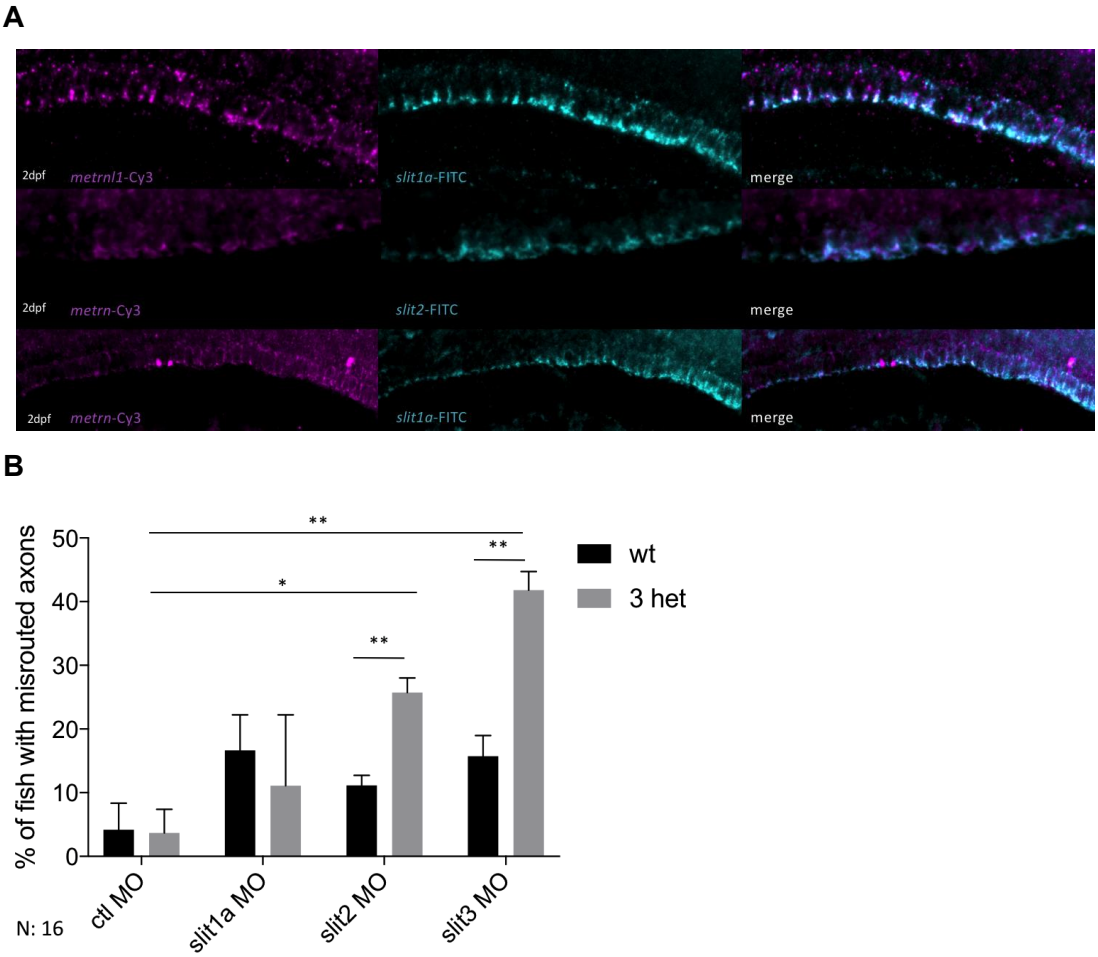

***Figure 4: Metrns* and *slits* are expressed in the same cell populations in the hindbrain floorplate as well as spinal cord and they genetically interact on the level of the AC: A)** Double fluorescent *in situ* hybridization on zebrafish spinal cord visualizing examples for *metrns* and *slits* co-localization. **B)** Quantification of AC phenotype at 28hpf for morpholino (MO) injections into wt and into triplMut$^{+/-}$ (3 het) embryos showing a significant increase in misrouted axons for *slit2* MO and *slit3* MO injected 3 het samples and indicating for a genetic interaction between Meteorins and Slits, p-values evaluated with Fisher exact test indicating statistical significance, **p*-value < 0.01 and ***p*-value < 0.001.

These results are consistent with the hypothesis that Slits might genetically interact with Metrn proteins for the proper AC formation. Hence, we assume that Meteorins and Slits could have similar roles during the embryonic nervous system patterning and that Meteorins indeed could be involved as new axonal guidance factors in axonal pathfinding.

Meteorins generically interact with Integrins *ItgαV* and *Itgβ1b* on the level of commissure development

In a previous publication we could demonstrate a novel role for Meteorin proteins during embryonic development, showing that they are required for the proper formation of the KV. We revealed that Metrns act together with ItgαV and Itgβ1b, and that they are essential for DFC clustering and migration by mediating necessary cellular interactions. Integrin αV was shown to be implemented during early developmental processes as *αV* mutant mice suffered from disturbed embryonic cerebral blood vessel formation and defects in the axon and glia interactions in the CNS [26]–[28]. Additionally, several *in vitro* studies connected $\alpha V\beta 1$ to neurodevelopmental processes. For instance $\alpha V\beta 1$ was shown to be implicated in embryonic astrocytes and oligodendrocyte precursors migration in rodents [29], in neural cell adhesion molecule L1 cell binding [30] and β1 Integrins are crucial for proper cerebral cortex development [31].

Subsequently, we were wondering if there might be a connection between Meteorins and ItgαV/ Itgβ1b also on the level of the AC formation. Therefore, we injected morpholinos (MO) for *itgβ1b* (0.5 ng) or *itgαV* (0.41ng) into 1 to 4 -cell-stage triplMut$^{+/-}$ embryos to generate insufficient doses of both proteins in heterozygous *metrns* background. The injection of the MO at these doses and sufficient doses (*itgβ1b:* 0.7ng, *itgαV:* 1.25ng) reproduced the previously reported defects on DFCs [32] Therefore we maintained these concentrations also in the context of the AC formation. The single injection of low dose *itgβ1b* or *itgαV* MO into wt embryo controls did not affect the AC phenotype and formation. But surprisingly, the injection of either morpholino at low dose into triplMut$^{+/-}$ embryos lead to a significant increase in the percentage with embryos misrouted axons of the AC (Figure 5A-B).

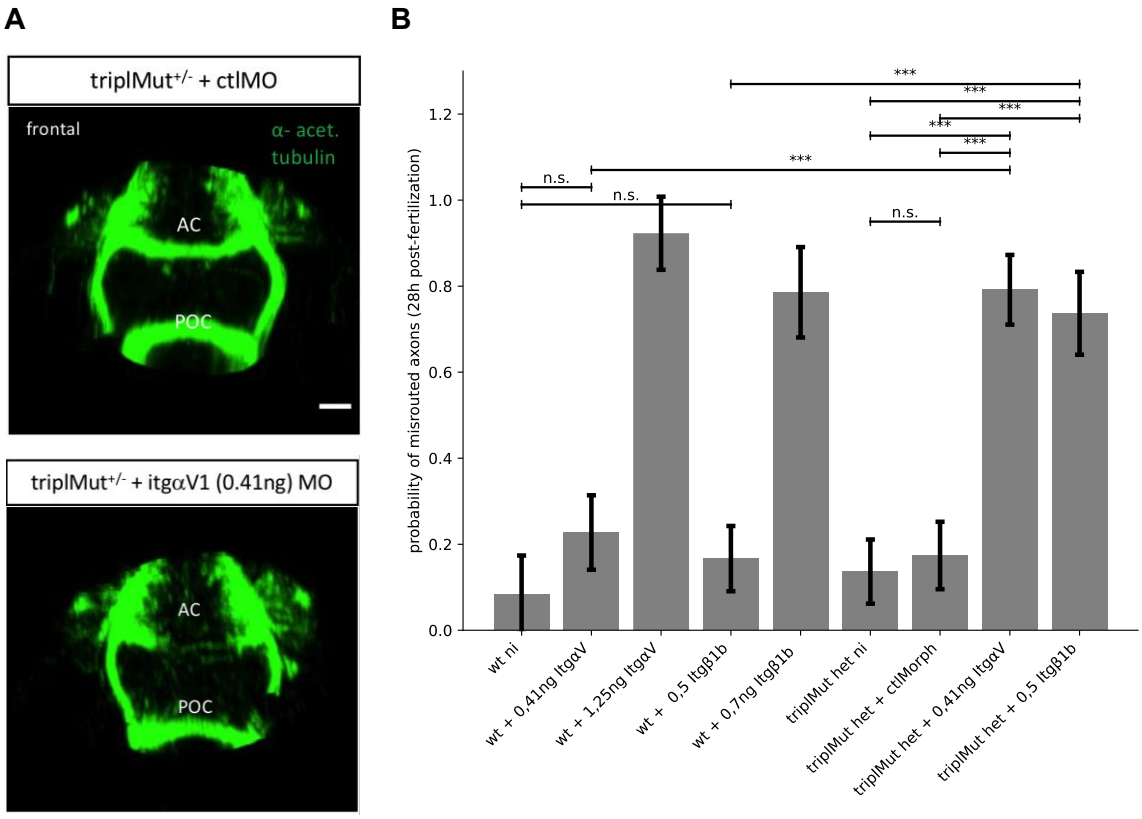

Figure 5: **Meteorins generically interact with Integrins ItgαV and Itgβ1b on the level of the AC development: A)** AC and POC in the rostral forebrain of a 28hpf zebrafish embryo from a control (triplMut$^{+/-}$ + ctl MO) and a *itgαV*1 MO injected fish (triplMut$^{+/-}$ + *itgαV*1 (0.41ng) MO), visualizing a fully developed AC and POC in the control fish while *itgαV*1 MO injected fish shows incomplete development of the AC (scale bar: 30 µm). **B)** Quantification of AC phenotype at 28hpf for MO injections into wt and into triplMut$^{+/-}$ embryos showing a significant increase in misrouted axons for *itgαV*1 MO and *itgβ1b* MO injected triplMut$^{+/-}$ samples (wt ni N= 12, wt+*itgαV* MO-0.41ng N=22, wt+*itgαV* MO-1.25ng N=13, wt+*itgβ1b* MO-0.5ng N=24, wt+*itgβ1b* MO-0.7ng N=14, triplMut$^{+/-}$ ni N=22, triplMut$^{+/-}$+ctl MO N=23, triplMut$^{+/-}$+i*tgαV* MO-0.41ng N=24, triplMut$^{+/-}$+*itgβ1b* MO-0.5ng N=19), p-values evaluated with Fisher exact test indicating statistical significance, **p*-value < 0.01, ***p*-value < 0.001 and ****p*-value < 0.0001 and n.s. = not significant.

These results indicate that beside Slits, both Integrins ItgαV and Itgβ1b might genetically interact with Metrn proteins for the development of the AC and that the signaling pathways of Meteorins including their co-factors play an important role in axonal pathfinding of commissural neurons.

DISCUSSION

By using a LOF approach for all three members of the Meteorin family in zebrafish, we could characterize axonal development defects in *meteorins* mutant fish including defects in the development of AC neurons. Besides, we could show that Metrns act together with proteins of the Slit family as well as Integrins αV and β1 on the level of the AC formation. Additionally, we observed that Metrns also colocalize at the spinal cord and the ventral midline with Slits proteins, which are well established axonal guidance factors. Thus, we hypothesize that Metrns as novel axonal guidance factors, play an important role during the development of the vertebrate CNS and axonal midline crossing, especially in commissural axon guidance.
Significantly, the expression patterns of *metrn* genes in a spatiotemporal manner is consistent with their hypothesized role of modulating of axonal navigation.

Truly, in both zebrafish and mouse, *Metrns* expression can be detected in glia and neuronal progenitor cells the floor plate and midline. Both structures are known to be crucial for the secretion of guidance factors directing the navigation of elongating axons. The colocalization of *metrns* and three slit paralogues (*slit1a, slit1b* and *slit2*) at the level of hindbrain floor plate cells and spinal cord cells indicates that *metrns* are at least partly expressed within the same population of cells which is essential and responsible for some of the leading axonal guidance cues during embryonic brain development.

Investigating for possible functions of Meteorins using our *metrns* LOF fish, we could observe axonal navigation defects in *metrns* mutant fish, demonstrating that Meteorin signaling is influencing at least three neuronal populations. We assume that different axons could respond to different Meteorin proteins combinations, since for instance AC axons seem to be solely influenced by Metrn and trigeminal neurons are sensitive to the synergistic activity of Metrn and Metrnl1. In the case of the laminar organization of RGC we think that Meteorins act redundantly, as we could not observe and disruptions in single *metrns* mutants.

Slit proteins and their receptors are key regulators in midline crossing axonal guidance and for instance were shown to determine commissure development in zebrafish. The reduction of Slit1a, Slit2 and/or Slit3 was shown to result in defasciculation of the POC, indicating for a crucial role of these Slit proteins during the navigation of POC axons across the midline [33]. Strikingly, we could observe that the mRNA encoding for *metrn* and *metrnl1* as well as for three out of the four slit paralogues in zebrafish (*slit1a, slit1b* and *slit2*) are co-localizing at the floor plate region in the zebrafish hindbrain. Additionally, we could find out a possible genetic interaction between Meteorin proteins and Slits (Slit2, Slit3) on the level of the AC. These

observations highlight that the Meteorins and Slits are, at least in part, produced by the same population of cells. Furthermore, Meteorins, in contrast to Slit2 and Slit3 which are necessary for proper POC development, are required for the formation of the AC and could therefore in synergy with Slit2 and Slit3 in controlling the navigation of commissural axons. Hence, the possible functional cooperation between these two classes of molecules supports the hypothesized role of Meteorins on the level of axonal guidance.

Additionally, we could determine that Meteorin proteins are also connected to IntegrinαV and β1 on the level of AC development. Mainly due to their broad expression in connection with other integrins as well as the lack of αVβ1 specific inhibitors and antibodies specific, αVβ1 has not yet been studied extensively in mammals. However, several *in vitro* studies connected αVβ1 to processes during embryonic neurodevelopmental. For instance αVβ1 was shown to be implicated in neural cell adhesion molecule L1 cell binding [30] as well as in embryonic astrocytes and oligodendrocyte precursors migration [29]. Interestingly, we recently discovered that αV/β1b might genetically interact with Metrn proteins for the proper DFC clustering during early left-right patterning processes (Eggeler et al. in preperation). αVβ1 is known to dimerize additionally with the β3, β5, β6, β8 subunits as well as with the αIIb subunit. Therefore, it might be possible that Metrns as potential novel axonal guidance factors have functional cooperation with additional Integrin subunits and especially with Integrinβ1 as it is associated to numerous axonal pathfinding processes [34].

Since the receptor(s) of Metrns in the context of axon guidance remain to be identified, whether the effect of Metrns is directly linked to the binding of Meteorin proteins to their receptor located on the targeted axons or if it is caused by the modulation of other axonal navigation pathways is still unknown.

In conclusion, our results are revealing a novel role for the proteins of the Meteorin family in embryonic CNS patterning, suggesting Metrns as a new class of axonal guidance factors, essential for the formation of complex axonal projection patterns in the developing vertebrate brain and giving a solid base for further investigations about Meteorin proteins and their role in establishing embryonic neural circuits.

MATERIAL AND METHODS

Zebrafish husbandry

Zebrafish (*Danio rerio*) were maintained at 28°C o.n. a 14h light/10h dark cycle. Fish were housed in the animal facility of our laboratory which was built according to the respective local animal welfare standards. Animal handling and experimental procedures were approved by the Committee on ethics of animal experimentation. All animal procedures were performed in accordance with French and European Union animal welfare guidelines.

CRISPR-Cas9-mediated mutagenesis of *metrn*, *metrnl1* and *metrnl2* and genotyping

The establishment of single, double as well triple Meteorins mutants (*metrn*$^{-/-}$; *metrnl1*$^{-/-}$; *metrnl2*$^{-/-}$; *metrn*$^{-/-}$, *metrnl1*$^{-/-}$; *metrn*$^{-/-}$, *metrnl2*$^{-/-}$; *metrnl1*$^{-/-}$, *metrnl2*$^{-/-}$; *metrn*$^{-/-}$, *metrnl1*$^{-/-}$, *metrnl2*$^{-/-}$) and the respective genotyping was performed as described in Eggeler et al. (in preparation).

Whole embryo DNA extraction

For genomic DNA extraction, 25 5-dpf embryos were pooled and digested for 1 h at 55°C with proteinase K (0.17 mg/mL) in 0.5mL lysis buffer (10 mM Tris, pH 8.0, 10 mM NaCl, 10 mM EDTA, and 2% SDS). Proteinase K inactivation was achieved by a following 95°C incubation for 10min. To analyze the frequency of indel mutations, target genomic loci were amplified by PCR using the Phusion High-Fidelity DNA polymerase Following, PCR amplicons were cloned into the pCR-bluntII-TOPO vector. Plasmid DNA was extracted from single colonies and sent for Sanger sequencing. Mutant alleles were identified by aligning with the respective wild-type sequence.

Whole embryo RNA extraction and cDNA synthesis

Whole embryo RNA was extracted from zebrafish embryos in the respective developmental stage with TRIzol reagent and the TURBO DNA-free kit.

For cDNA synthesis 1µg RNA was retrotranscribed using the SuperScript III First-Strand Synthesis system and random primers. The quality and concentration of extracted RNA and synthesized cDNA was determined with a NanoDrop spectrophotometer.

single and double fluorescent *in situ* hybridization

Respective cDNA fragments were amplified by PCR from zebrafish cDNA using the following primers:

	Sequence (5'->3')
metrn-fw	GAAGTGGACTTTCTCAGGC
metrn-rev	CAAGGATTGTTTGGCCTGTTCG
metrnl1-fw	GTATTTGCTGTCGGTTGTGC
metrnl1-rev	CAGGGGTTGGTCCCTTGCTGCCG
metrnl2-fw	CTGAAGGCTCTCTGCAGTGG
metrnl2-rev	ATCACAGCGCTGCAGAATCT
slit1a-fw	TGAGCAGCTGGTTGAGGAAC
slit1a-rev	GTAGCCGTCTGTCTGATCCG
slit1b-fw	CACGGACTTAACCTGGCAGA
slit1b-rev	TTGGGTGGACAAACAGGCTT
slit2-fw	TTGCTGATTTGGCCTGTCCA
slit2-rev	TGTGAACTCGTTGCCATCGA

In vitro transcription of Digoxigenin/Fluorescent-labeled *in situ* probes was executed using a RNA Labeling Kit according to company's instructions. Zebrafish embryos were manually dechorionated at the appropriate developmental stage(s) and fixed in 4% paraformaldehyde (in PBS, pH 7.4) for 2 hours at room temperature or 4°C o.n. Whole-mount *in situ* hybridizations were performed as described in Thisse and Thisse 2008 [35].

Vibratome sections

Whole-mount embryos at respective stages were washed twice in 1X PBS/0.1% Tween-20 (PBS-Tw) solution and then were embedded in gelatin/albumin with 4% of Glutaraldehyde. The samples were sectioned (20 mm) with a VT1000 S vibrating blade microtome (Leica)and subsequently mounted in Fluoromount Aqueous Monting Medium (Sigma).

Molecular cloning

The p*isl2b*:Gal4:GFP-Caax plasmid was produced by a Gateway reaction (MultiSite GatewayThree-FragmentVector Construction Kit, ThermoFisher Scientific, Waltham, MA) using the p5E-Isl2b39, pME-GFP-caax, p3E-pA and the pDest-Tol2;cmlc2:eGFP40 constructs.

Design and injection of antisense morpholino oligonucleotides

Used antisense morpholino oligonucleotides were previously published from Barresi et al., 2005 [33] and Ablooglu et al., 2010 [32]. The sequences were as following:

	Sequence (5'->3')
slit1a	GACAACATCCTCCTCTCGCAGGCAT
slit2	CATCACCGCTGTTTCCTCAA GTTCT
slit3	TATATCCTCTGAGGCTGATAGCAGC
itgαV1	AGTGTTTGCCCATGTTTTGAGTCTC
itgβ1b1	GGAGCAGCCTTACGTCCATCTTAAC
standard control	CCTCTTACCTCAGTTACAATTTATA

All MOs were obtained from Gene Tools (Philomath, OR, USA). MOs were injected in 1- to 4-cell-stage zebrafish embryos.

Whole-mount immunohistochemistry

Embryos were fixed at their respective stage in 4% paraformaldehyde (in PBS-Tween) for 2h at RT or o.n. at 4°C and subsequently washed three times in PBS-Tween. To promote permeabilization, the samples were incubated for 30min in 1% Triton X 100 (in PBS-Tween) and subsequently, for 1h at RT in blocking solution (10% Normal Goat Serum, in PBS-Tw). This followed an o.n. incubation, at 4 °C, with a mouse anti acetylated tubulin monoclonal antibody (1/200 dilution in blocking solution). After five washes in PBS-Tween, the samples were incubated with an Alexa Fluor 488 anti- mouse IgG secondary antibody (final concentration 1/200 in blocking solution) o.n. at 4°C. The next day embryos were washed five times in PBS-Tween before mounted with 1% low melting point agarose in glass-bottom cell tissue culture dishes.

Microscopy and image analysis

In situ samples were imaged on a Leica MZ10F stereomicroscope. Fluorescent *in situ* hybridization samples were imaged on a Leica MZ FLIII stereomicroscope equipped with a Leica DFC310FX digital camera. Images were processed and analyzed using ImageJ software. Color balance, brightness and contrast and were applied uniformly. For Whole-mount immunohistochemistry imaging an inverted confocal microscope Olympus FV-1000 was used, employing a 20x oil immersion objective or 40x water immersion objective. Z-volumes were acquired with a 0,5- 2µm resolution and images were processed and analyzed using IMARIS software. For *in vivo* imaging, embryos were anesthetized with 0.02% tricaine and mounted in 1% low melting- point agarose in cell tissue culture dish with glass-bottom.

REFERENCES

[1] S. Tole, G. Gutin, L. Bhatnagar, R. Remedios, and J. M. Hébert, “Development of midline cell types and commissural axon tracts requires Fgfr1 in the cerebrum,” *Developmental Biology*, vol. 289, no. 1, pp. 141–151, Jan. 2006, doi: 10.1016/j.ydbio.2005.10.020.

[2] R. J. Ferland *et al.*, “Abnormal cerebellar development and axonal decussation due to mutations in AHI1 in Joubert syndrome,” *Nat Genet*, vol. 36, no. 9, pp. 1008–1013, Sep. 2004, doi: 10.1038/ng1419.

[3] A. A. Nugent, A. L. Kolpak, and E. C. Engle, “Human disorders of axon guidance,” *Current Opinion in Neurobiology*, vol. 22, no. 5, pp. 837–843, Oct. 2012, doi: 10.1016/j.conb.2012.02.006.

[4] E. Y. Van Battum, S. Brignani, and R. J. Pasterkamp, “Axon guidance proteins in neurological disorders,” *The Lancet Neurology*, vol. 14, no. 5, pp. 532–546, May 2015, doi: 10.1016/S1474-4422(14)70257-1.

[5] V. Corset, K. T. Nguyen-Ba-Charvet, C. Forcet, E. Moyse, A. Chédotal, and P. Mehlen, “Netrin-1-mediated axon outgrowth and cAMP production requires interaction with adenosine A2b receptor,” *Nature*, vol. 407, no. 6805, pp. 747–750, Oct. 2000, doi: 10.1038/35037600.

[6] K. L. Whitford *et al.*, “Regulation of Cortical Dendrite Development by Slit-Robo Interactions,” *Neuron*, vol. 33, no. 1, pp. 47–61, Jan. 2002, doi: 10.1016/S0896-6273(01)00566-9.

[7] Y.-Y. Kim *et al.*, “Meteorin Regulates Mesendoderm Development by Enhancing Nodal Expression,” *PLoS ONE*, vol. 9, no. 2, p. e88811, Feb. 2014, doi: 10.1371/journal.pone.0088811.

[8] H. S. Lee, J. Han, S.-H. Lee, J. A. Park, and K.-W. Kim, “Meteorin promotes the formation of GFAP-positive glia via activation of the Jak-STAT3 pathway,” *Journal of Cell Science*, vol. 123, no. 11, pp. 1959–1968, Jun. 2010, doi: 10.1242/jcs.063784.

[9] J. Nishino, K. Yamashita, H. Hashiguchi, H. Fujii, T. Shimazaki, and H. Hamada, “Meteorin: a secreted protein that regulates glial cell differentiation and promotes axonal extension,” *EMBO J*, vol. 23, no. 9, pp. 1998–2008, May 2004, doi: 10.1038/sj.emboj.7600202.

[10] J. R. Jørgensen *et al.*, “Characterization of Meteorin—An Evolutionary Conserved Neurotrophic Factor,” *J Mol Neurosci*, vol. 39, no. 1–2, pp. 104–116, Sep. 2009, doi: 10.1007/s12031-009-9189-4.

[11] J. R. Jørgensen *et al.*, “Cometin is a novel neurotrophic factor that promotes neurite outgrowth and neuroblast migration in vitro and supports survival of spiral ganglion neurons in vivo,” *Experimental Neurology*, vol. 233, no. 1, pp. 172–181, Jan. 2012, doi: 10.1016/j.expneurol.2011.09.027.

[12] S. Zheng, Z. Li, J. Song, J. Liu, and C. Miao, “Metrnl: a secreted protein with new emerging functions,” *Acta Pharmacol Sin*, vol. 37, no. 5, pp. 571–579, May 2016, doi: 10.1038/aps.2016.9.

[13] T. W. Jung *et al.*, “METRNL attenuates lipid-induced inflammation and insulin resistance via AMPK or PPARδ-dependent pathways in skeletal muscle of mice,” *Exp Mol Med*, vol. 50, no. 9, p. 122, Sep. 2018, doi: 10.1038/s12276-018-0147-5.

[14] J. A. Park *et al.*, “Meteorin regulates angiogenesis at the gliovascular interface,” *Glia*, vol. 56, no. 3, pp. 247–258, Feb. 2008, doi: 10.1002/glia.20600.

[15] Z.-Y. Li *et al.*, “Subfatin is a Novel Adipokine and Unlike Meteorin in Adipose and Brain Expression,” *CNS Neurosci Ther*, vol. 20, no. 4, pp. 344–354, Apr. 2014, doi: 10.1111/cns.12219.

[16] M. S. Cooper and L. A. D’amico, “A Cluster of Noninvoluting Endocytic Cells at the Margin of the Zebrafish Blastoderm Marks the Site of Embryonic Shield Formation,” *Developmental Biology*, vol. 180, no. 1, pp. 184–198, Nov. 1996, doi: 10.1006/dbio.1996.0294.

[17] J. J. Essner, J. D. Amack, M. K. Nyholm, E. B. Harris, and H. J. Yost, “Kupffer’s vesicle is a ciliated organ of asymmetry in the zebrafish embryo that initiates left-right development of the brain, heart and gut,” *Development*, vol. 132, no. 6, pp. 1247–1260, Mar. 2005, doi: 10.1242/dev.01663.

[18] M. Placzek and J. Briscoe, “The floor plate: multiple cells, multiple signals,” *Nat Rev Neurosci*, vol. 6, no. 3, pp. 230–240, Mar. 2005, doi: 10.1038/nrn1628.

[19] Z. Kaprielian, E. Runko, and R. Imondi, “Axon guidance at the midline choice point,” *Dev. Dyn.*, vol. 221, no. 2, pp. 154–181, Jun. 2001, doi: 10.1002/dvdy.1143.

[20] B. B. Gore, K. G. Wong, and M. Tessier-Lavigne, “Stem Cell Factor Functions as an Outgrowth-Promoting Factor to Enable Axon Exit from the Midline Intermediate Target,” *Neuron*, vol. 57, no. 4, pp. 501–510, Feb. 2008, doi: 10.1016/j.neuron.2008.01.006.

[21] J. Hjorth and B. Key, “Development of axon pathways in the zebrafish central nervous system.,” *Int. J. Dev. Biol.*, vol. 46, no. 4, Art. no. 4, Jul. 2004, doi: 10.1387/ijdb.12141449.

[22] R. Macdonald *et al.*, “The Pax protein Noi is required for commissural axon pathway formation in the rostral forebrain,” *Development*, vol. 124, no. 12, pp. 2397–2408, Jun. 1997, doi: 10.1242/dev.124.12.2397.

[23] S. Shanmugalingam *et al.*, “Ace/Fgf8 is required for forebrain commissure formation and patterning of the telencephalon,” *Development*, vol. 127, no. 12, pp. 2549–2561, Jun. 2000, doi: 10.1242/dev.127.12.2549.

[24] K. J. Svensson *et al.*, “A Secreted Slit2 Fragment Regulates Adipose Tissue Thermogenesis and Metabolic Function,” *Cell Metabolism*, vol. 23, no. 3, pp. 454–466, Mar. 2016, doi: 10.1016/j.cmet.2016.01.008.

[25] R. R. Rao *et al.*, “Meteorin-like Is a Hormone that Regulates Immune-Adipose Interactions to Increase Beige Fat Thermogenesis,” *Cell*, vol. 157, no. 6, pp. 1279–1291, Jun. 2014, doi: 10.1016/j.cell.2014.03.065.

[26] J. H. McCarty *et al.*, “Selective ablation of αv integrins in the central nervous system leads to cerebral hemorrhage, seizures, axonal degeneration and premature death,” *Development*, vol. 132, p. 12, Jan. 2005, doi: 10.1242/dev.01551.

[27] J. H. McCarty *et al.*, “Defective Associations between Blood Vessels and Brain Parenchyma Lead to Cerebral Hemorrhage in Mice Lacking alpha-v Integrins,” *MOL. CELL. BIOL.*, vol. 22, p. 11, Nov. 2002, doi: 10.1128/MCB.22.21.7667–7677.2002.

[28] B. L. Bader, H. Rayburn, D. Crowley, and R. O. Hynes, “Extensive Vasculogenesis, Angiogenesis, and Organogenesis Precede Lethality in Mice Lacking All alpha-v Integrins,” *Cell*, vol. 95, p. 13, Nov. 1998, doi: 10.1016/s0092-8674(00)81618-9.

[29] R. Milner, G. Edwards, and C. Streuli, “A Role in Migration for the avb1 Integrin Expressed on Oligodendrocyte Precursors,” *The Journal of Neuroscience*, vol. 15, p. 13, Nov. 1996, doi: 10.1523/JNEUROSCI.16-22-07240.1996.

[30] B. Felding-Habermann *et al.*, “A Single Immunoglobulin-like Domain of the Human Neural Cell Adhesion Molecule L1 Supports Adhesion by Multiple Vascular and Platelet Integrins,” *Journal of Cell Biology*, vol. 139, no. 6, pp. 1567–1581, Dec. 1997, doi: 10.1083/jcb.139.6.1567.

[31] R. Belvindrah, D. Graus-Porta, S. Goebbels, K.-A. Nave, and U. Muller, “1 Integrins in Radial Glia But Not in Migrating Neurons Are Essential for the Formation of Cell Layers in the Cerebral Cortex,” *Journal of Neuroscience*, vol. 27, no. 50, pp. 13854–13865, Dec. 2007, doi: 10.1523/JNEUROSCI.4494-07.2007.

[32] A. J. Ablooglu, E. Tkachenko, J. Kang, and S. J. Shattil, “Integrin αV is necessary for gastrulation movements that regulate vertebrate body asymmetry,” *Development*, vol. 137, no. 20, pp. 3449–3458, Oct. 2010, doi: 10.1242/dev.045310.

[33] M. J. F. Barresi, “Hedgehog regulated Slit expression determines commissure and glial cell position in the zebrafish forebrain,” *Development*, vol. 132, no. 16, pp. 3643–3656, Jul. 2005, doi: 10.1242/dev.01929.

[34] J. P. Myers, M. Santiago-Medina, and T. M. Gomez, “Regulation of axonal outgrowth and pathfinding by integrin-ecm interactions,” *Devel Neurobio*, vol. 71, no. 11, pp. 901–923, Nov. 2011, doi: 10.1002/dneu.20931.

[35] C. Thisse and B. Thisse, “High-resolution in situ hybridization to whole-mount zebrafish embryos,” *Nat Protoc*, vol. 3, no. 1, pp. 59–69, Jan. 2008, doi: 10.1038/nprot.2007.514.

3.3 Hunting for Meteorin receptors

Since the discovery of Meteorins as secreted proteins over 15 years their receptor(s) were unknown for a long time. Just recently the first receptor for Meteorin and also the first receptor for Metrnl were published.

The first METRNL receptor published is the stem cell factor receptor KIT (KIT receptor tyrosine kinase). *Metrnl* was found to be highly expressed in myeloid cells of an infarct region of the left heart ventricle. Via chemical cross-linking mass spectrometry, KIT was detected as a possible METRNL receptor. The physical interaction was validated by co-immunoprecipitation assay using HEK-293 cells expressing KIT as well as METRNL. Finally, it was suggested that METNL by binding to KIT is promoting heart infarct repair [6]. Just three months after the first Metrnl receptor also the first Metrn receptor was identified. It was demonstrated that Metrn regulates the homeostasis of hematopoietic stem/progenitor cells by Htr2b interaction. *Metrn* expression was shown to be induced in macrophages under hypoxia and that by interacting with Htr2b Metrn is regulating reactive oxygen species levels in hematopoietic stem/progenitor cells via phospholipase C signaling targeting. Via a GST-pulldown assays Metrn interaction with the Htr2b N-terminus was demonstrated. Still, how the authors decided to test specifically Htr2b for possible Metrn binding is not extensively explained.

However, both published receptors are quite specific for their expression patterns and their functions. For instance, in zebrafish *kita* expression starts around 9hpf and is restricted to the prechordal plate. *Kitb* expression can be detected from 11hpf in the anterior ventral mesoderm (Figure 22A). However, since the onset for zebrafish *kits* expression is “too late” and *kit* expression cannot be found in proximity to DFCs and the forming KV and *htr2b* expression could not be even detected at these early stages (expression start around 2dpf, Figure 22B), we believe that Metrns act through other/additional receptors during early patterning processes.

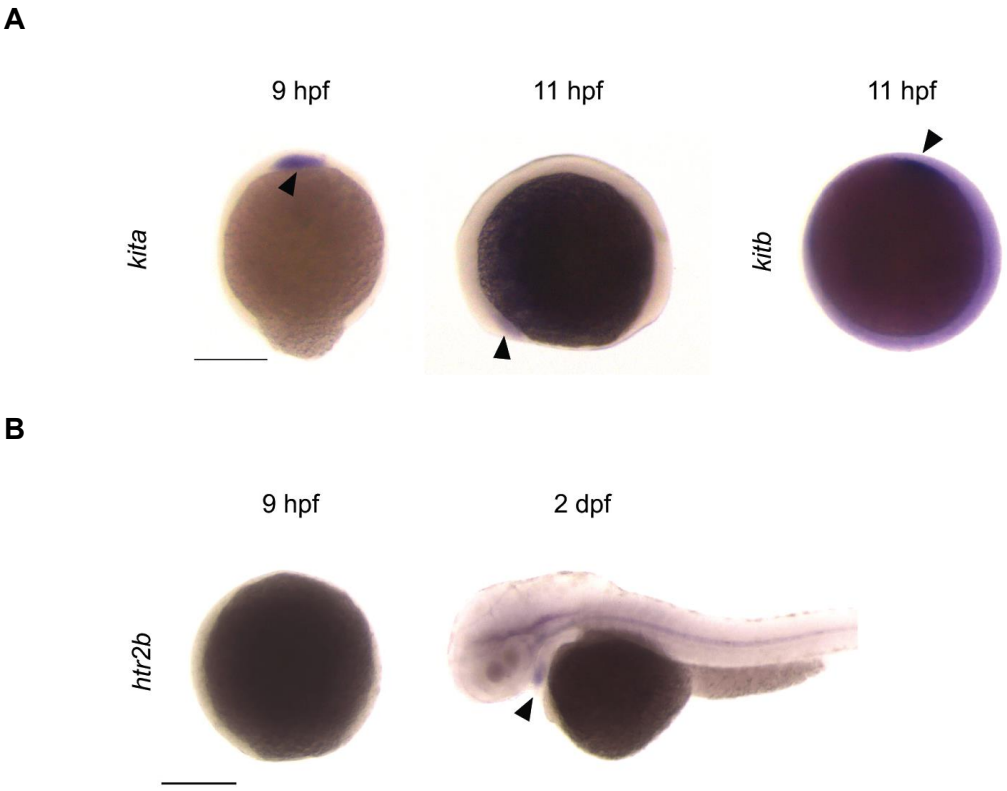

Figure 22: **Antisense RNA probe *in situ* hybridization for *kita, kitb* and *htr2b* reveal distinct expression patterns*:* A** At 9hpf *kita* is expressed in the prechordal plate (black arrow) and from 11hpf in the lateral borders of the anterior neural plate (black arrow). K*itb* expression could be detected from 11hpf in the anterior ventral mesoderm (black arrow). (scale: 0.25mm) **B** At *9hpf htr2b* expression was undetectable, solely from 2dpf *htr2b* transcripts could be visualized in the developing heart. (scale: 0.25mm)

We hypothesize that there might be more Meteorin receptors and that their function in connection with Meteorins could be depending on the tissue and developmental stage. Hence, we have hunted and are still hunting for new Meteorin receptors with several approaches to fully elucidate their biochemical signaling pathways and to understand their diverse roles. We think in using independent approaches to identify Metrns receptors we greatly increase the chances of success of a receptor identification and putative common candidates identified with several approaches will have greater chance to be *bona fide* physiological receptors.

3.3.1 Candidate approach with AVEXIS

A first approach to identify putative receptors, we used the Avidity-based extracellular interaction screen (AVEXIS) method. This method is suited for the detection of low–affinity extracellular protein interaction networks with a half-life ≤ 0.1 sec [348]. AVEXIS is a well-established method in zebrafish, based on an ELISA-like assay using receptor library prey complexes to probe on a ligand coated screening plate. Entire ectodomains of cell surface

proteins are expressed as soluble recombinant proteins in mammalian cell culture to maintain extracellular binding function without the insoluble transmembrane region. Protein ectodomains are expressed as a monomeric biotinylated “bait”- as well as pentamerized “prey” form (Figure 23A and B). Baits are captured in an oriented manner on streptavidin-coated microtiter plates whereas preys are tagged with lactamase to allow detection. For the interaction screen, bait ectodomains are probed with soluble pentameric lactamase-tagged prey ectodomains and positive binding can be visualized and analyzed by colorimetric enzymatic activity (Figure 23C). Prey-pentamerization enhances the avidity of the interaction as well as the detection sensitivity [348].

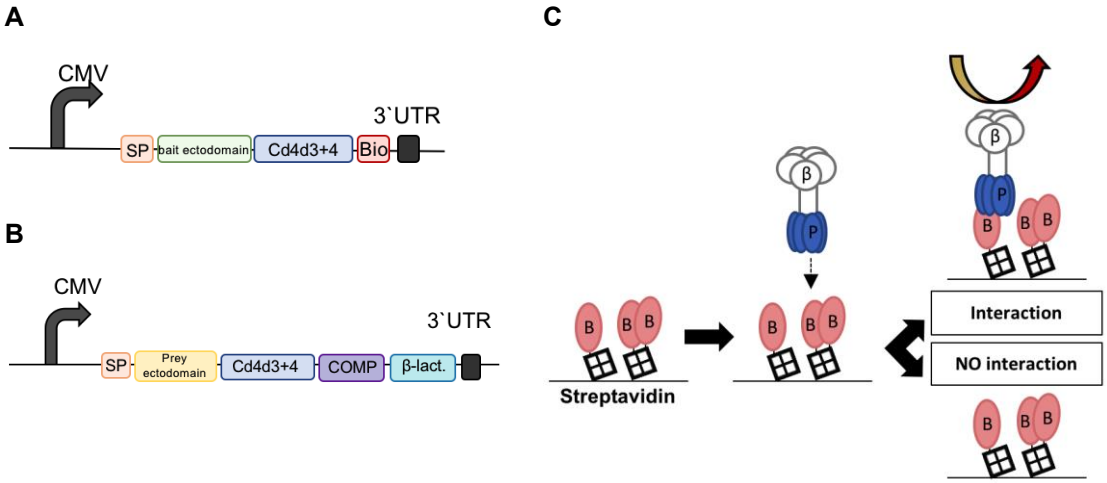

Figure 23: **The AVEXIS approach is based on monomeric biotinylated “bait”- as well as pentamerized “prey” forms and positive binding can be visualized and analyzed by colorimetric enzymatic activity: A** Scheme for the bait expression construct, containing the bait ectodomain, flanked by AscI and NotI restriction sites and a Cd4d3+4 tag. The bait is monobiotinylated via the co-transfection of a plasmid which is expressing the secreted BirA enzyme. Modified from [349]. **B** Scheme for the prey expression construct, containing the prey ectodomain, flanked by AscI and NotI restriction sites and a Cd4d3+4 tag, followed by a cartilage oligomeric matrix protein (COMP) pentamerisation sequence and a β-lactamase enzyme. Modified from [349]. **C** Schematic illustration of the AVEXIS approach, showing biotinylated bait ectodomains (pink) which are captured on a streptavidin-coated microtiter plate in an orientated manner. Baits are probed with soluble pentameric prey ectodomains with a lactamase tag (blue). Positive binding is visualized via nitrocefin’s colorimetric enzymatic turnover from yellow to red. Modified from [348].

To perform the AVEXIS screen, I visited the lab of Rob Meijers at the EMBL Hamburg with whom we have established a collaboration for this project. I performed the Meteorin receptor screen using their established zebrafish receptor library. We tested following bait and prey soluble recombinant proteins:

Bait	Metrn, Metrnl1, Netrin1a, Netrin1b, DSCAM
Prey	Robo1, Robo3, Robo4, DSCAM, Fizzled8, Unc5b, Dcc, Neo, Metrn, Metrnl1, Csf1a, Csf1b, Shha, Shhb, Draxin, SDK, L1CAM

In total, we screened 19 different Meteorin receptor candidates and we used metrn and metrnl1 as preys as well baits to already decrease the chance of false-positive results. The lab from Rob Meijers previously found that Netrins cannot be expressed as pentamers hence, Netrin1a and Netrin1b were screened as baits only. In contrast, all other 17 possible receptor candidates were expressed and screened as preys. Performing the AVEXIS screen with prey and bait Metrn/Metrnl1 we could not detect any positive interaction with one of the selected candidates. Furthermore, the addition of different concentrations of Heparan sulfate, which is known to be a positive modulator of Robo/Slit or DCC/Netrin signaling at the midline [351], did not reveal any positive interaction of Metrn/Metrnl1 either. On the other hand, we could detect as expected netrin binding to Unc5b, Dcc or Neo (neogenin), indicating that the general execution of the AVEXIS was successful and indeed metrn/metrnl was not binding to any of the tested candidates under these experimental conditions.

Nevertheless, since the AVEXIS is an approach for detecting also very transient interactions, with a very low false-positive rate, and it is not specific for one organism, we still plan to use this technique in the future. It would be possible to use the AVEXIS approach for the receptor candidate validation after another indenpendent candidate approach or a screening approach, which will be explained in the next paragraphs.

3.3.2 Candidate approach with AP-binding assays

Another approach we performed to visualize the distribution of possible Metrns receptor(s) and to identify putative Meteorins receptors were AP-binding assays. Therefore, constructs were cloned to produce Metrn-AP/Metrnl1-AP fusion proteins. AP-fusion proteins have been demonstrated to be an efficient tool for the investigation of the cellular distribution of putative receptors [352]. The Metrn-AP/Metrnl1-AP fusion proteins were then used as probes to detected possible binding on sections or to receptor candidates expressed in COS7 cells. Positive binding could be then visualized using an αAP-antibody and following an HRP tagged secondary antibody.

Advantages for an AP-binding assay are that it is very fast and several receptor candidates can be tested in parallel. Additionally, the read out for positive interaction is simple. Positive binding results in deep blue staining due to the reaction of the AP with BCIP (5-Bromo-4-chloro-3-indolyl phosphate) and NBT (nitro blue tetrazolium) causing the production of a dark blue/purple precipitation. On the other hand, the sensitivity and specificity of an AP-binding

assay is lower than of the AVEXIS, therefore the probabilities of getting false positive as well as false negative results is higher.

We used the AP-binding assay approach to validate if Metrns are able to bind axons expressing their hypothesized receptor(s) and to test for possible binding as we screened for putative receptor candidates.

We could show that Metrns AP-fusion proteins bind close to the midline of the spinal cord. This supports the hypothesis of Metrns as novel axonal guidance factors facilitating midline crossing, and possible receptors are located where axons just crossed the midline (*Figure 24*).

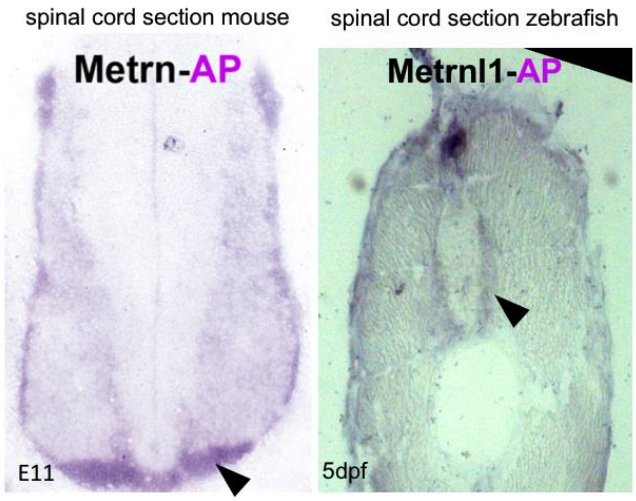

Figure 24: **The identification of Meteorin receptor(s) is crucial for fully understanding their biochemical signaling pathways:** Spinal cord sections of E11 mouse and 5dpf zebrafish probed with Metrn-AP or Metrnl1-AP, visualizing possible Metrns receptor(s) location, close to the midline of the spinal cord (black arrows).

During our hunt for Meteorins receptor(s) we tested the following receptor candidates with the AP-binding assay: IntegrinαV, Integrinβ1b and Gp130. IntegrinαV ad well as Integrinβ1b were tested as possible receptors since we investigated that both integrins might genetically interact with Metrn proteins for the proper clustering of DFCs (see 3.1.2). Gp130 was tested since it was described that Meteorin activates the tyrosine phosphorylation of gp130 and recruits Gp130 as it is activating the Jak-STAT3 pathway [2].

Performing an AP-binding assay we could not detect any binding between Metrn or Metrnl and IntegrinαV, Integrinβ1b or Gp130. Also, for IntegrinαV together with Integrinβ1b we did not detect any positive interaction with Metrn or Metrnl (see example in Figure 25). Therefore, we did not pursue any further binding assays for these proteins.

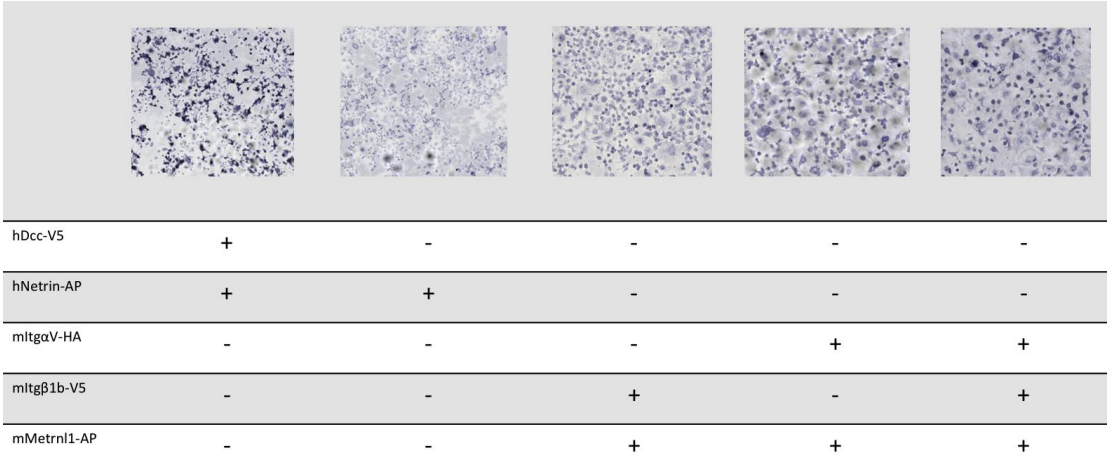

hDcc-V5	+	-	-	-	-
hNetrin-AP	+	+	-	-	-
mItgαV-HA	-	-	-	+	+
mItgβ1b-V5	-	-	+	-	+
mMetrnl1-AP	-	-	+	+	+

Figure 25: **Via an AP-binding assay no positive interaction between Metrnl1 and IntegrinαV/Integrinβ1b could be detected:** An example of an AP-binding assay showing positive interaction (dark colored cells) in the control between the *Dcc* receptor expressed in COS7 cells and Netrin-AP. No interaction (just light blue colored cells) could be detected between IntegrinαV and/or Integrinβ1b and Metrnl1.

3.3.3 Establishing a receptor candidate library with Ecto-Fc ligand-receptor interaction screen

Since we were not successful through our receptor identification approaches (AVEXIS or AP-binding assays), we opted to apply an unbiased high-throughput proteomic screening to establish a receptor candidate library for Meteorins. We decided for an Ecto-FC ligand-receptor interaction screen as published from Savas et al. [8]. This was described to be specific for ligand-receptor interactions with high sensitivity, to have a short duration of analysis and to be a robust and reproducible technique. For the Ecto-FC ligand-receptor interaction screen approach candidate ligands - in our case Meteorins and Netrin as control - are cloned into an FC-tag vector including an N-terminal bovine prolactine signal peptide, a signal peptide for stable and efficient secretion as shown *in vitro* [353] and *in vivo* [354] studies. These Ecto-Fc baits are then purified after transfection into HEK293 cells, and serve ultimately as baits in a binding assay using prey endogenous proteins extracted from E13 embryonic mouse brains. After incubation, the bait-prey protein mix is eluted, in-gel purified, trypsin-digested and proteins are identified by mass spectrometry (MS) (Figure 26) [8]. By adding in parallel the Netrin-Fc bait as control we expected to differentially identify known Netrin receptors and most importantly new specific Meteorins receptor candidates.

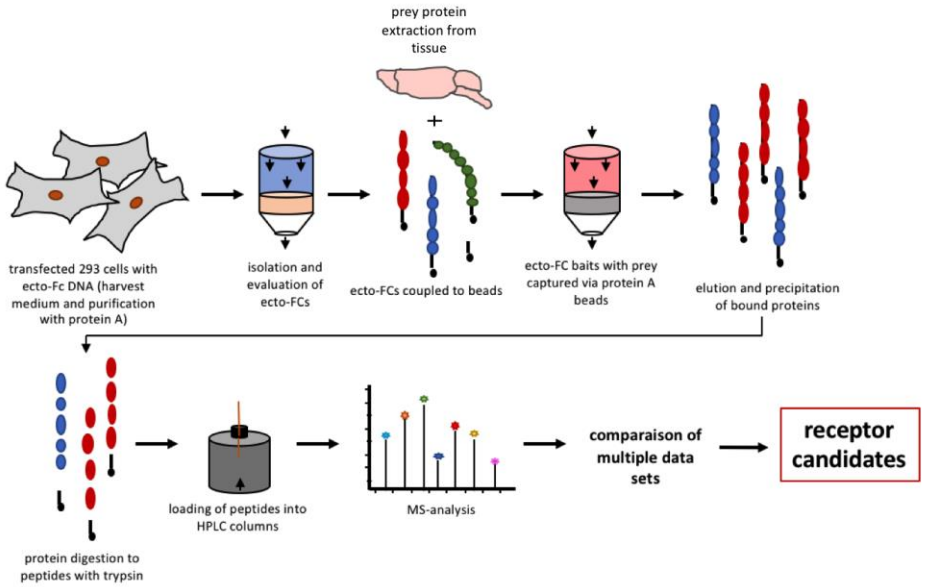

Figure 26: **Hunting for the Meteorins receptors via the Ecto-FC ligand-receptor interaction screen:** Schematic representation of the Ecto-FC approach displaying the different steps from bait-FC proteins production, prey protein extraction from mouse tissue, the purification of bait-prey proteins and analysis via MS. Adapted from [8].

The published approach and protocol from Savas et al. [8] performs ligands identifications and uses transmembrane receptors as ecto-Fc bait proteins. In our case, we were hunting for putative receptors and our ligands were used as ecto-Fc bait proteins. Therefore, we had to perform several optimization steps to the original protocol, especially in respect to the prey protein extraction methodology.

As a preliminary step we evaluated the purity and quality of our Ecto-FC bait proteins. To this end, we MS-analyzed purified single bait FC-tagged proteins. For all tested Ecto-Fc bait proteins the inserted gene of interest (Meteorin, Meteorin-like, Netrin) corresponds to the most abundant protein identified, confirming the successful production and the adequate purification yield of our bait proteins.

We expect the Meteorin receptor(s) to be transmembrane (TM) proteins. Therefore, to select membrane proteins among all the MS-identified interactors we used a custom made “Transmembrane-Filter”, to sort out all detected proteins with an annotated transmembrane domain. We performed the first MS experiment with the Netrin-FC bait and a standard whole protein extract obtained from 4 embryonic brains. The overall number of identified proteins was low (323), only a little fraction could be annotated as transmembrane proteins (12) and Netrin known receptors like DCC or NEO1 could not be identified (Figure 27A). Hence, we assumed that the quantity of total proteins and the resulting small number of transmembrane proteins were not enough to identify even established Netrin interactors.

Subsequently, to improve the proteomic screening method we first increased the number of dissected embryonic brains (from 4 to 16) to generate higher amount of prey proteins. Second, as Meteorin receptor(s) are likely to be transmembrane proteins, we decided to use a specific plasma membrane extraction kit. Indeed it's well known that plasma membrane protein identification is challenging because of their low abundance and their water-insolubility due the membrane's lipid layer in which they are embedded [355].

We performed prey protein extraction from dissected embryonic mouse nervous tissue, and not from zebrafish. This choice has been made because our collaborators from Alain Chédotal's team have already experience in protein extraction methods from mouse nervous tissue. Since meteorins are highly –conserved among vertebrates [3], [17], [21], [22], we expect to identify similar protein partners in both species.

By combining the increase of initial prey protein quantity and the use of the plasma membrane extraction kit we were able to significantly increase the total number of identified proteins (2348/323~ 7fold increase) after a first FC interaction experiment. Interestingly we also obtained a 4.5fold enrichment in the number of annotated membrane proteins (16.8% rather then 3.7%, Figure 27A/B). Moreover, DCC and NEO1 were efficiently identified in the Netrin-FC sample (DCC peptides=22 NEO1 peptides=24). These results confirm that our hunting receptor approach works well and it can be used to perform the Metrns receptor candidate screening (Figure 27C).

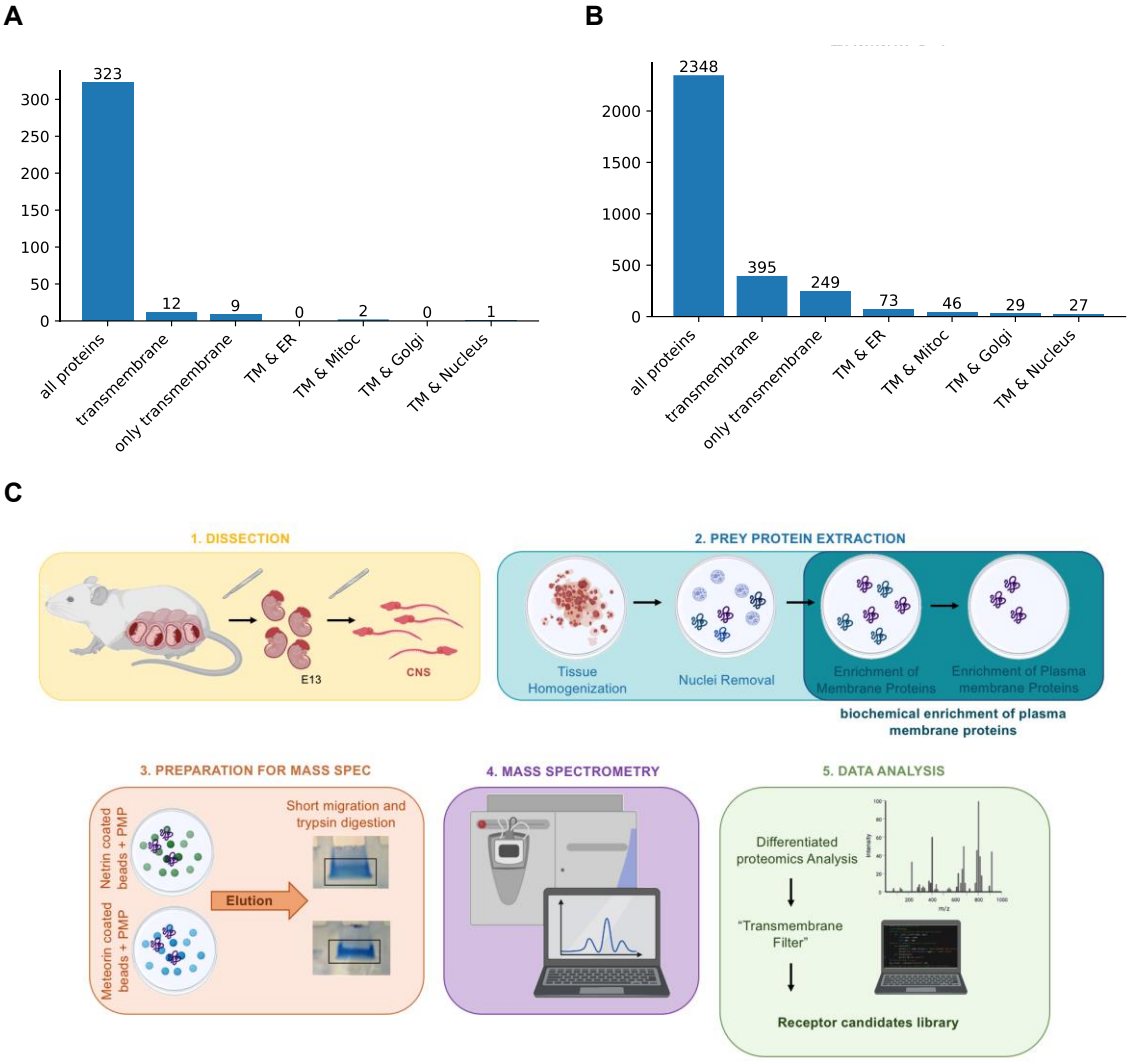

Figure 27: **Ecto-Fc interaction screen optimization and experimental workflow set up.** **A** Example of MS results using the "Transmembrane Filter, showing the number of identified proteins (all proteins= all identified proteins without filter; transmembrane= identified protein has an annotated transmembrane domain; only transmembrane= identified protein has an annotated transmembrane domain and is not located at the ER, Mitochondrium, Golgi or Nucleus; TM & ER= identified protein has an annotated transmembrane domain and is located at the ER; TM & Mitoc= identified protein has an annotated transmembrane domain and is located at the Mitochondrium; TM & Golgi= identified protein has an annotated transmembrane domain and is located at the Golgi; TM & Nucleus= identified protein has an annotated transmembrane domain and is located at the Nucleus). Proteins are considered identified if at least 2 peptides are detected and if Unique>1. **B** Analogous to A but after optimization of sample preparation. **C** Schematic for the optimized experimental workflow for Metrns receptor identification after the enrichment of plasma membrane proteins (PMP).

So far, we performed two independent Ecto-FC ligand-receptor interaction experiments followed by MS identification. The principle of the screening is to bring to the fore specific Meteorin interactors by comparing all the identified Meteorin and Netrin partners. To fulfill this aim, a quantitative analysis has to be made since candidate enrichement rather then presence/absence is frequently reported in this type of protein interaction screening. It's known that the number of MS-MS spectra obtained for each protein is correlated with its abundance. Thus, for each identified protein the log2 ratio between the number of spectra detected in the FC-Meteorin and in the FC-Netrin samples is calculated.

In the first experiment we identified 2348 proteins with 395 annotated as transmembrane proteins. We found >150 enriched candidates for Ntn1, including DCC and NEO1 Ntn1 receptors (Figure 28). The >150 enriched candidates for Ntn1 might be due to unspecific binding.

For Metrn we could identify around 42 enriched candidates and remarkably, two proteins were identified only in the Metrn-FC sample (*Figure 28*A, candidate 1=6 peptides; candidate 2=7 peptides). In the second experiment we identified 5322 proteins with 1055 annotated as transmembrane proteins. DCC and NEO1 were specifically identified in the Ntn1-FC sample. Most importantly the same two Mtrn candidates identified in the first experiment were found only in the Metrn-FC samples (*Figure 28*B, candidate1= 4 peptides; candidate 2=5 peptides). These new Mtrn interaction partners are annotated as membrane proteins. Although a high number of FC-Ntn1 and FC-Mtrn bound proteins were identified in both experiments, the identification of the same two Mtrn interaction partners in two independent screenings make us confident on the robustness of our data results and indicate that we have potentially identified two novel Metrn interactors. These results are very promising and pave the way to the discovery of Mtrn receptors in embryonic nervous tissue. Definitive proof requires however further extensive validation, starting with additional Ecto-FC ligand-receptor interaction experiments to unambiguously confirm the identified candidates.

A

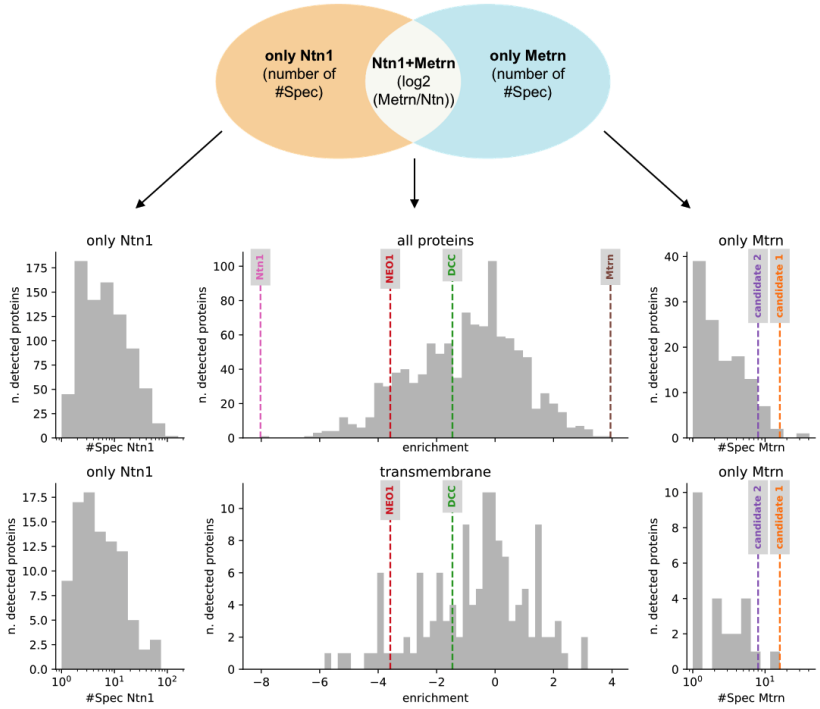

B

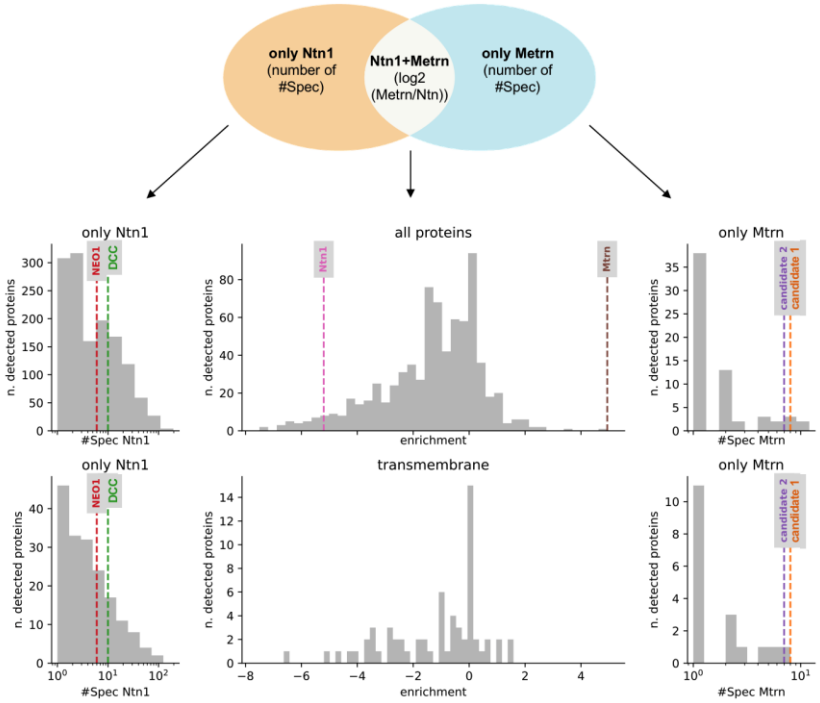

Figure 28: **Analyses of FC-Mtrn/FC-Ntn1 differential proteomic screenings. A** Protein enrichment analysis (log2(Metrn/Ntn)) for the first proteomic screening. The graph shows the number of all identified proteins (upper panel) and after including the “Transmembrane-Filter” (lower panel). Proteins only identified in the Netrin interaction sample (only Ntn1, left) or only in the Meteorin interaction sample (only Metrn, right panel) are visualized according to the number of Spectra (# Spec). **B** Analogous to A but for the second replicate.

4 DISCUSSION AND PERSPECTIVES

4.1 Meteorins during the establishment of the left-right axis throughout early embryonic development

Externally, the body plans of vertebrates appear bilaterally symmetric. But, from the inside the positioning and morphology of internal organs display a significant asymmetry. Therefore, during early development, the vertebrate embryo has to establish three main body axes, the anterior-posterior, the dorsal-ventral and the left-right axis. To achieve these axes specifications the distributions of specific signaling molecules at the right place and the right time within the developing embryo are essential for proper cell fate specification and pattern coordination. The left-right body axis is one of the last one to be defined during early embryonic development. One major regulator for the establishment of this axis is Nodal, a ligand belonging to the TGFβ protein family [112], [166]–[170]. It was shown that in vertebrates, Nodal signaling is activated in the left LPM, but remains inactive in the right LPM, and consequently is creating an embryo-scale left-right asymmetry [168]. In mouse, symmetry-breaking is initiated in the Node, with equivalent structures in for instance chicken (Hensen's node) and in zebrafish (KV) [194]–[196]. Within the node (or equivalents) a leftward flow of extraembryonic fluid is achieved by an oriented rotation of node cilia and this so called "Nodal flow" is assumed to be the essence for vertebrate L-R symmetry breaking. Nevertheless, the knowledge of early developmental biology and embryonic patterning processes increased enormously during the last two decades the whole mystery of how cell know exactly at the right time and the right place what do and where to go is far from being solved.

Excitingly, we could demonstrate that Meteorin proteins are required for the proper formation of the zebrafish KV and thus we aim to establish a novel role of Meteorins as proteins during embryonic left-right patterning.

We hypothesize that Meteorin proteins act in left-right patterning by regulating the level of correct DFC clustering. In the absence of Meteorins, DFCs are not able to assemble properly, which leads to deceleration of their migration towards the VP, resulting in an incomplete formation of the KV. This incomplete formation causes an insufficient Nodal flow and thus altered expression of Nodal factors, wind up in left-right patterning defects, like the proper positioning of organs as the heart.

Mechanisms underlying left-right patterning are known to be highly conserved within vertebrates. Hence, the first question we raised was if the Meteorin protein family is conserved across different species. As verified from our lab and also described from Zheng et al. 2016 [21], genes coding for *metrn* and *metrnl* are existing in several vertebrate classes, but could

be found in genomes of invertebrates. Therefore, we suggest that Metrn proteins arose after the vertebrate evolution and their putative function in the establishment of the left-right axis is specific for vertebrates. Also, the presence of highly conserved modules of amino acids within the Metrns sequences support a putative conservation of the Metrns biological activity during vertebrate evolution. One of these conserved features is the signal peptide on the N-terminal region of each member of the Meteorin protein family, supporting the idea that all Meteorins are secreted in the extracellular environment, where they, most likely, function via interacting with a receptor of their target cells.

Supporting the hypothesis of Metrns being essential for correct DFC clustering and KV formation, we could show that two members of the zebrafish Meteorin family (*metrn, metrnl1*) are expressed during early developmental stages within and around the KV structure and specifically in DFCs. Furthermore, we could analyze a significant increase of disorganized DFC assembly with occasional gaps in *metrn-/-, metrnl1-/-* and triplMut zebrafish embryos. These results indicate that both, Metrn and Metrnl1, cooperatively are necessary for proper DFC assembly. Nevertheless, the exact way how Meteorins are involved in this process is still elusive.

One theory could be that Meteorins have a direct effect on DFCs. Since *meteorins* are expressed in DFCs, but known to be secreted proteins, it is possible that Meteorins act via autocrine signaling. Several factors of the Nodal pathway and also Nodal itself are known to signal in an autocrine manner within development and proliferation processes [356]–[359].

However, autocrine Metrn signaling in DFCs would require that the Meteorins receptor(s) is/are located on the cell membrane of DFCs as well.

Remarkably, it was recently shown that during the onset of gastrulation in zebrafish, Nodal ligands act in an autocrine manner to introduce the sorting of endodermal cells in cooperation with sox32 (casanova)-dependent endodermal specification trough the acvr1ba receptor [358]. These finding indicate that autocrine Meteorin signaling would indeed fit into signaling pathways crucial for early embryonic patterning processes.

Therefore, one possibility could be, that Meteorins interact with cell-adhesion molecules (for instance cdherin1 and cadherin2 are known to be expressed within DFCs) located on the DFC cell membrane, since the disaggregation phenotype we observe in our *meteorin* mutants possibly suggests an involvement of cell adhesion [360], [361]. Additionally, several zebrafish studies demonstrated that proper DFC clustering is crucial for KV ciliogenesis and LR patterning [362]–[364] and that the disruption of genes encoding for cell-adhesion molecules belonging to the Cadherin family result in broken-up DFC phenotypes [363]. Thus, in the absence of Meteorins, the cell adhesion within DFCs would be disturbed, which would result in our observed DFC disassembly phenotypes.

Another possibility could be that Meteorins are cooperating with Ephrin signaling on the level of the DFC, since Ephrins are known to be able to signal in an autocrine manner [365]. Interestingly, it was shown that the gene for the Ephrin receptor *ephb4b* is expressed significantly in DFCs, that Ephrin ligands are expressed in close proximity to the cluster of DFCs and that the knockdown of either one of them is sufficient to cause scattering of the DFC cluster [364]. Hence, it would be imaginable that Meteorins are necessary for the proper binding of Ephrin ligands to their respective Ephrin receptors or synergize downstream with this signaling pathway and therefore influence the mediation of cell-cell contact-reliant repulsion between their neighboring cells and DFCs, crucial for correct KV formation.
Intriguingly, Ephrins and their receptors also belong to the family of canonical axonal guidance cues, which could indicate that Meteorins might interact with Ephrins during left-right patterning but also in the context of axonal guidance as described in 3.2.2.
To investigate the above-mentioned theories of Meteorins affecting on DFCs via autocrine signaling, several approaches could be performed. Via HCR and/or fluorescent double in-situ hybridizations the possible colocalization of *metrn/metrnl1* and possible interactors (*ephrins, cadherins*) could be analyzed. Furthermore, to assess possible relationships between Metrns potential interactors, the genetic interaction on the level of DFCs clustering could be analyzed with insufficient dosages of respective morpholinos, as described in 2.10, 3.1.2 and 3.2.2. To analyze if Meteorins are directly interacting during the above-mentioned theories, AP-binding assays and Co-IP approaches could be used.
Supported by our demonstrated genetic interaction of Metrns and IntegrinαVβ1 on the level of DFC clustering, another option would be that Meteorins interact with Integrins located on the membranes of DFCs. Importantly in this hypothesis, a couple of *in vitro* studies connected αVβ1 to migration and cell adhesion during developmental processes. For instance αVβ1 was shown to be implicated in neural cell adhesion molecule L1 cell binding [214] and in embryonic astrocytes and oligodendrocyte precursors migration [213]. Moreover, alike *meteorins*, both *integrins* were shown to be expressed in DFCs [209]. Therefore, it could be possible that Metrns interaction with αV and/or β1 influences the Integrin's adhesive functions and/or the further signaling, necessary for proper DFC clustering. Consequently, the absence of Meteorins would possibly lead to disturbed adhesion and/or Integrin signaling, resulting in DFC assembly defects and disturbed KV development, as discovered in *metrn* mutants. Via an AP-binding assay we were not able to detect significant direct interaction between Metrns/Metrnl1 and αV and/or β1, which could indicate that Meteorins and αVβ1 signaling pathways are linked but that αV and β1Intergins don't act as Metrns receptors. Therefore, specific interactions and concrete molecular signaling pathways of Metrns together with αVβ1 are still elusive. Further, we hypothesize that αV and/or β1 might still be involved in direct Meteorin interaction, even

after out negative AP-binding results. Integrins are known to interact and signal with numerous cofactor(s) and form complex dimers with additional Integrin subunits. For instance, αVβ1 is known to dimerize additionally with the β3, β5, β6, β8 subunits as well as with the αIIb subunit. Hence, it should not be excluded that Meteorins indeed interact with αV and/or β1 since an additional cofactor or further Integrin subunit might be necessary for accurate interaction and not present in our AP-binding assay.

Intriguingly, in several *metrns* LOF embryos, the connection between DFC and YSL/EVL seems to be disrupted, indicating that the DFC migration and clustering defect in our *meteorin* mutants appears to be not only involved in mediolateral DFC clustering. Also, we could observe that in mutants some DFCs are detached from the EVL during epiboly movements and therefore are not able to migrate properly. Since the connection between DFC and EVL normally enables a subset of DFCs to have apical contacts with the EVL and to be prepolarized, another hypothesis could be that Metrns are partly important for the polarization of the DFCs [199]–[201]. Since polarized DFCs initiated developing cilia at their membrane domain facing the lumen, it was further demonstrated, that KV lumen development was directly connected to ciliogenesis [200]. These findings emphasize that DFC polarization is essential for correct KV formation and ciliogenesis. Hence, the impaired polarization in embryos lacking Meteorins possibly disturbs the physical tissue linkage of EVL and DFCs and the correct formation of the KV which results in our described incorrect clustering of DFCs and properties of the KV. Nevertheless, the possible role of Metrns in the polarization of DFCs still hast to be investigated.

Hence, it might be useful to visualize DFC polarization via immunohistochemistry using for instance an antibody against the epithelial atypical Protein Kinase C (aPKC) [366]. A live *in vivo* approach via imaging a *Tg(sox17/cas:GFP)* transgenic reporter line in wt as well as *metrn* mutants backgrounds could provide further information about possible GFC migratory defects and polarization defects.

Another hypothesis could be that Meteorins signaling occurs in a paracrine manner, with Meteorins affecting cells and tissues surrounding DFCs. For instance, Meteorins could signal through interaction with receptor(s) located on the membrane of EVL cells and therefore affect the important connection between DFC and EVL [199]–[201]. Another option would be that Meteorins interact with Cadherins as described above, but in a paracrine manner. *Cdh1* as well as *cdh2* are expressed within the DFCs but also in the surrounding tissue [363], [367]. Hence, in the case of *metrn* LOF cell-adhesions of DFC surrounding cells could be disturbed, which would lead to disrupted DFC assembly and migration as observed in our *metrns* mutants. The same could be possible also for the interaction between Meteorins and αVβ1.

Both Intergins are described to be expressed within but also around the DFC tissue [209], [210].

Importantly, the theories and hypotheses discussed above are not mutually exclusive. Meteorins could interact and cooperate in an autocrine but also paracrine manner. To analyze the direct effect of *metrns* LOF in specifically DFCs or the cells of the surrounding tissue the 2C-Cas9 system could be used [368]. With this it would be possible to knock-out *meteorins* exclusively in DFCs (*cas9* expression under *cas* or *sox17* promoter) or in surrounding tissue like the YSL (*cas9* expression under *rab5b* or *slc3a2a* promoter [369]). The establishment of *metrn* and *metrnl1* transgenic lines, in which *meteorins* express fluorescent reporters would further support the effect(s) of Meteorins on DFC clustering and migration.

However, in all the above-described scenarios, it is possible that for successful Meteorins autocrine and/or paracrine signaling on the level of the DFCs additional co-factors are necessary. Therefore, the above-mentioned approaches to validate Meteorins interactions can just inform if Meteorins directly interact with Ephrins, Cadherins etc. To identify possible co-factors, our established Ecto-FC ligand-receptor interaction screen mass spec data could be used and analyzed for molecules, specifically involved in early developmental cell migration processes. However, it should be mentioned that until now we used mouse spinal cord, hindbrain and forebrain from stage E13 for prey protein extraction. Consequently, we cannot be sure that we miss possible co-factors in the context of early embryonic patterning due to the wrong “stage” and location of our prey extraction samples.

In addition, our work does not exclude the possibility that Metrns are also involved in later KV developmental and/or left-right patterning events, especially considering the specific expression of *metrn* and *metrnl1* around the zebrafish KV. To analyze the specific role of Meteorins during later KV developmental and left-right patterning stages, their genes could be inactivated after completed DFC clustering and migration. In this way, the role of Meteorins during embryonic left-right patterning could be investigated independently from DFC clustering and migration.

We hypothesize that disturbed KV properties, the impaired Nodal flow and the randomization of laterality organs are results of impaired DFC clustering and migration in *metrn* loss-of-function zebrafish. In conclusion, we can assume that Metrn proteins are novel factors involved in establishing the L-R asymmetry during embryonic development. The identification of Meteorins interaction partners would critically advance our understanding of their biological functions during early embryonic left-right patterning processes.

4.2 Meteorin proteins during the development of the vertebrate CNS and axonal midline crossing

During the last decades, the knowledge of molecular mechanisms responsible for the formation of functional neural circuits, especially within the CNS midline, has increased significantly, driven by the discovery and identification of axonal guidance factors, proteins which are modulating the elongation of axons during embryonic neuro development. The extensive study of these instructive molecular guidance molecules has allowed scientists to decipher the key aspects of biological processes guiding axonal pathfinding across the midline. These mechanisms appear to be highly conserved across evolution. Despite the complexity, the mystery of the midline crossing puzzle is nowhere near from being solved in its totality and especially the involvement of additional molecules within the midline crossing navigation still has to be investigated.

Meteorins are a small group of secreted proteins, known to regulate axonal extension and neuronal progenitor differentiation, *in vitro.* By using the CNS of our favorite organism, the zebrafish, as a model, we aim to understand *in vivo* if Meteorins play indeed a role during embryonic neurodevelopment, more precisely, if they are acting as factors regulating axonal pathfinding. Identical to their assumed role during embryonic left-right patterning, we suggest that the putative function of Meteorins in the processes of CNS patterning are specific for vertebrates.

The hypothesis of Metrns as novel axonal pathfinding factors was encouraged by a supposed NTR-like domain, present at the C-terminal region of the zebrafish Metrnl1. Nonetheless, the NTR-like domain was not detected in other Metrn proteins in zebrafish (Metrn, Metrnl2). Based on preliminary bioinformatic analysis, we hypothesize that this domain existing also in other orthologues or paralogues although its detection is impaired by a lower conservation of its canonical sequence. Up to date it is still unknown if the Metrnl1 NTR-like domain has a functional meaning, but interestingly it is also present in Netrins as well as other proteins. The domain was shown to be involved in ECM components interactions, like with HSPGs, but without showing any chemorepellent or chemoattractant properties and was further associated as an Integrin binding domain [370], [371]. Hence, it seems reasonable to assume that the putative NTR-like domain could contribute to the regulation of Metrnl1's activity via the modulation of the spatial distribution in the extracellular compartment and/or Intergin interaction.

We suggest, das Metrns are involved in defining axonal trajectories during embryonic neurodevelopment. To support this hypothesis, we demonstrated *metrns* expression in the embryonic zebrafish CNS. Similar to the mouse orthologues, *metrn* genes transcription can be detected in glia and neuronal progenitors [3], [22]. Strikingly, *metrn-* and *metrnl1* are also

transcribed from numerous cells located at the FP and along the midline. The FP as well as the midline represent well-characterized regions acting as guideposts for elongating axons and key areas for the generation of the numerous environmental cues orchestrating the navigation of growing axons [233], [372].

Previous work in the laboratory has generated loss-of-function alleles for all three zebrafish genes from the Meteorin family of secreted proteins. Interestingly, we could characterize specific axonal development defects in these mutant fish including defects in several commissural neuron populations. In particular, we could observe that AC commissural axons, trigeminal neurons as well as RGC projections are affected by Metrn signaling. In more detail, since AC development defects (defects in its fasciculation and elongation) could be observed in triplMut and single *metrn*$^{-/-}$ mutants, but not in *metrnl1*$^{-/-}$ or *metrnl2*$^{-/-}$ single mutants, we hypothesize that Metrn is the only paralogue in zebrafish impacting AC development. Contrarily, our results indicate that all three Metrn paralogues could act redundantly on the level RGC axon laminar patterning and that Metrn and Metrnl1, but not Metrnl2, are having a possible instructive role for the trigeminal nerve fasciculation.

Remarkably, we could investigate that mRNA encoding for *metrn* and *metrnl1* co-localize at the FP region in the hindbrain as well as at the spinal cord with three out of the four zebrafish slit paralogues (*slit1a, slit1b* and *slit2*). These observations let us assume that, *metrns* and *slits* are, at least in part, expressed from the same cell populations and that there might be a functional interaction between the two molecules. Indeed, we could describe a possible genetic interaction between Meteorin proteins and Slits (Slit2, Slit3) on the level of the AC. These results indicate that, beside Slit2 and Slit3 which are necessary for proper POC development, Meteorins are required for the formation of the AC and could therefore act as a pendant to Slit2 and Slit3 on the navigation of commissural axons. Nonetheless, the detailed molecular mechanisms of the functional interaction between Metrn and Slit signaling and the issue if the effects of Metrns are directly linked to the binding of Slits to their receptor on the targeted axons or on the other hand are a result of the modulation of the axonal navigation pathway, still have to be investigated.

We could also analyze a functional interaction between Metrns and IntegrinαV and β1 on the level of the development of the zebrafish AC. Remarkably, these results could connect the suggested Meteorin signaling during axonal pathfinding with the previous discussed embryonic left-right axis establishment. *IntegrinαV* and *β1* are broadly expressed and often are connected with other Integrins, however the interaction with Meteorins could represent a possible conservation of Meteorins signaling cascade, especially during embryonic developmental processes.

Overall, our phenotypic and molecular analysis of Meteorins during zebrafish neurodevelopment demonstrates a role of our favorite protein family in the defining of axonal

projection patterns in several neuronal types, focusing in the fact that different combinations of Meteorins are affecting distinct axonal populations. But, despite our results suggest a novel rule of Meteorin proteins as new class of factors in regulating axonal elongation, it is still elusive in which way the activity of Meteorins is able to impact axonal behavior. Therefore, in the next paragraph we will hypothesize possible mechanisms to provide a functional explanation how Meteorin proteins could modulate axonal guidance.

4.2.1 Possible models for modulation of axonal pathfinding induced by Meteorin proteins: direct interaction and/or FP induction

A first theory hypothesizes that Meteorin proteins themselves are directly able to control choices of axonal navigation. Therefore, Metrns would act as novel and uncharacterized axonal guidance molecules, or through direct interaction or regulation of already established axonal guidance pathways. As we could reveal, Meteorins secretion occurs at the “right time” and also the “right place” within the embryonic CNS and therefore could represent a likely candidate within the family of axonal guidance molecules. To indeed orchestrate the processes of axonal elongation, Meteorin proteins have to interact with a specific receptor, which should be expressed at elongating axons. Subsequently, the interaction could result in the activation of signaling pathways which in turn lead to axonal behavior changes. Strikingly, we could demonstrate that Metrns-AP fusion proteins are able to bind to commissural axons on spinal cord sections of mouse as well zebrafish, and particular to the commissural axons post-crossing segment. These results encourage the hypothesis of Meteorin proteins as novel axonal guidance factors and emphasize on the urge to identify putative receptor(s) to fully understand the biological activity of Meteorins in the context of axonal navigation. Another possible way of how Meteorin proteins are able to control choices of axonal navigation is that they collaborate with canonical guidance pathways by the regulation of their activity and therefore influencing their effect on axonal navigation. One possible idea could be that Meteorins are acting in one of the Slit signaling pathways. Since it was demonstrated that Slits as well as Metrns are impacting DRG explants and promoting axonal branching and neurite extension, this hypothesis could be tempting [3], [22], [373]. Remarkably, it was also shown that a cleaved fragment of Slit2 (Slit2-C) exerts the same function as Metrnl in adipose tissue [54]. Additionally, we could also show that the expression patterns of *meteorins* and *slits* display a partial overlap and that Meteorin proteins and Slits (Slit2, Slit3) are genetically linked on the level of AC formation. Since axons pathfinding choices in *metrn* LOF are also influenced by the activity of Slits [333], [374], the hypothesis of a Metrns-Slit functional interaction is further reinforced. Via the AVEXIS we could not detect a direct interaction between Meteorins and Robo receptors. Therefore, it could be possible that Meteorins effect axonal responses to the Slit-Robo pathway by first forming a complex with Slit proteins and subsequently interacting

with Robo receptors. Instead, another possibility would be that Metrns via binding to a so far unknown receptor, located on the membrane of growing axons, activate a signaling cascade which in turn leads to expression level changes of Robo receptors, resulting in changed sensitive of growing axons to the Slit-mediated repulsion.

Several *in vitro* studies connected Integrin αVβ1 to processes acting during the development of the CNS neurodevelopmental. IntegrinαVβ1 was shown to be implicated in neural cell adhesion molecule L1 cell binding [214] as well as in embryonic astrocytes and oligodendrocyte precursors migration [213]. Additionally, Integrins were shown to influence the regulation of the dynamic detachment-attachment of growth cones through laminins interactions [375]. Interestingly, it was shown in Drosophila, that Integrins are able to regulate the responsiveness of growing axons to the Slit-mediated repulsion and that they are directly associated to commissural development [376], [377]. Encouraged by our observation of a possible genetic interaction between Meteorins and Integrins on the level of AC formation, we hypothesize that Meteorins effect axonal pathfinding via Integrin interaction. Meteorins could bind directly or in concert with other co-factors to Integrins expressed close to the growth cone and affect the navigation of the growing axons through ways as just described how Meteorins might affect axonal responses to the Slit-Robo pathway.

A second hypothesis would be that Meteorins would act more indirectly, in fact on the differentiation and patterning of midline glia cells, which are responsible for generating instructive axon guidance cues. This theory would also span the bridge to the role of Meteorins during embryonic left-right patterning and the described function of Metrn as a possible positive regulator of Nodal signaling during mesendoderm development [4]. Notably, in zebrafish *cyc* (*ndr2*) mutants the ventral midline is not able to differentiate properly leading to severe guidance defects, indicating that Nodal activity is crucial for FP induction [378]. Therefore, if Meteorins indeed would act as Nodal enhancers, the FP in *metrns* LOF fish would not fully develop, leading to a disturbed guidance molecules production, resulting in axonal pathfinding defects. Nevertheless, anatomical observations, stable *ntl* expression around the notochord and randomized visceral organs positioning in triplMut zebrafish embryos let assume that the FP development is not influenced by *metrns* LOF [247], [379], [380] (Eggeler et al. in preperation).

Consequently, an alternative hypothesis for the role of Meteorins during the differentiation and patterning of midline glia cells would be an involvement within the modulation of glia specification. It was shown via the exposure to exogenous Metrn the differentiation into GFAP-positive glia cells wad induced in P19 embryonic cells or cultured neurospheres [2], [3]. The balance of neuron/glia is known to be crucial for the homeostasis of the developing brain, since it was shown to be responsible for orchestrating the right dosages of guidance and trophic factors [381]. Hence, if Meteorins indeed would influence glia differentiation, the LOF would

result in glia differentiation defects and therefore in an unbalanced guidance factors production, as observed in our mutants. Interestingly, Integrin αV was shown to be important for proper axon and glia interactions in the CNS [205]–[207]. Therefore, it might be possible that Meteorins beside αV are involved in the regulation of this interactions as well. Hence, it might be useful to label glia cells and post-mitotic neurons differently and subsequently stain the two cell types via immunohistochemistry using for instance a GFAP and HuC antibody. A live *in vivo* approach via generating transgenic reporter lines for the two cell populations would be an additional approach to investigate a possible role of Metrns for correct axon and glia interactions. Preliminary results (data not shown) however, show that *gfap* mRNA levels as well as the number of *gfap* expressing cells are not altered in *metrns* LOF embryos. These observations would therefore argue against the hypothesis for the role of Meteorins in the context of differentiation and patterning of midline glia cells.

Again, as mentioned in the context of LR patterning, the hypothesis and theories discussed above are not mutually exclusive. Considering, the numerous discovered functions of Meteorin during diverse a broad spectrum of developmental, metabolical, regenerative processes, it is likely possible that our favorite proteins (Meteorins) have also multiple functions during axonal guidance processes. They could be involved in the differentiation of neurons and glia at early developmental stages and subsequently regulate axonal navigation within later developmental processes. To analyze the specific role of Meteorins during early and later developmental stages, their genes could be inactivated after completed neuronal differentiation. Hence, Metrns function within axonal guidance could be investigated impartially from the process of glia and FP differentiation. However, considering the significant decrease of *meteorins* expression after 2dpf and the absence of obvious neurodevelopmental defects in adult zebrafish we assume that Meteorins function in aspect of axonal development and guidance is just required during the developmental of the CNS and not its maintenance.

4.3 The (long) Meteorins receptor hunt….to be continued

In spite of the recent advancement in understanding the numerous functions of Meteorins, we assume that the totality of all Metrns receptor(s) are still unknown. Thus, the identification of additional Metrn receptor(s) is essential for fully understanding downstream signaling pathways and biological functions of proteins from the Meteorin family. To hunt for Meteorins receptors we made use of several independent approaches.

The AVEXIS, one of the first methods we performed during our receptor hunt, is described as a high-throughput interaction screen for even very transient interactions and with a low false-positive rate, seeming perfect for the search for our receptor(s). Additionally, it is not bound to one specific species, giving us the possibility to analyze possible binding in zebrafish and mouse in parallel. On the other hand, it is only suited for single transmembrane domain receptor candidates and therefore might rule out possible multiple transmembrane domain receptor candidates. For instance, Htr2b, the recent published receptor for Metrn displays seven transmembrane domains [7] and could not be detected with the AVEXIS. Further, AVEXIS is described to be not suitable for homophilic extracellular interaction detection either, caused by avid prey–prey associations. AVEXIS is indeed a high throughput approach, however only if possible candidates are available and known. It is not suited as a screening approach, since each single receptor candidate needs individual cloning in the respective backbone and expression validation. I was very fortunate to receive a travelling fellowship to visit the lab of Rob Meijers at the EMBL Hamburg, with whom we have established a collaboration for the Meteorin project. I was able to perform the AVEXIS Meteorin receptor screen under their guidance and using their established zebrafish receptor library. The Meijers lab has already extensive experience with this method, successfully identifying various receptor/ligand interactions involved in axon guidance [382], [383]. Unfortunately, we were not able to detect any positive interaction between Meteorins and our tested receptor candidates. However, due to its ability to detect very transient interactions and with its low false-positive rate, it would be a powerful approach to validate possible Meteorin receptor candidates, determined via another screening approaches.

The second candidate approach we tried was the AP-binding assay. As already discussed in 4.1, although we were not able to detect positive interactions between the tested Integrins and Meteorins with the AP-binding assay, it might be still possible that Integrins could act as Meteorins receptors.

Unable to establish receptor candidates via the AVEXIS or AP-binding assays, we decided to perform a screening approach prior to further candidate approaches. Hence, we performed an Ecto-FC ligand-receptor interaction screen as published from Savas et al. [8] to establish a list of possible Meteorin receptors. The Ecto-FC ligand-receptor interaction screen is described to

be highly sensitive, with a short duration of analysis and as robust and reproducible technique. The approach is based on Ecto-Fc proteins, which serve as baits for prey proteins, extracted from mouse tissues. By capturing bait proteins, bound to possible interaction partners/receptors and subsequent MS-analysis, the Ecto-FC ligand-receptor interaction approach enables to fish for possible interaction partners from a pool of the main relevant biological source, containing native post-translational modifications and without the need of a priority candidate. However, similarly to the AVEXIS approach, interactions with multiple transmembrane domain proteins are close to impossible to detect with the Ecto-FC. Further, the protocol requires extensive washing and elution steps, which could interfere with very low affinity interactions. In our case, the purification of the prey proteins from mouse tissue was optimized and to achieve a final proper amount of prey protein, a quite high number of samples was necessary. Additionally, the purification of specifically transmembrane proteins could be just achieved using a specific kit. Moreover, we could detect significantly more interactors for our Netrin control compared to the Meteorin sample and known Netrin interactors as DCC or NEO1 were not the most enriched within the group of detected Netrin interactors. These results could indicate that Netrin might attract numerous molecules for unspecific binding, probably due to unfolding. Therefore, for future MS experiments and analysis another internal control could be used. On the other hand, the low number of possible Meteorin interactors could be specifically linked to Meteorin. It could be possible that in our Ecto-FC approach the stechiometry between bait and prey is not optimal, especially if the affinity beween Meteorin and its receptor(s) is relatively weak. Indeed, by using 400ug of prey for 5ug of bait we were performing the interaction screen with “just” 100 times more prey, which could be not enough to detect Meteorin interaction with its putative receptor(s). Therefore, it could be possible that by increasing the number of embryonic brains and/or by further optimizing prey protein extraction the yield of prey protein could be increased and the potential number of identified interactors could be improved.

However, after the analysis of two independent MS data sets from the Ecto-FC ligand-receptor interaction screen, we identified two novel receptor candidates for Meteorins. However, to demonstrate their biological interest, the use of independent approaches to validate the receptor candidates will greatly increase the chances of success of this receptor identification. Putative common candidates identified with these approaches will have greater chance to be *bona fide* physiological receptors. Approaches to investigate possible interaction could be an AP-binding assay as already performed during the candidate approach (see 3.3.2) or a Co-IP. For the AP-binding assay respective receptor candidates could be cloned into a pCX-HA and pCX-V5 expression vector to induce their expression in COS7 with an HA- or V5-tag. After confirming the membrane localization of the receptor candidates, the AP-binding assay could be performed with our already established Metrns-AP fusion proteins as probes. However, the

AP-binding assay is a suitable method to detect interaction with a cell membrane receptor. Therefore, if the possible Meteorins receptor candidate is located within another membrane of the cell (ER, lysosome, Golgi ect.) a co-immunoprecipitation would be more relevant to investigate possible interaction. Co-IP is a well-established technique for the identification of protein–protein interactions via the usage of antibodies specific for the target protein to directly capture proteins interacting to the specific target protein. Since there are so far no reliable working antibodies for Meteorins available, HA or V5-tagged Meteorin fusion proteins could be used beside HA or V5-tagged receptor candidate fusion proteins in a pull-down assay.

However, both the Co-IP method and the Ecto-FC ligand-receptor interaction screen are *in vitro* approaches far away from the natural environment of the cell. Proteins need to be extracted in presence of detergents, which could alter folding as well as subcellular localization. Hence, a more "*in vivo*" driven approach would be crucial to confirm putative Meteorins interactions as described for instance from Hein et al. [384] or Cho et al. [385]. Therefore, our proteins of interest (Metrn, Metrnl ect.) and putative receptor candidates could be tagged with fluorophores via CRISPR-Cas9 gene editing following homologous recombination using single-stranded oligonucleotides donors [385]. This generated library of cells expressing targeted fluorophore-tagged proteins under near-endogenous conditions could then be used for Live-cell 3D confocal microscopy or further MS analysis. With this approach, it would be possible to analyze endogenous protein localization patterns and more strikingly, it enables to identify molecular interactions in unaffected cell environment.

As discussed in 4.2, we assume that the Metrn family is conserved across different vertebrate species. Moreover, we think that Meteorin interactors are conserved as well. Therefore, it would be exciting to performed parts of the receptor hunt, like the Ecto-FC ligand-receptor interaction screen also in zebrafish and/or human. Investigating if the recent published receptors for Metrnl and Metrn are also interactors for the zebrafish Meteorin family would be interesting to support the hypothesis of conserved Meteorin interactions. A possible approach would be an AP-binding assay expressing zebrafish *htr2b* or *kit* in cell culture and using the established Metrns-AP fusion proteins as probes.

After a hopefully successful validation of one (or more) receptor candidates, the screening of their role in embryonic patterning, neurodevelopment and axon guidance would be crucial to fully understand the role of Meteorin signaling during these processes. Therefore, *in situ* hybridizations (or HCR) for the respective receptor candidates could be performed in zebrafish, to visualize the general expression pattern and analyze if the candidate(s) is/are expressed in proximity to the hypothesized places of *meteorin* expression and function (commissures, DFCs). Furthermore, the CRISPR/Cas9 gene editing technique could be used to establish a knock out zebrafish line(s) (if not already existing) for the selected Metrns receptor(s) and analyze commissure development and embryonic patterning in the mutant backgrounds. To

test the cell autonomous role of Metrns receptor molecules in the axon guidance of commissural neurons, the inactivation of the receptor(s) gene expression in selected neuronal population in zebrafish would be necessary. For this, a cell specific expression of the *cas9* enzyme in genetically defined neuronal populations would be a possible approach [368]. Further, to visualize the Metrns receptor(s) *in vivo,* a transgenic reporter lines could be created using a CRISPR/Cas9-mediated knock-in method [386].

Since nothing is known so far about the molecular nature of the Metrn receptor(s) in the contexts of axonal guidance and embryonic patterning among many others, new Meteorin receptors will pave new research avenues to address how Meteorins are involved in numerous functions.

4.4 CONCLUSION

Meteorin proteins, belonging to the family of secreted proteins, are highly conserved among vertebrates. They display a great variety of biological functions and those are far from fully understood. Meteorin was allotted a role in neurogenesis, angiogenesis and mesendoderm development among others. Meteorin-like was assigned a possible role on diabetes and thermogenesis inter alia.

In this thesis we focused on the analysis of the so far unknown and putative conserved function of proteins belonging to the Meteorin family during early embryonic left-right axis establishment and the patterning of the embryonic CNS during development.

We could reveal that Meteorin proteins are new essential components for left-right patterning during embryonic vertebrate development and that in *metrns* LOF zebrafish embryos DFC disorganization and Nodal flow formation defects within the KV lead to left-right patterning defects like inverted positioning of organs like the heart. Further we could show that *metrn* genes are expressed at the FP and along the midline in the developing CNS mouse as well zebrafish and that the LOF results pathfinding defects in several populations of axons.

Furthermore, our biochemical approach to identify novel putative Metrn receptors lead to the discovery of two interesting candidates that will be further validated.

In summary, these results propose Metrns as potential novel factors for vertebrate left-right patterning and axonal midline crossing and thus represent an important improvement of the understanding of mechanisms directing patterning of the embryo in its first hours of development as well as the navigation of growing axons.

5 REFERENCES

[1] A. R. Ypsilanti, Y. Zagar, and A. Chedotal, “Moving away from the midline: new developments for Slit and Robo,” *Development*, vol. 137, no. 12, pp. 1939–1952, Jun. 2010, doi: 10.1242/dev.044511.

[2] H. S. Lee, J. Han, S.-H. Lee, J. A. Park, and K.-W. Kim, “Meteorin promotes the formation of GFAP-positive glia via activation of the Jak-STAT3 pathway,” *Journal of Cell Science*, vol. 123, no. 11, pp. 1959–1968, Jun. 2010, doi: 10.1242/jcs.063784.

[3] J. Nishino, K. Yamashita, H. Hashiguchi, H. Fujii, T. Shimazaki, and H. Hamada, “Meteorin: a secreted protein that regulates glial cell differentiation and promotes axonal extension,” *EMBO J*, vol. 23, no. 9, pp. 1998–2008, May 2004, doi: 10.1038/sj.emboj.7600202.

[4] Y.-Y. Kim *et al.*, “Meteorin Regulates Mesendoderm Development by Enhancing Nodal Expression,” *PLoS ONE*, vol. 9, no. 2, p. e88811, Feb. 2014, doi: 10.1371/journal.pone.0088811.

[5] T. G. Montague, J. A. Gagnon, and A. F. Schier, “Conserved regulation of Nodal-mediated left-right patterning in zebrafish and mouse,” *Development*, vol. 145, no. 24, p. dev171090, Dec. 2018, doi: 10.1242/dev.171090.

[6] M. R. Reboll *et al.*, “Meteorin-like promotes heart repair through endothelial KIT receptor tyrosine kinase,” *Science*, vol. 376, no. 6599, pp. 1343–1347, Jun. 2022, doi: 10.1126/science.abn3027.

[7] Y.-W. Dai *et al.*, “Meteorin links the bone marrow hypoxic state to hematopoietic stem/progenitor cell mobilization,” *Cell Reports*, vol. 40, no. 12, p. 111361, Sep. 2022, doi: 10.1016/j.celrep.2022.111361.

[8] J. N. Savas, J. De Wit, D. Comoletti, R. Zemla, A. Ghosh, and J. R. Yates, “Ecto-Fc MS identifies ligand-receptor interactions through extracellular domain Fc fusion protein baits and shotgun proteomic analysis,” *Nat Protoc*, vol. 9, no. 9, pp. 2061–2074, Sep. 2014, doi: 10.1038/nprot.2014.140.

[9] Z. Xie, Y. Jia, and H. Li, “Studying Protein–Protein Interactions by Biotin AP-Tagged Pulldown and LTQ-Orbitrap Mass Spectrometry,” in *Proteomics for Drug Discovery: Methods and Protocols*, Springer, 2017, pp. 129–138. doi: 10.1007/978-1-4939-7201-2_8.

[10] A. M. Benham, “Protein Secretion and the Endoplasmic Reticulum,” *Cold Spring Harbor Perspectives in Biology*, vol. 4, no. 8, pp. a012872–a012872, Aug. 2012, doi: 10.1101/cshperspect.a012872.

[11] S. Keerthikumar and Department of Biochemistry and Genetics, La Trobe Institute for Molecular Science, La Trobe University, Melbourne, Victoria 3086, Australia, “A

catalogue of human secreted proteins and its implications," *AIMS Biophysics*, vol. 3, no. 4, pp. 563–570, 2016, doi: 10.3934/biophy.2016.4.563.

[12] A. Falkenhagen, M. Ameli, S. Asad, S. E. Read, and S. Joshi, "A novel gene therapy strategy using secreted multifunctional anti-HIV proteins to confer protection to gene-modified and unmodified target cells," *Gene Ther*, vol. 21, no. 2, pp. 175–187, Feb. 2014, doi: 10.1038/gt.2013.70.

[13] M. Baay, A. Brouwer, P. Pauwels, M. Peeters, and F. Lardon, "Tumor Cells and Tumor-Associated Macrophages: Secreted Proteins as Potential Targets for Therapy," *Clinical and Developmental Immunology*, vol. 2011, pp. 1–12, 2011, doi: 10.1155/2011/565187.

[14] J. L. Robinson, A. Feizi, M. Uhlén, and J. Nielsen, "A Systematic Investigation of the Malignant Functions and Diagnostic Potential of the Cancer Secretome," *Cell Reports*, vol. 26, no. 10, pp. 2622-2635.e5, Mar. 2019, doi: 10.1016/j.celrep.2019.02.025.

[15] M. Stastna and J. E. Van Eyk, "Secreted proteins as a fundamental source for biomarker discovery," *Proteomics*, vol. 12, no. 4–5, pp. 722–735, Feb. 2012, doi: 10.1002/pmic.201100346.

[16] M. Ramialison *et al.*, "Rapid identification of PAX2/5/8 direct downstream targets in the otic vesicle by combinatorial use of bioinformatics tools," *Genome Biol*, vol. 9, no. 10, p. R145, 2008, doi: 10.1186/gb-2008-9-10-r145.

[17] J. R. Jørgensen *et al.*, "Cometin is a novel neurotrophic factor that promotes neurite outgrowth and neuroblast migration in vitro and supports survival of spiral ganglion neurons in vivo," *Experimental Neurology*, vol. 233, no. 1, pp. 172–181, Jan. 2012, doi: 10.1016/j.expneurol.2011.09.027.

[18] Z.-Y. Li *et al.*, "Subfatin is a Novel Adipokine and Unlike Meteorin in Adipose and Brain Expression," *CNS Neurosci Ther*, vol. 20, no. 4, pp. 344–354, Apr. 2014, doi: 10.1111/cns.12219.

[19] C. Bridgewood *et al.*, "The novel cytokine Metrnl/IL-41 is elevated in Psoriatic Arthritis synovium and inducible from both entheseal and synovial fibroblasts," *Clinical Immunology*, vol. 208, p. 108253, Nov. 2019, doi: 10.1016/j.clim.2019.108253.

[20] I. Ushach *et al.*, "Meteorin-like/Meteorin-β Is a Novel Immunoregulatory Cytokine Associated with Inflammation," *J.I.*, vol. 201, no. 12, pp. 3669–3676, Dec. 2018, doi: 10.4049/jimmunol.1800435.

[21] S. Zheng, Z. Li, J. Song, J. Liu, and C. Miao, "Metrnl: a secreted protein with new emerging functions," *Acta Pharmacol Sin*, vol. 37, no. 5, pp. 571–579, May 2016, doi: 10.1038/aps.2016.9.

[22] J. R. Jørgensen *et al.*, "Characterization of Meteorin—An Evolutionary Conserved Neurotrophic Factor," *J Mol Neurosci*, vol. 39, no. 1–2, pp. 104–116, Sep. 2009, doi: 10.1007/s12031-009-9189-4.

[23] I. Ushach *et al.*, “METEORIN-LIKE is a cytokine associated with barrier tissues and alternatively activated macrophages,” *Clinical Immunology*, vol. 156, no. 2, pp. 119–127, Feb. 2015, doi: 10.1016/j.clim.2014.11.006.

[24] W. Gong, Y. Liu, Z. Wu, S. Wang, G. Qiu, and S. Lin, “Meteorin-Like Shows Unique Expression Pattern in Bone and Its Overexpression Inhibits Osteoblast Differentiation,” *PLoS ONE*, vol. 11, no. 10, p. e0164446, Oct. 2016, doi: 10.1371/journal.pone.0164446.

[25] Z. Li *et al.*, “Intestinal Metrnl released into the gut lumen acts as a local regulator for gut antimicrobial peptides,” *Acta Pharmacol Sin*, vol. 37, no. 11, pp. 1458–1466, Nov. 2016, doi: 10.1038/aps.2016.70.

[26] J. A. Park *et al.*, “Meteorin regulates angiogenesis at the gliovascular interface,” *Glia*, vol. 56, no. 3, pp. 247–258, Feb. 2008, doi: 10.1002/glia.20600.

[27] R. H. Garman, “Histology of the Central Nervous System,” *Toxicol Pathol*, vol. 39, no. 1, pp. 22–35, Jan. 2011, doi: 10.1177/0192623310389621.

[28] A. Volterra and J. Meldolesi, “Astrocytes, from brain glue to communication elements: the revolution continues,” *Nat Rev Neurosci*, vol. 6, no. 8, pp. 626–640, Aug. 2005, doi: 10.1038/nrn1722.

[29] N. J. Abbott, L. Rönnbäck, and E. Hansson, “Astrocyte–endothelial interactions at the blood–brain barrier,” *Nat Rev Neurosci*, vol. 7, no. 1, pp. 41–53, Jan. 2006, doi: 10.1038/nrn1824.

[30] M. E. Hamby and M. V. Sofroniew, “Reactive astrocytes as therapeutic targets for CNS disorders,” *Neurotherapeutics*, vol. 7, no. 4, pp. 494–506, Oct. 2010, doi: 10.1016/j.nurt.2010.07.003.

[31] H. S. Lee, S.-H. Lee, J.-H. Cha, J. H. Seo, B. J. Ahn, and K.-W. Kim, “Meteorin is upregulated in reactive astrocytes and functions as a negative feedback effector in reactive gliosis,” *Molecular Medicine Reports*, vol. 12, no. 2, pp. 1817–1823, Aug. 2015, doi: 10.3892/mmr.2015.3610.

[32] M. V. Sofroniew, “Reactive Astrocytes in Neural Repair and Protection,” *Neuroscientist*, vol. 11, no. 5, pp. 400–407, Oct. 2005, doi: 10.1177/1073858405278321.

[33] J. F. Robinson *et al.*, “Cadmium-Induced Differential Toxicogenomic Response in Resistant and Sensitive Mouse Strains Undergoing Neurulation,” *Toxicological Sciences*, vol. 107, no. 1, pp. 206–219, Jan. 2009, doi: 10.1093/toxsci/kfn221.

[34] S. Balmer, S. Nowotschin, and A.-K. Hadjantonakis, “Notochord morphogenesis in mice: Current understanding & open questions: Notochord Morphogenesis in Mice,” *Dev. Dyn.*, vol. 245, no. 5, pp. 547–557, May 2016, doi: 10.1002/dvdy.24392.

[35] T. Taga and K. Nakashima, “Mechanisms Underlying Cytokine-Mediated Cell-Fate Regulation in the Nervous System,” *MN*, vol. 25, no. 3, pp. 233–244, 2002, doi: 10.1385/MN:25:3:233.

[36] K. Nakashima, “Synergistic Signaling in Fetal Brain by STAT3-Smad1 Complex Bridged by p300,” *Science*, vol. 284, no. 5413, pp. 479–482, Apr. 1999, doi: 10.1126/science.284.5413.479.

[37] O. Islam, X. Gong, S. Rose-John, and K. Heese, “Interleukin-6 and Neural Stem Cells: More Than Gliogenesis,” *MBoC*, vol. 20, no. 1, pp. 188–199, Jan. 2009, doi: 10.1091/mbc.e08-05-0463.

[38] C. Ménard *et al.*, “An Essential Role for a MEK-C/EBP Pathway during Growth Factor-Regulated Cortical Neurogenesis,” *Neuron*, vol. 36, no. 4, pp. 597–610, Nov. 2002, doi: 10.1016/S0896-6273(02)01026-7.

[39] M. Simard, G. Arcuino, T. Takano, Q. S. Liu, and M. Nedergaard, “Signaling at the Gliovascular Interface,” *J. Neurosci.*, vol. 23, no. 27, pp. 9254–9262, Oct. 2003, doi: 10.1523/JNEUROSCI.23-27-09254.2003.

[40] M. D. Tran and J. T. Neary, “Purinergic signaling induces thrombospondin-1 expression in astrocytes,” *Proceedings of the National Academy of Sciences*, vol. 103, no. 24, pp. 9321–9326, Jun. 2006, doi: 10.1073/pnas.0603146103.

[41] K. Watanabe *et al.*, “Latent process genes for cell differentiation are common decoders of neurite extension length,” *Journal of Cell Science*, vol. 125, no. 9, pp. 2198–2211, May 2012, doi: 10.1242/jcs.097709.

[42] D. W. Y. Sah, M. H. Ossipo, and F. Porreca, “Neurotrophic factors as novel therapeutics for neuropathic pain,” *Nat Rev Drug Discov*, vol. 2, no. 6, pp. 460–472, Jun. 2003, doi: 10.1038/nrd1107.

[43] J. R. Jørgensen *et al.*, “Meteorin reverses hypersensitivity in rat models of neuropathic pain,” *Experimental Neurology*, vol. 237, no. 2, pp. 260–266, Oct. 2012, doi: 10.1016/j.expneurol.2012.06.027.

[44] J. R. Jørgensen *et al.*, “Lentiviral delivery of Meteorin protects striatal neurons against excitotoxicity and reverses motor deficits in the quinolinic acid rat model,” *Neurobiology of Disease*, vol. 41, no. 1, pp. 160–168, Jan. 2011, doi: 10.1016/j.nbd.2010.09.003.

[45] Z. Wang *et al.*, “Meteorin is a Chemokinetic Factor in Neuroblast Migration and Promotes Stroke-Induced Striatal Neurogenesis,” *J Cereb Blood Flow Metab*, vol. 32, no. 2, pp. 387–398, Feb. 2012, doi: 10.1038/jcbfm.2011.156.

[46] J. L. Wright, C. M. Ermine, J. R. Jørgensen, C. L. Parish, and L. H. Thompson, “Over-Expression of Meteorin Drives Gliogenesis Following Striatal Injury,” *Front. Cell. Neurosci.*, vol. 10, Jul. 2016, doi: 10.3389/fncel.2016.00177.

[47] K. Jin *et al.*, “Directed migration of neuronal precursors into the ischemic cerebral cortex and striatum,” *Molecular and Cellular Neuroscience*, vol. 24, no. 1, pp. 171–189, Sep. 2003, doi: 10.1016/S1044-7431(03)00159-3.

[48] K. Jin *et al.*, “Evidence for stroke-induced neurogenesis in the human brain,” *Proceedings of the National Academy of Sciences*, vol. 103, no. 35, pp. 13198–13202, Aug. 2006, doi: 10.1073/pnas.0603512103.

[49] A. Arvidsson, T. Collin, D. Kirik, Z. Kokaia, and O. Lindvall, “Neuronal replacement from endogenous precursors in the adult brain after stroke,” *Nat Med*, vol. 8, no. 9, pp. 963–970, Sep. 2002, doi: 10.1038/nm747.

[50] J. Tornøe *et al.*, “Encapsulated cell-based biodelivery of Meteorin is neuroprotective in the quinolinic acid rat model of neurodegenerative disease,” *Restorative Neurology and Neuroscience*, vol. 30, no. 3, pp. 225–236, 2012, doi: 10.3233/RNN-2012-110199.

[51] J.-J. Wang *et al.*, “Circular RNA-ZNF609 regulates retinal neurodegeneration by acting as miR-615 sponge,” *Theranostics*, vol. 8, no. 12, pp. 3408–3415, 2018, doi: 10.7150/thno.25156.

[52] H. Cao, “Adipocytokines in obesity and metabolic disease,” *Journal of Endocrinology*, vol. 220, no. 2, pp. T47–T59, Feb. 2014, doi: 10.1530/JOE-13-0339.

[53] R. R. Rao *et al.*, “Meteorin-like Is a Hormone that Regulates Immune-Adipose Interactions to Increase Beige Fat Thermogenesis,” *Cell*, vol. 157, no. 6, pp. 1279–1291, Jun. 2014, doi: 10.1016/j.cell.2014.03.065.

[54] K. J. Svensson *et al.*, “A Secreted Slit2 Fragment Regulates Adipose Tissue Thermogenesis and Metabolic Function,” *Cell Metabolism*, vol. 23, no. 3, pp. 454–466, Mar. 2016, doi: 10.1016/j.cmet.2016.01.008.

[55] J. Y. Bae, J. Woo, S. Kang, and K. O. Shin, “Effects of detraining and retraining on muscle energy-sensing network and meteorin-like levels in obese mice,” *Lipids Health Dis*, vol. 17, no. 1, p. 97, Dec. 2018, doi: 10.1186/s12944-018-0751-3.

[56] J. Y. Bae, “Aerobic Exercise Increases Meteorin-Like Protein in Muscle and Adipose Tissue of Chronic High-Fat Diet-Induced Obese Mice,” *BioMed Research International*, vol. 2018, pp. 1–8, 2018, doi: 10.1155/2018/6283932.

[57] J. O. Lee *et al.*, “The myokine meteorin-like (metrnl) improves glucose tolerance in both skeletal muscle cells and mice by targeting AMPKα2,” *FEBS J*, vol. 287, no. 10, pp. 2087–2104, May 2020, doi: 10.1111/febs.15301.

[58] Y. Amano, Y. Nonaka, R. Takeda, Y. Kano, and D. Hoshino, “Effects of electrical stimulation-induced resistance exercise training on white and brown adipose tissues and plasma meteorin-like concentration in rats,” *Physiol Rep*, vol. 8, no. 16, Aug. 2020, doi: 10.14814/phy2.14540.

[59] M. Eaton, C. Granata, J. Barry, A. Safdar, D. Bishop, and J. P. Little, “Impact of a single bout of high-intensity interval exercise and short-term interval training on interleukin-6, FNDC5, and METRNL mRNA expression in human skeletal muscle,” *Journal of Sport*

and Health Science, vol. 7, no. 2, pp. 191–196, Apr. 2018, doi: 10.1016/j.jshs.2017.01.003.

[60] M. Berghoff, A. Höpfinger, R. Rajendran, T. Karrasch, A. Schmid, and A. Schäffler, "Evidence of a Muscle–Brain Axis by Quantification of the Neurotrophic Myokine METRNL (Meteorin-Like Protein) in Human Cerebrospinal Fluid and Serum," *JCM*, vol. 10, no. 15, p. 3271, Jul. 2021, doi: 10.3390/jcm10153271.

[61] J. J. O'Shea, Y. Kanno, and A. C. Chan, "In Search of Magic Bullets: The Golden Age of Immunotherapeutics," *Cell*, vol. 157, no. 1, pp. 227–240, Mar. 2014, doi: 10.1016/j.cell.2014.03.010.

[62] S. Zhang, Y. Lei, T. Sun, Z. Gao, Z. Li, and H. Shen, "Elevated levels of Metrnl in rheumatoid arthritis: Association with disease activity," *Cytokine*, vol. 159, p. 156026, Nov. 2022, doi: 10.1016/j.cyto.2022.156026.

[63] C. Atri, F. Guerfali, and D. Laouini, "Role of Human Macrophage Polarization in Inflammation during Infectious Diseases," *IJMS*, vol. 19, no. 6, p. 1801, Jun. 2018, doi: 10.3390/ijms19061801.

[64] B. H. Sobieh, D. H. Kassem, Z. M. Zakaria, and H. O. El-Mesallamy, "Potential emerging roles of the novel adipokines adipolin/CTRP12 and meteorin-like/METRNL in obesity-osteoarthritis interplay," *Cytokine*, vol. 138, p. 155368, Feb. 2021, doi: 10.1016/j.cyto.2020.155368.

[65] A. Tanaka *et al.*, "The molecular skin pathology of familial primary localized cutaneous amyloidosis," *Experimental Dermatology*, vol. 19, no. 5, pp. 416–423, May 2010, doi: 10.1111/j.1600-0625.2010.01083.x.

[66] B. Kerget, D. E. Afşin, F. Kerget, S. Aşkın, and M. Akgün, "Is Metrnl an Adipokine İnvolved in the Anti-inflammatory Response to Acute Exacerbations of COPD?," *Lung*, vol. 198, no. 2, pp. 307–314, Apr. 2020, doi: 10.1007/s00408-020-00327-4.

[67] J. A. Knipper, A. Ivens, and M. D. Taylor, "Helminth-induced Th2 cell dysfunction is distinct from exhaustion and is maintained in the absence of antigen," *PLoS Negl Trop Dis*, vol. 13, no. 12, p. e0007908, Dec. 2019, doi: 10.1371/journal.pntd.0007908.

[68] H. M. A. Javaid, N. E. Sahar, D.-L. ZhuGe, and J. Y. Huh, "Exercise Inhibits NLRP3 Inflammasome Activation in Obese Mice via the Anti-Inflammatory Effect of Meteorin-like," *Cells*, vol. 10, no. 12, p. 3480, Dec. 2021, doi: 10.3390/cells10123480.

[69] Z.-Y. Li *et al.*, "Adipocyte Metrnl Antagonizes Insulin Resistance Through PPARg Signaling," *Diabetes*, vol. 64, p. 12, Dec. 2015, doi: 10.2337/db15-0274.

[70] K. Choi and Y.-B. Kim, "Molecular Mechanism of Insulin Resistance in Obesity and Type 2 Diabetes," *Korean J Intern Med*, vol. 25, no. 2, p. 119, 2010, doi: 10.3904/kjim.2010.25.2.119.

[71] S. Tyagi, S. Sharma, P. Gupta, A. Saini, and C. Kaushal, “The peroxisome proliferator-activated receptor: A family of nuclear receptors role in various diseases,” *J Adv Pharm Tech Res*, vol. 2, no. 4, p. 236, 2011, doi: 10.4103/2231-4040.90879.

[72] D. Löffler *et al.*, “METRNL decreases during adipogenesis and inhibits adipocyte differentiation leading to adipocyte hypertrophy in humans,” *Int J Obes*, vol. 41, no. 1, pp. 112–119, Jan. 2017, doi: 10.1038/ijo.2016.180.

[73] T. W. Jung *et al.*, “Meteorin-like protein (METRNL)/IL-41 improves LPS-induced inflammatory responses via AMPK or PPARδ–mediated signaling pathways,” *Advances in Medical Sciences*, vol. 66, no. 1, pp. 155–161, Mar. 2021, doi: 10.1016/j.advms.2021.01.007.

[74] K. Landgraf *et al.*, “Evidence of Early Alterations in Adipose Tissue Biology and Function and Its Association With Obesity-Related Inflammation and Insulin Resistance in Children,” *Diabetes*, vol. 64, no. 4, pp. 1249–1261, Apr. 2015, doi: 10.2337/db14-0744.

[75] T. W. Jung *et al.*, “METRNL attenuates lipid-induced inflammation and insulin resistance via AMPK or PPARδ-dependent pathways in skeletal muscle of mice,” *Exp Mol Med*, vol. 50, no. 9, p. 122, Sep. 2018, doi: 10.1038/s12276-018-0147-5.

[76] C. Rupérez *et al.*, “Meteorin-like/Meteorin-β protects heart against cardiac dysfunction,” *Journal of Experimental Medicine*, vol. 218, no. 5, p. e20201206, May 2021, doi: 10.1084/jem.20201206.

[77] W. Hu, R. Wang, and B. Sun, “Meteorin-Like Ameliorates β Cell Function by Inhibiting β Cell Apoptosis of and Promoting β Cell Proliferation via Activating the WNT/β-Catenin Pathway,” *Frontiers in Pharmacology*, vol. 12, p. 10, Mar. 2021, doi: 10.3389/fphar.2021.627147.

[78] A. Gastaldelli, “Role of beta-cell dysfunction, ectopic fat accumulation and insulin resistance in the pathogenesis of type 2 diabetes mellitus,” *Diabetes Research and Clinical Practice*, vol. 93, pp. S60–S65, Aug. 2011, doi: 10.1016/S0168-8227(11)70015-8.

[79] Y. C. Long, “AMP-activated protein kinase signaling in metabolic regulation,” *Journal of Clinical Investigation*, vol. 116, no. 7, pp. 1776–1783, Jul. 2006, doi: 10.1172/JCI29044.

[80] L. Xu, Y. Cai, Y. Wang, and C. Xu, “Meteorin-Like (METRNL) Attenuates Myocardial Ischemia/Reperfusion Injury-Induced Cardiomyocytes Apoptosis by Alleviating Endoplasmic Reticulum Stress via Activation of AMPK-PAK2 Signaling in H9C2 Cells,” *Med Sci Monit*, vol. 26, Jun. 2020, doi: 10.12659/MSM.924564.

[81] M. F. Garcés *et al.*, “Maternal Serum Meteorin Levels and the Risk of Preeclampsia,” *PLoS ONE*, vol. 10, no. 6, p. e0131013, Jun. 2015, doi: 10.1371/journal.pone.0131013.

[82] J. H. Lee *et al.*, “Serum Meteorin-like protein levels decreased in patients newly diagnosed with type 2 diabetes,” *Diabetes Research and Clinical Practice*, vol. 135, pp. 7–10, Jan. 2018, doi: 10.1016/j.diabres.2017.10.005.

[83] S. R. Khan *et al.*, “The discovery of novel predictive biomarkers and early-stage pathophysiology for the transition from gestational diabetes to type 2 diabetes,” *Diabetologia*, vol. 62, no. 4, pp. 687–703, Apr. 2019, doi: 10.1007/s00125-018-4800-2.

[84] H. S. Chung *et al.*, “Implications of circulating Meteorin-like (Metrnl) level in human subjects with type 2 diabetes,” *Diabetes Research and Clinical Practice*, vol. 136, pp. 100–107, Feb. 2018, doi: 10.1016/j.diabres.2017.11.031.

[85] R. Wang, D. Hu, X. Zhao, and W. Hu, “Correlation of serum meteorin-like concentrations with diabetic nephropathy,” *Diabetes Research and Clinical Practice*, vol. 169, p. 108443, Nov. 2020, doi: 10.1016/j.diabres.2020.108443.

[86] J. C. Pickup, G. D. Chusney, S. M. Thomas, and D. Burt, “Plasma interleukin-6, tumour necrosis factor a and blood cytokine production in type 2 diabetes,” *Life Sciences*, vol. 67, p. 10, 2000, doi: 10.1016/s0024-3205(00)00622-6.

[87] Y. Du *et al.*, “Inverse relationship between serum Metrnl levels and visceral fat obesity (VFO) in patients with type 2 diabetes,” *Diabetes Research and Clinical Practice*, vol. 161, p. 108068, Mar. 2020, doi: 10.1016/j.diabres.2020.108068.

[88] M. Dadmanesh, H. Aghajani, R. Fadaei, and K. Ghorban, “Lower serum levels of Meteorin-like/Subfatin in patients with coronary artery disease and type 2 diabetes mellitus are negatively associated with insulin resistance and inflammatory cytokines,” *PLoS ONE*, vol. 13, no. 9, p. e0204180, Sep. 2018, doi: 10.1371/journal.pone.0204180.

[89] Z.-X. Liu *et al.*, “Serum Metrnl is associated with the presence and severity of coronary artery disease,” *J Cell Mol Med*, vol. 23, no. 1, pp. 271–280, Jan. 2019, doi: 10.1111/jcmm.13915.

[90] H. M. El-Ashmawy, F. O. Selim, T. A. M. Hosny, and H. N. Almassry, “Association of low serum Meteorin like (Metrnl) concentrations with worsening of glucose tolerance, impaired endothelial function and atherosclerosis,” *Diabetes Research and Clinical Practice*, vol. 150, pp. 57–63, Apr. 2019, doi: 10.1016/j.diabres.2019.02.026.

[91] Ö. Tok, “Effects of increased physical activity and/or weight loss diet on serum myokine and adipokine levels in overweight adults with impaired glucose metabolism,” *Journal of Diabetes and Its Complications*, vol. 35, p. 9, Feb. 2021, doi: 10.1016/j.jdiacomp.2021.107892.

[92] A. Schmid, T. Karrasch, and A. Schäffler, “Meteorin-Like Protein (Metrnl) in Obesity, during Weight Loss and in Adipocyte Differentiation,” *JCM*, vol. 10, no. 19, p. 4338, Sep. 2021, doi: 10.3390/jcm10194338.

[93] K. Wang *et al.*, “Serum Levels of Meteorin-Like (Metrnl) Are Increased in Patients with Newly Diagnosed Type 2 Diabetes Mellitus and Are Associated with Insulin Resistance,” *Med Sci Monit*, vol. 25, pp. 2337–2343, Mar. 2019, doi: 10.12659/MSM.915331.

[94] AlKhairi *et al.*, “Increased Expression of Meteorin-Like Hormone in Type 2 Diabetes and Obesity and Its Association with Irisin,” *Cells*, vol. 8, no. 10, p. 1283, Oct. 2019, doi: 10.3390/cells8101283.

[95] C. Wang *et al.*, “Serum Metrnl Level is Correlated with Insulin Resistance, But Not with β-Cell Function in Type 2 Diabetics,” *Med Sci Monit*, vol. 25, pp. 8968–8974, Nov. 2019, doi: 10.12659/MSM.920222.

[96] Z. Yao, P. Lin, C. Wang, K. Wang, and Y. Sun, “Administration of metrnl delays the onset of diabetes in non-obese diabetic mice,” *Endocr J*, vol. 68, no. 2, pp. 179–188, 2021, doi: 10.1507/endocrj.EJ20-0351.

[97] J. M. Moreno-Navarrete *et al.*, “Irisin Is Expressed and Produced by Human Muscle and Adipose Tissue in Association With Obesity and Insulin Resistance,” *The Journal of Clinical Endocrinology & Metabolism*, vol. 98, no. 4, pp. E769–E778, Apr. 2013, doi: 10.1210/jc.2012-2749.

[98] P. Boström *et al.*, “A PGC1-α-dependent myokine that drives brown-fat-like development of white fat and thermogenesis,” *Nature*, vol. 481, no. 7382, pp. 463–468, Jan. 2012, doi: 10.1038/nature10777.

[99] S. Pellitero *et al.*, “Opposite changes in meteorin-like and oncostatin m levels are associated with metabolic improvements after bariatric surgery,” *Int J Obes*, vol. 42, no. 4, pp. 919–922, Apr. 2018, doi: 10.1038/ijo.2017.268.

[100] C. Grander *et al.*, “Hepatic Meteorin-like and Krüppel-like Factor 3 are Associated with Weight Loss and Liver Injury,” *Exp Clin Endocrinol Diabetes*, vol. 130, no. 06, pp. 406–414, Aug. 2021, doi: 10.1055/a-1537-8950.

[101] M. H. Jamal *et al.*, “Effect of sleeve gastrectomy on the expression of meteorin-like (METRNL) and Irisin (FNDC5) in muscle and brown adipose tissue and its impact on uncoupling proteins in diet-induced obesity rats,” *Surgery for Obesity and Related Diseases*, vol. 16, no. 12, pp. 1910–1918, Dec. 2020, doi: 10.1016/j.soard.2020.07.022.

[102] A. Rutkovskiy, K.-O. Stensløkken, and I. J. Vaage, “Osteoblast Differentiation at a Glance,” *Med Sci Monit Basic Res*, vol. 22, pp. 95–106, Sep. 2016, doi: 10.12659/MSMBR.901142.

[103] E. F. Wagner and R. Eferl, “Fos/AP-1 proteins in bone and the immune system,” *Immunol Rev*, vol. 208, no. 1, pp. 126–140, Dec. 2005, doi: 10.1111/j.0105-2896.2005.00332.x.

[104] N. L. Kikel-Coury *et al.*, “Identification of astroglia-like cardiac nexus glia that are critical regulators of cardiac development and function,” *PLoS Biol*, vol. 19, no. 11, p. e3001444, Nov. 2021, doi: 10.1371/journal.pbio.3001444.

[105]C. Hu *et al.*, “Meteorin-like protein attenuates doxorubicin-induced cardiotoxicity via activating cAMP/PKA/SIRT1 pathway,” *Redox Biology*, vol. 37, p. 101747, Oct. 2020, doi: 10.1016/j.redox.2020.101747.

[106]J. B. Gurdon and P.-Y. Bourillot, “Morphogen gradient interpretation,” *Nature*, vol. 413, no. 6858, pp. 797–803, Oct. 2001, doi: 10.1038/35101500.

[107]E. M. De Robertis, “Spemann’s organizer and self-regulation in amphibian embryos,” *Nat Rev Mol Cell Biol*, vol. 7, no. 4, pp. 296–302, Apr. 2006, doi: 10.1038/nrm1855.

[108]K. Fukuda and Y. Kikuchi, “Endoderm development in vertebrates: fate mapping, induction and regional specification,” *Dev Growth Differ*, vol. 47, no. 6, pp. 343–355, Aug. 2005, doi: 10.1111/j.1440-169X.2005.00815.x.

[109]F. B. Tuazon and M. C. Mullins, “Temporally coordinated signals progressively pattern the anteroposterior and dorsoventral body axes,” *Seminars in Cell & Developmental Biology*, vol. 42, pp. 118–133, Jun. 2015, doi: 10.1016/j.semcdb.2015.06.003.

[110]A. F. Schier, “Nodal Morphogens,” *Cold Spring Harbor Perspectives in Biology*, vol. 1, no. 5, pp. a003459–a003459, Nov. 2009, doi: 10.1101/cshperspect.a003459.

[111]A. F. Schier, “Nodal Signaling in Vertebrate Development,” *Annu. Rev. Cell Dev. Biol.*, vol. 19, no. 1, pp. 589–621, Nov. 2003, doi: 10.1146/annurev.cellbio.19.041603.094522.

[112]X. Zhou, L. Lowe, H. Sasaki, B. L. M. Hogan, and M. R. Kuehn, “Nodal is a novel TGF-β-like gene expressed in the mouse node during gastrulation,” *Nature*, vol. 361, no. 6412, pp. 543–547, Feb. 1993, doi: 10.1038/361543a0.

[113]P.-F. Xu, N. Houssin, K. F. Ferri-Lagneau, B. Thisse, and C. Thisse, “Construction of a Vertebrate Embryo from Two Opposing Morphogen Gradients,” *Science*, vol. 344, no. 6179, pp. 87–89, Apr. 2014, doi: 10.1126/science.1248252.

[114]M. M. Shen, “Nodal signaling: developmental roles and regulation,” *Development*, vol. 134, no. 6, pp. 1023–1034, Mar. 2007, doi: 10.1242/dev.000166.

[115]M. M. Shen and A. F. Schier, “The EGF-CFC gene family in vertebrate development,” *Trends in Genetics*, vol. 16, no. 7, pp. 303–309, Jul. 2000, doi: 10.1016/S0168-9525(00)02006-0.

[116]A. F. Schier and M. M. Shen, “Nodal signalling in vertebrate development,” *Nature*, vol. 403, no. 6768, pp. 385–389, Jan. 2000, doi: 10.1038/35000126.

[117]M. Yamamoto *et al.*, “The transcription factor FoxH1 (FAST) mediates Nodal signaling during anterior-posterior patterning and node formation in the mouse,” *Genes Dev.*, vol. 15, no. 10, pp. 1242–1256, May 2001, doi: 10.1101/gad.883901.

[118]Y. Chen and A. F. Schier, “Lefty Proteins Are Long-Range Inhibitors of Squint-Mediated Nodal Signaling,” *Current Biology*, vol. 12, no. 24, pp. 2124–2128, Dec. 2002, doi: 10.1016/S0960-9822(02)01362-3.

[119]C. Chen and M. M. Shen, “Two Modes by which Lefty Proteins Inhibit Nodal Signaling,” *Current Biology*, vol. 14, no. 7, pp. 618–624, Apr. 2004, doi: 10.1016/j.cub.2004.02.042.

[120]C. Chen *et al.*, “The Vg1-related protein Gdf3 acts in a Nodal signaling pathway in the pre-gastrulation mouse embryo,” *Development*, vol. 133, p. 11, Nov. 2005, doi: 10.1242/dev.02210.

[121]S. K. Cheng, F. Olale, J. T. Bennett, A. H. Brivanlou, and A. F. Schier, “EGF-CFC proteins are essential coreceptors for the TGF-beta signals Vg1 andGDF1,” *Genes & Development*, vol. 17, p. 6, Jan. 2003, doi: 10.1101/gad.1041203.

[122]O. Andersson, E. Reissmann, H. Jörnvall, and C. F. Ibáñez, “Synergistic interaction between Gdf1 and Nodal during anterior axis development,” *Developmental Biology*, vol. 293, p. 12, Mar. 2006, doi: 10.1016/j.ydbio.2006.02.002.

[123]H. Fu *et al.*, “A Nodal enhanced micropeptide NEMEP regulates glucose uptake during mesendoderm differentiation of embryonic stem cells,” *Nat Commun*, vol. 13, no. 1, p. 3984, Jul. 2022, doi: 10.1038/s41467-022-31762-x.

[124]Y.-T. Yan *et al.*, “Dual Roles of Cripto as a Ligand and Coreceptor in the Nodal Signaling Pathway,” *Mol Cell Biol*, vol. 22, no. 13, pp. 4439–4449, Jul. 2002, doi: 10.1128/MCB.22.13.4439-4449.2002.

[125]C.-Y. Yeo and M. Whitman, “Nodal Signals to Smads through Cripto-Dependent and Cripto-Independent Mechanisms,” *Molecular Cell*, vol. 7, no. 5, pp. 949–957, May 2001, doi: 10.1016/S1097-2765(01)00249-0.

[126]E. Reissmann *et al.*, “The orphan receptor ALK7 and the Activin receptor ALK4 mediate signaling by Nodal proteins during vertebrate development,” *Genes Dev.*, vol. 15, no. 15, pp. 2010–2022, Aug. 2001, doi: 10.1101/gad.201801.

[127]K. Dorey and C. S. Hill, “A novel Cripto-related protein reveals an essential role for EGF-CFCs in Nodal signalling in Xenopus embryos,” *Developmental Biology*, vol. 292, no. 2, pp. 303–316, Apr. 2006, doi: 10.1016/j.ydbio.2006.01.006.

[128]S. K. Cheng, F. Olale, A. H. Brivanlou, and A. F. Schier, “Lefty Blocks a Subset of TGFβ Signals by Antagonizing EGF-CFC Coreceptors,” *PLoS Biol*, vol. 2, no. 2, p. e30, Feb. 2004, doi: 10.1371/journal.pbio.0020030.

[129]C. Meno *et al.*, “Mouse Lefty2 and Zebrafish Antivin Are Feedback Inhibitors of Nodal Signaling during Vertebrate Gastrulation,” *Molecular Cell*, vol. 4, no. 3, pp. 287–298, Sep. 1999, doi: 10.1016/S1097-2765(00)80331-7.

[130]B. Feldman *et al.*, “Lefty Antagonism of Squint Is Essential for Normal Gastrulation,” *Current Biology*, vol. 12, p. 7, Dec. 2022, doi: 10.1016/s0960-9822(02)01361-1.

[131]S. Piccolo *et al.*, “The head inducer Cerberus is a multifunctional antagonist of Nodal, BMP and Wnt signals,” *Nature*, vol. 397, no. 6721, pp. 707–710, Feb. 1999, doi: 10.1038/17820.

[132]S. Marques, A. C. Borges, A. C. Silva, S. Freitas, M. Cordenonsi, and J. A. Belo, “The activity of the Nodal antagonist *Cerl-2* in the mouse node is required for correct L/R body axis,” *Genes Dev.*, vol. 18, no. 19, pp. 2342–2347, Oct. 2004, doi: 10.1101/gad.306504.

[133]A. C. Silva, M. Filipe, K.-M. Kuerner, H. Steinbeisser, and J. A. Belo, “Endogenous Cerberus activity is required for anterior head specification in *Xenopus*,” *Development*, vol. 130, no. 20, pp. 4943–4953, Oct. 2003, doi: 10.1242/dev.00705.

[134]J. Massagué, J. Seoane, and D. Wotton, “Smad transcription factors,” *Genes Dev.*, vol. 19, no. 23, pp. 2783–2810, Dec. 2005, doi: 10.1101/gad.1350705.

[135]S. Germain, M. Howell, G. M. Esslemont, and C. S. Hill, “Homeodomain and winged-helix transcription factors recruit activated Smads to distinct promoter elements via a common Smad interaction motif,” *Genes Dev.*, vol. 14, no. 4, pp. 435–451, Feb. 2000, doi: 10.1101/gad.14.4.435.

[136]R. A. Randall, M. Howell, C. S. Page, A. Daly, P. A. Bates, and C. S. Hill, “Recognition of Phosphorylated-Smad2-Containing Complexes by a Novel Smad Interaction Motif,” *Mol Cell Biol*, vol. 24, no. 3, pp. 1106–1121, Feb. 2004, doi: 10.1128/MCB.24.3.1106-1121.2004.

[137]T. Dickmeis *et al.*, “Identification of nodal signaling targets by array analysis of induced complex probes,” *Dev. Dyn.*, vol. 222, no. 4, pp. 571–580, Dec. 2001, doi: 10.1002/dvdy.1220.

[138]H. Adachi *et al.*, “Determination of left/right asymmetric expression of nodal by a left side-specific enhancer with sequence similarity to a lefty-2 enhancer,” *Genes & Development*, vol. 13, no. 12, pp. 1589–1600, Jun. 1999, doi: 10.1101/gad.13.12.1589.

[139]D. P. Norris and E. J. Robertson, “Asymmetric and node-specific nodal expression patterns are controlled by two distinct cis-acting regulatory elements,” *Genes & Development*, vol. 13, no. 12, pp. 1575–1588, Jun. 1999, doi: 10.1101/gad.13.12.1575.

[140]Y. Saijoh *et al.*, “Two nodal-responsive enhancers control left-right asymmetric expression ofNodal,” *Dev. Dyn.*, vol. 232, no. 4, pp. 1031–1036, Apr. 2005, doi: 10.1002/dvdy.20192.

[141]S. D. Vincent, D. P. Norris, J. Ann Le Good, D. B. Constam, and E. J. Robertson, “Asymmetric Nodal expression in the mouse is governed by the combinatorial activities of two distinct regulatory elements,” *Mechanisms of Development*, vol. 121, no. 11, pp. 1403–1415, Nov. 2004, doi: 10.1016/j.mod.2004.06.002.

[142]D. P. Norris, J. Brennan, E. K. Bikoff, and E. J. Robertson, “The Foxh1-dependent autoregulatory enhancer controls the level of Nodal signals in the mouse embryo,” *Development*, vol. 129, no. 14, pp. 3455–3468, Jul. 2002, doi: 10.1242/dev.129.14.3455.

[143]H. L. Ashe and J. Briscoe, “The interpretation of morphogen gradients,” *Development*, vol. 133, no. 3, pp. 385–394, Feb. 2006, doi: 10.1242/dev.02238.

[144] C. Meno *et al.*, “Diffusion of Nodal Signaling Activity in the Absence of the Feedback Inhibitor Lefty2,” *Developmental Cell*, vol. 1, no. 1, pp. 127–138, Jul. 2001, doi: 10.1016/S1534-5807(01)00006-5.

[145] R. Sakuma *et al.*, “Inhibition of Nodal signalling by Lefty mediated through interaction with common receptors and efficient diffusion: Inhibition of Nodal signalling by Lefty,” *Genes to Cells*, vol. 7, no. 4, pp. 401–412, Apr. 2002, doi: 10.1046/j.1365-2443.2002.00528.x.

[146] N. Ben-Haim *et al.*, “The Nodal Precursor Acting via Activin Receptors Induces Mesoderm by Maintaining a Source of Its Convertases and BMP4,” *Developmental Cell*, vol. 11, p. 11, Sep. 2006, doi: 10.1016/j.devcel.2006.07.005.

[147] M. Morkel *et al.*, “β-Catenin regulates Cripto- and Wnt3-dependent gene expression programs in mouse axis and mesoderm formation,” *Development*, vol. 130, no. 25, pp. 6283–6294, Dec. 2003, doi: 10.1242/dev.00859.

[148] B. Feldman *et al.*, “Zebrafish organizer development and germ-layer formation require nodal-related signals,” *Nature*, vol. 395, no. 6698, pp. 181–185, Sep. 1998, doi: 10.1038/26013.

[149] A. F. Schier and W. S. Talbot, “The zebrafish organizer,” *Current Opinion in Genetics & Development*, vol. 8, no. 4, pp. 464–471, Aug. 1998, doi: 10.1016/S0959-437X(98)80119-6.

[150] S. T. Dougan, R. M. Warga, D. A. Kane, A. F. Schier, and W. S. Talbot, “The role of the zebrafish *nodal* -related genes *squint* and *cyclops* in patterning of mesendoderm,” *Development*, vol. 130, no. 9, pp. 1837–1851, May 2003, doi: 10.1242/dev.00400.

[151] D. Mesnard, M. Guzman-Ayala, and D. B. Constam, “Nodal specifies embryonic visceral endoderm and sustains pluripotent cells in the epiblast before overt axial patterning,” *Development*, vol. 133, no. 13, pp. 2497–2505, Jul. 2006, doi: 10.1242/dev.02413.

[152] A. Perea-Gomez *et al.*, “Nodal Antagonists in the Anterior Visceral Endoderm Prevent the Formation of Multiple Primitive Streaks,” *Developmental Cell*, vol. 3, no. 5, pp. 745–756, Nov. 2002, doi: 10.1016/S1534-5807(02)00321-0.

[153] J. Rossant and P. P. L. Tam, “Emerging Asymmetry and Embryonic Patterning in Early Mouse Development,” *Developmental Cell*, vol. 7, no. 2, pp. 155–164, Aug. 2004, doi: 10.1016/j.devcel.2004.07.012.

[154] S. D. Vincent, N. R. Dunn, S. Hayashi, D. P. Norris, and E. J. Robertson, “Cell fate decisions within the mouse organizer are governed by graded Nodal signals,” *Genes Dev.*, vol. 17, no. 13, pp. 1646–1662, Jul. 2003, doi: 10.1101/gad.1100503.

[155] M. Hammerschmidt, G. N. Serbedzija, and A. P. McMahon, “Genetic analysis of dorsoventral pattern formation in the zebrafish: requirement of a BMP-like ventralizing activity and its dorsal repressor.,” *Genes Dev.*, vol. 10, no. 19, pp. 2452–2461, Oct. 1996, doi: 10.1101/gad.10.19.2452.

[156]Y. Kishimoto, K.-H. Lee, L. Zon, M. Hammerschmidt, and S. Schulte-Merker, “The molecular nature of zebrafish swirl: BMP2 function is essential during early dorsoventral patterning,” *Development*, vol. 124, p. 10, Nov. 1997, doi: 10.1242/dev.124.22.4457.

[157]A. V. Gore, S. Maegawa, A. Cheong, P. C. Gilligan, E. S. Weinberg, and K. Sampath, “The zebrafish dorsal axis is apparent at the four-cell stage,” *Nature*, vol. 438, p. 7, Dec. 2005, doi: 10.1038/nature04184.

[158]T. O. Aoki, J. Mathieu, L. Saint-Etienne, and M. R. Rebagliati, “Regulation of Nodal Signalling and Mesendoderm Formation by TARAM-A, a TGFℒ-Related Type I Receptor,” *Developmental Biology*, vol. 241, p. 16, 2001, doi: 10.1006/dbio.2001.0510.

[159]J. Brennan, C. C. Lu, D. P. Norris, T. A. Rodriguez, R. S. P. Beddington, and E. J. Robertson, “Nodal signalling in the epiblast patterns the early mouse embryo,” *Nature*, vol. 411, p. 5, Jun. 2001, doi: 10.1038/35082103.

[160]J. Ding *et al.*, “Cripto is required for correct orientation of the anterior–posterior axis in the mouse embryo,” *Nature*, vol. 395, no. 6703, pp. 702–707, Oct. 1998, doi: 10.1038/27215.

[161]L. A. Lowe, S. Yamada, and M. R. Kuehn, “Genetic dissection of nodal function in patterning the mouse embryo,” *Development*, vol. 128, p. 13, Apr. 2001, doi: 10.1242/dev.128.10.1831.

[162]K. Takaoka *et al.*, “The Mouse Embryo Autonomously Acquires Anterior-Posterior Polarity at Implantation,” *Developmental Cell*, vol. 10, p. 9, Apr. 2006, doi: 10.1016/j.devcel.2006.02.017.

[163]M. Yamamoto *et al.*, “Nodal antagonists regulate formation of the anteroposterior axis of the mouse embryo,” *Nature*, vol. 428, no. 6981, pp. 387–392, Mar. 2004, doi: 10.1038/nature02418.

[164]R. Brandenberger *et al.*, “Transcriptome characterization elucidates signaling networks that control human ES cell growth and differentiation,” *Nat Biotechnol*, vol. 22, no. 6, pp. 707–716, Jun. 2004, doi: 10.1038/nbt971.

[165]L. Vallier, D. Reynolds, and R. A. Pedersen, “Nodal inhibits differentiation of human embryonic stem cells along the neuroectodermal default pathway,” *Developmental Biology*, vol. 275, no. 2, pp. 403–421, Nov. 2004, doi: 10.1016/j.ydbio.2004.08.031.

[166]M. Blum, K. Feistel, T. Thumberger, and A. Schweickert, “The evolution and conservation of left-right patterning mechanisms,” *Development*, vol. 141, no. 8, pp. 1603–1613, Apr. 2014, doi: 10.1242/dev.100560.

[167]M. Blum and T. Ott, “Animal left–right asymmetry,” *Current Biology*, vol. 28, no. 7, pp. R301–R304, Apr. 2018, doi: 10.1016/j.cub.2018.02.073.

[168]D. T. Grimes and R. D. Burdine, “Left–Right Patterning: Breaking Symmetry to Asymmetric Morphogenesis,” *Trends in Genetics*, vol. 33, no. 9, pp. 616–628, Sep. 2017, doi: 10.1016/j.tig.2017.06.004.

[169]A. Kawasumi *et al.*, “Left–right asymmetry in the level of active Nodal protein produced in the node is translated into left–right asymmetry in the lateral plate of mouse embryos,” *Developmental Biology*, vol. 353, no. 2, pp. 321–330, May 2011, doi: 10.1016/j.ydbio.2011.03.009.

[170]W. W. Branford and H. J. Yost, “Nodal Signaling: CrypticLefty Mechanism of Antagonism Decoded,” *Current Biology*, vol. 14, no. 9, pp. R341–R343, May 2004, doi: 10.1016/j.cub.2004.04.020.

[171]H. Hamada, C. Meno, D. Watanabe, and Y. Saijoh, “Establishment of vertebrate left–right asymmetry,” *Nat Rev Genet*, vol. 3, no. 2, pp. 103–113, Feb. 2002, doi: 10.1038/nrg732.

[172]M. Fujinaga, “Development of sidedness of asymmetric body structures in vertebrates,” *Int. J. Dev. Biol.*, vol. 41, p. 34, Apr. 1997.

[173]S. Nonaka, H. Shiratori, Y. Saijoh, and H. Hamada, “Determination of left–right patterning of the mouse embryo by artificial nodal flow,” *Nature*, vol. 418, no. 6893, pp. 96–99, Jul. 2002, doi: 10.1038/nature00849.

[174]S. Nonaka *et al.*, “Randomization of Left–Right Asymmetry due to Loss of Nodal Cilia Generating Leftward Flow of Extraembryonic Fluid in Mice Lacking KIF3B Motor Protein,” p. 9.

[175]Y. Okada, S. Takeda, Y. Tanaka, J.-C. I. Belmonte, and N. Hirokawa, “Mechanism of Nodal Flow: A Conserved Symmetry Breaking Event in Left-Right Axis Determination,” *Cell*, vol. 121, no. 4, pp. 633–644, May 2005, doi: 10.1016/j.cell.2005.04.008.

[176]K. Sulik *et al.*, “Morphogenesis of the murine node and notochordal plate,” *Dev. Dyn.*, vol. 201, no. 3, pp. 260–278, Nov. 1994, doi: 10.1002/aja.1002010309.

[177]L. A. Lowe *et al.*, “Conserved left–right asymmetry of nodal expression and alterations in murine situs inversus,” *Nature*, vol. 381, no. 6578, pp. 158–161, May 1996, doi: 10.1038/381158a0.

[178]S. Long, N. Ahmad, and M. Rebagliati, “The zebrafish *nodal* -related gene *southpaw* is required for visceral and diencephalic left-right asymmetry,” *Development*, vol. 130, no. 11, pp. 2303–2316, Jun. 2003, doi: 10.1242/dev.00436.

[179]M. Levin, R. L. Johnson, C. D. Sterna, M. Kuehn, and C. Tabin, “A molecular pathway determining left-right asymmetry in chick embryogenesis,” *Cell*, vol. 82, no. 5, pp. 803–814, Sep. 1995, doi: 10.1016/0092-8674(95)90477-8.

[180]J. Collignon, I. Varlet, and E. J. Robertson, “Relationship between asymmetric nodal expression and the direction of embryonic turning,” *Nature*, vol. 381, no. 6578, pp. 155–158, May 1996, doi: 10.1038/381155a0.

[181]C. Meno *et al.*, “Two closely-related left-right asymmetrically expressed genes, *lefty-1* and *lefty-2* : their distinct expression domains, chromosomal linkage and direct neuralizing

activity in *Xenopus* embryos," *Genes Cells*, vol. 2, no. 8, pp. 513–524, Aug. 1997, doi: 10.1046/j.1365-2443.1997.1400338.x.

[182] J. Brennan, D. P. Norris, and E. J. Robertson, "Nodal activity in the node governs left-right asymmetry," *Genes Dev.*, vol. 16, no. 18, pp. 2339–2344, Sep. 2002, doi: 10.1101/gad.1016202.

[183] Y. Saijoh, S. Oki, S. Ohishi, and H. Hamada, "Left–right patterning of the mouse lateral plate requires Nodal produced in the node," *Developmental Biology*, p. 13, 2003, doi: 10.1016/s0012-1606(02)00121-5.

[184] C. Meno *et al.*, "lefty-1 Is Required for Left-Right Determination as a Regulator of lefty-2 and nodal," *Cell*, vol. 94, no. 3, pp. 287–297, Aug. 1998, doi: 10.1016/S0092-8674(00)81472-5.

[185] T. Nakamura *et al.*, "Generation of Robust Left-Right Asymmetry in the Mouse Embryo Requires a Self-Enhancement and Lateral-Inhibition System," *Developmental Cell*, vol. 11, no. 4, pp. 495–504, Oct. 2006, doi: 10.1016/j.devcel.2006.08.002.

[186] Y. Komatsu and Y. Mishina, "Establishment of left–right asymmetry in vertebrate development: the node in mouse embryos," *Cell. Mol. Life Sci.*, vol. 70, no. 24, pp. 4659–4666, Dec. 2013, doi: 10.1007/s00018-013-1399-9.

[187] J. D. Lee and K. V. Anderson, "Morphogenesis of the node and notochord: The cellular basis for the establishment and maintenance of left-right asymmetry in the mouse," *Dev. Dyn.*, vol. 237, no. 12, pp. 3464–3476, Dec. 2008, doi: 10.1002/dvdy.21598.

[188] N. Hirokawa, Y. Tanaka, Y. Okada, and S. Takeda, "Nodal Flow and the Generation of Left-Right Asymmetry," *Cell*, vol. 125, no. 1, pp. 33–45, Apr. 2006, doi: 10.1016/j.cell.2006.03.002.

[189] Y. Yamanaka, O. J. Tamplin, A. Beckers, A. Gossler, and J. Rossant, "Live Imaging and Genetic Analysis of Mouse Notochord Formation Reveals Regional Morphogenetic Mechanisms," *Developmental Cell*, vol. 13, no. 6, pp. 884–896, Dec. 2007, doi: 10.1016/j.devcel.2007.10.016.

[190] H. Hagiwara, N. Ohwada, and K. Takata, "Cell Biology of Normal and Abnormal Ciliogenesis in the Ciliated Epithelium," in *International Review of Cytology*, vol. 234, Academic Press, 2004, pp. 101–141. doi: 10.1016/S0074-7696(04)34003-9.

[191] A. Schweickert *et al.*, "Cilia-Driven Leftward Flow Determines Laterality in Xenopus," *Current Biology*, vol. 17, no. 1, pp. 60–66, Jan. 2007, doi: 10.1016/j.cub.2006.10.067.

[192] Y. Tanaka, Y. Okada, and N. Hirokawa, "FGF-induced vesicular release of Sonic hedgehog and retinoic acid in leftward nodal flow is critical for left–right determination," *Nature*, vol. 435, no. 7039, pp. 172–177, May 2005, doi: 10.1038/nature03494.

[193] R. P. Harvey, "Links in the Left/Right Axial Pathway," *Cell*, vol. 94, no. 3, pp. 273–276, Aug. 1998, doi: 10.1016/S0092-8674(00)81468-3.

[194] J. J. Essner, J. D. Amack, M. K. Nyholm, E. B. Harris, and H. J. Yost, “Kupffer’s vesicle is a ciliated organ of asymmetry in the zebrafish embryo that initiates left-right development of the brain, heart and gut,” *Development*, vol. 132, no. 6, pp. 1247–1260, Mar. 2005, doi: 10.1242/dev.01663.

[195] J. Gros, K. Feistel, C. Viebahn, M. Blum, and C. J. Tabin, “Cell Movements at Hensen’s Node Establish Left/Right Asymmetric Gene Expression in the Chick,” *Science*, vol. 324, no. 5929, pp. 941–944, May 2009, doi: 10.1126/science.1172478.

[196] P. Vick *et al.*, “Flow on the right side of the gastrocoel roof plate is dispensable for symmetry breakage in the frog Xenopus laevis,” *Developmental Biology*, vol. 331, no. 2, pp. 281–291, Jul. 2009, doi: 10.1016/j.ydbio.2009.05.547.

[197] M. Hojo *et al.*, “Right-elevated expression of charon is regulated by fluid flow in medaka Kupffer’s vesicle: Left-right asymmetric expression of charon,” *Development, Growth & Differentiation*, vol. 49, no. 5, pp. 395–405, Jun. 2007, doi: 10.1111/j.1440-169X.2007.00937.x.

[198] A. Kuntz, “Notes on the Embryology and Larval Development of Five Species of Teleostean Fishes,” *U.S. Government Printing Office*, vol. 34, p. 23, 1916.

[199] M. S. Cooper and L. A. D’amico, “A Cluster of Noninvoluting Endocytic Cells at the Margin of the Zebrafish Blastoderm Marks the Site of Embryonic Shield Formation,” *Developmental Biology*, vol. 180, no. 1, pp. 184–198, Nov. 1996, doi: 10.1006/dbio.1996.0294.

[200] P. Oteíza, M. Köppen, M. L. Concha, and C.-P. Heisenberg, “Origin and shaping of the laterality organ in zebrafish,” *Development*, vol. 135, no. 16, pp. 2807–2813, Aug. 2008, doi: 10.1242/dev.022228.

[201] L. Solnica-Krezel *et al.*, “Mutations affecting cell fates and cellular rearrangements during gastrulation in zebrafish,” *Development*, vol. 123, no. 1, pp. 67–80, Dec. 1996, doi: 10.1242/dev.123.1.67.

[202] E. Pulgar *et al.*, “Apical contacts stemming from incomplete delamination guide progenitor cell allocation through a dragging mechanism,” *eLife*, vol. 10, p. e66483, Aug. 2021, doi: 10.7554/eLife.66483.

[203] G. Wang, A. B. Cadwallader, D. S. Jang, M. Tsang, H. J. Yost, and J. D. Amack, “The Rho kinase Rock2b establishes anteroposterior asymmetry of the ciliated Kupffer’s vesicle in zebrafish,” *Development*, vol. 138, p. 10, 2011, doi: 10.1242/dev.052985.

[204] G. Wang, M. L. Manning, and J. D. Amack, “Regional cell shape changes control form and function of Kupffer’s vesicle in the zebrafish embryo,” *Developmental Biology*, vol. 370, no. 1, pp. 52–62, Oct. 2012, doi: 10.1016/j.ydbio.2012.07.019.

[205] J. H. McCarty *et al.*, “Selective ablation of αv integrins in the central nervous system leads to cerebral hemorrhage, seizures, axonal degeneration and premature death,” *Development*, vol. 132, p. 12, Jan. 2005, doi: 10.1242/dev.01551.

[206] J. H. McCarty *et al.*, “Defective Associations between Blood Vessels and Brain Parenchyma Lead to Cerebral Hemorrhage in Mice Lacking alpha-v Integrins,” *MOL. CELL. BIOL.*, vol. 22, p. 11, Nov. 2002, doi: 10.1128/MCB.22.21.7667–7677.2002.

[207] B. L. Bader, H. Rayburn, D. Crowley, and R. O. Hynes, “Extensive Vasculogenesis, Angiogenesis, and Organogenesis Precede Lethality in Mice Lacking All alpha-v Integrins,” *Cell*, vol. 95, p. 13, Nov. 1998, doi: 10.1016/s0092-8674(00)81618-9.

[208] Y. Takada, X. Ye, and S. Simon, “The integrins,” *Genome Biol*, vol. 8, no. 5, p. 215, 2007, doi: 10.1186/gb-2007-8-5-215.

[209] A. J. Ablooglu, E. Tkachenko, J. Kang, and S. J. Shattil, “Integrin αV is necessary for gastrulation movements that regulate vertebrate body asymmetry,” *Development*, vol. 137, no. 20, pp. 3449–3458, Oct. 2010, doi: 10.1242/dev.045310.

[210] A. J. Ablooglu, J. Kang, R. I. Handin, D. Traver, and S. J. Shattil, “The zebrafish vitronectin receptor: Characterization of integrin *αV* and *β3* expression patterns in early vertebrate development,” *Dev. Dyn.*, vol. 236, no. 8, pp. 2268–2276, Aug. 2007, doi: 10.1002/dvdy.21229.

[211] M. Delannet, F. Martin, B. Bossy, D. A. Cheresh, L. F. Reichardt, and J.-L. Duband, “Specific roles of the αVβ1, αVβ3 and αVβ5 integrins in avian neural crest cell adhesion and migration on vitronectin,” *Development*, vol. 120, p. 16, Sep. 1994, doi: 10.1242/dev.120.9.2687.

[212] S. Testaz, M. Delannet, and D. Jean-Loup, “Adhesion and migration of avian neural crest cells on fibronectin require the cooperating activities of multiple integrins of the β1 and β3 families,” *Journal of Cell Science*, vol. 112, p. 14, Nov. 1999, doi: 10.1242/jcs.112.24.4715.

[213] R. Milner, G. Edwards, and C. Streuli, “A Role in Migration for the avb1 Integrin Expressed on Oligodendrocyte Precursors,” *The Journal of Neuroscience*, vol. 15, p. 13, Nov. 1996, doi: 10.1523/JNEUROSCI.16-22-07240.1996.

[214] B. Felding-Habermann *et al.*, “A Single Immunoglobulin-like Domain of the Human Neural Cell Adhesion Molecule L1 Supports Adhesion by Multiple Vascular and Platelet Integrins,” *Journal of Cell Biology*, vol. 139, no. 6, pp. 1567–1581, Dec. 1997, doi: 10.1083/jcb.139.6.1567.

[215] J. Yang T and H. Richard O, “Fibronectin Receptor Functions in Embryonic Cells Deficient in a541 Integrin Can Be Replaced by av Integrins,” *Molecular Biology of the Cell*, vol. 7, p. 12, Nov. 1996, doi: 10.1091/mbc.7.11.1737.

[216] G. Niu and X. Chen, “Why Integrin as a Primary Target for Imaging and Therapy,” *Theranostics*, vol. 1, pp. 30–47, 2011, doi: 10.7150/thno/v01p0030.

[217] H. Hashimoto *et al.*, “The Cerberus/Dan-family protein Charon is a negative regulator of Nodal signaling during left-right patterning in zebrafish,” *Development*, vol. 131, pp. 1741–1753, Apr. 2004, doi: 10.1242/dev.01070.

[218] C. Tanaka, R. Sakuma, T. Nakamura, H. Hamada, and Y. Saijoh, “Long-range action of Nodal requires interaction with GDF,” *Genes & Development*, vol. 21, p. 12, Dec. 2007, doi: 10.1101/gad.1623907.

[219] K. Minegishi, H. Masakazu, A. Rieko, T. Katsuyoshi, S. Hidetaka, and H. Hiroshi, “A Wnt5 Activity Asymmetry and Intercellular Signaling via PCP Proteins Polarize Node Cells for Left-Right Symmetry Breaking,” *Developmental Cell*, vol. 40, p. 19, Mar. 2014, doi: 10.1016/j.devcel.2017.02.010.

[220] M. Hashimoto and H. Hiroshi, “Planar polarization of node cells determines the rotational axis of node cilia,” *Nature Cell Biology*, vol. 12, no. 2, p. 18, Jan. 2010, doi: 10.1038/ncb2020.

[221] C. J. Derrick, A. Santos-Ledo, L. Eley, I. A. Paramita, J. Henderson, and B. Chaudhry, “Sequential action of JNK genes establishes the embryonic left-right axis,” *Development*, vol. 149, p. 16, 2022, doi: 10.1242/dev.200136.

[222] A. Chedotal and L. J. Richards, “Wiring the Brain: The Biology of Neuronal Guidance,” *Cold Spring Harbor Perspectives in Biology*, vol. 2, no. 6, pp. a001917–a001917, Jun. 2010, doi: 10.1101/cshperspect.a001917.

[223] S. Tole, G. Gutin, L. Bhatnagar, R. Remedios, and J. M. Hébert, “Development of midline cell types and commissural axon tracts requires Fgfr1 in the cerebrum,” *Developmental Biology*, vol. 289, no. 1, pp. 141–151, Jan. 2006, doi: 10.1016/j.ydbio.2005.10.020.

[224] R. J. Ferland *et al.*, “Abnormal cerebellar development and axonal decussation due to mutations in AHI1 in Joubert syndrome,” *Nat Genet*, vol. 36, no. 9, pp. 1008–1013, Sep. 2004, doi: 10.1038/ng1419.

[225] Y. Huang *et al.*, “Novel dominant and recessive variants in human ROBO1 cause distinct neurodevelopmental defects through different mechanisms,” *Human Molecular Genetics*, vol. 31, no. 16, pp. 2751–2765, Aug. 2022, doi: 10.1093/hmg/ddac070.

[226] E. Cortés, J. S. Pak, and E. Özkan, “Structure and evolution of neuronal wiring receptors and ligands,” *Developmental Dynamics*, p. dvdy.512, Jul. 2022, doi: 10.1002/dvdy.512.

[227] S. J. Araújo and G. Tear, “Axon guidance mechanisms and molecules: lessons from invertebrates,” *Nat Rev Neurosci*, vol. 4, no. 11, pp. 910–922, Nov. 2003, doi: 10.1038/nrn1243.

[228] E. Tamariz and A. Varela-EchavarrÃ-a, “The discovery of the growth cone and its influence on the study of axon guidance,” *Front. Neuroanat.*, vol. 9, May 2015, doi: 10.3389/fnana.2015.00051.

[229] E. Tanaka and J. Sabry, “Making the connection: Cytoskeletal rearrangements during growth cone guidance,” *Cell*, vol. 83, no. 2, pp. 171–176, Oct. 1995, doi: 10.1016/0092-8674(95)90158-2.

[230] D. Bentley and T. P. O’Connor, “Cytoskeletal events in growth cone steering,” *Current Opinion in Neurobiology*, vol. 4, no. 1, pp. 43–48, Jan. 1994, doi: 10.1016/0959-4388(94)90030-2.

[231] F. Schneider, I. Metz, and M. B. Rust, “Regulation of actin filament assembly and disassembly in growth cone motility and axon guidance,” *Brain Research Bulletin*, vol. 192, pp. 21–35, Jan. 2023, doi: 10.1016/j.brainresbull.2022.10.019.

[232] J. Raper and C. Mason, “Cellular Strategies of Axonal Pathfinding,” *Cold Spring Harbor Perspectives in Biology*, vol. 2, no. 9, pp. a001933–a001933, Sep. 2010, doi: 10.1101/cshperspect.a001933.

[233] Z. Kaprielian, E. Runko, and R. Imondi, “Axon guidance at the midline choice point,” *Dev. Dyn.*, vol. 221, no. 2, pp. 154–181, Jun. 2001, doi: 10.1002/dvdy.1143.

[234] A. L. Kolodkin and M. Tessier-Lavigne, “Mechanisms and Molecules of Neuronal Wiring: A Primer,” *Cold Spring Harbor Perspectives in Biology*, vol. 3, no. 6, pp. a001727–a001727, Jun. 2011, doi: 10.1101/cshperspect.a001727.

[235] B. J. Dickson, “Molecular Mechanisms of Axon Guidance,” *Science*, vol. 298, p. 8, Dec. 2002, doi: 10.1126/science.1072165.

[236] M. Placzek and J. Briscoe, “The floor plate: multiple cells, multiple signals,” *Nat Rev Neurosci*, vol. 6, no. 3, pp. 230–240, Mar. 2005, doi: 10.1038/nrn1628.

[237] B. B. Gore, K. G. Wong, and M. Tessier-Lavigne, “Stem Cell Factor Functions as an Outgrowth-Promoting Factor to Enable Axon Exit from the Midline Intermediate Target,” *Neuron*, vol. 57, no. 4, pp. 501–510, Feb. 2008, doi: 10.1016/j.neuron.2008.01.006.

[238] T. Yamada, M. Placzek, H. Tanaka, J. Dodd, and T. M. Jessell, “Control of cell pattern in the developing nervous system: Polarizing activity of the floor plate and notochord,” *Cell*, vol. 64, no. 3, pp. 635–647, Feb. 1991, doi: 10.1016/0092-8674(91)90247-V.

[239] C. Klämbt, J. R. Jacobs, and C. S. Goodman, “The midline of the drosophila central nervous system: A model for the genetic analysis of cell fate, cell migration, and growth cone guidance,” *Cell*, vol. 64, no. 4, pp. 801–815, Feb. 1991, doi: 10.1016/0092-8674(91)90509-W.

[240] P. Bovolenta and J. Dodd, “Perturbation of neuronal differentiation and axon guidance in the spinal cord of mouse embryos lacking a floor plate: analysis of Danforth’s short- tail mutation,” *Development*, vol. 113, pp. 625–639, Oct. 1991, doi: 10.1242/dev.113.2.625.

[241]M. P. Matise, M. Lustig, T. Sakurai, M. Grumet, and A. L. Joyner, “Ventral midline cells are required for the local control of commissural axon guidance in the mouse spinal cord,” *Development*, vol. 126, no. 16, pp. 3649–3659, Aug. 1999, doi: 10.1242/dev.126.16.3649.

[242]J. B. Thomas, S. T. Crews, and C. S. Goodman, “Molecular genetics of the single-minded locus: A gene involved in the development of the Drosophila nervous system,” *Cell*, vol. 52, no. 1, pp. 133–141, Jan. 1988, doi: 10.1016/0092-8674(88)90537-5.

[243]W. T. Farmer *et al.*, “Pioneer longitudinal axons navigate using floor plate and Slit/Robo signals,” *Development*, vol. 135, no. 22, pp. 3643–3653, Nov. 2008, doi: 10.1242/dev.023325.

[244]A. Dumoulin, N. H. Wilson, K. L. Tucker, and E. T. Stoeckli, “A cell-autonomous role for primary cilia in long-range 1 commissural axon guidance,” *bioRixv*, p. 53, 2022, doi: https://doi.org/10.1101/2022.08.15.503894.

[245]S. G. Varadarajan *et al.*, “Netrin1 Produced by Neural Progenitors, Not Floor Plate Cells, Is Required for Axon Guidance in the Spinal Cord,” *Neuron*, vol. 94, no. 4, pp. 790-799.e3, May 2017, doi: 10.1016/j.neuron.2017.03.007.

[246]C. Dominici *et al.*, “Floor-plate-derived netrin-1 is dispensable for commissural axon guidance,” *Nature*, vol. 545, no. 7654, pp. 350–354, May 2017, doi: 10.1038/nature22331.

[247]B. W. Bisgrove, J. J. Essner, and H. J. Yost, “Multiple pathways in the midline regulate concordant brain, heart and gut left-right asymmetry,” *Development*, vol. 127, no. 16, p. 13, Aug. 2000, doi: 10.1242/dev.127.16.3567.

[248]H. J. Yost, “Left–right development in Xenopus and zebrafish,” *Seminars in Cell & Developmental Biology*, vol. 9, no. 1, pp. 61–66, Feb. 1998, doi: 10.1006/scdb.1997.0191.

[249]K. L. Whitford *et al.*, “Regulation of Cortical Dendrite Development by Slit-Robo Interactions,” *Neuron*, vol. 33, no. 1, pp. 47–61, Jan. 2002, doi: 10.1016/S0896-6273(01)00566-9.

[250]V. Corset, K. T. Nguyen-Ba-Charvet, C. Forcet, E. Moyse, A. Chédotal, and P. Mehlen, “Netrin-1-mediated axon outgrowth and cAMP production requires interaction with adenosine A2b receptor,” *Nature*, vol. 407, no. 6805, pp. 747–750, Oct. 2000, doi: 10.1038/35037600.

[251]H. Blockus and A. Chédotal, “Slit-Robo signaling,” *Development*, vol. 143, no. 17, pp. 3037–3044, Sep. 2016, doi: 10.1242/dev.132829.

[252]A. Chédotal, “Chemotropic Axon Guidance Molecules in Tumorigenesis,” in *Progress in Experimental Tumor Research*, K. S. Zänker and F. Entschladen, Eds. Basel: KARGER, 2007, pp. 78–90. doi: 10.1159/000100048.

[253]K. Brose and M. Tessier-Lavigne, “Slit proteins: key regulators of axon guidance, axonal branching, and cell migration,” *Current Opinion in Neurobiology*, vol. 10, no. 1, pp. 95–102, Feb. 2000, doi: 10.1016/S0959-4388(99)00066-5.

[254]K. H. Wang *et al.*, “Biochemical Purification of a Mammalian Slit Protein as a Positive Regulator of Sensory Axon Elongation and Branching,” *Cell*, vol. 96, no. 6, pp. 771–784, Mar. 1999, doi: 10.1016/S0092-8674(00)80588-7.

[255]T. Kidd *et al.*, “Roundabout Controls Axon Crossing of the CNS Midline and Defines a Novel Subfamily of Evolutionarily Conserved Guidance Receptors,” *Cell*, vol. 92, no. 2, pp. 205–215, Jan. 1998, doi: 10.1016/S0092-8674(00)80915-0.

[256]T. Kidd, K. S. Bland, and C. S. Goodman, “Slit Is the Midline Repellent for the Robo Receptor in Drosophila,” *Cell*, vol. 96, no. 6, pp. 785–794, Mar. 1999, doi: 10.1016/S0092-8674(00)80589-9.

[257]M. Seeger, G. Tear, D. Ferres-Marco, and C. S. Goodman, “Mutations affecting growth cone guidance in drosophila: Genes necessary for guidance toward or away from the midline,” *Neuron*, vol. 10, no. 3, pp. 409–426, Mar. 1993, doi: 10.1016/0896-6273(93)90330-T.

[258]S. Rajagopalan and E. Nicolas, “Crossing the Midline: Roles and Regulation of Robo Receptors,” *Neuron*, vol. 28, pp. 767–777, Dec. 2000, doi: 10.1016/s0896-6273(00)00152-5.

[259]J. H. Simpson, K. S. Bland, R. D. Fetter, and C. S. Goodman, “Short-Range and Long-Range Guidance by Slit and Its Robo Receptors: A Combinatorial Code of Robo Receptors Controls Lateral Position,” *Cell*, vol. 103, p. 14, Dec. 2000, doi: 10.1016/s0092-8674(00)00206-3.

[260]B. J. Dickson and G. F. Gilestro, “Regulation of Commissural Axon Pathfinding by Slit and its Robo Receptors,” *Annu. Rev. Cell Dev. Biol.*, vol. 22, no. 1, pp. 651–675, Nov. 2006, doi: 10.1146/annurev.cellbio.21.090704.151234.

[261]C. Morlot *et al.*, “Structural insights into the Slit-Robo complex,” *Proc. Natl. Acad. Sci. U.S.A.*, vol. 104, no. 38, pp. 14923–14928, Sep. 2007, doi: 10.1073/pnas.0705310104.

[262]H. Long *et al.*, “Conserved Roles for Slit and Robo Proteins in Midline Commissural Axon Guidance,” *Neuron*, vol. 42, no. 2, pp. 213–223, Apr. 2004, doi: 10.1016/S0896-6273(04)00179-5.

[263]A. Jaworski, H. Long, and M. Tessier-Lavigne, “Collaborative and Specialized Functions of Robo1 and Robo2 in Spinal Commissural Axon Guidance,” *Journal of Neuroscience*, vol. 30, no. 28, pp. 9445–9453, Jul. 2010, doi: 10.1523/JNEUROSCI.6290-09.2010.

[264]P. Zelina, B. Heike, Z. Yvrick, P. Amélié, F. Francois, and C. Alain, “Signaling Switch of the Axon Guidance Receptor Robo3 during Vertebrate Evolution,” *Neuron*, vol. 84, pp. 1258–1272, Dec. 2014, doi: 10.1016/j.neuron.2014.11.004.

[265] V. Marillat *et al.*, “The Slit Receptor Rig-1/Robo3 Controls Midline Crossing by Hindbrain Precerebellar Neurons and Axons,” *Neuron*, vol. 43, no. 1, pp. 69–79, Jul. 2004, doi: 10.1016/j.neuron.2004.06.018.

[266] C. Sabatier *et al.*, “The Divergent Robo Family Protein Rig-1/Robo3 Is a Negative Regulator of Slit Responsiveness Required for Midline Crossing by Commissural Axons,” *Cell*, vol. 117, no. 2, pp. 157–169, Apr. 2004, doi: 10.1016/S0092-8674(04)00303-4.

[267] K. L. W. Sun, J. P. Correia, and T. E. Kennedy, “Netrins: versatile extracellular cues with diverse functions,” *Development*, vol. 138, no. 11, pp. 2153–2169, Jun. 2011, doi: 10.1242/dev.044529.

[268] N. Krahn, M. Meier, R. Reuten, M. Koch, J. Stetefeld, and T. R. Patel, “Solution Structure of C. elegans UNC-6: A Nematode Paralogue of the Axon Guidance Protein Netrin-1,” *Biophysical Journal*, vol. 116, no. 11, pp. 2121–2130, Jun. 2019, doi: 10.1016/j.bpj.2019.04.033.

[269] N. Ishii, G. Wadsworth, B. D. Stern, J. G. Culotti, and E. M. Hedgecock, “UNC-6, a laminin-Related Protein, Guides Cell and Pioneer Axon Migrations in C. elegans,” *Neuron*, vol. 9, p. 9, Nov. 1992, doi: 10.1016/0896-6273(92)90240-e.

[270] S. W. Moore, M. Tessier-Lavigne, and T. E. Kennedy, “Netrins and Their receptors,” in *Axon Growth and Guidance*, vol. 621, D. Bagnard, Ed. New York, NY: Springer New York, 2007, pp. 17–31. doi: 10.1007/978-0-387-76715-4_2.

[271] K. Xu *et al.*, “Structures of netrin-1 bound to two receptors provide insight into its axon guidance mechanism,” *Science*, vol. 344, no. 6189, pp. 1275–1279, Jun. 2014, doi: 10.1126/science.1255149.

[272] T. Serafini *et al.*, “Netrin-1 Is Required for Commissural Axon Guidance in the Developing Vertebrate Nervous System,” *Cell*, vol. 87, no. 6, pp. 1001–1014, Dec. 1996, doi: 10.1016/S0092-8674(00)81795-X.

[273] T. Serafini, T. E. Kennedy, M. J. Gaiko, C. Mirzayan, T. M. Jessell, and M. Tessier-Lavigne, “The netrins define a family of axon outgrowth-promoting proteins homologous to C. elegans UNC-6,” *Cell*, vol. 78, no. 3, pp. 409–424, Aug. 1994, doi: 10.1016/0092-8674(94)90420-0.

[274] D. Bradford, S. J. Cole, and H. M. Cooper, “Netrin-1: Diversity in development,” *The International Journal of Biochemistry & Cell Biology*, vol. 41, no. 3, pp. 487–493, Mar. 2009, doi: 10.1016/j.biocel.2008.03.014.

[275] T. E. Kennedy, T. Serafini, JoséR. de la Torre, and M. Tessier-Lavigne, “Netrins are diffusible chemotropic factors for commissural axons in the embryonic spinal cord,” *Cell*, vol. 78, no. 3, pp. 425–435, Aug. 1994, doi: 10.1016/0092-8674(94)90421-9.

[276] T. E. Kennedy, “Axon Guidance by Diffusible Chemoattractants: A Gradient of Netrin Protein in the Developing Spinal Cord,” *Journal of Neuroscience*, vol. 26, no. 34, pp. 8866–8874, Aug. 2006, doi: 10.1523/JNEUROSCI.5191-05.2006.

[277] O. Pourchet *et al.*, “Loss of floor plate Netrin-1 impairs midline crossing of corticospinal axons and leads to mirror movements,” *Cell Reports*, vol. 34, no. 3, p. 108654, Jan. 2021, doi: 10.1016/j.celrep.2020.108654.

[278] E. R. Fearon *et al.*, “Identification of a Chromosome 18q Gene that Is Altered in Colorectal Cancers,” *Science*, vol. 247, no. 4938, pp. 49–56, Jan. 1990, doi: 10.1126/science.2294591.

[279] K. Keino-Masu *et al.*, “1035 DCC (Deleted in colorectal cancer) encodes a netrin receptor,” *Neuroscience Research*, vol. 28, p. S128, Jan. 1997, doi: 10.1016/S0168-0102(97)90340-0.

[280] R. P. Kruger, “Mapping Netrin Receptor Binding Reveals Domains of Unc5 Regulating Its Tyrosine Phosphorylation,” *Journal of Neuroscience*, vol. 24, no. 48, pp. 10826–10834, Dec. 2004, doi: 10.1523/JNEUROSCI.3715-04.2004.

[281] B. V. Geisbrecht, K. A. Dowd, R. W. Barfield, P. A. Longo, and D. J. Leahy, “Netrin Binds Discrete Subdomains of DCC and UNC5 and Mediates Interactions between DCC and Heparin,” *Journal of Biological Chemistry*, vol. 278, no. 35, pp. 32561–32568, Aug. 2003, doi: 10.1074/jbc.M302943200.

[282] G. Liu *et al.*, “DSCAM functions as a netrin receptor in commissural axon pathfinding,” *Proc. Natl. Acad. Sci. U.S.A.*, vol. 106, no. 8, pp. 2951–2956, Feb. 2009, doi: 10.1073/pnas.0811083106.

[283] R. Klein, “Eph/ephrin signaling in morphogenesis, neural development and plasticity,” *Current Opinion in Cell Biology*, vol. 16, no. 5, pp. 580–589, Oct. 2004, doi: 10.1016/j.ceb.2004.07.002.

[284] D. A. Feldheim and D. D. M. O’Leary, “Visual Map Development: Bidirectional Signaling, Bifunctional Guidance Molecules, and Competition,” *Cold Spring Harbor Perspectives in Biology*, vol. 2, no. 11, pp. a001768–a001768, Nov. 2010, doi: 10.1101/cshperspect.a001768.

[285] K. Kullander and R. Klein, “Mechanisms and functions of eph and ephrin signalling,” *Nat Rev Mol Cell Biol*, vol. 3, no. 7, pp. 475–486, Jul. 2002, doi: 10.1038/nrm856.

[286] K. Shen and C. W. Cowan, “Guidance Molecules in Synapse Formation and Plasticity,” *Cold Spring Harbor Perspectives in Biology*, vol. 2, no. 4, pp. a001842–a001842, Apr. 2010, doi: 10.1101/cshperspect.a001842.

[287] U. Yazdani and J. R. Terman, “[No title found],” *Genome Biol*, vol. 7, no. 3, p. 211, 2006, doi: 10.1186/gb-2006-7-3-211.

[288]K. Alex L, M. David J, and G. Corey S, “Fasciclin IV: Sequence, Expression, and Function during Growth Cone Guidance in the Grasshopper Embryo,” *Neuron*, vol. 9, p. 15, Nov. 1992, doi: 10.1016/0896-6273(92)90237-8.

[289]Y. Luo, D. Raible, and J. A. Raper, “Collapsin: A protein in brain that induces the collapse and paralysis of neuronal growth cones,” *Cell*, vol. 75, no. 2, pp. 217–227, Oct. 1993, doi: 10.1016/0092-8674(93)80064-L.

[290]L. Tamagnone and P. M. Comoglio, “Signalling by semaphorin receptors: cell guidance and beyond,” *Trends in Cell Biology*, vol. 10, no. 9, pp. 377–383, Sep. 2000, doi: 10.1016/S0962-8924(00)01816-X.

[291]T. S. Tran, A. L. Kolodkin, and R. Bharadwaj, “Semaphorin Regulation of Cellular Morphology,” *Annu. Rev. Cell Dev. Biol.*, vol. 23, no. 1, pp. 263–292, Nov. 2007, doi: 10.1146/annurev.cellbio.22.010605.093554.

[292]T. Kitsukawa *et al.*, “Neuropilin–Semaphorin III/D-Mediated Chemorepulsive Signals Play a Crucial Role in Peripheral Nerve Projection in Mice,” *Neuron*, vol. 19, no. 5, pp. 995–1005, Nov. 1997, doi: 10.1016/S0896-6273(00)80392-X.

[293]G. Vaccaro, A. Dumoulin, N. R. Zuñiga, C. E. Bandtlow, and E. T. Stoeckli, “The Nogo-66 Receptors NgR1 and NgR3 Are Required for Commissural Axon Pathfinding,” *J. Neurosci.*, vol. 42, no. 20, pp. 4087–4100, May 2022, doi: 10.1523/JNEUROSCI.1390-21.2022.

[294]M. Rehman and L. Tamagnone, “Semaphorins in cancer: Biological mechanisms and therapeutic approaches,” *Seminars in Cell & Developmental Biology*, vol. 24, no. 3, pp. 179–189, Mar. 2013, doi: 10.1016/j.semcdb.2012.10.005.

[295]Z. Meng *et al.*, “The Hippo pathway mediates Semaphorin signaling,” *Sci. Adv.*, vol. 8, no. 21, p. eabl9806, May 2022, doi: 10.1126/sciadv.abl9806.

[296]J. P. Myers, M. Santiago-Medina, and T. M. Gomez, “Regulation of axonal outgrowth and pathfinding by integrin-ecm interactions,” *Devel Neurobio*, vol. 71, no. 11, pp. 901–923, Nov. 2011, doi: 10.1002/dneu.20931.

[297]C. E. Holt and B. J. Dickson, “Sugar Codes for Axons?,” *Neuron*, vol. 46, no. 2, pp. 169–172, Apr. 2005, doi: 10.1016/j.neuron.2005.03.021.

[298]M. W. Rochlin, R. O’Connor, R. J. Giger, J. Verhaagen, and A. I. Farbman, “Comparison of neurotrophin and repellent sensitivities of early embryonic geniculate and trigeminal axons,” *J. Comp. Neurol.*, vol. 422, no. 4, pp. 579–593, Jul. 2000, doi: 10.1002/1096-9861(20000710)422:4<579::AID-CNE7>3.0.CO;2-G.

[299]G. López-Bendito *et al.*, “Tangential Neuronal Migration Controls Axon Guidance: A Role for Neuregulin-1 in Thalamocortical Axon Navigation,” *Cell*, vol. 125, no. 1, pp. 127–142, Apr. 2006, doi: 10.1016/j.cell.2006.01.042.

[300]A. Ebens *et al.*, “Hepatocyte Growth Factor/Scatter Factor Is an Axonal Chemoattractant and a Neurotrophic Factor for Spinal Motor Neurons,” *Neuron*, vol. 17, no. 6, pp. 1157–1172, Dec. 1996, doi: 10.1016/S0896-6273(00)80247-0.

[301]E. R. Kramer *et al.*, “Cooperation between GDNF/Ret and ephrinA/EphA4 Signals for Motor-Axon Pathway Selection in the Limb,” *Neuron*, vol. 50, no. 1, pp. 35–47, Apr. 2006, doi: 10.1016/j.neuron.2006.02.020.

[302]R. Shirasaki, J. W. Lewcock, K. Lettieri, and S. L. Pfaff, “FGF as a Target-Derived Chemoattractant for Developing Motor Axons Genetically Programmed by the LIM Code,” *Neuron*, vol. 50, no. 6, pp. 841–853, Jun. 2006, doi: 10.1016/j.neuron.2006.04.030.

[303]S. Yoshikawa, R. D. McKinnon, M. Kokel, and J. B. Thomas, “Wnt-mediated axon guidance via the Drosophila Derailed receptor,” *Nature*, vol. 422, no. 6932, pp. 583–588, Apr. 2003, doi: 10.1038/nature01522.

[304]A. I. Lyuksyutova *et al.*, “Anterior-Posterior Guidance of Commissural Axons by Wnt-Frizzled Signaling,” *Science*, vol. 302, no. 5652, pp. 1984–1988, Dec. 2003, doi: 10.1126/science.1089610.

[305]K. Yamauchi, K. D. Phan, and S. J. Butler, “BMP type I receptor complexes have distinct activities mediating cell fate and axon guidance decisions,” *Development*, vol. 135, no. 6, pp. 1119–1128, Mar. 2008, doi: 10.1242/dev.012989.

[306]F. Charron, E. Stein, J. Jeong, A. P. McMahon, and M. Tessier-Lavigne, “The Morphogen Sonic Hedgehog Is an Axonal Chemoattractant that Collaborates with Netrin-1 in Midline Axon Guidance,” *Cell*, vol. 113, no. 1, pp. 11–23, Apr. 2003, doi: 10.1016/S0092-8674(03)00199-5.

[307]F. Trousse, E. Martí, P. Gruss, M. Torres, and P. Bovolenta, “Control of retinal ganglion cell axon growth: a new role for Sonic hedgehog,” *Development*, vol. 128, no. 20, pp. 3927–3936, Oct. 2001, doi: 10.1242/dev.128.20.3927.

[308]A. Dumoulin and E. T. Stoeckli, “Looking for Guidance – Models and Methods to Study Axonal Navigation,” *Neuroscience*, p. S0306452222004080, Aug. 2022, doi: 10.1016/j.neuroscience.2022.08.005.

[309]J. Hjorth and B. Key, “Development of axon pathways in the zebrafish central nervous system,” *Int. J. Dev. Biol.*, vol. 46, no. 4, p. 11, Jul. 2004, doi: 10.1387/ijdb.12141449.

[310]R. Macdonald *et al.*, “The Pax protein Noi is required for commissural axon pathway formation in the rostral forebrain,” *Development*, vol. 124, no. 12, pp. 2397–2408, Jun. 1997, doi: 10.1242/dev.124.12.2397.

[311]M. A. Wolman, “Repulsion and Attraction of Axons by Semaphorin3D Are Mediated by Different Neuropilins In Vivo,” *Journal of Neuroscience*, vol. 24, no. 39, pp. 8428–8435, Sep. 2004, doi: 10.1523/JNEUROSCI.2349-04.2004.

[312] A. Gaudin, W. Hofmeister, and B. Key, “Chemoattractant axon guidance cues regulate de novo axon trajectories in the embryonic forebrain of zebrafish,” *Developmental Biology*, vol. 367, no. 2, pp. 126–139, Jul. 2012, doi: 10.1016/j.ydbio.2012.04.032.

[313] M. J. F. Barresi, L. D. Hutson, C.-B. Chien, and R. O. Karlstrom, “Hedgehog regulated Slit expression determines commissure and glial cell position in the zebrafish forebrain,” *Development*, vol. 132, no. 16, pp. 3643–3656, Aug. 2005, doi: 10.1242/dev.01929.

[314] S. Shanmugalingam *et al.*, “Ace/Fgf8 is required for forebrain commissure formation and patterning of the telencephalon,” *Development*, vol. 127, no. 12, pp. 2549–2561, Jun. 2000, doi: 10.1242/dev.127.12.2549.

[315] M. J. F. Barresi, “Hedgehog regulated Slit expression determines commissure and glial cell position in the zebrafish forebrain,” *Development*, vol. 132, no. 16, pp. 3643–3656, Jul. 2005, doi: 10.1242/dev.01929.

[316] Y. Guo, C. F. Oliveros, and T. Ohshima, “CRMP2 and CRMP4 are required for the formation of commissural tracts in the developing zebrafish forebrain,” *Developmental Neurobiology*, vol. 82, no. 6, pp. 533–544, 2022, doi: 10.1002/dneu.22897.

[317] L. Garcia-Campmany, F. J. Stam, and M. Goulding, “From circuits to behaviour: motor networks in vertebrates,” *Current Opinion in Neurobiology*, vol. 20, no. 1, pp. 116–125, Feb. 2010, doi: 10.1016/j.conb.2010.01.002.

[318] C. B. Moens and V. E. Prince, “Constructing the hindbrain: Insights from the zebrafish,” *Dev. Dyn.*, vol. 224, no. 1, pp. 1–17, May 2002, doi: 10.1002/dvdy.10086.

[319] H. A. Burgess, S. L. Johnson, and M. Granato, “Unidirectional startle responses and disrupted left-right co-ordination of motor behaviors in *robo3* mutant zebrafish,” *Genes, Brain and Behavior*, vol. 8, no. 5, pp. 500–511, Jul. 2009, doi: 10.1111/j.1601-183X.2009.00499.x.

[320] S.-Y. Yeo *et al.*, “Involvement of Islet-2 in the Slit signaling for axonal branching and defasciculation of the sensory neurons in embryonic zebrafish,” *Mechanisms of Development*, vol. 121, no. 4, pp. 315–324, Apr. 2004, doi: 10.1016/j.mod.2004.03.006.

[321] R. A. Jain, H. Bell, A. Lim, C.-B. Chien, and M. Granato, “Mirror Movement-Like Defects in Startle Behavior of Zebrafish dcc Mutants Are Caused by Aberrant Midline Guidance of Identified Descending Hindbrain Neurons,” *Journal of Neuroscience*, vol. 34, no. 8, pp. 2898–2909, Feb. 2014, doi: 10.1523/JNEUROSCI.2420-13.2014.

[322] H. Baier, S. Klostermann, T. Trowe, R. O. Karlstrom, C. Nüsslein-Volhard, and F. Bonhoeffer, “Genetic dissection of the retinotectal projection,” *Development*, vol. 123, p. 11, Dec. 1996, doi: 10.1242/dev.123.1.415.

[323] H. Baier, “Synaptic Laminae in the Visual System: Molecular Mechanisms Forming Layers of Perception,” *Annu. Rev. Cell Dev. Biol.*, vol. 29, no. 1, pp. 385–416, Oct. 2013, doi: 10.1146/annurev-cellbio-101011-155748.

[324] J. D. Burrill and S. S. Easter, “Development of the retinofugal projections in the embryonic and larval zebrafish (Brachydanio rerio),” *J. Comp. Neurol.*, vol. 346, no. 4, pp. 583–600, Aug. 1994, doi: 10.1002/cne.903460410.

[325] C. Stuermer, “Retinotopic organization of the developing retinotectal projection in the zebrafish embryo,” *J. Neurosci.*, vol. 8, no. 12, pp. 4513–4530, Dec. 1988, doi: 10.1523/JNEUROSCI.08-12-04513.1988.

[326] E. Robles, A. Filosa, and H. Baier, “Precise Lamination of Retinal Axons Generates Multiple Parallel Input Pathways in the Tectum,” *Journal of Neuroscience*, vol. 33, no. 11, pp. 5027–5039, Mar. 2013, doi: 10.1523/JNEUROSCI.4990-12.2013.

[327] T. Trowe *et al.*, “Mutations disrupting the ordering and topographic mapping of axons in the retinotectal projection of the zebrafish, Danio rerio,” *Development*, vol. 123, p. 12, Dec. 1996, doi: 10.1242/dev.123.1.439.

[328] R. O. Karlstrom *et al.*, “Zebrafish mutations affecting retinotectal axon pathfinding,” *Development*, vol. 123, p. 12, Dec. 1996, doi: 10.1242/dev.123.1.427.

[329] L. D. Hutson and C.-B. Chien, “Pathfinding and Error Correction by Retinal Axons: The Role of astray/robo2,” *Neuron*, vol. 33, p. 13, Jan. 2022, doi: 10.1016/s0896-6273(01)00579-7.

[330] A. Seth *et al.*, “*belladonna* /(*lhx2*) is required for neural patterning and midline axon guidance in the zebrafish forebrain,” *Development*, vol. 133, no. 9, pp. 1856–1856, May 2006, doi: 10.1242/dev.02390.

[331] J.-S. Lee *et al.*, “Axon Sorting in the Optic Tract Requires HSPG Synthesis by ext2 (dackel) and extl3 (boxer),” *Neuron*, vol. 44, no. 6, pp. 947–960, Dec. 2004, doi: 10.1016/j.neuron.2004.11.029.

[332] C. Fricke, J.-S. Lee, S. Geiger-Rudolph, F. Bonhoeffer, and C.-B. Chien, “*astray* , a Zebrafish *roundabout* Homolog Required for Retinal Axon Guidance,” *Science*, vol. 292, no. 5516, pp. 507–510, Apr. 2001, doi: 10.1126/science.1059496.

[333] T. Xiao, W. Staub, E. Robles, N. J. Gosse, G. J. Cole, and H. Baier, “Assembly of Lamina-Specific Neuronal Connections by Slit Bound to Type IV Collagen,” *Cell*, vol. 146, no. 1, pp. 164–176, Jul. 2011, doi: 10.1016/j.cell.2011.06.016.

[334] C. Davison, G. Bedó, and F. R. Zolessi, “Zebrafish Slit2 and Slit3 act together to regulate retinal axon crossing at the midline,” Developmental Biology, preprint, Aug. 2022. doi: 10.1101/2022.08.12.503757.

[335] E. Stoeckli, “Where does axon guidance lead us?,” *F1000Res*, vol. 6, p. 78, Jan. 2017, doi: 10.12688/f1000research.10126.1.

[336] G. J. Bashaw and R. Klein, “Signaling from Axon Guidance Receptors,” *Cold Spring Harbor Perspectives in Biology*, vol. 2, no. 5, pp. a001941–a001941, May 2010, doi: 10.1101/cshperspect.a001941.

[337]H. Nawabi and V. Castellani, “Axonal commissures in the central nervous system: how to cross the midline?,” *Cell. Mol. Life Sci.*, vol. 68, no. 15, pp. 2539–2553, Aug. 2011, doi: 10.1007/s00018-011-0691-9.

[338]I. Dudanova and R. Klein, “Integration of guidance cues: parallel signaling and crosstalk,” *Trends in Neurosciences*, vol. 36, no. 5, pp. 295–304, May 2013, doi: 10.1016/j.tins.2013.01.007.

[339]F. Friocourt *et al.*, “Recurrent DCC gene losses during bird evolution,” *Sci Rep*, vol. 7, no. 1, p. 37569, Apr. 2017, doi: 10.1038/srep37569.

[340]W. Y. Hwang *et al.*, “Efficient genome editing in zebrafish using a CRISPR-Cas system,” *Nat Biotechnol*, vol. 31, no. 3, pp. 227–229, Mar. 2013, doi: 10.1038/nbt.2501.

[341]R. Tang, A. Dodd, D. Lai, W. C. McNabb, and D. R. Love, “Validation of Zebrafish (Danio rerio) Reference Genes for Quantitative Real-time RT-PCR Normalization,” *ABBS*, vol. 39, no. 5, pp. 384–390, May 2007, doi: 10.1111/j.1745-7270.2007.00283.x.

[342]M. Valcu and C.-M. Valcu, “Data transformation practices in biomedical sciences,” *Nat Methods*, vol. 8, no. 2, pp. 104–105, Feb. 2011, doi: 10.1038/nmeth0211-104.

[343]C. Thisse and B. Thisse, “High-resolution in situ hybridization to whole-mount zebrafish embryos,” *Nat Protoc*, vol. 3, no. 1, pp. 59–69, Jan. 2008, doi: 10.1038/nprot.2007.514.

[344]A. Streit and C. D. Stern, “Combined Whole-Mount in Situ Hybridization and Immunohistochemistry in Avian Embryos,” *Methods*, vol. 23, no. 4, pp. 339–344, Apr. 2001, doi: 10.1006/meth.2000.1146.

[345]A. Borovina, S. Superina, D. Voskas, and B. Ciruna, “Vangl2 directs the posterior tilting and asymmetric localization of motile primary cilia,” *Nat Cell Biol*, vol. 12, no. 4, p. 16, Apr. 2010, doi: 10.1038/ncb2042.

[346]I. F. Sbalzarini and P. Koumoutsakos, “Feature point tracking and trajectory analysis for video imaging in cell biology,” *Journal of Structural Biology*, vol. 151, no. 2, pp. 182–195, 2005, doi: 10.1016/j.jsb.2005.06.002.

[347]N. Tarantino *et al.*, “TNF and IL-1 exhibit distinct ubiquitin requirements for inducing NEMO–IKK supramolecular structures,” *Journal of Cell Biology*, vol. 204, no. 2, pp. 231–245, Jan. 2014, doi: 10.1083/jcb.201307172.

[348]K. M. Bushell, C. Sollner, B. Schuster-Boeckler, A. Bateman, and G. J. Wright, “Large-scale screening for novel low-affinity extracellular protein interactions,” *Genome Research*, vol. 18, no. 4, pp. 622–630, Mar. 2008, doi: 10.1101/gr.7187808.

[349]J. S. Kerr and G. J. Wright, “Avidity-based Extracellular Interaction Screening (AVEXIS) for the Scalable Detection of Low-affinity Extracellular Receptor-Ligand Interactions,” *JoVE*, no. 61, p. 3881, Mar. 2012, doi: 10.3791/3881.

[350]D. T. Grimes, V. L. Patterson, G. Luna-Arvizu, J. Schottenfeld-Roames, Z. H. Irons, and R. D. Burdine, “Left-right asymmetric heart jogging increases the robustness of dextral

heart looping in zebrafish," *Developmental Biology*, vol. 459, no. 2, pp. 79–86, Mar. 2020, doi: 10.1016/j.ydbio.2019.11.012.

[351] S.-A. Hussain *et al.*, "A Molecular Mechanism for the Heparan Sulfate Dependence of Slit-Robo Signaling," *Journal of Biological Chemistry*, vol. 281, no. 51, pp. 39693–39698, Dec. 2006, doi: 10.1074/jbc.M609384200.

[352] J. G. Flanagan and H.-J. Cheng, "Alkaline phosphatase fusion proteins for molecular characterization and cloning of receptors and their ligands," in *Methods in Enzymology*, vol. 327, Elsevier, 2000, pp. 198–210. doi: 10.1016/S0076-6879(00)27277-7.

[353] V. R. Lingappa, A. Devillers-Thiery, and G. Blobel, "Nascent prehormones are intermediates in the biosynthesis of authentic bovine pituitary growth hormone and prolactin.," *Proc. Natl. Acad. Sci. U.S.A.*, vol. 74, no. 6, pp. 2432–2436, Jun. 1977, doi: 10.1073/pnas.74.6.2432.

[354] K. Simon, E. Perara, and V. R. Lingappa, "Translocation of globin fusion proteins across the endoplasmic reticulum membrane in Xenopus laevis oocytes.," *The Journal of Cell Biology*, vol. 104, no. 5, pp. 1165–1172, May 1987, doi: 10.1083/jcb.104.5.1165.

[355] S.-H. Lin and G. Guidotti, "Chapter 35 Purification of Membrane Proteins," in *Methods in Enzymology*, vol. 463, R. R. Burgess and M. P. Deutscher, Eds. Academic Press, 2009, pp. 619–629. doi: 10.1016/S0076-6879(09)63035-4.

[356] J. A. L. Good *et al.*, "Nodal Stability Determines Signaling Range," *Current Biology*, vol. 15, no. 1, pp. 31–36, Jan. 2005, doi: 10.1016/j.cub.2004.12.062.

[357] Z. He, J. Jiang, M. Kokkinaki, and M. Dym, "Nodal Signaling via an Autocrine Pathway Promotes Proliferation of Mouse Spermatogonial Stem/Progenitor Cells through Smad2/3 and Oct-4 Activation," *Stem Cells*, vol. 27, no. 10, pp. 2580–2590, Oct. 2009, doi: 10.1002/stem.198.

[358] Z. Liu, S. Woo, and O. D. Weiner, "Nodal signaling has dual roles in fate specification and directed migration during germ layer segregation in zebrafish," *Development*, vol. 145, no. 17, p. dev163535, Sep. 2018, doi: 10.1242/dev.163535.

[359] M. Tang, D. Naidu, P. Hearing, S. Handwerger, and S. Tabibzadeh, "LEFTY, a Member of the Transforming Growth Factor-β Superfamily, Inhibits Uterine Stromal Cell Differentiation: A Novel Autocrine Role," *Endocrinology*, vol. 151, no. 3, pp. 1320–1330, Mar. 2010, doi: 10.1210/en.2009-1081.

[360] L. Wang, Z. Liu, H. Lin, D. Ma, Q. Tao, and F. Liu, "Epigenetic regulation of left–right asymmetry by DNA methylation," *EMBO J*, vol. 36, no. 20, pp. 2987–2997, Oct. 2017, doi: 10.15252/embj.201796580.

[361] T. Matsui, I. Hiroshi, and B. Yasumasa, "Cell collectivity regulation within migrating cell cluster during Kupffer's vesicle formation in zebrafish," *Frontiers in Cell and Developmental Biology*, vol. 3, p. 8, 2015, doi: 10.3389/fcell.2015.00027.

[362]P. Oteiza *et al.*, “Planar cell polarity signalling regulates cell adhesion properties in progenitors of the zebrafish laterality organ,” *Development*, vol. 137, no. 20, pp. 3459–3468, Oct. 2010, doi: 10.1242/dev.049981.

[363]T. Matsui *et al.*, “Canopy1, a positive feedback regulator of FGF signaling, controls progenitor cell clustering during Kupffer’s vesicle organogenesis,” *Proc Natl Acad Sci U S A*, vol. 108, no. 24, pp. 9881–9886, Jun. 2011, doi: 10.1073/pnas.1017248108.

[364]J. Zhang, Z. Jiang, X. Liu, and A. Meng, “Eph/ephrin signaling maintains the boundary of dorsal forerunner cell cluster during morphogenesis of the zebrafish embryonic left-right organizer,” *Development*, vol. 143, no. 14, pp. 2603–2615, Jul. 2016, doi: 10.1242/dev.132969.

[365]L. Atapattu, M. Lackmann, and P. W. Janes, “The role of proteases in regulating Eph/ephrin signaling,” *Cell Adh Migr*, vol. 8, no. 4, pp. 294–307, Oct. 2014, doi: 10.4161/19336918.2014.970026.

[366]J. D. Amack, X. Wang, and H. J. Yost, “Two T-box genes play independent and cooperative roles to regulate morphogenesis of ciliated Kupffer’s vesicle in zebrafish,” *Developmental Biology*, vol. 310, no. 2, pp. 196–210, Oct. 2007, doi: 10.1016/j.ydbio.2007.05.039.

[367]F. A. Giger and N. B. David, “Endodermal germ-layer formation through active actin-driven migration triggered by N-cadherin,” *Proceedings of the National Academy of Sciences*, vol. 114, no. 38, pp. 10143–10148, Sep. 2017, doi: 10.1073/pnas.1708116114.

[368]F. De Santis, V. Di Donato, and F. Del Bene, “Clonal analysis of gene loss of function and tissue-specific gene deletion in zebrafish via CRISPR/Cas9 technology,” in *Methods in Cell Biology*, vol. 135, Elsevier, 2016, pp. 171–188. doi: 10.1016/bs.mcb.2016.03.006.

[369]B. Thisse *et al.*, “Spatial and Temporal Expression of the Zebrafish Genome by Large-Scale In Situ Hybridization Screening,” in *Methods in Cell Biology*, vol. 77, Academic Press, 2004, pp. 505–519. doi: 10.1016/S0091-679X(04)77027-2.

[370]M. Bekhouche *et al.*, “Role of the Netrin-like Domain of Procollagen C-Proteinase Enhancer-1 in the Control of Metalloproteinase Activity,” *Journal of Biological Chemistry*, vol. 285, no. 21, pp. 15950–15959, May 2010, doi: 10.1074/jbc.M109.086447.

[371]A. Stanco *et al.*, “Netrin-1–α3β1 integrin interactions regulate the migration of interneurons through the cortical marginal zone,” *Proc Natl Acad Sci U S A*, vol. 106, no. 18, pp. 7595–7600, May 2009, doi: 10.1073/pnas.0811343106.

[372]G. Tear, “Axon guidance at the central nervous system midline,” *CMLS, Cell. Mol. Life Sci.*, vol. 55, no. 11, pp. 1365–1376, Aug. 1999, doi: 10.1007/s000180050377.

[373]K. Zinn and Q. Sun, “Slit Branches Out: A Secreted Protein Mediates Both Attractive and Repulsive Axon Guidance,” *Cell*, vol. 97, no. 1, pp. 1–4, Apr. 1999, doi: 10.1016/S0092-8674(00)80707-2.

[374]Y. A. Pan, M. Choy, D. A. Prober, and A. F. Schier, “Robo2 determines subtype-specific axonal projections of trigeminal sensory neurons,” *Development*, vol. 139, no. 3, pp. 591–600, Feb. 2012, doi: 10.1242/dev.076588.

[375]L. McKerracher, M. Chamoux, and C. O. Arregui, “Role of laminin and integrin interactions in growth cone guidance,” *Mol Neurobiol*, vol. 12, no. 2, pp. 95–116, Apr. 1996, doi: 10.1007/BF02740648.

[376]D. Oliver *et al.*, “Integrins Have Cell-Type-Specific Roles in the Development of Motor Neuron Connectivity,” *J Dev Biol*, vol. 7, no. 3, p. 17, Aug. 2019, doi: 10.3390/jdb7030017.

[377]A. Stevens and J. R. Jacobs, “Integrins Regulate Responsiveness to Slit Repellent Signals,” *J. Neurosci.*, vol. 22, no. 11, pp. 4448–4455, Jun. 2002, doi: 10.1523/JNEUROSCI.22-11-04448.2002.

[378]K. Sampath *et al.*, “Induction of the zebrafish ventral brain and floorplate requires cyclops/nodal signalling,” *Nature*, vol. 395, no. 6698, pp. 185–189, Sep. 1998, doi: 10.1038/26020.

[379]M. E. Halpern *et al.*, “Genetic Interactions in Zebrafish Midline Development,” *Developmental Biology*, vol. 187, no. 2, pp. 154–170, Jul. 1997, doi: 10.1006/dbio.1997.8605.

[380]S. L. Amacher, B. W. Draper, B. R. Summers, and C. B. Kimmel, “The zebrafish T-box genes *no tail* and *spadetail* are required for development of trunk and tail mesoderm and medial floor plate,” *Development*, vol. 129, no. 14, pp. 3311–3323, Jul. 2002, doi: 10.1242/dev.129.14.3311.

[381]C. Chotard and I. Salecker, “Neurons and glia: team players in axon guidance,” *Trends in Neurosciences*, vol. 27, no. 11, pp. 655–661, Nov. 2004, doi: 10.1016/j.tins.2004.09.001.

[382]Y. Liu *et al.*, “Structural Basis for Draxin-Modulated Axon Guidance and Fasciculation by Netrin-1 through DCC,” *Neuron*, vol. 97, no. 6, pp. 1261-1267.e4, Mar. 2018, doi: 10.1016/j.neuron.2018.02.010.

[383]L. I. Finci *et al.*, “Structure of unliganded membrane-proximal domains FN4-FN5-FN6 of DCC,” *Protein Cell*, vol. 8, no. 9, pp. 701–705, Sep. 2017, doi: 10.1007/s13238-017-0439-x.

[384]M. Y. Hein *et al.*, “A Human Interactome in Three Quantitative Dimensions Organized by Stoichiometries and Abundances,” *Cell*, vol. 163, no. 3, pp. 712–723, Oct. 2015, doi: 10.1016/j.cell.2015.09.053.

[385]N. H. Cho *et al.*, “OpenCell: Endogenous tagging for the cartography of human cellular organization,” *Science*, vol. 375, no. 6585, p. eabi6983, Mar. 2022, doi: 10.1126/science.abi6983.

[386] T. O. Auer, K. Duroure, A. De Cian, J.-P. Concordet, and F. Del Bene, “Highly efficient CRISPR/Cas9-mediated knock-in in zebrafish by homology-independent DNA repair,” *Genome Research*, vol. 24, no. 1, pp. 142–153, Jan. 2014, doi: 10.1101/gr.161638.113.

[386] X. Xu, C. Zhang, Y. Xia, and J. Yu, “Over expression of *METRN* predicts poor clinical prognosis in colorectal cancer,” *Mol Genet Genomic Med*, vol. 8, no. 3, Mar. 2020, doi: 10.1002/mgg3.1102.

[387] K. Delaunay *et al.*, “Meteorin Is a Novel Therapeutic Target for Wet Age-Related Macular Degeneration,” J Clin Med. 2021 Jul 2;10(13):2973, doi: 10.3390/jcm10132973.

[388] M. Shivakumar, Y. Lee, L. Bang, T. Garg, K.-A. Sohn, and D. Kim, “Identification of epigenetic interactions between miRNA and DNA methylation associated with gene expression as potential prognostic markers in bladder cancer,” *BMC Med Genomics*, vol. 10, no. S1, p. 30, May 2017, doi: 10.1186/s12920-017-0269-y.

[389] G. Akkus, L. C. Koyuturk, M. Yilmaz, S. Hancer, I. H. Ozercan, and T. Kuloglu, “Asprosin and meteorin-like protein immunoreactivity in invasive ductal breast carcinoma stages,” *Tissue and Cell*, vol. 77, p. 101855, Aug. 2022, doi: 10.1016/j.tice.2022.101855.

VI. LIST OF FIGURES

Figure 1: Meteorins are an extremely interesting and diverse protein family: Overview about the different up-to-date known functions of Metrn and Metrnl. 19

Figure 2: ***Meteorins are small, secreted proteins:*** *Schematic for the three members of the Meteorin family in zebrafish, visualizing the signal peptide at the N-terminal of each protein and an NTR-like domain in Metrnl1.* 20

Figure 3: ***Metrnl is expressed in numerous tissues:*** *Schematic representation of examples for tissues with Metrnl expression.* 22

Figure 4: ***There are two published receptors for Meteorins so far, one each per member of the Meteorin family:*** *Schematic representation of the published receptors,* ***A*** *the KIT receptor (from www.uniprot.org/uniprotkb/A0A0U2N547/entry) and* ***B*** *Htr2b (adapted from [7])* 26

Figure 5: ***Metrnl is a regulator of beige fat thermogenesis:*** *Schematic representation of the role of Metrnl in beige fat thermogenesis visualizing the secretion of Metrnl induced by exercise or cold exposure, promoting adipocyte browning due to IL4/IL13 expression and secretion as well as macrophage activation. Adapted from [53].* 29

Figure 6: ***Metrnl as an important player within diabetes pathogenesis:*** *Schematic representation of the described influence of secreted Metrnl on the expression of PPARδ and resulting effects on the expression of pro-inflammatory cytokines leading to decreased insulin resistance, inflammation as well as fatty acid oxidation as described in [69], [72]–[76].* 33

Figure 7: ***Metrnl is improving glucose tolerance:*** *Schematic representation of the described influence of Metrnl treatment on fatty acid synthesis, fatty acid oxidation and glucose uptake as published from [57].* 34

Figure 8: ***Nodal ligands are conserved in vertebrates:*** *Schematic for Nodal signaling with Nodal binding to type I and type II serine-threonine kinase receptors (possible inhibition via Leftys), inducing Smad2 phosphorylation, which leads to interaction with Smad4 resulting in transcriptional complex formation within the nucleus acting as transcriptional activators with FoxH1. Modified from [123].* 39

Figure 9: ***Nodal signaling is regulated by positive- and negative-feedback loops:*** ***A*** *Schematic model for the cross-regulation between zebrafish Squint, Cyclops, Lefty1 and Lefty2 during the germ layer specification. Adapted from [130].* ***B*** *Schemata for endoderm and mesoderm induction in the zebrafish embryo, with cyclops, squint and leftys being expressed close to the YSL*

and acting with long-range activity (squint, leftys) and short-range activity (cyclops). Adapted from [110]. *41*

Figure 10: ***Nodal signaling is the key player for the L-R axis specification:*** *Simplified model for the establishment of the left-right axis by Nodal and Lefty visualizing Nodal/GDF1 heterodimers formed at the node, activating Nodal signaling in the LPM. Caused by the leftward Nodal flow, Nodal activation is biased toward the left, succeeding the autoregulation of Nodal, Lefty expression induction as well as Lefty's long-range inhibition towards the right. Adapted from [110].* *44*

Figure 11: ***In zebrafish the KV is the organ of laterality:*** *Drawing from a teleostean fish egg at 24hpf highlighting the Kupffer's vesicle [198].* *45*

Figure 12: ***The KV is formed by DFCs and is important for asymmetric Nodal gene expression: A*** *Schematic representation of an 8hpf zebrafish embryo visualizing animal pole (AP) to vegetal pole (VP) dorsal forerunner cell (DFC) migration. EVL, enveloping layer; DC, deep cells; YSL, yolk syncytial layer* ***B*** *Schematic for the asymmetric Nodal flow within the ciliated KV which results in asymmetric Nodal gene expression.* *46*

Figure 13: ***The Integrins α and β can form heterodimers: A*** *Schematic overview for known Integrin α and β interactions. Adapted from [216].* ***B*** *Schematic representation of an Integrin $\alpha\beta$ heterodimer.* *47*

Figure 14: ***Nodal related genes are important for the establishment of the left-right axis:*** *Schematic for the expression patterns in zebrafish at 6 somite stage (left) and 12 somite stage (right) for spaw, dand5 as well as lefty1. LPM, lateral plate mesoderm; KV, Kupffer's vesicle; N, notochord* *48*

Figure 15: ***General mechanisms of axonal guidance: A*** *Schematic representation of a growth cone highlighting its central domain, enriched with microtubules (green) and the organization of its peripheral domain housing actin filaments cytoskeletal components.* ***B*** *Schematic representation of the different possible guidance cues acting on the growth cone and the developing axon including long-range attractant and long-range repellent enabling axonal navigation and short-range repulsion as well as attractive cues keeping the growing axon in a tight bundle.* *53*

Figure 16: ***Axonal guidance at the midline: A*** *Schematic representation of a mouse embryonic spinal cord section and an axon crossing the midline, guided by repulsive and attracting guidance cues.* ***B*** *Schematic representation of a sd or gli mouse mutant missing the floorplate, which results in commissural axons stuck at the midline.* *55*

Figure 17: ***Receptors of canonical axonal guidance factors:*** *Schematic representation of the DCC, Unc5, Robo, Neuropilin, Plexin and Eph-receptor.* *61*

Figure 18: ***Development of the first commissural tracts in zebrafish:*** *Frontal representation of the zebrafish anterior commissure (AC) and post-optic commissure (POC) at around 24hpf showing DRC neurons extending to and forming the SOT and AC. Beside VRC neurons are establishing the POC. 62*

Figure 19: ***Example for a short migration in an SDS-PAGE gel of an Meteorin- and Netrin-interaction sample.*** *(cut regions marked with squares) 81*

Figure 20: ***Metrns LOF fish show DFC phenotype, which cannot be rescued by an ectopic source of metrns and is mimicked by metrns overexpression: A*** *Quantification of DFC malformation phenotypes in triplMut at 9hpf with metrns mRNA injection.* ***B*** *Quantification of DFC malformation phenotypes in wt samples at 9hpf with metrns mRNA injection..... 120*

Figure 21: ***Metrns LOF fish show heart looping phenotype, which can partially be rescued by an ectopic source of metrns and is not strongly influenced by metrns overexpression:*** *Analysis of heart looping phenotypes in triplMut at 2dpf with metrns mRNA injections and in wt samples at 2dpf with metrns mRNA injections. 121*

Figure 22: ***Antisense RNA probe in situ hybridization for kita, kitb and htr2b reveal distinct expression patterns: A*** *At 9hpf kita is expressed in the prechordal plate (black arrow) and from 11hpf in the lateral borders of the anterior neural plate (black arrow). Kitb expression could be detected from 11hpf in the anterior ventral mesoderm (black arrow). (scale: 0.25mm)* ***B*** *At 9hpf htr2b expression was undetectable, solely from 2dpf htr2b transcripts could be visualized in the developing heart. (scale: 0.25mm) 144*

Figure 23: ***The AVEXIS approach is based on monomeric biotinylated "bait"- as well as pentamerized "prey" forms and positive binding can be visualized and analyzed by colorimetric enzymatic activity: A*** *Scheme for the bait expression construct, containing the bait ectodomain, flanked by AscI and NotI restriction sites and a Cd4d3+4 tag. The bait is monobiotinylated via the co-transfection of a plasmid which is expressing the secreted BirA enzyme. Modified from [349].* ***B*** *Scheme for the prey expression construct, containing the prey ectodomain, flanked by AscI and NotI restriction sites and a Cd4d3+4 tag, followed by a cartilage oligomeric matrix protein (COMP) pentamerisation sequence and a β-lactamase enzyme. Modified from [349].* ***C*** *Schematic illustration of the AVEXIS approach, showing biotinylated bait ectodomains (pink) which are captured on a streptavidin-coated microtiter plate in an orientated manner. Baits are probed with soluble pentameric prey ectodomains with a lactamase tag (blue). Positive binding is visualized via nitrocefin's colorimetric enzymatic turnover from yellow to red. Modified from [348]. 145*

Figure 24: ***The identification of Meteorin receptor(s) is crucial for fully understanding their biochemical signaling pathways:*** *Spinal cord sections of E11 mouse and 5dpf zebrafish probed*

with Metrn-AP or Metrnl1-AP, visualizing possible Metrns receptor(s) location, close to the midline of the spinal cord (black arrows). 147

Figure 25: ***Via an AP-binding assay no positive interaction between Metrnl1 and IntegrinαV/Integrinβ1b could be detected:*** *An example of an AP-binding assay showing positive interaction (dark colored cells) in the control between the Dcc receptor expressed in COS7 cells and Netrin-AP. No interaction (just light blue colored cells) could be detected between IntegrinαV and/or Integrinβ1b and Metrnl1. ..... 148*

Figure 26: ***Hunting for the Meteorins receptors via the Ecto-FC ligand-receptor interaction screen:*** *Schematic representation of the Ecto-FC approach displaying the different steps from bait-FC proteins production, prey protein extraction from mouse tissue, the purification of bait-prey proteins and analysis via MS. Adapted from [8]. 149*

Figure 27: ***Ecto-Fc interaction screen optimization and experimental workflow set up. A*** *Example of MS results using the "Transmembrane Filter, showing the number of identified proteins (all proteins= all identified proteins without filter; transmembrane= identified protein has an annotated transmembrane domain; only transmembrane= identified protein has an annotated transmembrane domain and is not located at the ER, Mitochondrium, Golgi or Nucleus; TM & ER= identified protein has an annotated transmembrane domain and is located at the ER; TM & Mitoc= identified protein has an annotated transmembrane domain and is located at the Mitochondrium; TM & Golgi= identified protein has an annotated transmembrane domain and is located at the Golgi; TM & Nucleus= identified protein has an annotated transmembrane domain and is located at the Nucleus). Proteins are considered identified if at least 2 peptides are detected and if Unique>1.* ***B*** *Analogous to A but after optimization of sample preparation.* ***C*** *Schematic for the optimized experimental workflow for Metrns receptor identification after the enrichment of plasma membrane proteins (PMP). 151*

Figure 28: ***Analyses of FC-Mtrn/FC-Ntn1 differential proteomic screenings. A*** *Protein enrichment analysis (log2(Metrn/Ntn)) for the first proteomic screening. The graph shows the number of all identified proteins (upper panel) and after including the "Transmembrane-Filter" (lower panel). Proteins only identified in the Netrin interaction sample (only Ntn1, left) or only in the Meteorin interaction sample (only Metrn, right panel) are visualized according to the number of Spectra (# Spec).* ***B*** *Analogous to A but for the second replicate. 153*

VII. ANNEX

ARTICLE:

Myosin-1b regulates intestinal epithelial morphogenesis and its function is impaired in human UNC45A deficiency

Céline Revenu[1], Marion Rosello[1,2], Rémi Duclaux-Loras[3], Karine Duroure[1,2], Ophélie Nicolle[4], Fanny Eggeler[2], Marie-Thérèse Prospéri[5], Julie Stoufflet[1], Juliette Vougny[1], Corinne Lebreton[3], Priscilla Lépine[5], Grégoire Michaux[4], Nadine Cerf-Benssusan[3], Evelyne Coudrier[5], Marianna Parlato[3‡], Filippo Del Bene[1,2 ‡]

[1]Institut Curie, PSL Research University, INSERM U934, CNRS UMR3215, 75248 Paris Cedex 05, France.

[2] Sorbonne Université, INSERM, CNRS, Institut de la Vision, F-75012 Paris, France

[3] INSERM, UMR1163, Laboratory of Intestinal Immunity and Institut Imagine, 75015 Paris, France.

[4]CNRS, UMR6290, Institut de Génétique et Développement de Rennes, F-35043 15 Rennes, France.

[5]Institut Curie, PSL Research University, CNRS UMR144, 75248 Paris Cedex 05, France.

‡Authors for correspondence: filippo.del-bene@inserm.fr, marianna.parlato@inserm.fr

Keywords

Myosin 1b, intestine, zebrafish, UNC45A, villous atrophy

Summary statement

Myosin-1b is important for intestinal epithelium folding during zebrafish development and participates in the villous atrophy clinical manifestation downstream UNC45A deficiency.

Abstract

Vesicle trafficking and the establishment of apico-basal polarity are essential processes in epithelium morphogenesis. Myosin-1b, an actin-motor able to bind membranes, regulates membrane shaping and vesicle trafficking. Here, we investigate Myosin-1b function in gut morphogenesis and congenital disorders using cell line and zebrafish larvae as well as patient biopsies. In a 3D Caco-2 cyst model, lumen formation is impaired in absence of Myosin-1b. In zebrafish, both Morpholino knock-down and genetic mutation of *myo1b* result in intestinal bulb epithelium folding defects associated with vesicle accumulation, reminiscent of a villous atrophy phenotype. We show that Myosin-1b interacts with the chaperone UNC45A, genetic deletion of which also results in gut folding defects in zebrafish. Loss of function mutations in *UNC45A* have been reported in complex hereditary syndromes, notably exhibiting intestinal disorders associated with villous atrophy. In UNC45A-depleted cells and in patient biopsies, Myosin-1b protein level is strikingly decreased. The appearance of Myosin-1b aggregates upon proteasome inhibition in cells points at a degradation mechanism of misfolded Myosin-1b in the absence of its chaperone. In conclusion, Myosin-1b plays an unexpected role in the development of the intestinal epithelium folds or villi downstream UNC45A, establishing its role in the gut defects reported in UNC45A patients.

Introduction

The establishment of apico-basal polarity and lumen formation are two fundamental steps during vertebrate intestinal epithelial morphogenesis (Chin et al., 2017). The actin cytoskeleton and the vectorial vesicle trafficking play a major role in the initiation and maintenance of this process, leading to a stable single layer of cells with distinct apical and basolateral domains (Lubarsky and Krasnow, 2003, Martin-Belmonte and Mostov, 2008). The apical membrane of the enterocyte is further organized in microvilli, plasma membrane protrusions, which are supported by bundles of parallel actin filaments and interacting proteins interconnected at the basis through a network of actin, spectrin, and myosins known as terminal web (Revenu et al., 2004). The interaction between neighboring polarized cells is further strengthened by the formation of cadherin-based adherens junctions and claudin-based tight junctions. A proper polarization of the intestinal epithelium is essential to achieve its main physiological roles, such as fluids and nutrient absorption and secretion. Indeed, defects in intestinal epithelial cell polarity and apical lumen formation result in early onset intestinal disorders, usually appearing in the first days of life (Kwon et al., 2020). Recently, loss of function (LOF) variants in the chaperone *UNC45A* were reported in families presenting complex phenotypes including congenital diarrhea and several degrees of villous atrophy (Esteve et al., 2018). UNC45A belongs to the conserved UCS protein family (UNC-45/CRO1/She4p) of myosin co-chaperones.

Myosins 1 are single-headed actin motors targeted to membranes. Myosin1b (Myo1b) was detected in mouse enterocyte brush borders in a mass spectrometry analysis (Revenu et al., 2012). Studies in cell cultures reported that Myo1b associates with organelles and regulates membrane trafficking by controlling their morphology (Almeida et al., 2011). Myo1b can pull out membrane tubes along actin bundles immobilized on a solid substrate (Yamada et al., 2014) and it controls the formation of repulsive filopodia, the redistribution of actomyosin fibres driving cell repulsion (Prosperi et al., 2015) as well as the formation of axons in cultured neurons by controlling actin waves (Iuliano et al., 2018). Despite this progress in understanding Myo1b function *in vitro* and in cellular systems, its function in tissue biology, especially in the intestinal epithelium where it is expressed, remains unexplored. This work investigates this question in the context of gut epithelium development and morphogenesis. MYO1B localizes at the apical brush border of intestinal epithelial cells in humans and loss of MYO1B in enterocyte like Caco-2 cells impairs epithelial morphogenesis. In zebrafish, genetic inactivation of Myo1b affects intestinal bulb fold formation revealing its conserved function during normal intestinal epithelium development. Finally, here we show that MYO1B is one of UNC-45A clients, suggesting a role for myosin1b in the pathogenesis of UNC45A deficiency.

Results

Myo1b concentrates apically in the gut epithelium but has no major impact on epithelial cell differentiation of zebrafish intestinal bulb

To investigate the implication of Myo1b in intestinal epithelium morphogenesis in vivo, we turned to zebrafish as a good model for gut development. There is one single myo1b gene with several splicing isoforms in the current zebrafish genome assembly. The corresponding Myo1b protein shares 80% identity with the Homo sapiens and Mus musculus homologues (Fig. 1C). In order to determine the expression pattern of myo1b during zebrafish development, we performed whole mount in situ hybridization labelling with specific antisense probes. Myo1b transcripts were unambiguously detected at 3dpf in the digestive tract of zebrafish (Fig. 1D) coinciding with the onset of gut morphogenesis (Ng et al., 2005, Wallace et al., 2005). Myo1b transcripts were also observed at 5dpf (Fig. 1D) when the intestine becomes functional and compartmentalised in bulb, mid and posterior intestines. At this stage, the transcripts were restricted to the intestinal bulb, the anterior part of the gut that forms large folds. Due to the lack of a zebrafish specific antibody, endogenous Myo1b sub-cellular localisation could not be assessed in zebrafish larvae. However, expressing eGFP-tagged Myo1b revealed apical accumulation of the protein (Fig. 1E). The zebrafish intestinal epithelium differentiates from 3 days post fertilisation (dpf) where it is essentially a flat monolayered tube. At 5dpf, epithelial folds are present, especially in the anterior most part of the gut, the intestinal bulb (Wallace et al., 2005). These folds are equivalent to the mammalian villi, and although no crypts are present in zebrafish, the region between folds will have a crypt-like role (Crosnier et al., 2005). First, we designed a splice blocking Morpholino (Myo1b-MO) that is efficiently preventing proper splicing of myo1b as determined by RT-PCR (supplemental Fig. 1A-B). At the concentration used, Myo1b MO displayed no overt phenotype, despite occasionally a slight heart oedema (supplemental Fig. 1C). To extend these results with a genetic loss of function model, we also generated a mutated allele at the myo1b locus using the CRISPR/Cas9 system, resulting in the insertion of a single base at the beginning of the open reading frame, as confirmed by sequencing (supplemental Fig. 1D). This leads to a premature stop codon and to the lack of detection of the protein by Western blot in gut lysates from adult homozygote mutants (myo1b-/-, supplemental Fig. 1E). As myo1b mRNA is maternally provided (supplemental Fig.1F), maternal contribution was suppressed by crossing myo1b-/- mothers. As for the MO injections, the resulting maternal-zygotic homozygous mutant larvae displayed no overt phenotype (supplemental Fig. 1C). In cross-sections (Fig. 3A), the intestinal bulbs of Myo1b MO and myo1b-/- larvae appeared smaller compared to controls. A significant reduction of the number of cells per cross-section was observed for both Myo1b MO and myo1b-/-

intestinal bulbs at 3 and 5dpf compared to their respective controls (Fig. 3B). A reduction in the total cell number in the intestinal bulb could be the consequence of increased apoptosis or reduced cell proliferation. No significant difference with controls in the proportion of proliferative cells could be detected at 3 and 5dpf (supplemental Fig. 2A). A slight increase in the proportion of apoptotic cells could be detected at 5dpf but not at 3dpf (supplemental Fig. 2B). This later increase in apoptosis can however not account for the reduced cell number per section reported from 3dpf on and could more be a readout of increased cellular stress level upon prolonged absence of Myo1b, as reported after the KO of other Myosins 1 in mouse and drosophila (Hegan et al., 2007, Tyska et al., 2005). Using specific markers for secreting and absorptive cell lineages, defects in enterocyte differentiation could also be excluded (supplemental Fig. 2 C-D). Finally, the microvilli marker Villin appeared properly localised apically, lining the lumen together with F-actin (Fig. 3C), suggesting that apical polarity is not affected in Myo1b MO and myo1b -/- intestinal epithelium in vivo.

Myo1b loss of function zebrafish display villus atrophy-like features in the intestinal bulb epithelium

To analyse in 3D intestinal bulb epithelium morphogenesis in zebrafish, we used the BAC line *cldn15la:cldn15la*-GFP that specifically labels the gut epithelium (Alvers et al., 2014). Both MO and KO intestinal bulbs revealed single continuous lumen suggesting that early steps of lumen fusion events were not affected (Alvers et al., 2014, Horne-Badovinac et al., 2001). However, in Myo1b MO larvae, the intestinal bulb epithelium appeared most of the time flat at 5dpf, not developing the expected folds observed in controls (Fig. 3D). Consistently with this phenotype, in the KO model, we detected a significant reduction in fold length in KO versus control samples (Fig. 3E). In an attempt to understand this milder phenotype in the mutant compared to the MO condition, we analysed potential compensation mechanisms by other myosins 1 performing RT-QPCR. On the 4 myosins 1 tested (myo1ca, myo1cb, myo1d and myo1eb), myo1eb showed a reproducible increase of on average 60% of the WT expression level in the mutant using EF1a (supplemental Fig. 1G) and RPL13a (not shown) as reference genes. Myo1eb is broadly expressed in early developmental stages but has restricted expression patterns after 2dpf (mostly branchial arches and pharynx) (Thisse and Thisse, 2004). A partial compensation of the loss of myo1b by an upregulation of myo1eb could thus potentially explain the subtler and more restricted phenotype of the mutant larvae compared to the knock-downs.

To further characterize the architecture of Myo1b-deficient intestinal bulb epithelium, a histological analysis by transmission electron microscopy (TEM) was performed on 5dpf larvae. It confirmed the affected folding of the intestinal bulb epithelium in MO and KO samples, and the preserved apico-basal polarity of enterocytes (Fig. 4A-B). Quantifying microvilli length

and density did not reveal any significant defect resulting from Myo1b downregulation or absence, although packing looked less regular (Fig. 4C). In contrast, a darker sub-apical band was visible in Myo1b affected samples compared to controls, likely corresponding to modifications of the terminal web (Fig. 4C). Moreover, this ultrastructural analysis showed an important accumulation of vesicles in MO and KO samples compared to controls (Fig. 4B insets) suggesting defects in membrane trafficking. These TEM observations (epithelium folding impaired, modifications of the apical pole ultrastructure and trafficking defects) overall indicate that myo1b-deficient enterocytes display some microvillus inclusion disease-like features.

Myo1b is expressed apically in intestinal epithelial cells and contributes to lumenogenesis

To determine whether human MYO1B plays a conserved role in controlling intestinal epithelial cell morphogenesis, we first used the human epithelial colorectal Caco-2 cell line, a widely used model of intestinal epithelial cells. These cells organize into polarized cysts with a spherical architecture when embedded in a reconstituted basement membrane such as Matrigel therefore enabling to screen for morphogenesis defects. *MYO1B* accumulated apically in polarised Caco-2 cysts, as demonstrated by its colocalization with the F-actin marker phalloidin demonstrating a localisation in actin-rich area, microvilli and/or the subjacent terminal web (Fig. 1B). *MYO1B* was then knocked-out using CRISPR/Cas9 in Caco-2 cells (*MYO1B* KO, Fig. 1 A-B). The global apico-basal polarity of Caco-2 cysts was not affected in *MYO1B* KO cells compared to controls as shown by the correct apical concentration of F-actin, pERM and villin (Fig. 2 A-B). Despite the absence of major polarisation defects, *MYO1B* KO Caco-2 cells were more prone than controls to the formation of cysts with multiple lumen (Fig. 2 A-B). Indeed, after 5 days in matrigel, *MYO1B* KO cells showed a 50% drop in the percentage of well-formed cysts with single hollow central lumen compared to controls (Fig. 2C), overall pointing to a role for MYO1B in controlling lumen morphogenesis in intestinal epithelial cells.

Myosin 1B interacts with UNC45A and is misfolded in UNC45A deficiency

Loss of function (LOF) variants in the chaperone *UNC45 homolog A* have recently been associated with rare human genetic syndromes notably presenting intestinal disorders, including chronic diarrhea and villous atrophy of variable penetrance (Esteve et al., 2018 + PMID: 35575086). In complex with HSP90, UNC45A acts as a critical cochaperone for the folding and stability of type II myosins (PMID: 23332754). A pull-down assay performed to detect potential Myo1b partners identified UNC45A as the most abundant protein interacting with Myo1b in a mouse neuronal cell model (Supplementary table 1). Immunoprecipitation

coupled to mass spectrometry using UNC45A as bait in Caco-2 cells identified MYO1B as part of UNC45A interactome in Caco-2 cells (PMID: 35575086). Lysates from myc/flag-tagged UNC45A Caco-2 cells and from myc/flag-tagged empty vector (EV) control Caco-2 cells were immunoprecipitated with myc-Ab and pulled-downs analysed by western blot, confirming the interaction of WT-UNC45A with both myosin 1B and HSP90 (data not shown). Accordingly, *UNC45A* KO Caco-2 cells showed reduced MYO1B expression by both western blot and immunofluorescence (Fig. 5A), suggesting that in UNC45A deficient condition, MYO1B fails to fold properly and is redirected for proteasome degradation. Blocking the proteasome machinery with the proteasome inhibitor MG132 induced the appearance of protein aggregates both in control and UNC45A KO Caco-2 cells (Fig. 5B). Myo1b staining partly co-localised with the aggresomes in the UNC45A KO condition (Fig. 5B). Strikingly, while in control duodenal tissues, MYO1B was detected apically at the base of the villi and in crypts, partially colocalising with Villin (Fig. 5C), in duodenal tissues from UNC45A-deficient patients, Villin was still localised apically whereas MYO1B was barely detectable (Fig. 5D). Overall, these findings confirm MYO1B as client of the chaperone complex UNC45A/HSP90 and indicate that MYO1B is misfolded, degraded and therefore not functional in UNC45A deficient condition.

Discussion

This work identifies Myo1b, an actin motor, as an unexpected player in the regulation of the morphogenesis of the intestinal epithelium during gut development. In zebrafish, we report defects in epithelial folding and villous atrophy when Myo1b is depleted. This phenotype is similar to the ones reported in zebrafish and in human patients with loss of function variants in *UNC45A*. In intestinal epithelial cells, we show that MYO1B belongs to the UNC45A interactome and that MYO1B is misfolded in absence of UNC45A.

For this study, we analysed both *myo1b* mutant- and Morpholino-induced phenotypes. It is now well established that Morpholino knock-downs often result in more severe overt phenotypes than the corresponding knock-outs, at least partially due to the induction of genetic compensation mechanisms in the mutants (Kok et al., 2015, Rossi et al., 2015). In the *myo1b* null case, we observed a more subtle outcome than the Morpholino, which could be due to compensation mechanisms (El-Brolosy and Stainier, 2017) as supported by the RT-QPCR of *myo1eb*. Here, the intestinal bulb phenotypes observed with both approaches converged on reduced cell number of intestinal bulb sections and impaired epithelial folding.

Up to now, myosins 1a, c, d and e had been identified in intestinal brush borders constituting the apical pole of differentiated enterocytes (Benesh et al., 2010). Several class I myosins have been implicated in the maintenance of intestinal epithelial differentiated state. Myo1a, which is associated with the highly organised actin network of differentiated enterocytes in mammals

(Revenu et al., 2012, Tyska et al., 2005), but seems to lack in the zebrafish and *Drosophila* genomes, is important for enterocyte polarity and participates in the structure and composition of the brush border (Mazzolini et al., 2012, Tyska et al., 2005). The phenotype of the *myo1a* KO mice is however mild, with reports of clear compensations by other class I myosins (Benesh et al., 2010, Tyska et al., 2005). Likewise, two of the known class I myosins in *Drosophila* are also localised in the apical pole of differentiated enterocytes and *Drosophila* Myo61F is necessary for the stability of enterocyte apical organisation (Hegan et al., 2007). We report the expression of another myosin 1 in the gut epithelium, Myo1b, and its apical localisation in Caco-2 cells and in enterocytes of duodenal human tissues and of zebrafish intestinal bulb. Myo1b localisation in microvilli had previously been reported in kidney epithelial cells (Komaba and Coluccio, 2015). In human duodenum, Myo1b is expressed at the base of the villi and in crypts suggesting a specific role in the proliferative compartment and not in enterocyte differentiated state. We did not detect global polarisation defects at the cell level or impaired differentiation in absence of Myo1b, whereas both the Caco-2 3D model and the zebrafish model demonstrate morphogenetic defects at the tissue level, respectively single lumen formation and folding.

Proliferation, apoptosis or differentiation defects do not account for the reduced cell number observed on transverse sections of the intestinal bulb from 3dpf. As the sections give a 2D overview of a 3D organ, this reduced cell number is thus likely the readout of the different organisation in space of the epithelium. A specificity of the zebrafish intestinal bulb is the early folding of the epithelium that remains pronounced to adulthood (Ng et al., 2005). The reduced folding and villi formation in the mutants and morphants are clear signs of a different architecture of the tissue. Also the mechanisms underlying intestinal epithelium folding are not yet fully understood, the impact of tension and forces at the cell and tissue level driving compression, cell intercalation and invagination through apical constriction have been investigated in other tissues during development (Mammoto and Ingber, 2010). Myosins are central in the control of actin cytoskeleton dynamics and in force generation (Reymann et al., 2012). In particular, Myo1b deforms membranes and participates in organelle formation and trafficking (Almeida et al., 2011, Coudrier and Almeida, 2011). It also remodels the actin cytoskeleton (Iuliano et al., 2018, Pernier et al., 2019, Prosperi et al., 2015). Its roles in membrane traffic and in the dynamic organisation of actin structures make it a plausible actor in the morphogenesis of the gut epithelium. The electron microscopy data show a strong accumulation of intra-cellular vesicles in Myo1b mutant and Morpholino tissues suggesting impaired trafficking, in agreement with its role in the formation of post Golgi carriers and protein transport at the level of multivesicular endosomes (Almeida et al., 2011, Salas-Cortes et al., 2005). Electron microscopy also reveals modifications of the terminal web area, the apical actin belt linking adherens junctions in the epithelium, in agreement with its role in actin dynamics.

Myosin 1b function on actin dynamics and consequently on membrane remodelling and membrane trafficking must impact cell and tissue mechanics (Buske et al., 2012), and this way contributes to impaired intestinal epithelial folding in the absence or down-regulation of *myo1b*. Myo1b restricted localisation at the base of the villi in human biopsies may indicate a specific mechanical role in crypts morphogenesis.

Villous atrophy is a phenotype associated with various intestinal disorders including some rare hereditary syndromes presenting congenital diarrhea like microvillous inclusion disease (MVID). Mutations in MyosinVb are the main cause of MVID (Muller et al., 2008) and have notably been associated with defective trafficking. A zebrafish mutant of *myoVb* develops a flat intestinal epithelium (Sidhaye et al., 2016). Recently, loss of function (LOF) mutations in the chaperone *UNC45A* were reported in families presenting complex phenotypes including congenital diarrhea and several degrees of villous atrophy (Esteve et al., 2018). A zebrafish mutant for *UNC45A* also exhibit loss of intestinal epithelium folding (Esteve et al., 2018). UNC45A is a chaperone participating in the conformational maturation of, among others, some Myosins (Barral et al., 2002, Lee et al., 2014, Lehtimaki et al., 2017). Here we confirm that UNC45A in concert with HSP90 participates to the folding of MYO1B. Our results in enterocyte-like Caco-2 cells and in patient tissues indicate a strong reduction in the protein level of MYO1B in absence of a functional UNC45A, pointing to the degradation of misfolded and destabilised MYO1B. The intestinal phenotypes associated with LOF variants in *UNC45A* could hence partly be the consequence of the reduced protein level of MYO1B. In conclusion, Myosin 1b contributes to gut morphogenesis and appears as a potential player in the complex intestinal phenotype of the UNC45A deficiency.

Materials and Methods

CRISPR- Cas9 genome editing of MYO1B in Caco2 cells and 3D culture. The lentiCRISPRv2 plasmid was a gift from F. Zhang (Massachusetts Institute of Technology, Boston, MA; plasmid no. 98290, Addgene). The single-guide RNAs (sgRNAs) were designed using the CRISPR Design Tool (Massachusetts Institute of Technology) and cloned into the BsmbI site. sgRNA sequences: for-5- CACCGATCCCTACGAGATCAAGATA -3, rev-5- AAAC TA TCT TGA TCT CGT AGG GAT C -3. Following production of lentiviral particles, the lentiCRISPRv2 plasmids were transduced in Caco2 cells. Positively transduced cells were selected by puromycin (10μg/ml).
For 3D culture, CaCo2 cells were resuspended at a concentration of 10^4 cells/mL in DMEM (Gibco) with 20% FCS containing 4% Matrigel (BD Biosciences) and 2.5 10^4 cells/well were plated in 8-wells chamber slide IBIDI (Biovalley), previously precoated with 100 µL of Matrigel. Cells were grown for 5 days to obtain cysts. To detect aggregation-prone proteins, the proteasome inhibitor MG132 (Sigma-Aldrich) was added overnight in the culture medium at a concentration of 10 μM.

Western blot. Caco-2 cells were lysed in RIPA buffer (Sigma) supplemented with 1X proteinase inhibitor cocktail mix (Roche, Sigma). Adult zebrafish guts were dissected on ice and mechanically lysed in 200μL lysis buffer (10 mM HEPES + 300 mM KCl + 5 mM $MgCl_2$ + 0,45% triton X100 + 0,05% Tween20, pH7) with 10 mM ATP and Complete protease inhibitor (Roche). 40 μg of extracts in Laemmli buffer were loaded on a 4-12% polyacrylamide gradient concentration gel (ThermoFisher). Primary antibodies used were mouse anti-tubulin (1:12000, Sigma), rabbit anti-ratMyo1b (1,8 µg/µL, 1:500, (Salas-Cortes et al., 2005), anti GAPDH (#14C10, 1:1000, Cell Signaling), anti HSP90 (#4874, 1:1000, Cell Signaling), anti-FLAG (#F3165, 1:1000, Sigma-Aldrich).

Phylogenetic analysis. The Myo1b and Myo1a homologues in *Danio rerio, Homo sapiens, Mus Musculus, Gallus gallus and Drosophila melanogaster* were obtained from NCBI HomoloGene. Protein sequences were aligned and a phylogenetic tree was assembled using the online 'One Click' mode at Phylogeny.fr (Dereeper et al., 2008).

Molecular Cloning. The βactinhsp70:KalT4;cmlc2:eGFP construct was generated by combining four plasmids using the Multisite Gateway system (Invitrogen): p5E-bactinhsp70, pME-KalT4, p3E-polyA and pDEST-cmcl2:eGFP containing Tol2 sites (Kwan et al., 2007). The βactin promoter was cloned into the pCR-bluntII-TOPO vector (Invitrogen) and then inserted

in the p5E-MCS using KpnI and XhoI restriction sites. The 3' 638bp of the zebrafish hsp70 promoter (Dalgin et al., 2011) was inserted into this p5E-βactin vector linearized with XhoI using the Gibson Assembly Cloning Kit (New England Biolabs). The optimised Gal4 KalT4 (Distel et al., 2009) was amplified and inserted in a pDONR221 using the Multisite Gateway system (Invitrogen).
To generate the *14UAS:ubc-eGFP-Myo1b vector*, eGFP-Rat Myo1b cDNA was amplified from a previously published plasmid (Prosperi et al., 2015). It was inserted into the pT1UciMP plasmid containing 14xUAS-ubc and Tol1 sites (Horstick et al., 2015) linearized with Xho1 using the Gibson Assembly Cloning Kit (New England Biolabs).

Zebrafish (*Danio rerio*) husbandry. Wild-type Tupfel long fin zebrafish strains were used and raised according to standard protocols. Stable transgenic lines were generated by injection of the plasmids with *tol2* or *tol1 transposase* mRNA at 25ng/µL in one-cell stage zebrafish embryos. The transgenic BAC line claudin15-like-a fused to GFP (cldn15la:cldn15la-GFP) was kindly provided by Michel Bagnat (Alvers et al., 2014). For live-imaging, larvae were anaesthetised in 0.02% MS-222 and immobilised in 1% low melting point agarose. Imaging was performed on a Zeiss LSM 780 confocal. All animal procedures were performed in accordance with French and European Union animal welfare guidelines.

***In situ* hybridization.** *In situ* hybridizations (ISH) were performed on larvae treated with 1-phenyl-2-thiourea (PTU, Sigma-Aldrich) and fixed in freshly made 4% paraformaldehyde (PFA) 2-4h at RT and stored in 100% methanol at -20°C. After rehydration, larvae were treated with proteinase K (20 µg/ml; Roche diagnostics) at RT for 1h (3dpf) or 2h (5dpf) and fixed again in 4% PFA at RT for 20min. Digoxigenin-labelled antisense and sense RNA probes were synthesized by *in vitro* transcription using DIG-labelled UTP according to the manufacturer's instructions (DIG RNA labelling kit, Roche). Primers used were as follow: *myo1b* sense: CAA TAT GAT AGG GGT AGG GGA CAT G; antisense: TGG TTT GAA CTC AAT ATT TCC CAG C. Anti-DIG antibody conjugated to alkaline phosphatase allowed detection of hybridized riboprobes according to the manufacturer's instructions (Roche).

Myo1b zebrafish mutant generation with CRISPR/Cas9. The sgRNA sequence (sgB: CTTCTGACAAGGGCTCTAGG) was cloned into the BsaI digested pDR274 vector (Addgene). The sgRNAs were synthesized by in vitro transcription (Megascript T7 transcription kit, Ambion). After transcription, sgRNAs were purified using the RNAeasy Mini Kit (Quiagen). For injections at one cell stage, the synthesized sgB was injected at 300ng/µL after 5-minute incubation at RT with Cas9 protein (NEB) at 2µM final in 20mM Hepes-NaOH pH 7.5, 150mM KCl (Albadri et al., 2017). Injected embryos were grown to adulthood and crossed with wild-

types to identify founders. Pools of 20 embryos per clutch were lysed in NaOH 50mM at 95°C for at least 30min. PCR was performed on lysates to amplify the genomic region targeted by the sgB with primers forward 5'GGGTGTTGTTCAGCGATGGA and reverse 5'ATAGATCTCATTGTGATCGA using Phusion High-Fidelity DNA polymerase (Thermo Scientific). The amplicons were cloned in pCR-bluntII-TOPO vector (Zero Blunt Topo PCR cloning kit, Invitrogen) and sequenced (GATC Biotech) to identify indels and the corresponding founder fish. Sequences were analysed using Geneious. After selection of the founder, genotyping of the line was performed by PCR on fin clips with primers 5'AGATGAATGCAAGCAAGCCATT and 5'ATACGATCTGATTGTGATCGAATCGCT. The resulting product was digested with restriction enzyme FspBI, the site of which is lost in the mutant, resulting in 2 fragments (208 and 66bp) for the WT allele and only one (275bp) for the mutated allele.

Morpholino oligonucleotide design and injections. Myo1b splice blocking morpholino was designed to target the splice donor site downstream of exon 22 (Myo1b-MO, 5'-ATGAGAAACTGTGTTCATTACCTGG). Experiments were performed in parallel with a standard control-MO (5'-CCTCCTACCTCAGTTACAATTTATA) with no target in the zebrafish genome. Morpholinos (Gene Tools) diluted at 1mM in water, were injected in 1-cell stage embryos at a final concentration of 0.2mM. To validate Myo1b-MO knock-down, RT-PCR was performed on 3dpf larvae. Total RNA of 50 larvae was prepared with TRIzol and TURBO DNAse-free reagents (Invitrogen). mRNA (1µg) was retro-transcribed using oligo(dT) primers and the SuperScript III First-Strand Synthesis System (Invitrogen). To amplify the region targeted by the MO (supplemental Fig. 1A), PCR was performed on the cDNA with two different forward primers (primer 1 in exon21 was: 5'GGCTGCGATATTCTTGCCTCC, primer 2 at the edge of exon22 and the targeted intron was: 5'TCTTTCATTCGTGGATGGAAGGCC) and the reverse primer 5'AACCCAGGTAATGAACACAGTTTCTAT. PCR products were run on a gel (supplemental Fig. 2B) and bands were gel purified (Macherey-Nagel), inserted in a pCR-bluntII-Topo vector (Invitrogen) and sent for sequencing (GATC) to assess intron retention.

Quantitative RT-PCR. For each experiment, total RNA was prepared from 3 pools of 50 embryos per phenotype with TRIzol reagent and the TURBO DNA-free kit (ThermoFisher Scientific). RNA (1µg) was retro-transcribed using random primers and the SuperScript III First-Strand Synthesis system (ThermoFisher Scientific). For RT-QPCR, the SYBR Green PCR Master Mix (ThermoFisher Scientific) was used according to the manufacturer's instructions and PCR were performed on an ABI PRISM 7900HT instrument. Experimental triplicates of each sample were averaged and the relative expression level quantified with the log2ΔCT

method using EF1a and RPL13a reference genes. Shown are values normalised on the wild-type samples.

Immunohistochemistry. Caco-2 cells and cysts were fixed in 4% PFA 30min at 37°C and washed with PBS. They were permeabilised in PBS, 0.2%TX100, 1%BSA for 5min at RT and blocked in PBS 3%bBSA for 1-2 hours at RT. Primary antibodies used were rabbit anti-ratMyo1b (1,8 µg/µL, 1:100, (Salas-Cortes et al., 2005), mouse anti-Villin clone ID2C3 (1:300, (Robine et al., 1985), rabbit anti-pERM (1:100, abcam ab47293). After washes, they were incubated with Alexa Fluor 488 secondary antibody (Molecular probes), phalloidin-Alexa Fluor 568 and Dapi. To assess protein aggregation, the Proteostat Aggresome Detection Kit (ENZO, ENZ-51035) was used. Briefly, after the primary antibody rabbit anti-ratMyo1b, cells were incubated for 30min at RT with goat anti-rabbit-Alexa Fluor 635 antibody (1:400, Molecular probes), Proteostat 1:400 and Hoechst 1:800 (ENZO) in PBS 3%BSA. Zebrafish larvae were fixed for 2h at room temperature in 4% PFA and incubated in 30% sucrose/0.1% PBST overnight at 4°C. They were then frozen in Tissue-Tek OCT (Sakura) at -80°C and sectioned using a Cryostat (Leica). Zebrafish larvae sections were incubated in blocking buffer (10% serum in PBST, PBS 0.1%Tween20) and with mouse anti-Villin clone ID2C3 (1:300), mouse 2F11 antibody (1:100, Abcam ab71286) or 4E8 (1:100, Abcam ab73643) overnight at 4°C. After washes with PBST, they were incubated with Alexa Fluor 488 secondary antibody (Molecular probes), phalloidin-Alexa Fluor 568 and Dapi. To assess apoptosis, TUNEL assay was performed with reaction solutions from ApopTag Red In situ Apoptosis detection kit (Millipore) according to the manufacturer recommendations. To assess proliferation, larvae were injected in the yolk with 10mM 5-ethynyl-2'-deoxyuridine (EDU) in 1% DMSO and incubated in 100µM EdU, 0.4%DMSO for 20 hours after injection. Animals were fixed at indicated time and processed according to the Click-iT EdU Imaging Kit (Invitrogen).

Paraffin embedded sections of intestinal tissues from a UNC45A deficient patient and biopsies from controls were obtained for diagnosis or therapeutic purposes. Duodenal biopsies were routinely fixed in 4% buffered formalin for 24 hours and paraffin-embedded. Sections were heated for 1hr at 65°C and paraffin was removed by two 5-min washes in xylene. Sections were then hydrated with ethanol solutions of decreasing concentrations. Unmasking of the epitopes was performed at 100°C for 20 min in Citrate-based Antigen Unmasking Solution (Vector Laboratories). Sections were incubated for 30 min at room temperature in blocking buffer (3% BSA in PBS) and then overnight at 4°C with anti Myo1b antibody (1:200, Novus Biologicals NBP1-87739) in blocking. After washes with PBST, sections were incubated with goat anti rabbit Alexa Fluor 488 antibody (Molecular probes), phalloidin-Alexa Fluor 568 and Dapi for 2hrs at RT. After extensive washes and mounting in Vectashield (Vector Lab), all

stainings were imaged on a LSM780 confocal microscope (Zeiss). Images were processed and numbers of cells quantified using ImageJ.

TEM analysis on zebrafish larvae. 5dpf larvae were collected and stored at 4°C in Trump's fixative. Enhanced chemical fixation was performed in a mix of 4% PFA with 2.5% glutaraldehyde in 0.1 mol/L cacodylate buffer overnight at 4°C. A 1.5-hour incubation in 1% OsO4 was followed by a 1.5-hour incubation with 2% uranyl acetate at ambient temperature. Larvae were then dehydrated through graded ethanol solutions, cleared in acetone, infiltrated, and embedded in Epon-Araldite mix (EMS hard formula). We used adhesive frames (11560294 GENE-FRAME 65 µL; Thermo Fisher Scientific) for flat-embedding, as previously described (Kolotuev et al., 2012), to gain better anteroposterior orientation and sectioning. Ultrathin sections were cut on an ultramicrotome (UC7; Leica Microsystems) and collected on formvar-coated slot grids (FCF2010-CU, EMS). Each larva was sectioned transversally in five different places in intestinal bulb with ≥20 µm between each grid to examine the sample over a large region. Each grid contained at least 4-6 consecutive sections of 70 nm. TEM grids were observed using a JEM-1400 transmission electron microscope (JEOL) operated at 120 kV, equipped with a Gatan Orius SC1000 camera (Gatan) and piloted by the Digital Micrograph program. Microvilli length and density were quantified using Fiji on TEM pictures of at least 50 MV from 25 enterocytes of 3 larvae per condition.

Pull Down assay. 106 N1E115 cells were transfected with pEGFP Myo1b (Salas-Cortes et al., 2005) and lysed in TRIS 150mM, Nacl 150mM, EDTA 1mM, EGTA 1mM, ATP 10 mM, 10% glycerol, 1mM DTT, 0,5% triton and protease inhibitor 24 hours after transfection. The lysate was then incubated with 15 ml of GFP trap Beads (Chromotek) overnight. After washing the beads were resuspended in water and treated for mass spectrometry analysis. For immunoprecipitation, myc-tagged UNC45A Caco-2 cells and myc-tagged empty vector (EV) control Caco-2 cells were lysed in buffer (10 mM Tris/HCl, 150 mM NaCl, 0.5 mM EDTA, 0.5% NP40) with cOmplete protease inhibitors (Roche, Sigma-Aldrich), and myc-tagged proteins were immunoprecipitated by using the µMACS c-myc Isolation Kit (Miltenyi Biotec) according to the manufacturer's instructions.

Statistical analysis. The numbers of cells reported are coming from manual counting. No sample was excluded from the analysis, except for the total cell number per section where we made sure to analyse samples displaying single cell layers through the whole gut cross-sections and not the side of some villi. The sample size (n=) is defined as the number of larvae analysed (one section per larva). For statistical analysis, we applied the non-parametric Wilcoxon-Mann Whitney test.

Acknowledgements

The authors thank the Del Bene team for fruitful suggestions and discussions and members of the Institut Curie zebrafish facility and the pathologist Dr Marion Rabant from Necker Hospital who provided small intestinal tissues from UNC45A deficient patients. The authors acknowledge all members from the PICT-IBiSA Lhomond Imaging Platform (UMR144) and the Cell and Tissue Imaging Platform of the Genetics and Developmental Biology Department (UMR3215/U934) of Institut Curie, member of France-Bioimaging (ANR-10-INSB-04), for help with light microscopy and the electron microscopy unit of the MRic facility (Rennes, France).

Competing Interests

No competing interests declared.

Contributions

MP generated the KO cells. JS and CR generated the Myo1b null allele in zebrafish. MR generated the stable zebrafish transgenic lines. CR and FE performed immunofluorescence stainings. KD, JV and MR performed ISH. MR, CR and RDL performed WB. KD and CR did the RT-qPCR analysis. JS and JV genotyped the mutants. ON and GM did the TEM and analysis. MP and CL prepared cell culture samples. PL generated preliminary data with Morpholinos. MTP and EC performed the pull-down assay. CR analysed the results and wrote the paper. FDB, EC and NCB supervised the work. MR, MP, GM, EC and FDB edited the manuscript.

Funding

This work has been supported by Institut Curie, CNRS, INSERM and grants from the ANR (ANR-14-CE11-0005-03), ANR/e-RARE (ANR-12-RARE-0003-03), by ANR-20-CE17-0020-01 and the ARC foundation (grant n°SFI2012205571). E.C. group belongs to the CNRS consortium CellTiss and to the Laboratoire d'Excellence (LABEX) CelTisPhyBio 11-LBX-0038. FDB group is part of the LABEX DEEP 11-LABX-0044, and of the École des Neurosciences de Paris Ile-de-France network. CR was supported by a EU H2020 Marie Skłodowska-Curie Action fellowship (H2020-MSCA-IF-2014 #661527). MR was supported by the Fondation pour la Recherche Médicale (FRM grant number ECO20170637481).

References

Albadri, S., Del Bene, F. & Revenu, C. 2017. Genome editing using CRISPR/Cas9-based knock-in approaches in zebrafish. Methods, 121-122, 77-85.

Almeida, C. G., Yamada, A., Tenza, D., Louvard, D., Raposo, G. & Coudrier, E. 2011. Myosin 1b promotes the formation of post-Golgi carriers by regulating actin assembly and membrane remodelling at the trans-Golgi network. Nat Cell Biol, 13, 779-89.

Alvers, A. L., Ryan, S., Scherz, P. J., Huisken, J. & Bagnat, M. 2014. Single continuous lumen formation in the zebrafish gut is mediated by smoothened-dependent tissue remodeling. Development, 141, 1110-9.

Barral, J. M., Hutagalung, A. H., Brinker, A., Hartl, F. U. & Epstein, H. F. 2002. Role of the myosin assembly protein UNC-45 as a molecular chaperone for myosin. Science, 295, 669-71.

Benesh, A. E., Nambiar, R., Mcconnell, R. E., Mao, S., Tabb, D. L. & Tyska, M. J. 2010. Differential localization and dynamics of class I myosins in the enterocyte microvillus. Mol Biol Cell, 21, 970-8.

Buske, P., Przybilla, J., Loeffler, M., Sachs, N., Sato, T., Clevers, H. & Galle, J. 2012. On the biomechanics of stem cell niche formation in the gut--modelling growing organoids. FEBS J, 279, 3475-87.

Chin, A. M., Hill, D. R., Aurora, M. & Spence, J. R. 2017. Morphogenesis and maturation of the embryonic and postnatal intestine. Semin Cell Dev Biol, 66, 81-93.

Coudrier, E. & Almeida, C. G. 2011. Myosin 1 controls membrane shape by coupling F-Actin to membrane. Bioarchitecture, 1, 230-235.

Crosnier, C., Vargesson, N., Gschmeissner, S., Ariza-Mcnaughton, L., Morrison, A. & Lewis, J. 2005. Delta-Notch signalling controls commitment to a secretory fate in the zebrafish intestine. Development, 132, 1093-104.

Dalgin, G., Ward, A. B., Hao Le, T., Beattie, C. E., Nechiporuk, A. & Prince, V. E. 2011. Zebrafish mnx1 controls cell fate choice in the developing endocrine pancreas. Development, 138, 4597-608.

Dereeper, A., Guignon, V., Blanc, G., Audic, S., Buffet, S., Chevenet, F., Dufayard, J. F., Guindon, S., Lefort, V., Lescot, M., et al. 2008. Phylogeny.fr: robust phylogenetic analysis for the non-specialist. Nucleic Acids Res, 36, W465-9.

Distel, M., Wullimann, M. F. & Koster, R. W. 2009. Optimized Gal4 genetics for permanent gene expression mapping in zebrafish. Proc Natl Acad Sci U S A, 106, 13365-70.

El-Brolosy, M. A. & Stainier, D. Y. R. 2017. Genetic compensation: A phenomenon in search of mechanisms. PLoS Genet, 13, e1006780.

Esteve, C., Francescatto, L., Tan, P. L., Bourchany, A., De Leusse, C., Marinier, E., Blanchard, A., Bourgeois, P., Brochier-Armanet, C., Bruel, A. L., et al. 2018. Loss-of-Function Mutations in UNC45A Cause a Syndrome Associating Cholestasis, Diarrhea, Impaired Hearing, and Bone Fragility. Am J Hum Genet, 102, 364-374.

Hegan, P. S., Mermall, V., Tilney, L. G. & Mooseker, M. S. 2007. Roles for Drosophila melanogaster myosin IB in maintenance of enterocyte brush-border structure and resistance to the bacterial pathogen Pseudomonas entomophila. Mol Biol Cell, 18, 4625-36.

Horne-Badovinac, S., Lin, D., Waldron, S., Schwarz, M., Mbamalu, G., Pawson, T., Jan, Y., Stainier, D. Y. & Abdelilah-Seyfried, S. 2001. Positional cloning of heart and soul reveals multiple roles for PKC lambda in zebrafish organogenesis. Curr Biol, 11, 1492-502.

Horstick, E. J., Jordan, D. C., Bergeron, S. A., Tabor, K. M., Serpe, M., Feldman, B. & Burgess, H. A. 2015. Increased functional protein expression using nucleotide sequence features enriched in highly expressed genes in zebrafish. Nucleic Acids Res, 43, e48.

Iuliano, O., Yoshimura, A., Prosperi, M. T., Martin, R., Knolker, H. J. & Coudrier, E. 2018. Myosin 1b promotes axon formation by regulating actin wave propagation and growth cone dynamics. J Cell Biol.

Kok, F. O., Shin, M., Ni, C. W., Gupta, A., Grosse, A. S., Van Impel, A., Kirchmaier, B. C., Peterson-Maduro, J., Kourkoulis, G., Male, I., et al. 2015. Reverse genetic screening reveals poor correlation between morpholino-induced and mutant phenotypes in zebrafish. Dev Cell, 32, 97-108.

Kolotuev, I., Bumbarger, D. J., Labouesse, M. & Schwab, Y. 2012. Targeted ultramicrotomy: a valuable tool for correlated light and electron microscopy of small model organisms. Methods Cell Biol, 111, 203-22.

Komaba, S. & Coluccio, L. M. 2015. Myosin 1b Regulates Amino Acid Transport by Associating Transporters with the Apical Plasma Membrane of Kidney Cells. PLoS One, 10, e0138012.

Kwan, K. M., Fujimoto, E., Grabher, C., Mangum, B. D., Hardy, M. E., Campbell, D. S., Parant, J. M., Yost, H. J., Kanki, J. P. & Chien, C. B. 2007. The Tol2kit: a multisite gateway-based construction kit for Tol2 transposon transgenesis constructs. Dev Dyn, 236, 3088-99.

Kwon, O., Han, T. S. & Son, M. Y. 2020. Intestinal Morphogenesis in Development, Regeneration, and Disease: The Potential Utility of Intestinal Organoids for Studying Compartmentalization of the Crypt-Villus Structure. Front Cell Dev Biol, 8, 593969.

Lee, C. F., Melkani, G. C. & Bernstein, S. I. 2014. The UNC-45 myosin chaperone: from worms to flies to vertebrates. Int Rev Cell Mol Biol, 313, 103-44.

Lehtimaki, J. I., Fenix, A. M., Kotila, T. M., Balistreri, G., Paavolainen, L., Varjosalo, M., Burnette, D. T. & Lappalainen, P. 2017. UNC-45a promotes myosin folding and stress fiber assembly. J Cell Biol, 216, 4053-4072.

Lubarsky, B. & Krasnow, M. A. 2003. Tube morphogenesis: making and shaping biological tubes. Cell, 112, 19-28.

Mammoto, T. & Ingber, D. E. 2010. Mechanical control of tissue and organ development. Development, 137, 1407-20.

Martin-Belmonte, F. & Mostov, K. 2008. Regulation of cell polarity during epithelial morphogenesis. Curr Opin Cell Biol, 20, 227-34.

Mazzolini, R., Dopeso, H., Mateo-Lozano, S., Chang, W., Rodrigues, P., Bazzocco, S., Alazzouzi, H., Landolfi, S., Hernandez-Losa, J., Andretta, E., et al. 2012. Brush border myosin Ia has tumor suppressor activity in the intestine. Proc Natl Acad Sci U S A, 109, 1530-5.

Muller, T., Hess, M. W., Schiefermeier, N., Pfaller, K., Ebner, H. L., Heinz-Erian, P., Ponstingl, H., Partsch, J., Rollinghoff, B., Kohler, H., et al. 2008. MYO5B mutations cause microvillus inclusion disease and disrupt epithelial cell polarity. Nat Genet, 40, 1163-5.

Ng, A. N., De Jong-Curtain, T. A., Mawdsley, D. J., White, S. J., Shin, J., Appel, B., Dong, P. D., Stainier, D. Y. & Heath, J. K. 2005. Formation of the digestive system in zebrafish: III. Intestinal epithelium morphogenesis. Dev Biol, 286, 114-35.

Pernier, J., Kusters, R., Bousquet, H., Lagny, T., Morchain, A., Joanny, J. F., Bassereau, P. & Coudrier, E. 2019. Myosin 1b is an actin depolymerase. Nat Commun, 10, 5200.

Prosperi, M. T., Lepine, P., Dingli, F., Paul-Gilloteaux, P., Martin, R., Loew, D., Knolker, H. J. & Coudrier, E. 2015. Myosin 1b functions as an effector of EphB signaling to control cell repulsion. J Cell Biol, 210, 347-61.

Revenu, C., Athman, R., Robine, S. & Louvard, D. 2004. The co-workers of actin filaments: from cell structures to signals. Nat Rev Mol Cell Biol, 5, 635-46.

Revenu, C., Ubelmann, F., Hurbain, I., El-Marjou, F., Dingli, F., Loew, D., Delacour, D., Gilet, J., Brot-Laroche, E., Rivero, F., et al. 2012. A new role for the architecture of microvillar actin bundles in apical retention of membrane proteins. Mol Biol Cell, 23, 324-36.

Reymann, A. C., Boujemaa-Paterski, R., Martiel, J. L., Guerin, C., Cao, W., Chin, H. F., De La Cruz, E. M., Thery, M. & Blanchoin, L. 2012. Actin network architecture can determine myosin motor activity. Science, 336, 1310-4.

Robine, S., Huet, C., Moll, R., Sahuquillo-Merino, C., Coudrier, E., Zweibaum, A. & Louvard, D. 1985. Can villin be used to identify malignant and undifferentiated normal digestive epithelial cells? Proc Natl Acad Sci U S A, 82, 8488-92.

Rossi, A., Kontarakis, Z., Gerri, C., Nolte, H., Holper, S., Kruger, M. & Stainier, D. Y. 2015. Genetic compensation induced by deleterious mutations but not gene knockdowns. Nature, 524, 230-3.

Salas-Cortes, L., Ye, F., Tenza, D., Wilhelm, C., Theos, A., Louvard, D., Raposo, G. & Coudrier, E. 2005. Myosin Ib modulates the morphology and the protein transport within multi-vesicular sorting endosomes. J Cell Sci, 118, 4823-32.

Sidhaye, J., Pinto, C. S., Dharap, S., Jacob, T., Bhargava, S. & Sonawane, M. 2016. The zebrafish goosepimples/myosin Vb mutant exhibits cellular attributes of human microvillus inclusion disease. Mech Dev, 142, 62-74.

Thisse, B. & Thisse, C. 2004. Fast Release Clones: A High Throughput Expression Analysis. ZFIN Direct Data Submission (http://zfin.org).

Tyska, M. J., Mackey, A. T., Huang, J. D., Copeland, N. G., Jenkins, N. A. & Mooseker, M. S. 2005. Myosin-1a is critical for normal brush border structure and composition. Mol Biol Cell, 16, 2443-57.

Wallace, K. N., Akhter, S., Smith, E. M., Lorent, K. & Pack, M. 2005. Intestinal growth and differentiation in zebrafish. Mech Dev, 122, 157-73.

Yamada, A., Mamane, A., Lee-Tin-Wah, J., Di Cicco, A., Prevost, C., Levy, D., Joanny, J. F., Coudrier, E. & Bassereau, P. 2014. Catch-bond behaviour facilitates membrane tubulation by non-processive myosin 1b. Nat Commun, 5, 3624.

Figures

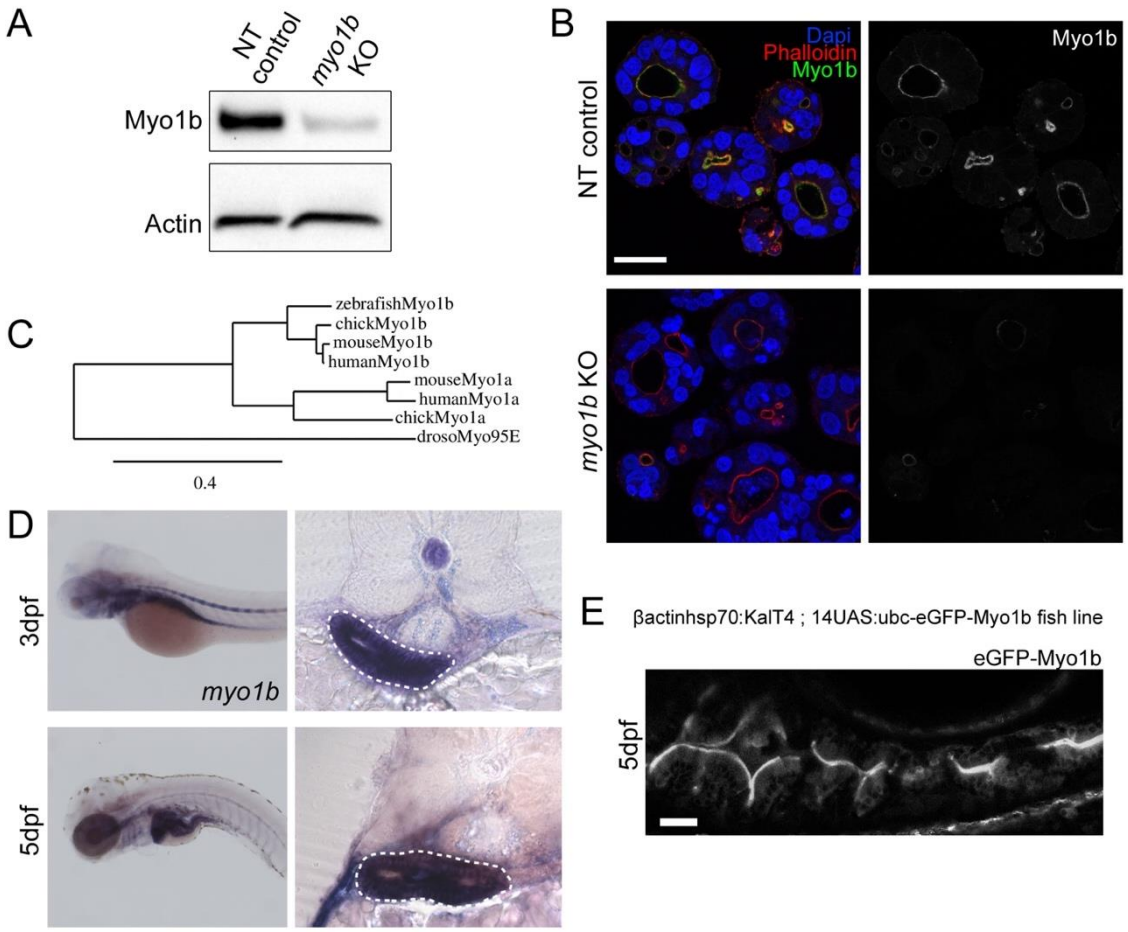

Revenu et al., Figure 1

Figure 1 **Myo1b expression and apical localisation in gut epithelial cells. A-** Western blot analysis of Myo1b expression in extracts from non-targeted (NT) control and myo1b targeted Caco-2 cells (KO) using CRISPR/Cas9. **B-** Confocal sections of Caco-2 3D cultures stained for Myo1b, F-actin (phalloidin) and nuclei (Dapi). **C-** Phylogenetic tree based on protein sequence of zebrafish, chick, human and mouse Myo1b and Myo1a and drosophila Myosin95E. **D-** *In situ* hybridization for myo1b transcripts on 3 and 5dpf zebrafish larvae whole mounts (left panel) and cross-sections at the level of the intestinal bulb (right panels). On sections, the forming intestinal bulb is circled with white dashed lines. **E-** Live, longitudinal (antero-posterior axis) confocal section of the intestinal bulb of a 5dpf zebrafish larva expressing the transcription activator KalT4 driving the expression of the eGFP-Myo1b transgene under the control of an upstream activating sequence (UAS). The precise construction of the transgenes is annotated in the panel. Scale bars 30µm.

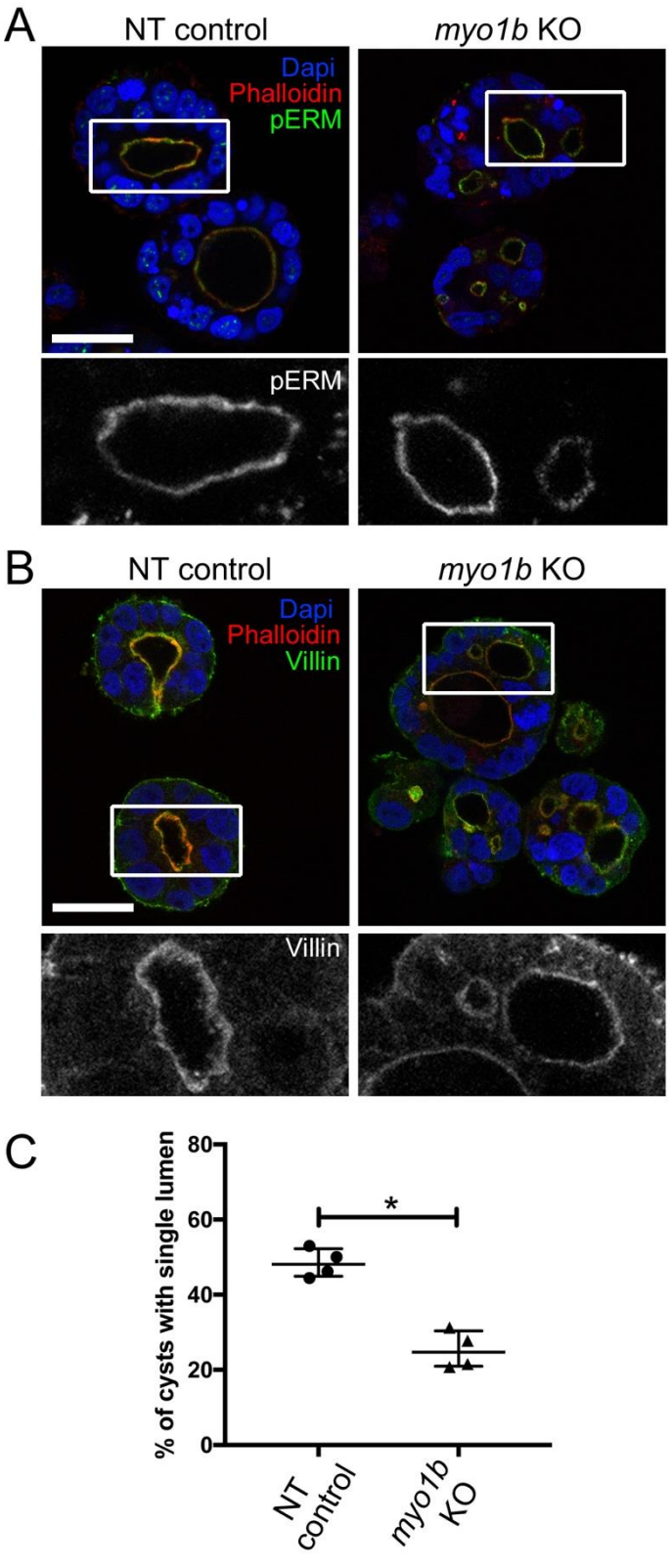

Revenu et al., Figure 2

Figure 2

Enterocyte 3D cyst organization is affected in the absence of Myo1b despite normal apico-basal polarization. Confocal sections of NT control and myo1b KO Caco-2 3D cultures stained for the apical and microvilli markers phospho-Ezrin (pERM, **A**) and Villin (**B**). F-actin (phalloidin) and nuclei (Dapi) are stained, scale bars 30µm, boxed areas showed in insets are enlarged 2.5x. **C-** Quantification of the percentage of well-formed cysts with a single central lumen in NT control and myo1b KO Caco-2 3D cultures. Data represented are median and interquartile range, Wilcoxon test, *p<0.05.

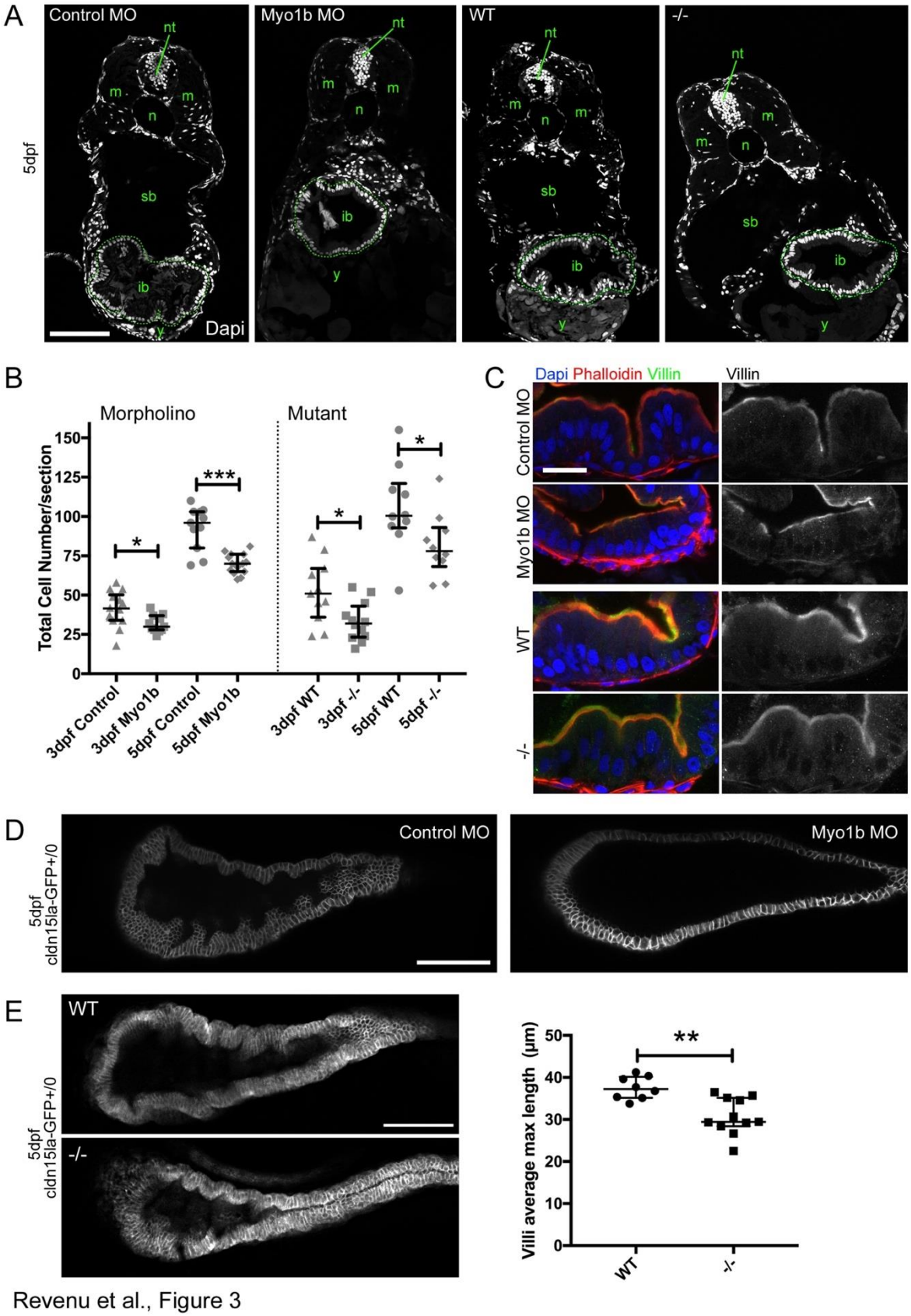

Revenu et al., Figure 3

Figure 3 **Myo1b knock-down and knock-out impair intestinal bulb fold development. A-** Confocal single optical sections stained with nuclear labelling (Dapi) of 5dpf larvae injected

with control and Myo1b Morpholinos (MO), and of 5dpf wild-type (WT) and myo1b-/- (-/-) larvae. ib intestinal bulb (circled with dashed lines), m muscles, n notochord, nt neural tube, sb swim bladder, y yolk. Scale bar=100µm. **B-** Quantifications from Dapi stained sections of the total number of cells per section at 3 and 5dpf in the four conditions. Data represented are median and interquartile range, Wilcoxon test, *p<0.05, ***p<0.001. **C-** Confocal optical sections of the intestinal bulb of 5dpf larvae in the four conditions stained for the microvilli marker Villin, F-actin (phalloidin) and nuclei (Dapi) showing the preserved apico-basal polarity of enterocytes when Myo1b is affected. Scale bar 20µm. **D-** Single confocal planes of live 5dpf larvae expressing Cldn15la-GFP injected with control MO (left) and Myo1b MO (right). Note the flat epithelium in the Myo1b MO condition. Scale bar=100µm. **E-** Single confocal planes of live 5dpf WT and myo1b -/- larvae expressing Cldn15la-GFP and quantification of the average length of the 3 longest folds per intestinal bulb analysed. Scale bar=100µm. Data presented are median and interquartile range, Wilcoxon test, **p<0.01.

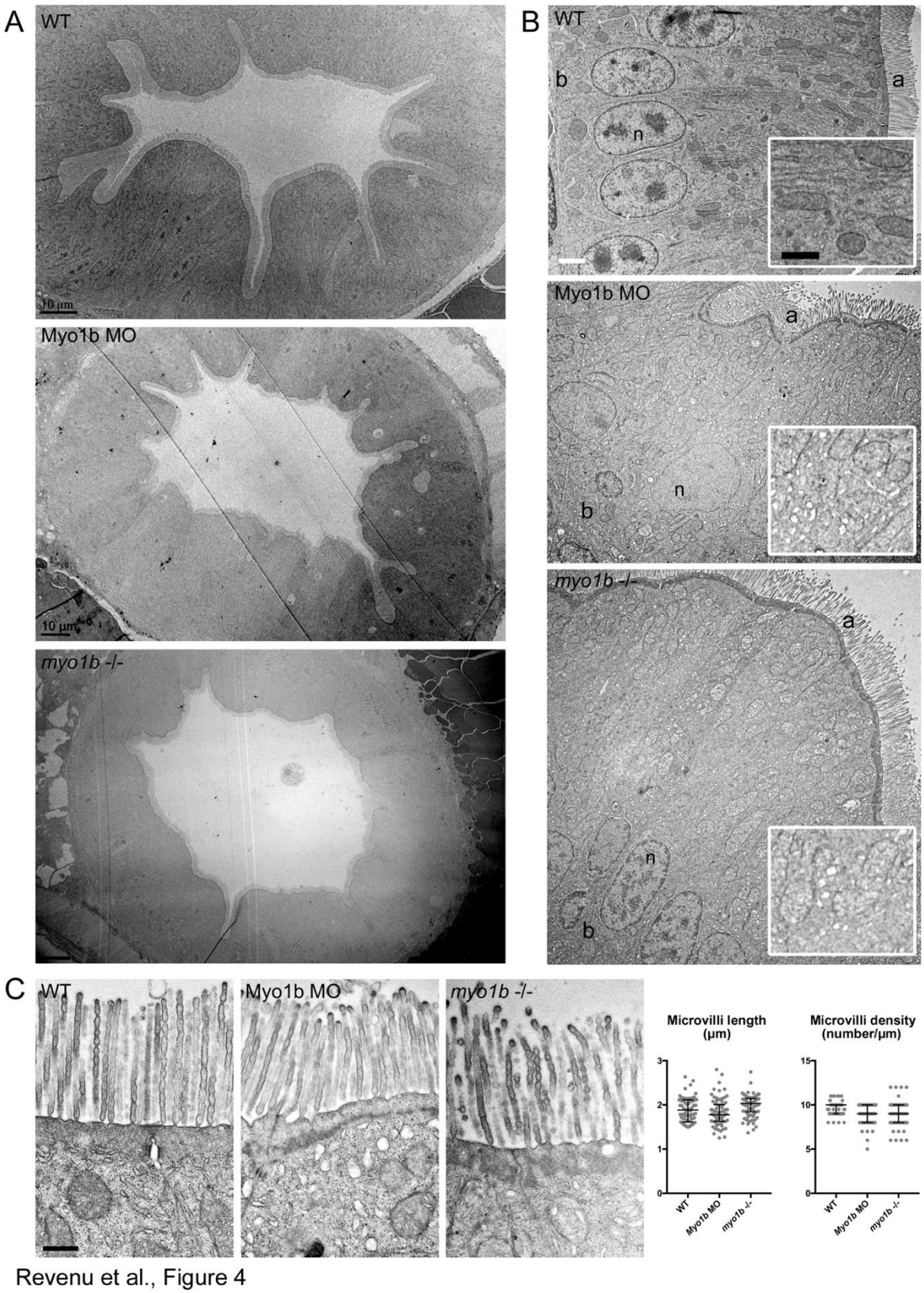

Revenu et al., Figure 4

Figure 4 **Electron Microscopy confirms folding defects and shows affected trafficking. A,B-** Transmission electron micrographs of sections of intestinal bulbs from WT, Myo1b MO and myo1b-/- 5dpf larvae presenting a general view of the folds of the epithelium (**A**, scale

bars 10µm) and of the apico-basally polarized enterocytes (**B**, scale bar 2µm; b basal, a apical, n nuclei). Insets in B, show higher magnifications of the cytoplasm region to highlight the accumulation of vesicles in Myo1b MO and myo1b-/- samples, scale bar 1µm. **C-** Transmission electron micrographs of sections of intestinal bulbs from WT, Myo1b MO and myo1b-/- 5dpf larvae illustrating the organization of the brush border, and quantifications of the average length and density of the intestinal microvilli in the different conditions. Data presented are median and interquartile range. Scale bar 500 nm.

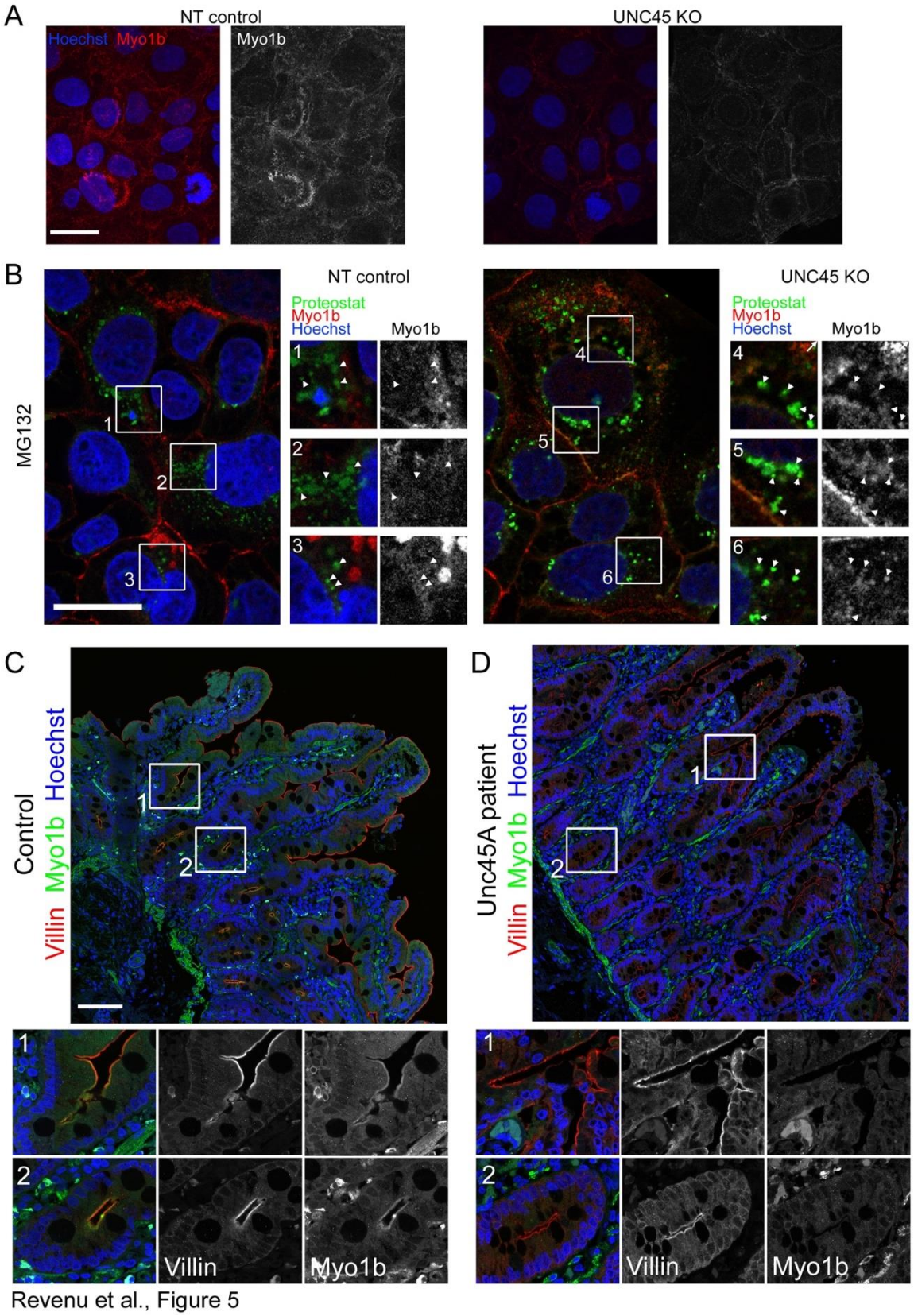

Figure 5 **Myo1b expression is destabilized in UNC45A depleted cells and in biopsies from UNC45A mutated patients. A-** Immunohistochemistry analyses of Myo1b in non-targeted (NT) control and UNC45A deficient (KO) Caco-2 cells show decreased Myo1b levels.

Pictures are maximal projections of confocal stacks, Hoechst labels nuclei, scale bar 30µm. **B-** Confocal sections of NT control and UNC45A KO Caco-2 cells treated with the proteasome inhibitor MG132 and stained for Myo1b and the aggresome probe Proteostat. Hoechst labels nuclei, scale bar 30µm. Boxed areas showed in insets are enlarged 2x, arrowheads point at Proteostat-labelled protein aggregates and highlight colocalization with Myo1b proteins in UNC45A KO cells. **C, D-** Confocal sections of a human biopsy from a healthy patient (control, **C**) and from a UNC45A LOF patient (**D**) immuno-labelled for the microvilli marker Villin and for Myo1b; Hoechst labels nuclei, scale bar 100µm. Boxed areas showed in insets are enlarged 3x, and highlight the apical localisation of Myo1b in control tissue (**C**) at the base of the villi (1) and in crypts (2), which is essentially lost in the UNC45A LOF tissue (**D**).

Supplementary Figures and Table

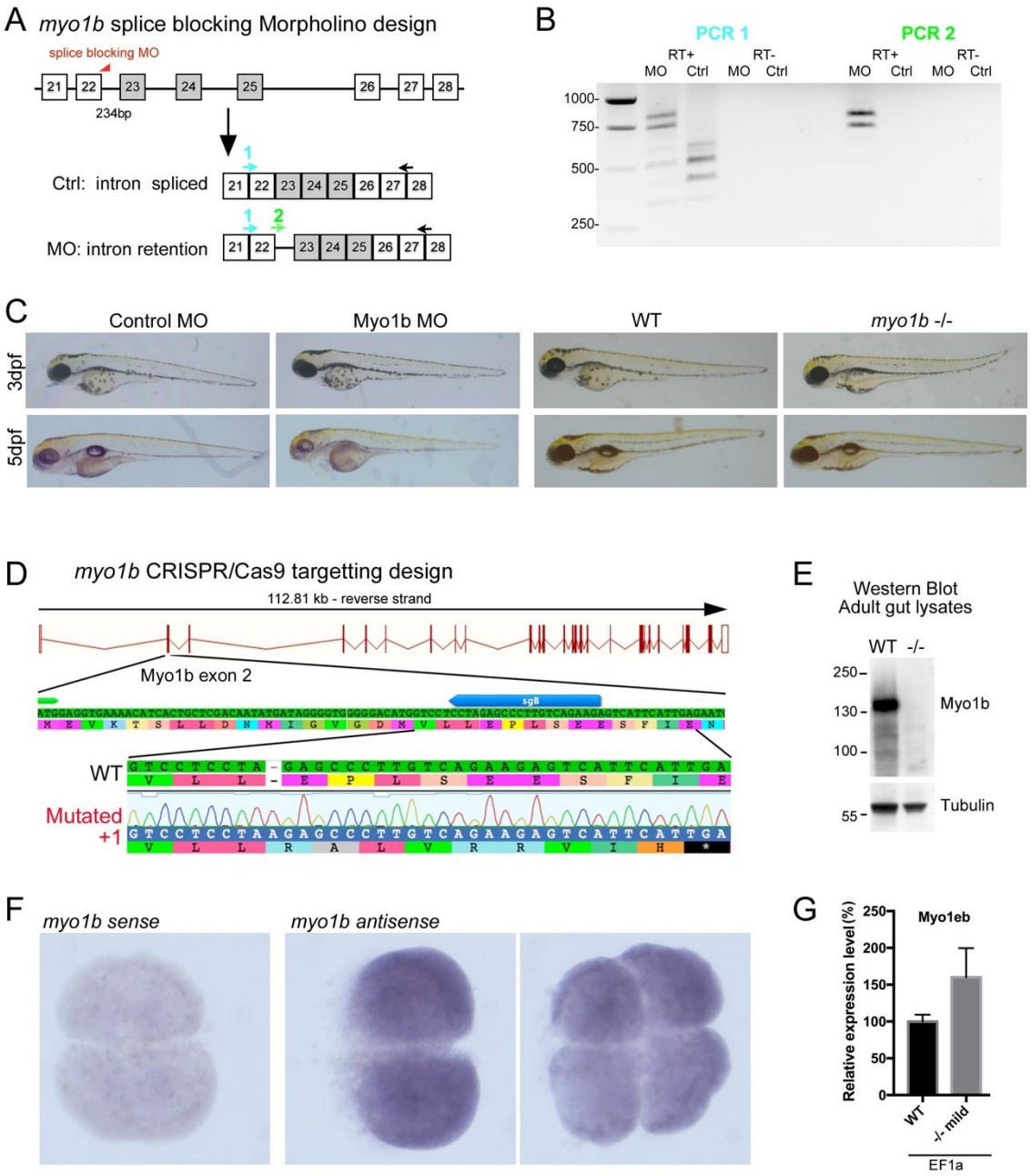

Revenu et al., Figure S1

Figure S1 **Myo1b Morpholino and CRISPR mutant design and validation. A-** Schematics of the design and **B-** DNA gel of the RT-PCR performed to control Myo1b-MO knock-down efficiency. Higher bands amplified in PCR1 MO compared to control and bands amplified in PCR2 MO correspond to Myo1b cDNA retaining the intron targeted by Myo1b-sMO, as verified by sequencing. In B, the multiple bands amplified, both in control and MO conditions, correspond to expected splicing variants of exons 23, 24 and 25 (highlighted in grey)

as checked by sequencing. RT- is the control RT without superscript compared to RT+. **C-** Bright field pictures of 3 and 5dpf larvae presenting the phenotypes of control and Myo1b Morpholinos, WT and myo1b-/- larvae. **D-** Schematics of CRISPR/Cas9-mediated gene disruption at the myo1b genomic locus. The sgRNA (sgB, blue arrow) was targeting exon 2 downstream the start codon (ATG, green arrow). Compared to the WT sequence, the mutated allele displayed an insertion of 1bp generating a frame shift from amino-acid 21 and a premature STOP codon after 29 amino-acids. **E-** Western Blot with antibodies against Myo1b and Tubulin on lysates of dissected guts from WT and -/- adults. **F-** Negative control with a sense probe and in situ hybridisation with a myo1b anti-sense probe on wild-type embryos at 2 and 4 cell-stages showing maternal contribution for myo1b mRNA. **G-** RT-QPCR of myo1eb expression at 3dpf with EF1a used as reference gene, normalised on expression of the WT samples. Shown are mean and sem (WT=100.0±9.2, -/- =160.1±39.5 , n=6).

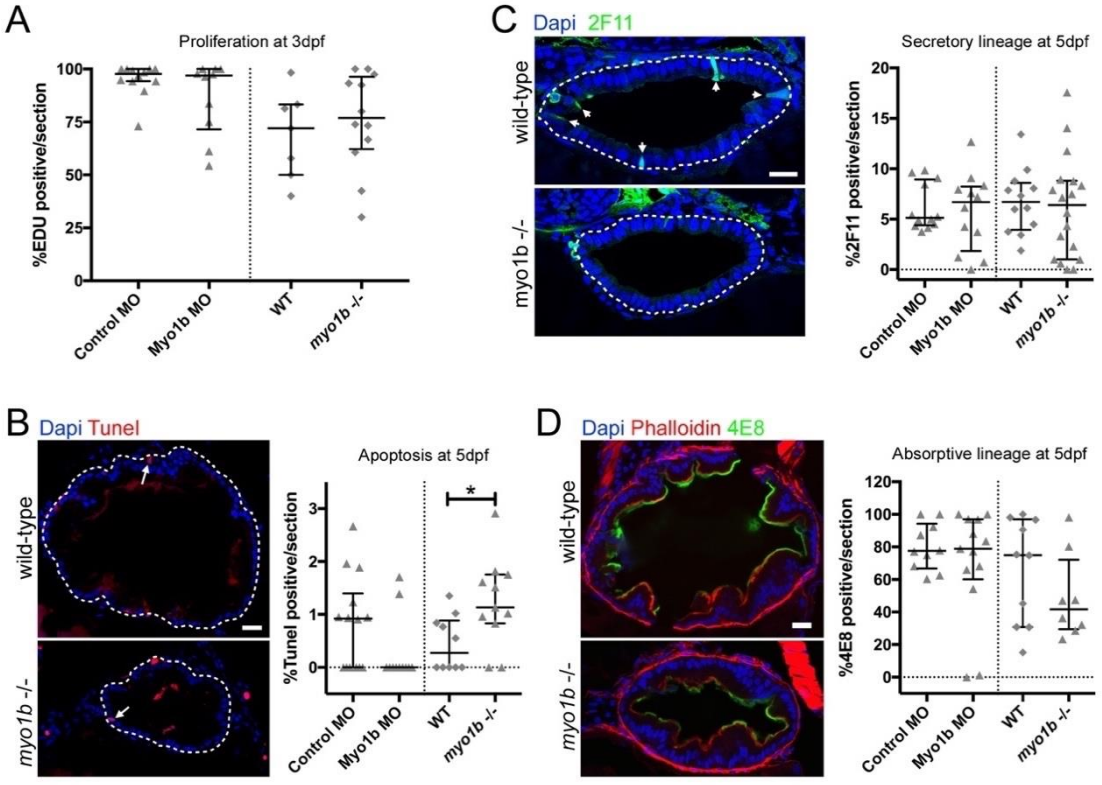

Revenu et al., Figure S2

Figure S2 **Proliferation, apoptosis and differentiation are essentially unaffected in Myo1b MO and mutant conditions. A-** Quantifications from EDU and Dapi stained sections of the proportion of cells in S-phase at 3dpf do not reveal significant differences in the proliferative rate of Control vs Myo1b MO and of WT vs *myo1b*-/- samples. **B-** Confocal sections of intestinal bulbs stained for apoptosis (Tunel, red) at 5dpf in WT and *myo1b*-/- samples and quantifications of the proportion of apoptotic cells in the four conditions. **C, D-** Confocal

sections of intestinal bulbs stained for differentiation markers in WT and *myo1b*-/- samples and quantifications of the proportion of differentiated cells in the four conditions. At 5dpf, neither differentiation of the secretory lineage (2F11, **C**) nor differentiation of the absorptive lineage (4E8, **D**) are significantly altered. For all quantifications, data represented are median and interquartile range, Wilcoxon test, *p<0.05. For confocal images, nuclei are counterstained with Dapi (blue), bars=20µm.

Rank	Accession	Description	MW [kDa]	Coverage %	#Unique Peptides	#PSMs
1	P46735	Unconventional myosin-Ib OS=Mus musculus [MYO1B_MOUSE]	128,483	65,31	102	633
2	Q99KD5	Protein unc-45 homolog A OS=Mus musculus [UN45A_MOUSE]	103,3818	22,14	24	53

Table S1 **Mass spectrometry result of the GFP-Myo1b pull down assay.** UNC45A ranks second, directly after Myo1b. MW, molecular weight; #Unique Peptides, number of distinct peptide sequences identified; # PSMs (peptide spectrum matches) total number of identified peptide sequences for the protein.